NEW CHARGE-TRANSPORT MATERIALS FOR OLED APPLICATIONS

KIRAN KAMTEKAR M.CHEM. (HONS) DUNELM MRSC

TREVELYAN COLLEGE

DEPARTMENT OF CHEMISTRY

UNIVERSITY OF DURHAM

A Thesis submitted for the degree of Doctor of Philosophy at the University of Durham

December 2006

STATEMENT OF COPYRIGHT

DECLARATION

The work described in this thesis was carried out in the Department of Chemistry at the University of Durham between October 2003 and September 2006. All the work was carried out by the author unless otherwise stated and has not previously been submitted for a degree at this or any other university.

Memorandum

The following conferences and symposia were attended during the period of study:

- **Organoboron Symposium**

University of Durham, Durham, UK 2004

- **6th International Symposium on Functional π-electron Systems**

Cornell University, Ithaca, USA 2004

- **Departmental 2nd Year PG Symposium**

University of Durham, Durham, UK 2005

Talk given entitled *Organic Materials*

- **Materials Chemistry 7: Functional Materials for the 21st Century**

University of Edinburgh, Edinburgh, UK 2005

- **Departmental 3rd Year PG Poster Session**

University of Durham, Durham, UK 2006

Poster presented entitled *New Electroluminescent Bipolar Compounds for Balanced Charge-transport and Tuneable Colour in Single-layer OLEDs*

- **SCI North Postgraduate Symposium**

University of York, York, UK 2006

Talk given entitled *New Electroluminescent Bipolar Compounds for Balanced Charge-Transport*

- **7th International Symposium on Functional π-electron Systems**

Osaka, Japan 2006

Poster presented entitled *New Electroluminescent Bipolar Compounds for Balanced Charge-transport and Tuneable Colour in Single-layer OLEDs*

The following papers are based on work described in this thesis:

K. T. Kamtekar, C. S. Wang, S. L. Bettington, A. S. Batsanov, I. F. Perepichka, M. R. Bryce, J. H. Ahn, M. Rabinal and M. C. Petty, **New electroluminescent bipolar compounds for balanced charge-transport and tuneable colour in organic light-emitting diodes: triphenylamine-oxadiazole-fluorene triad molecules**, *Journal of Materials Chemistry*, 2006, **16**, 3823

N. E. Widdowson, J. H. Ahn, K. T. Kamtekar, C. Wang, C. Pearson, M. R. Bryce and M. C. Petty, **Lifetime studies of blended layer organic light-emitting diodes**, *J. Appl. Phys.*, Document in preparation

C. Pearson, C Wang, J. H. Ahn, K. T. Kamtekar, M. R. Bryce and M. C. Petty, **Switching and memory effects in organic thin films of electroactive compounds**, *Appl. Phys. Lett.*, Document in preparation

Table of Contents

Abstract

New Charge-Transport Materials for OLED Applications

Kiran Kamtekar, University of Durham, 2006

Novel fluorene-1,3,4-oxadiazole and spirobifluorene-1,3,4-oxadiazole compounds **202** and **211**, respectively, have been synthesised. Compound **202** was blended with MEH-PPV in various ratios and incorporated into organic light-emitting diodes (OLEDs). The devices were found to emit light purely from MEH-PPV up to very high doping levels. When the device architecture ITO/PEDOT:PSS/MEH-PPV:**202**/Ca:Al was used it was found that increasing the amount of **202** increases the lifetime of the device.

Novel bipolar fluorene-1,3,4-oxadiazole-triphenylamine molecules **237** and **240** were synthesised using silicon protecting groups. When incorporated into devices with architecture ITO/PEDOT:PSS/**237** or **240**/Ca:Al it was found that the materials facilitated the transport of electrons and holes as well as acting as blue-green emitters with efficiencies of up to 0.26%/0.6 cd A^{-1}. Compound **237** also performed well when blended with MEH-PPV giving rise to efficiencies two orders of magnitude greater than for pure MEH-PPV devices.

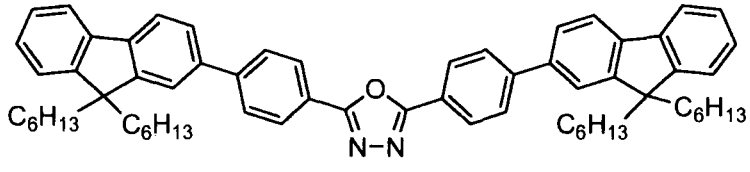

202

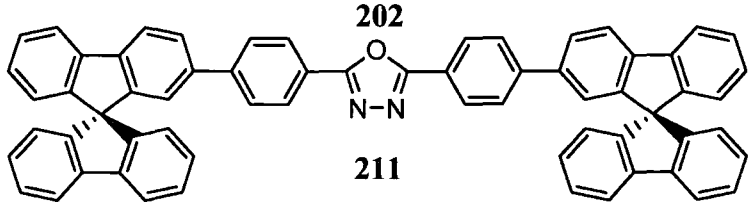

211

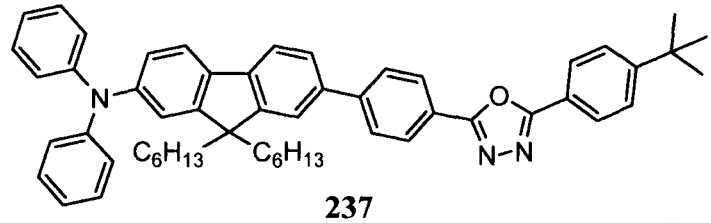

237

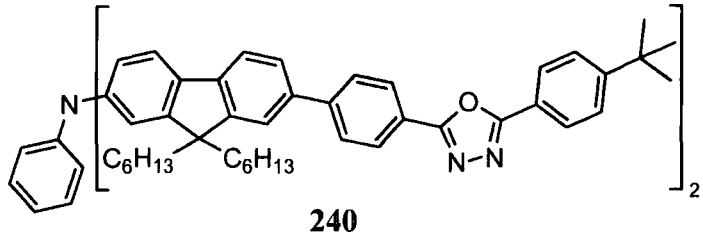

240

Acknowledgements

After the lengthy challenge of writing this thesis I'm now faced with the possibly greater challenge of thanking everyone who has helped me over the last three years.

Firstly I'd like to thank my supervisor Martin Bryce for welcoming me into his research group back in 2002, encouraging me to develop my ideas and solving problems as well as enabling me to attend several international conferences.

I'd especially like to thank Dr Changsheng Wang and Dr Sylvia Bettington who have helped me enormously by demonstrating practical techniques and offering potential solutions to many synthetic problems. Changsheng's gift of an OLED device on my first day in the lab has helped me to keep the wider picture in mind. Thanks must also go to the other members of CG104 past and present (in no particular order) Kara, Conny, Kate, Pete, Carl, Amy, Ste, Mustafa, Xianshun, Igor and undergraduates Ryan, Ed and Laura who have all helped maintain a friendly working environment and provided great entertainment on conferences.

This thesis would only be about half the size without the help of the group of Prof. Mike Petty in the Department of Engineering (especially Nick Widdowson and Dr Jin Ahn) who turned my materials into working OLED devices. Thanks to the technical staff (especially the NMR team) for enabling elucidation of structures and the stores team for sorting out our orders and conference matters.

I've been lucky enough to have made many fantastic friends over my many years at Durham and I'd like to thank them all for the support they've given me – so much so I practically consider them family. Special thanks to my 4th year housemates Matt Cartwright, Alan Cooper and Ollie Cunningham – can you believe we've all done PhDs? I'd also like to thank the chemistry social group for helping me enjoy my last year in Durham. Many thanks to my parents for their support throughout my years at university. I hope I have made you proud. Finally Angharad: we may have only had a few months, but you made me believe in myself. Thank you.

For anyone who has believed in me

I have not failed. I've just found 10,000 ways that won't work.

- Thomas Alva Edison (1847 – 1931)

Abbreviations

acac	Acetonylacetate
Alq_3	Tris(8-hydroxyquinoline)aluminium, **3**
CIE	Commission Internationale de l'Eclairage
CV	Cyclic voltammetry
DCM	Dicholoromethane
DFT	Density functional theory
DMF	*N*,*N*-Dimethylformamide
EL	Electroluminescence
EQE	External quantum efficiency
ET	Electron transport
FIrpic	Iridium bis[(4,6-difluorophenyl)-pyridinato-N,C^2]picolinate, **172**
HOMO	Highest occupied molecular orbital
HT	Hole transporter
$Irppy_3$	Tris(2-phenylpyridine)iridium, **164**
ITO	Indium tin oxide
LUMO	Lowest unoccupied molecular orbital
MEH-PPV	Poly[2-(2-ethylhexyloxy)-5-methoxy-*p*-phenylenevinylene], **14**
mp	Melting point
NMR	Nuclear magnetic resonance
OLED	Organic light emitting diode
OXD	1,3,4-Oxadiazole
PBD	5-(4-Biphenyl)-2-(4-*tert*-butylphenyl)-1,3,4-oxadiazole, **5**
PEDOT	Poly(3,4-ethylenedioxythiophene), **20**
PL(QY)	Photoluminescence (quantum yield)
PMMA	Poly(methylmethacrylate), **56**
PPV	Poly(*p*-phenylene vinylene), **10**
PSS	Poly(styrene sulphonate), **21**
T_g	Glass transition temperature
THF	Tetrahydrofuran
TIPB	Triisopropyl borate
TPD	*N*,*N*'-Diphenyl-*N*,*N*'-bis(3-methylphenyl)(1,1'-biphenyl)-4,4'-diamine, **22**
UV-vis	Ultraviolet-visible

Chapter 1 – Introduction to Organic Light-Emitting Diodes

Since their inventions in the latter part of the 19th century, the cathode ray tube (CRT) and the tungsten light bulb have been the dominant technologies for display and lighting applications, respectively. Over a century later, their use is still widespread throughout the world. Organic light-emitting diodes (OLEDs) have the potential to replace both of these technologies in the near future, offering many attractive properties.

In the case of lighting, traditional filament bulbs emit over 90% of their energy as heat rather than light (giving approximately 15 lm W^{-1} luminous efficiency) and only offer

ca. 1000 hours of operational life. Fluorescent lighting is more efficient, but still wastes energy in transferring UV energy to a phosphor, contains toxic mercury and is a much more expensive solution. By contrast, solid state lighting (SSL) offers much higher efficiencies, lifetimes running to 100,000 hours and a substantial reduction in the amount of heat generated. LEDs (both inorganic and organic) are being developed with SSL applications in mind. Indeed, many world governments have invested funding (such as the US Department of Energy's *Solid-State Lighting Project Portfolio*) in SSL research to help meet targets on reducing greenhouse emissions. In addition, many companies are also seeing the benefit of "bulb-less" products. For example all new Boeing airliners, including the 747-8 and 787 Dreamliner, will feature SSL in a bid to increase efficiency and provide a more natural light to passengers.

Displays are beginning to move on from the traditional CRT. Liquid crystal displays (LCDs) and plasma displays, first developed in the 60s, are beginning to gain a larger market share. These replacements are not without their drawbacks; plasma displays are very fragile, expensive and prone to screen-burn whilst LCDs have slow response times (in the millisecond region), low viewing angles and require a backlight leading to poor contrast ratios. OLED displays offer quick response times (in the microsecond range), extremely high viewing angles and higher contrast ratios since they do not require backlights. In addition to being very thin, OLEDs offer the potential for flexible or "roll-up" screens when combined with suitable substrates and thin film transistors (TFTs). The first commercial OLED product, a car radio from Pioneer Corporation, was launched in 1997 and Eastman Kodak/Sanyo launched the first full-colour active matrix OLED (AMOLED) display on a digital camera in 2003. Today, small size (< 3") OLED screens are frequently used as displays in mobile phones, personal music players, PDAs and digital cameras as well as providing backlights for traditional LCDs. Several large-size displays ranging from high resolution WUXGA 21" through to WXGA 40" screens have been displayed at trade shows, but problems with lifetimes and colour purity need to be overcome before these kinds of displays are commercially viable. OLEDs promise to become a disruptive technology, replacing bulky CRT displays with ultra-thin, low power displays and wasteful, inefficient filament bulbs with lighting that can provide natural pure white light and change to a wide range of colours at the flick of a switch. Further innovations such as inkjet

printing of OLED materials and transparent OLEDs (TOLEDs) will allow OLEDs to be incorporated into many new and unexpected places.

Figure 1.1 Demonstrations of prototype OLED displays

It is estimated that the global OLED market will be worth $2.3 billion by 2008.[1] With many companies and academic groups around the globe working on this science, future advances and successful marketplace growth seem assured.

1.1 Organics for Photonics

1.1.1 Electroluminescence in Organic Materials

Electroluminescence (EL) was first reported by Pope *et al.* in 1963[2] by passing very large voltages through anthracene, **1**, crystals. Two years later Helfrich carried out further studies on anthracene systems, attributing the EL to the recombination of electrons and holes inside the crystals.[3] The high (*ca.* 400 V) voltages needed, due to the thickness of the crystals, meant that EL for displays and lighting would go uninvestigated for several decades. Indeed Helfrich went on to develop the twisted nematic (TN) LCD[4] which would help LCDs find commercial applications as displays. Operating voltages were reduced to *ca.* 30 V by Vincett *et al.* who reported EL from thin anthracene films sublimed onto oxidised aluminium electrodes.[5]

The major breakthrough came in 1987, when workers at Eastman Kodak developed a device incorporating thin films of diamine **2** and tris(8-hydroxyquinoline)aluminium (Alq_3, **3**).[6] The 750 Å diamine layer was incorporated to transport positive holes from the indium tin oxide (ITO) anode whilst the 600 Å Alq_3 layer produced the emission. A top electrode of Mg:Ag in a 10:1 ratio completed the diode. The cathode was chosen for Mg's low work function. Ag was incorporated to retard the atmospheric

degradation of the Mg via oxidation and corrosion. All the layers were deposited onto the ITO by vacuum deposition. On application of a potential difference across the device, light output was seen with as little as 2.5 V driving voltage. Brightnesses of over 1,000 cd m^{-2} (today's LCD screens are typically 200 – 300 cd m^{-2}) were seen at < 10 V and external quantum efficiencies (EQEs) of up to 1% were observed. The green emission (λ_{max} = 550 nm) was independent of the driving voltage, but changed with different layer thicknesses.

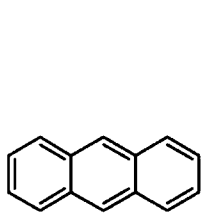

1

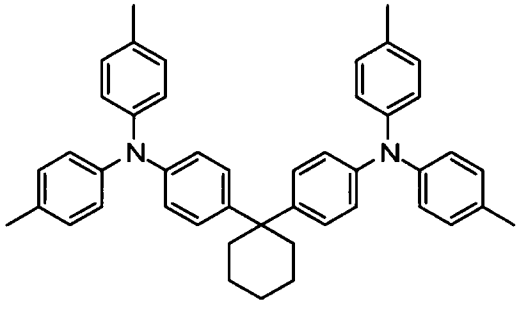

2

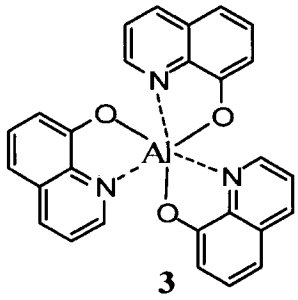

3

The EL spectrum matched the photoluminescence (PL) spectrum of Alq_3 indicating electron-hole recombination occurred within the Alq_3 layer. Further studies were carried out by Adachi *et al.* who fabricated a bilayer device consisting of NSD, **4**, a hole transporting luminescent material and electron transporting 1,3,4-oxadiazole derivative PBD, **5**.[7] Using the device configuration ITO/NSD/PBD/Mg:Ag, brightnesses of > 1,000 cd m^{-2} were achieved at operating voltages of 16 V giving a luminous efficiency of 0.2 lm W^{-1}. Efficiencies were four orders of magnitude greater than those obtained from single layer devices ITO/NSD/Mg:Ag. When a second hole transporting layer of diamine TPD, **6**, was incorporated into a device (ITO/TPD/NSD/Mg:Ag) a 10^2-fold increase in efficiency over the single layer device was obtained. The emission from the NSD/PBD device contained no trace of emission from PBD, suggesting that recombination occurred solely in the NSD layer. The PBD benefits the device by transporting electrons, blocking holes and preventing quenching of charge-carrying excitons at the emitter/cathode interface.

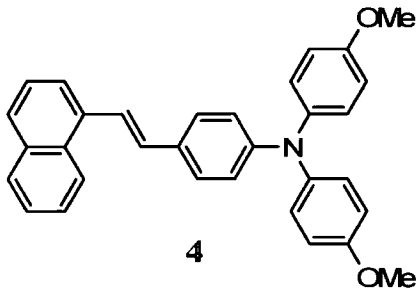

4

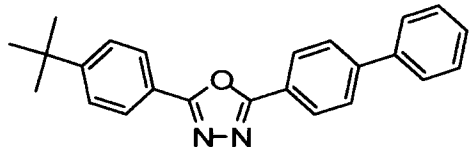

5

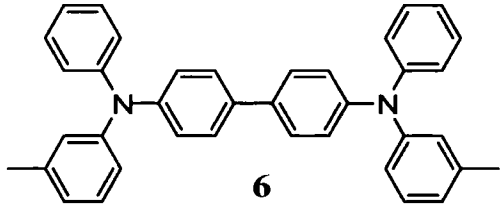

6

1.1.2 Polymeric Materials

The serendipitous discovery of the EL properties of poly(*p*-phenylenevinylene) (PPV, **10**) by workers at the University of Cambridge[8] gave rise to a new category of organic EL materials – conjugated polymers. Previous polymers studied in relation to EL applications[9] had been non-conjugated examples such as teflon, polyethylene and nylon-6. Conjugated polymers are semiconductors owing to their delocalised π molecular orbitals which enable charge to be transported quickly along polymer chains and, combined with the inherent processability of polymers, have the potential for very functional, flexible materials. A green-yellow glow was observed when a potential was applied to PPV which is an insoluble, intractable material. To create processable PPV films, a soluble sulphonium polymer precursor was spin-coated onto ITO and converted to PPV by heating in a vacuum. The route to PPV starting from α,α'-dichloro-*p*-xylene, **7**, is shown in Scheme 1.1. Compound **8** underwent polymerisation in a water/methanol mixture in the presence of base. After termination the reaction mixture was dialysed against distilled water. The solvent was removed and the polymer precursor, **9**, was redissolved in methanol from which it could easily be spin-coated. The temperature of conversion to PPV can be reduced down to 100 °C by using the bromide salt of the precursor **9**.

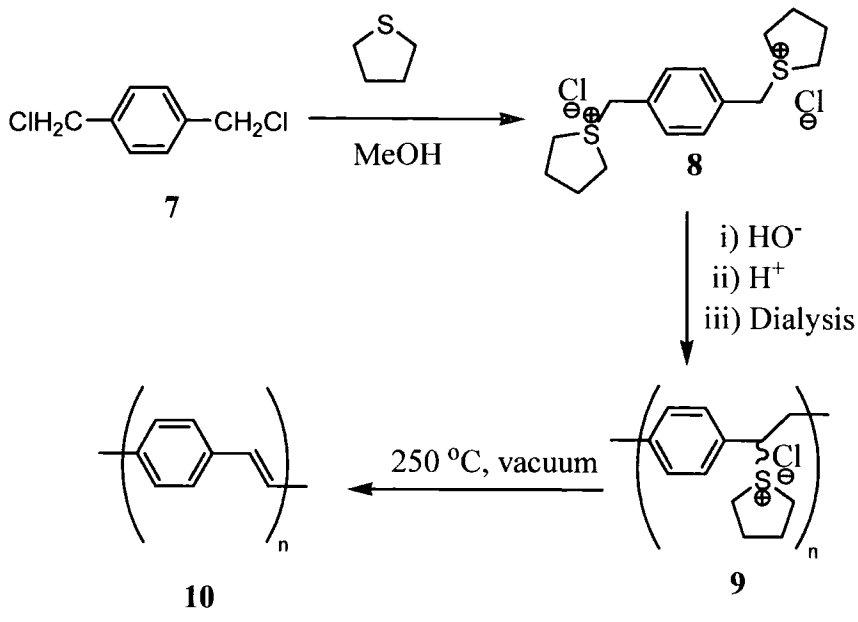

Scheme 1.1 Initial route to PPV

This route afforded homogeneous, uniform PPV films with a typical thickness of 100 nm. Devices with the structure ITO/PPV/Al emitted a green-yellow light (λ_{max} = 551, 520 nm) with an EQE of 0.05% and a threshold voltage of just below 14 V.

Several groups soon reported syntheses of PPV derivatives which are fully soluble in their polymeric form.[10, 11] Poly[2-methoxy-5-(2-ethylhexyloxy)-*p*-phenylenevinylene] (MEH-PPV, **14**) developed by Heeger and Braun is the most widely studied. Its solubility and air stability are derived from the alkoxy side chains. Due to MEH-PPV's excellent solubility in common solvents such as chloroform and THF it can be readily spin-coated without the need to thermally treat the cast film. Although MEH-PPV can be prepared using an analogous method to PPV, Gilch and Wheelwright developed a synthesis that shortens the preparation by two steps as shown in Scheme 1.2.[12]

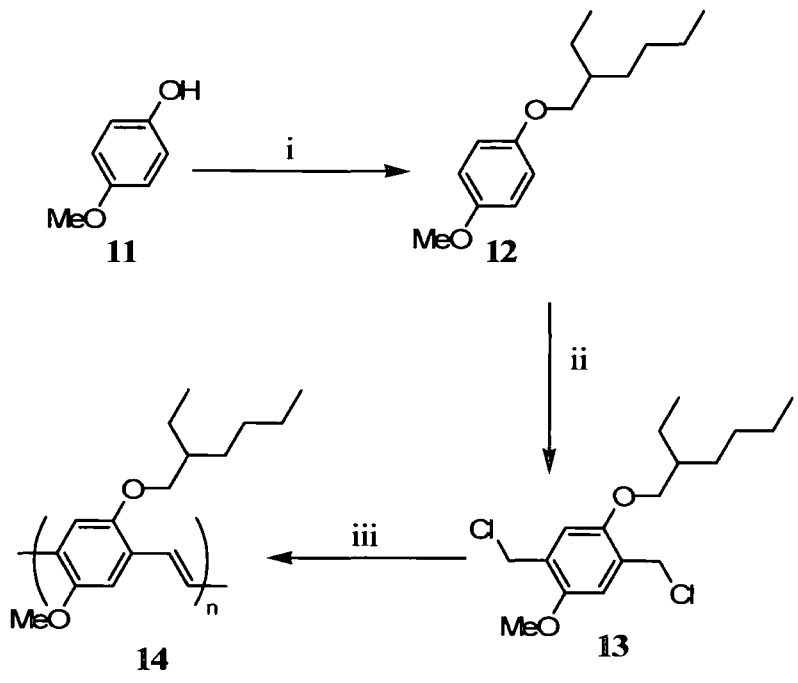

Scheme 1.2 Synthetic route to MEH-PPV; i, 3-(bromomethyl)heptane, KOH, reflux; ii, HCHO, *c*HCl, 20 °C then reflux; iii, KO^{t}Bu, 20 °C

Films of 120 nm thickness were spun from THF/xylene solutions containing 1% by weight MEH-PPV into devices comprising ITO/MEH-PPV/Ca and afforded orange-red light (λ_{max} = 626 nm) that became visible to the eye at driving voltages of 9 V. Compared to Mg:Ag alloy and Al, the use of a Ca cathode provides more efficient devices due to the lower work function of Ca which is more closely aligned with the LUMO of MEH-PPV. Device lifetime is sacrificed, however, due to the instability of Ca in the presence of atmospheric moisture.

Further studies by Gu at Uniax Corporation added a layer of polyaniline (PANI) protonated by (±)-10-camphor sulphonic acid (CSA) to form a device of structure ITO/PANI-CSA/MEH-PPV/Ca which turned on at 2 V and reached 100 cd m^{-2} at 2.4 V and 4,000 cd m^{-2} at < 4 V with an EQE of 2 – 2.5%.[13]

In 1997, Andersson, Yu and Heeger reported related alkyl and alkoxy substituted PPV derivatives **14** – **18**, related to MEH-PPV.[14]

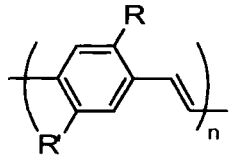

cpd	R	R'
14	2-ethylhexyloxy	methoxy
15	2-ethylhexyloxy	2-ethylhexyloxy
16	cholestanoloxy	cholestanoloxy
17	3-octyloxy	methoxy
18	ethylhexyl	butyl

It was found that when R = R' the polymer chains stacked closer together in a more ordered manner giving rise to lower PL efficiencies in films. Symmetrical polymers with large, bulky side groups such as BCHA-PPV, **16**, avoided this close packing with a resulting increase in PL efficiency (from 12% to 53%). The use of alkyl chains in the place of alkoxy chains gave rise to a blue-shifted emission due to the CH_2 groups adjacent to the phenyl ring which interfere with the chain's conjugation.

1.2 Structures and Modes of Operation

1.2.1 Theory

At their simplest OLEDs consist of an electroluminescent material sandwiched between two electrodes as shown in Figure 1.2. One of these electrodes must be at least semi-transparent to allow passage of the generated light out of the device. If both electrodes are transparent, then building OLEDs into vision-area applications such as displays on windows or vehicle windscreens becomes a possibility.

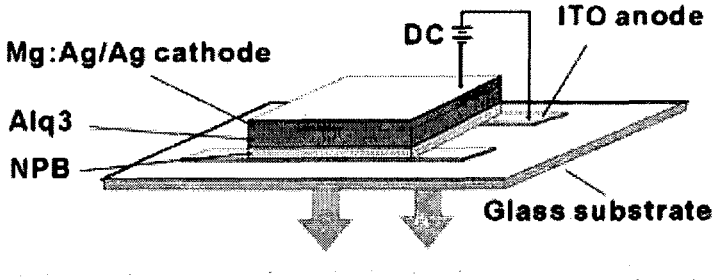

Figure 1.2 Schematic diagram of OLED device similar to that described in reference 6

When a potential is applied to the electrodes, electrons are injected into the LUMO of the organic layer from the low work function cathode to form anion radicals and positive holes are injected into the HOMO from the high work function anode to form cation radicals. These charge carriers then migrate towards the electrode of opposite polarity under the influence of the external electric field.[15] When these polarons meet an oppositely charged species, recombination occurs to form an excited state. This excited state can have either singlet or triplet multiplicity. In conventional fluorescent materials only the singlet states can relax to emit light. Spin statistics predict a 1:3 ratio of singlet:triplet states. There is currently ongoing debate over whether polymeric EL materials can obtain a higher ratio of singlet states.[16, 17]

Figure 1.3 shows the basic processes that occur inside a device when a potential is applied.[18] Internal quantum efficiency (η_{int}) is defined as "*the ratio of the total number of photons generated within the structure to the number of electrons injected*" and external quantum efficiency (η_{ext}) is defined as "*the ratio of the number of photons emitted by the OLED into the viewing direction to the number of electrons injected*".[19]

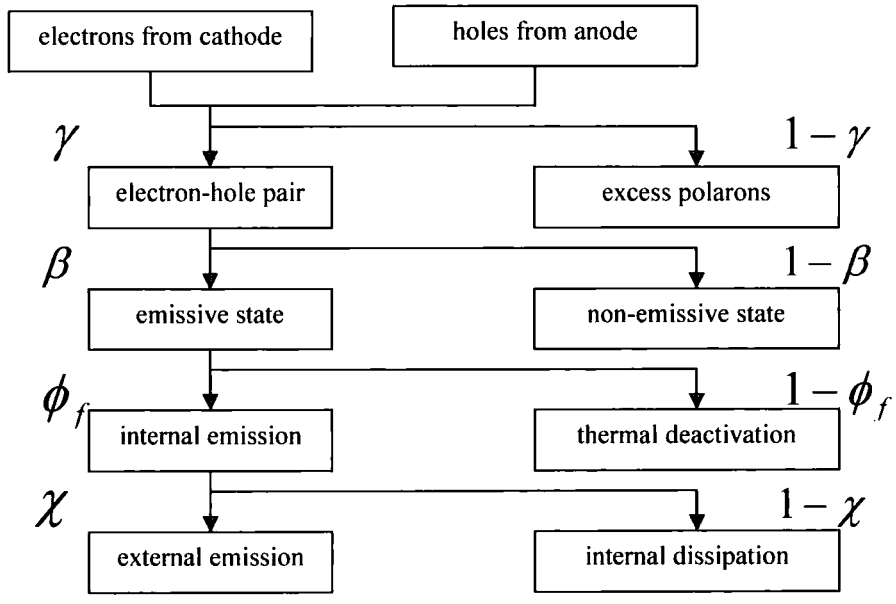

Figure 1.3 Possible routes for the polarons generated in devices to follow - reproduced from reference 18

The two efficiencies are linked by Equation (1) where χ is the light output coupling factor:

$$\eta_{ext} = \chi\eta_{int} \qquad (1)$$

The internal quantum efficiency is given by the Equation (2) where γ is the charge balance factor, β is the production efficiency of emissive excitons and φ_f is the fluorescence quantum yield:

$$\eta_{int} = \gamma\beta\phi_f \qquad (2)$$

In order to maximise efficiencies, all of these factors must be optimised. As mentioned above, fluorescent systems are limited by spin statistics allowing β to reach a maximum value of 0.25. In 1999 Forrest *et al.* developed a green emitter based on the iridium complex $Ir(ppy)_3$.[20] The heavy metal atom allows spin-orbit mixing of states such that emission can occur from triplet states allowing the value of β to rise to 1.0. These phosphorescent systems will be discussed later in Chapter 1.6. The synthesis of emitters with high fluorescent quantum yields has been an important target in research and many fluorescent materials with $\varphi_f > 0.8$ are now known.

The light output coupling factor, χ, takes into account all the light that never leaves the device and can be estimated by Equation (3) where n is the refractive index of the organic material:

$$\chi = 1 - \sqrt{1 - \frac{1}{n^2}} \qquad (3)$$

As most organic solids possess refractive indices of *ca.* 1.7 a further approximation (Equation (4)) is used:

$$\chi = \frac{1}{2n^2} \qquad (4)$$

This value is frequently taken to be 0.20, although it may reach close to 0.40 if planar orientation of the emissive centres is possible.

The optimisation of γ is discussed below, but it can be assumed that the values can reach 1.0. With the assumed values of $\chi = 0.20$, $\beta = 0.25$, $\gamma = 1$ and $\varphi_f = 1$, we arrive at a maximum external quantum efficiency of 0.05 or 5% for fluorescent materials.[18] This does not represent an actual ceiling of efficiency because, as noted above, some of these values can be increased. One feature of OLED development has been a lack of

consistency between research groups in the methods of device fabrication and measurements of performance. This is similar to the different methods used to measure performance of current LCD panels leading to some manufacturers claiming falsely improved specifications. Forrest *et al.* recently discussed these issues and suggested formal definitions to standardise results.[19] However, it remains inappropriate to directly compare results from different groups.

1.2.2 Balancing Charge Injection

The value of γ is a measure of how readily the electrons and holes within the device form excited states. If most of the injected charges simply pass through the device to the oppositely charged electrode, the value of γ will be low. This can occur if the organic material sandwiched between the electrodes does not favour the formation of either cation radicals and/or anion radicals. For example, in PPV cation radicals are the majority charge carriers due to the low electron affinity of the polymer, meaning holes are more likely to migrate through the device to the cathode than in devices with more balanced charge transporting properties.[15] There are several ways to address this issue. So far only simple "single layer" device structures have been discussed. By adding more layers to the device the charge transporting ability can be optimised. Figure 1.4 shows how OLED operation affects the frontier molecular orbitals.

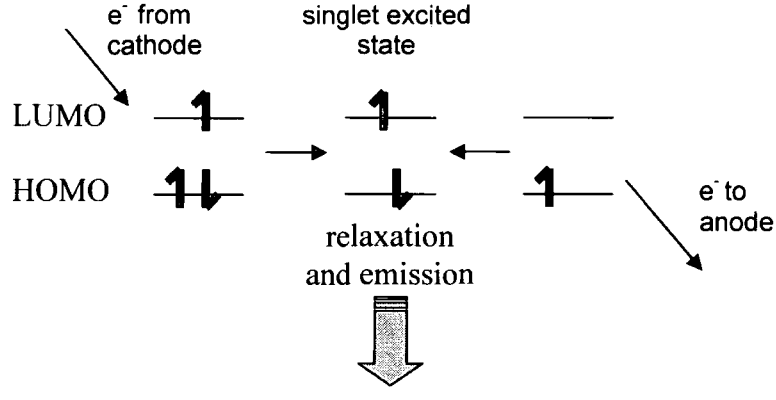

Figure 1.4 The role of the frontier orbitals in emissive materials

The charges are transported through the device by hopping from molecule to molecule and by delocalisation along polymer chains. When a cation radical and an anion radical are located on the same molecule triplet or singlet excited states are formed. Of these,

the singlets can emit light. A schematic energy level diagram for these single layer devices shows how an imbalance of charge injection occurs (Figure 1.5). There is a barrier to the injection of both holes (ΔE_h) and electrons (ΔE_e). If $\Delta E_h = \Delta E_e$ then there will be an equal abundance of positive and negative charge carriers in the device. This may still give a device for which $\gamma < 1$ as the carriers can still reach the opposing electrode. In the example shown in Figure 1.5, $\Delta E_h < \Delta E_e$ leads to a greater number of cation radicals.

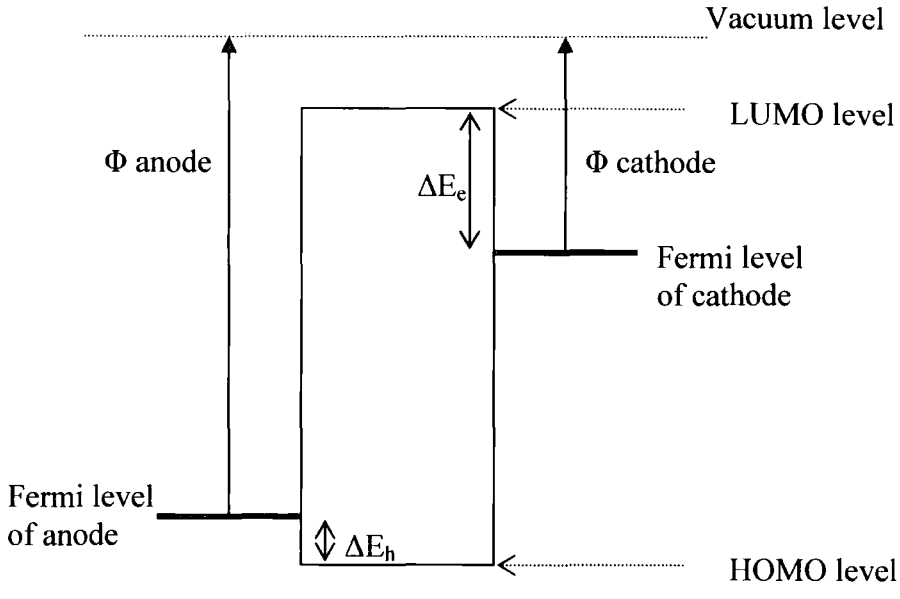

Figure 1.5 Energy levels for a single-layer device

To help address this imbalance, bilayer or multilayer devices can be constructed to balance and/or block transport of charge carriers. For example, the initial devices from Tang and VanSlyke required a diamine hole-transporting (HT) material with recombination and emission occurring in the predominantly electron-transporting Alq_3 layer.[6] In the case of MEH-PPV, an electron transporting (ET) layer is needed to promote the injection of electrons from the cathode and keep recombination in the hole-transporting MEH-PPV layer, away from the organic/cathode interface where emissions can be quenched. ET materials should possess LUMOs lying close to that of the work function of the cathode, whilst HT materials should possess HOMOs lying close to that of the anode. A schematic energy level diagram for a bilayer device is shown in Figure 1.6.

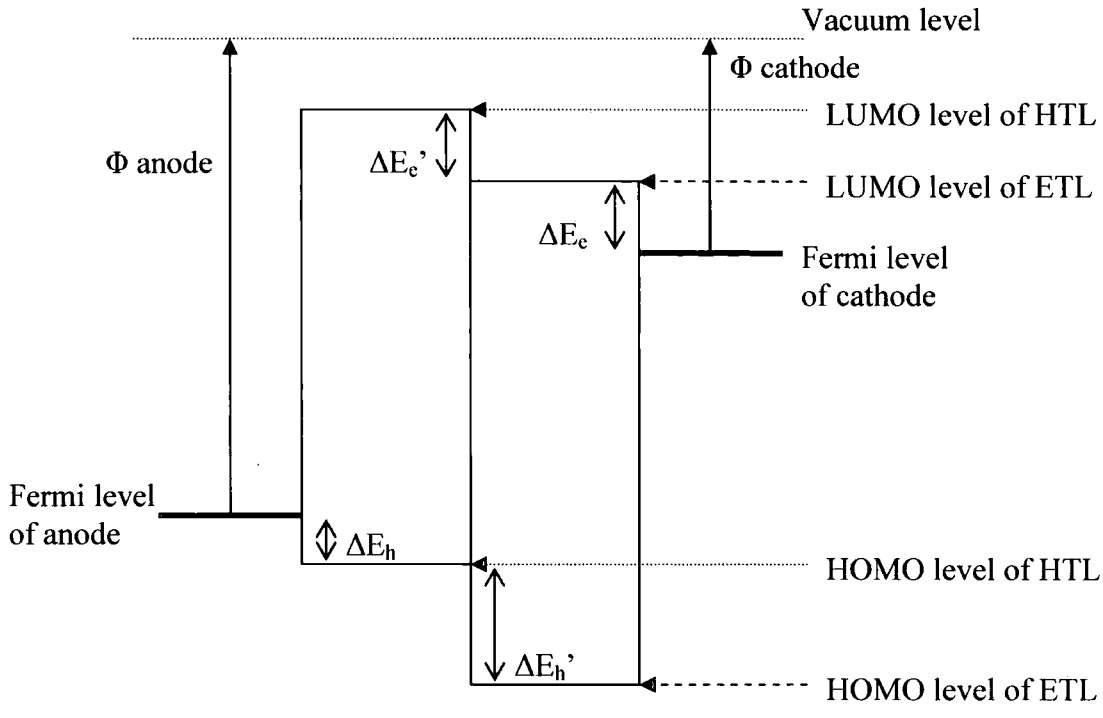

Figure 1.6 Energy levels for a bilayer device

Now ΔE_h is similar to ΔE_e which should allow for a more balanced injection of charges. Note also that $\Delta E_h' > \Delta E_e'$ indicating that the ET layer is also blocking the passage of holes from the HTL to the cathode, which promotes recombination in the HTL. Multilayer devices which contain an additional hole-transporting electron-blocking (HTEB) layer can also be fabricated. HTEB materials should possess HOMOs that closely match the work function of the ITO anode and have high-lying LUMO levels to inhibit electron movement. Increasing the number of layers which are incorporated into a device increases the difficulty and cost of fabrication. In the case of spin coating from solution and inkjet processes care must be taken to avoid dissolving previous layers when adding further materials and exciplex formation at interfaces can lead to red-shifted emission and poor device lifetimes.[21] Other methods employed to balance charge transport include (i) covalently attaching the desired charge transporting units onto the emitter itself which may require more complicated chemical synthesis and (ii) blending the emitter and transport material together and depositing this blend as a single layer which may suffer from phase separation on device operation.[15, 22, 23]

The surface of ITO can be rough on a microscopic scale leading to incomplete contact between the organic layer and the anode which can result in rapid device degradation. A thin hole-injecting buffer layer may be laid down before the HT layer to achieve a uniform surface which can improve device durability and result in lower driving voltages.[24] Common buffer layers include copper phthalocyanine (CuPc, **19**)[24] and poly(3,4-ethylenedioxythiophene) (PEDOT, **20**) doped with poly(styrene sulphonate) (PSS, **21**).[25] ITO is predominantly used as the anode due to its transparent properties. Its work function is 4.7 – 4.8 eV. There are several materials being considered for use as alternative anodes such as aluminium-doped zinc oxide.[26]

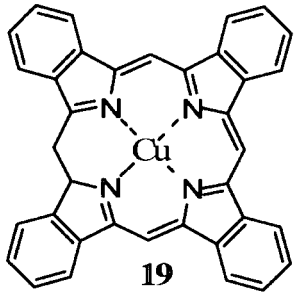

19

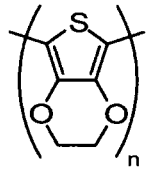

20

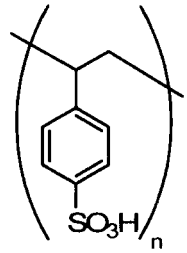

21

Work functions of a wide range of metals are shown in Table 1.1. However, several of these metals degrade in atmospheric conditions and so require another coating with a non-reactive metal or encapsulation. In a similar manner to ITO, a buffer layer of a material such as LiF can be inserted between the top organic layer and the cathode to aid electron injection.

Element	**Work Function /eV**[27]	**Element**	**Work Function /eV**[27]
Cesium	2.14	Lithium	2.90
Potassium	2.30	Magnesium	3.66
Barium	2.70	Silver	4.26
Sodium	2.75	Aluminium	4.28
Calcium	2.87		

Table 1.1 Workfunctions for selected metals

1.3 Molecular Design

In general, materials for use in OLED devices should possess the following attributes:

- Suitable HOMO and LUMO levels to match those of adjacent materials, i.e. the cathode, anode or another organic layer
- Ability to form pinhole-free films from a common deposition route (such as thermal evaporation, spin-coating or inkjet printing)
- Morphological and thermal stability

As already described, both small molecules and polymeric materials have enjoyed success in OLED displays. For small molecules to be useful in OLED devices, they need to form stable amorphous glasses. Understanding the relationship between structure and glass transition temperature (T_g) has aided the design of small molecules.[21] Starburst, rigid non-planar and spiro-type molecules can possess high T_gs that are in excess of the temperatures reached during device operation thus rendering these amorphous materials stable.

1.3.1 Hole Transporting Materials

Most HT materials are based on triarylamines.[18] As noted in Chapter 1.2.2, HT materials should possess a low electron affinity to prevent negative charge carriers reaching the anode whilst at the same time readily and reversibly forming cation radicals. *N,N'*-Bis(3-methylphenyl)-*N,N'*-diphenyl-[1,1'-biphenyl]-4,4'-diamine (TPD, **6**) has been widely used as an HT material in OLEDs despite its low T_g of 63 °C.[28] It was often found to crystallise, adversely affecting device lifetimes. Salbeck *et al.* used the spiro derivative spiro-TAD, **22**, in blue-emitting devices finding it possessed a higher T_g and thus imparted higher device stability over TPD.[29]

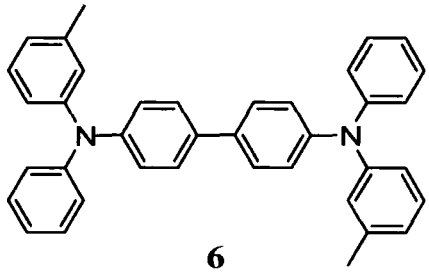

6

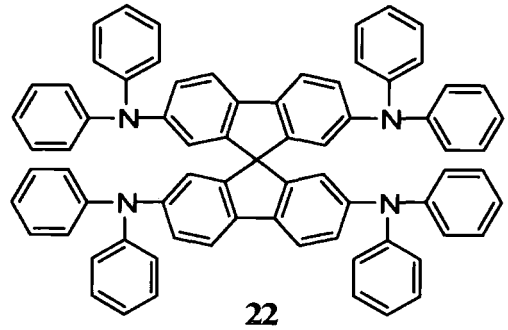

22

Other high T_g HT materials have been developed based on the 1,3,5-tris[*N*-(4-diphenylaminophenyl)phenylamino]benzene (*p*-DPA-TDAB, **23**),[30] 1,3,5-tris[4-(diphenylamino)phenyl]benzene (TDAPB, **24**)[31] and 4,4',4''-tri(*N*-carbazolyl)triphenylamine (TCTA, **25**)[32] families of compounds. These families provide much more thermal stability than TPD. More recently, higher T_g analogues of TPD have been developed including *N,N'*-di(1-naphthyl)-*N,N'*-diphenyl-[1,1'-biphenyl]-4,4'-diamine (α-NPD, **26**),[24] *N,N'*-di(9-phenanthryl)-*N,N'*-diphenyl-[1,1'-biphenyl]-4,4'-diamine (PPD, **27**),[33] 4,4'-di(*N*-carbazolyl)biphenyl (CBP, **28**),[34] 4-(iminodibenzyl)-4'-(iminostilbenyl)biphenyl (SSB, **29**),[34] *N,N'*-di(biphen-x-yl)-*N,N'*-diphenyl-[1,1'-biphenyl]-4,4'-diamine (*p/m/o*-BPD, **30**),[35] *N,N'*-bis(9,9-dimethylfluoren-2-yl)-*N,N'*-diphenyl-9,9-dimethylfluorene-2,7-diamine (PFFA, **31**), *N,N,N',N'*-tetrakis(9,9-dimethylfluoren-2-yl)-[1,1'-biphenyl]-4,4'-diamine (FFD, **32**)[36] and 4,4',4''-tris[9,9-dimethyl-2-fluorenyl(phenyl)amino]triphenylamine (TFATA, **33**).[36]

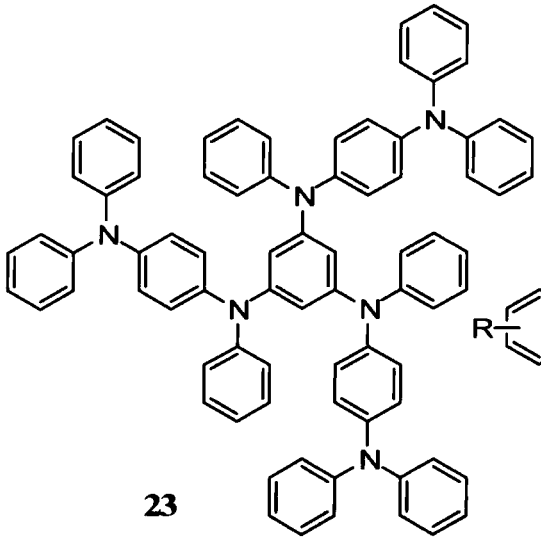

23

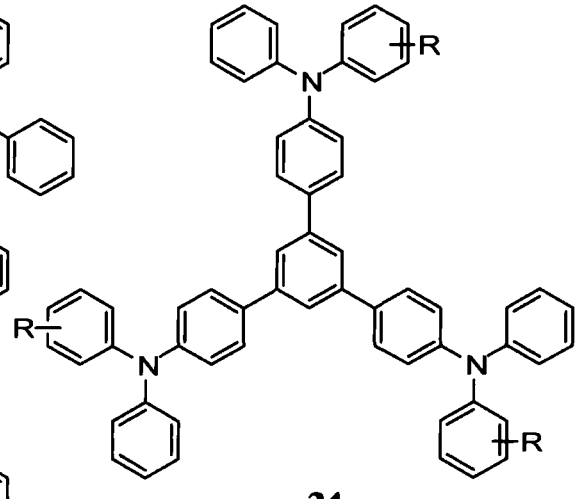

24

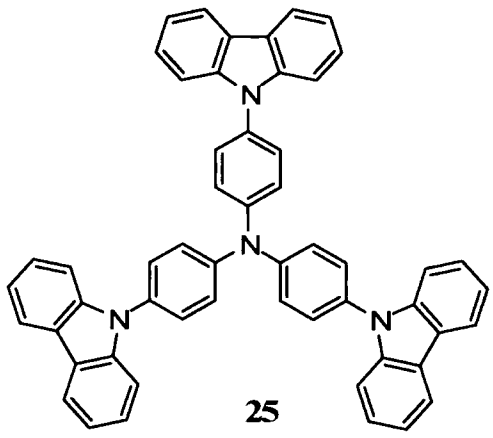

25

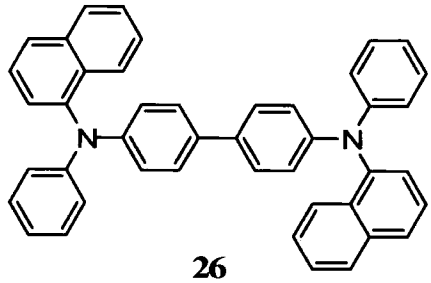

26

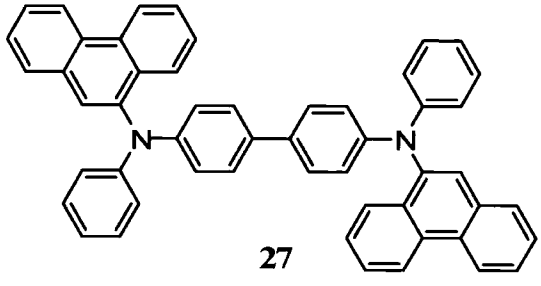

27

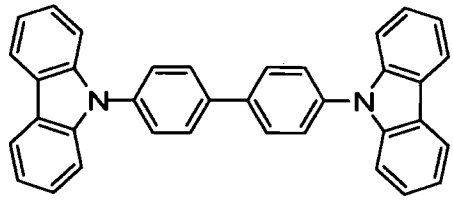

28

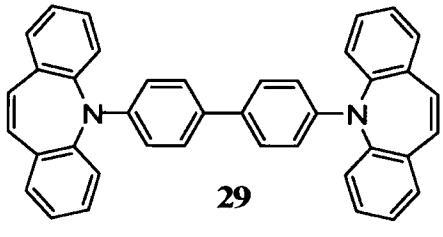

29

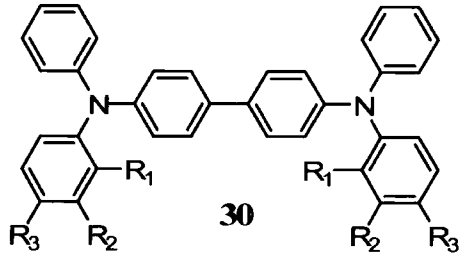

30

R_1	R_2	R_3	Name
H	H	Ph	*p*-BDP
H	Ph	H	*m*-BDP
Ph	H	H	*o*-BDP

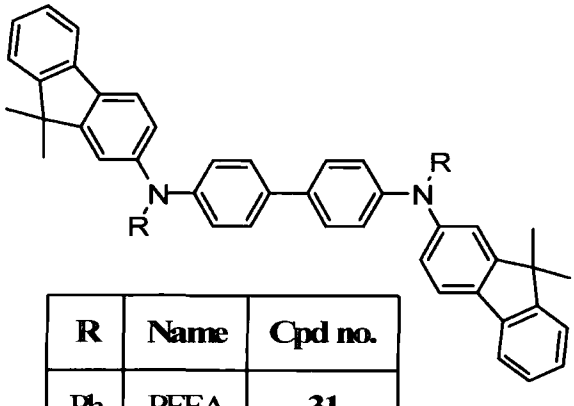

R	Name	Cpd no.
Ph	PFFA	31
Fl	FFD	32

Fl = 9,9-dimethylfluoren-2-yl

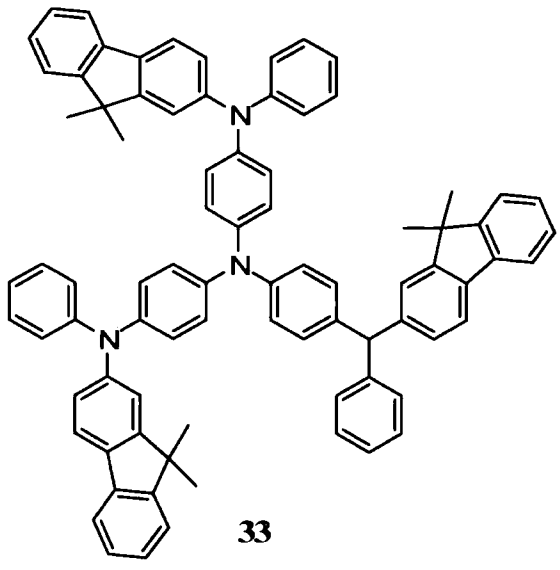

33

The T_gs of some of these materials are shown in Table 1.2.

Material	T_g /°C	Material	T_g /°C
α-NPD (**26**)	100	TPD (**6**)	60
SSB (**29**)	125	Spiro-TAD (**22**)	133
p-BPD (**30**)	102	*p*-DPA-TDAB (**23**)	108
PFFA (**31**)	135	TDAPB (**24**)	110
FFD (**32**)	165	TCTA (**25**)	151

Table 1.2 Selected glass transition temperatures from the above compounds

Several groups have fabricated devices incorporating two HT layers. Okumoto and Shirota constructed the device ITO/TFATA/FFD/Alq_3/Mg:Ag which turned on at 3.0 V emitting green light in agreement with the PL spectrum of Alq_3.[36] When the device's environment was raised to 170 °C, a luminance of over 200 cd m^{-2} was retained. After cooling back to room temperature the device continued to work. By comparison TPD-containing devices failed to work above 65 °C.

1.3.2 Electron Transporting Materials

Compared to hole transporters, ET materials should readily and reversibly form anion radicals to aid electron transport and possess a low-lying HOMO (high ionisation potential) to block the progress of holes from the emitting layer to the cathode. Once

again, high T_gs and the ability to form uniform pinhole-free holes are of the utmost importance. Most of the common polymeric emitters such as MEH-PPV, **14**, and polyfluorenes, **34**, inherently have a large barrier to electron injection, so the development of good ET materials was an industrial priority. There are several recent in-depth reviews of ET materials.[22, 37]

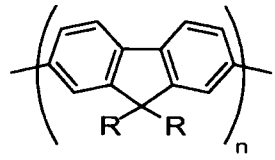

34

1.3.2.1 1,3,4-Oxadiazoles

1,3,4-Oxadiazole (OXD) derivatives, both molecular and polymeric, are the most widely studied class of ET materials for OLEDs. Most of the practical work presented in this thesis involves the OXD moiety. Since their discovery in 1961,[38] polymeric OXD materials have been known for their thermal and chemical stability as well as their high PL quantum yields, making them ideal for incorporation into OLED devices.[39-41] Syntheses of OXDs use cheap, readily available materials and generally proceed in high yields. The reactions all make use of an elimination-cyclisation reaction to form the heterocycle. As shown in Scheme 1.3, the simplest route to OXDs involves the reaction of a hydrazide with an acid chloride in basic solution such as pyridine. Hydrazides are readily obtained from acid chlorides, carboxylic acids and esters and are themselves widely commercially available. The resultant diacyl hydrazine derivative, **37**, is then converted to the oxadiazole by refluxing in a dehydrating solvent such as phosphorus oxychloride ($POCl_3$) or thionyl chloride ($SOCl_2$) or by heating *in vacuo*.[42] Symmetrical or polymeric OXD compounds can be made in this way by reacting diacid chlorides with hydrazine hydrate and then closing the heterocycles as above.

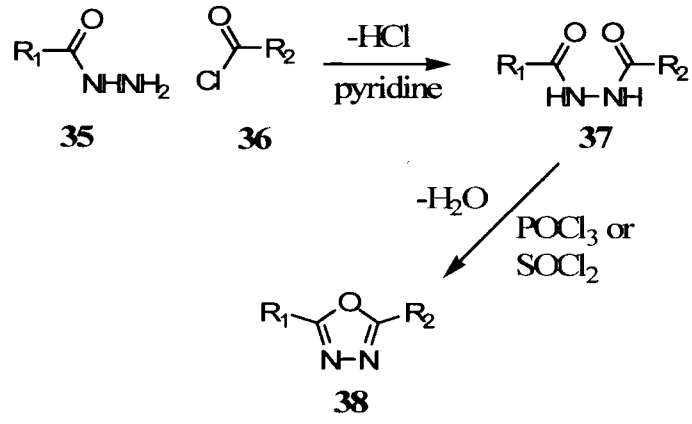

35 36 37 38

Scheme 1.3 Route to 1,3,4-oxadiazoles via a diacyl hydrazine

Similar methods to form polymeric OXD derivatives include the reaction of a bis(amidrazone) (e.g. compound **39**) with a diacid chloride followed by the elimination of ammonia upon heating in dichloroacetic acid. This can also be achieved in a one-pot reaction involving the reaction of the bis(amidrazone) with a dicarboxylic acid in the presence of methane sulphonic acid and phosphorous pentoxide as shown in Scheme 1.4.

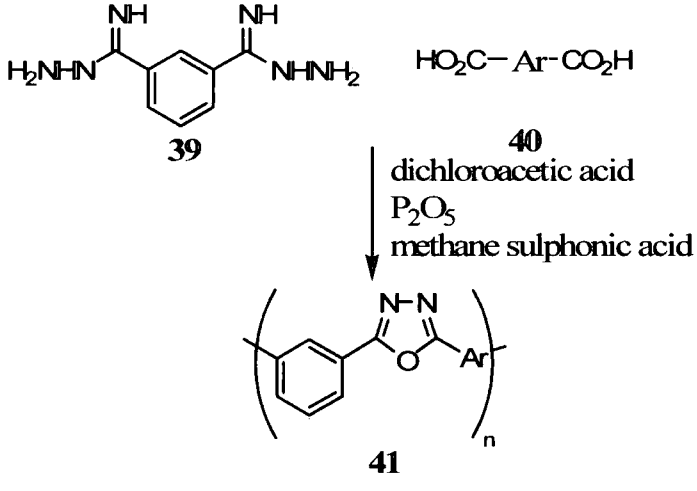

39 40 41

Scheme 1.4 Route to 1,3,4-oxadiazoles using bis(amidrazone)s

A second route using tetrazoles was developed by Huisgen in 1960. Tetrazoles are easily synthesised from cyano groups. The Huisgen route involves deprotonation of the tetrazole NH group and attack of the resulting anion on an acid chloride. Rearrangements with N_2^+ as a leaving group drives cyclisation to the oxadiazole as shown in Scheme 1.5.[43]

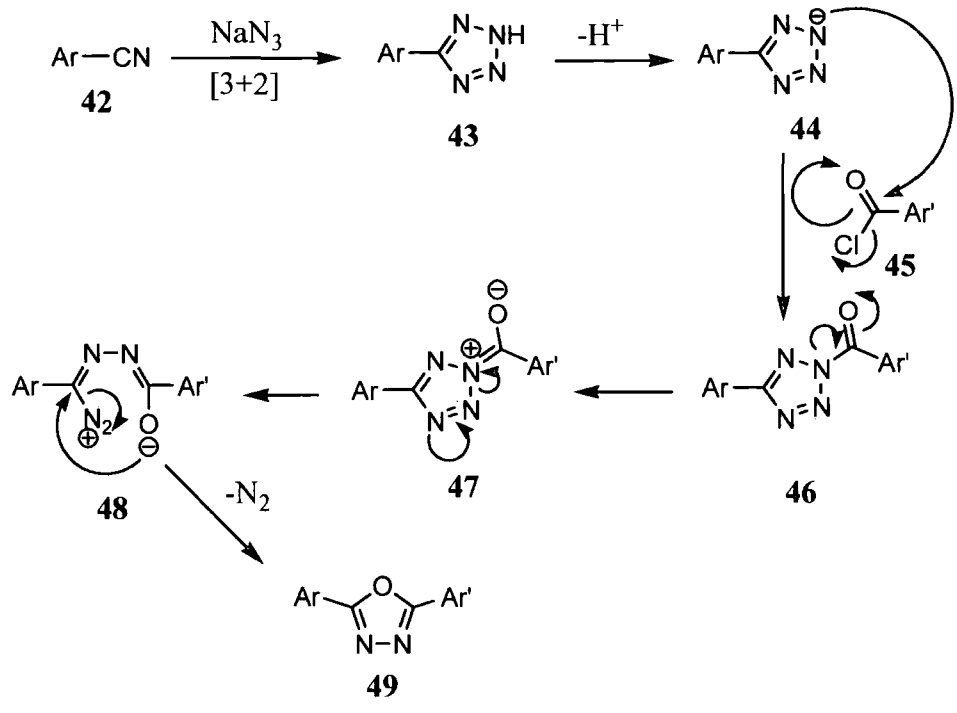

Scheme 1.5 Route to 1,3,4-oxadiazoles using tetrazoles

A route to OXDs with no substitution at the 5-position was described by Ainsworth in 1955.[44] This method involves the reflux of a hydrazide in ethyl orthoformate as shown in Scheme 1.6.

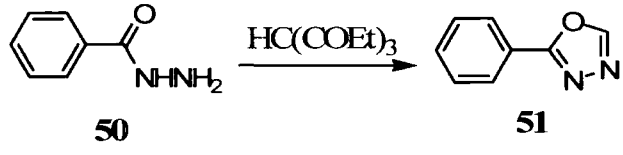

Scheme 1.6 Route to 1,3,4-oxadiazoles with no substitution at the 5-position

Alkyl groups can by placed at the 5-position by using the appropriate orthoformate and a wide range of aryl hydrazides can be used.

The first OXD material studied in relation to OLEDs was 2-(4-biphenyl)-5-(*tert*-butylphenyl)-1,3,4-oxadiazole (PBD, **5**) in 1989.[7] As previously mentioned, the bilayer device ITO/NSD/PBD/Mg:Ag was 10^4 times more efficient than the single layer device ITO/NSD/Mg:Ag. However, PBD – like TAD – suffers from a low (~60 °C) T_g and it crystallises over time in devices, shortening their lifetimes.[28] To overcome this problem Cao *et al.* blended PBD directly into a PPV derivative, poly[2-methoxy-5-

(3',7'-dimethyloctyloxy)-*p*-phenylenevinylene], **52**, leading to EQEs of 2 – 4%.[45] Similarly a blend of PBD and poly(methylmethacrylate) (PMMA, **53**) was spin-coated as an ET layer above PPV in the device ITO/PPV/PMMA:PBD/Ca giving an efficiency two orders of magnitude greater than that of the single layer PPV device.

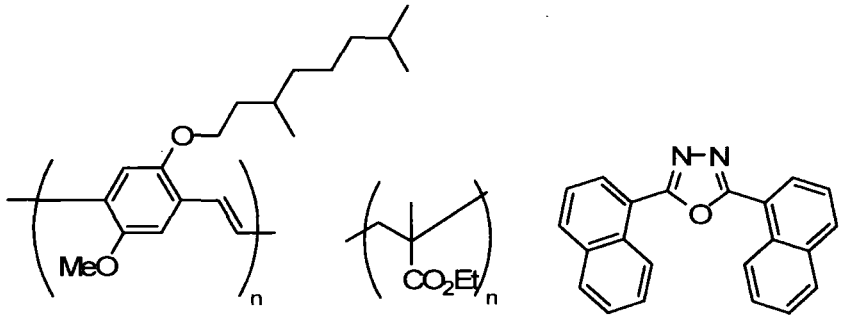

52 **53** **54**

2,5-Bis(naphthyl)-1,3,4-oxadiazole (BND, **54**) with similar properties to PBD has also been used in devices, again blended into PMMA.[46] It was noted that both PBD and BND do not possess a high enough ionisation potential to act as hole-blocking materials.

The oxadiazole dimer 3-bis[2-(4-*tert*-butylphenyl)-1,3,4-oxadiazol-5-yl]benzene (OXD-7, **61**) was synthesised as part of a range of compounds (**55** – **63**) by Tsutsui *et al.*[47] The complete list of molecules and their film forming abilities is shown below. When OXD-7 was incorporated into devices it formed homogeneous glassy films and no crystallisation was detected after thirty days. A device comprising ITO/TPD/OXD-8/OXD-7/Mg:Ag (where OXD-8 was used as the emissive layer) displayed a luminescence of 100 cd m^{-2} with no device degradation when operated at 77 K.

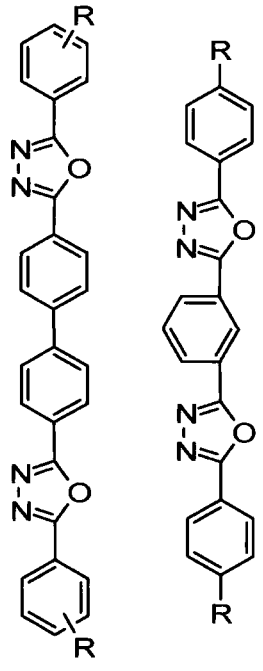

cpd	name	type	R	films
55	OXD-1	A	4-^{t}Bu	excellent
56	OXD-2	A	4-Cy	good
57	OXD-3	A	4-Ph	good
58	OXD-4	A	4-Et	good
59	OXD-5	A	2-Et	fair
60	OXD-6	A	4-NMe_2	excellent
61	OXD-7	B	4-^{t}Bu	excellent
62	OXD-8	B	4-NMe_2	excellent
63	OXD-9	B	4-Ph	good

Further derivatives of PBD were synthesised by Wang *et al.* in our group.[48-50] A series of bis[2-(4-*tert*-butylphenyl)-1,3,4-oxadiazol-5-yl] materials were used in ITO/MEH-PPV/OXD/Al bilayer devices where OXD represents the new derivatives **64** – **71**.

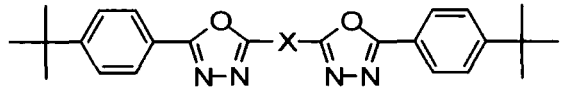

cpd	X	cpd	X
64	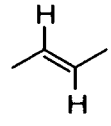	**68**	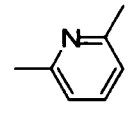
65	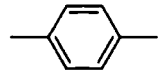	**69**	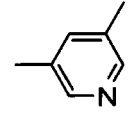
66	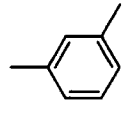	**70**	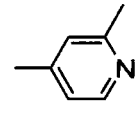
67	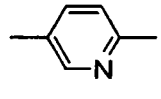	**71**	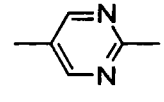

A comparison of OXD-7 with the pyridyl analogue 2,5-bis[2-(4-*tert*-butylphenyl)-1,3,4-oxadiazol-5-yl]pyridine (PDPyDP, **67**)[48] established that the latter produces devices twice as efficient as those using OXD-7 as the ET layer when using rubrene-doped MEH-PPV as the emitter. PDPyDP is more electron deficient due to the replacement of the central phenyl ring in OXD-7 by a pyridine ring which further decreases the LUMO level and brings it closer to the work function of the cathode. Crystal structures of PDPyDP showed that the material was partially crystalline which could afford it higher electron mobility than the other derivatives. Although the PDPyDP device was more efficient, it was more unstable than the OXD-7 device, with the sample current and efficiencies dropping dramatically after storage in low vacuum. The reason for this decrease was found to be the growth of dark spots on the device that do not emit light, thus lowering the current that can pass through the device. These spots failed to appear on storage of a device without the cathode added suggesting an interaction was occurring at the PDPyDP/Al interface. Aziz *et al.* observed dark spots in Alq_3 devices and reported that moisture caused the Alq_3 films to crystallise and delaminate from the cathode.[51] Devices fabricated incorporating a layer of Alq_3 between the PDPyDP and the Al electrode showed far fewer dark spots upon storage of the device. The device still degraded quickly on application of a constant current giving a half life of *ca.* 4 hours. When a buffer layer of CuPc was inserted between the ITO and the MEH-PPV(Ru) the devices showed a greatly improved lifetime. The OXD-7 isomer PDPDP, **65**, and the vinyl analogue PDVDP, **64**, were also studied. In bilayer devices comprising ITO/MEH-PPV/PDxDP/Al PDVDP doubled the efficiency compared to a single-layer device, PDPDP increased it six times and PDPyDP increased it by a factor of thirty. The extra electron-deficient nature of the pyridyl ring over that of the phenyl and vinylene units helps to explain the higher efficiencies. The results of a study using the other isomers and the 2,5-pyrimidine derivative, **71**, are shown in Table 1.3. The efficiencies of the individual devices could be improved by optimising the layer thicknesses. For example, a device comprising ITO/MEH-PPV(Ru) (90 nm)/**67** (55 nm)/Al showed an EQE of 0.7% .

cpd	EQE at 40 mA cm^{-2} /%	cpd	EQE at 40 mA cm^{-2} /%
65	0.11	**69**	0.04
66	0.06	**70**	0.05
67	0.14	**71**	0.12
68	0.14		

Table 1.3 Efficiencies of the OXD compounds 65 – 71

In all of the above devices the EL spectrum was that of MEH-PPV with no evidence of any emission from the oxadiazole derivatives indicating that recombination was confined to the MEH-PPV layer.

Recently, new OXD compounds were synthesised by Ichikawa *et al.*[52] Compounds **72** and **73** were found to possess T_gs of 106 and 114 °C respectively.

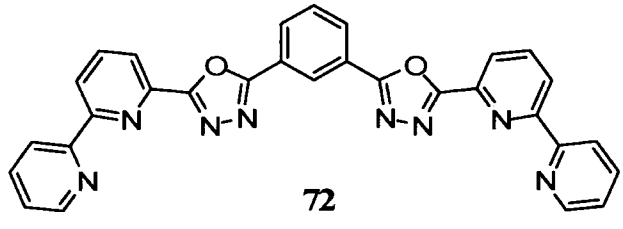

72

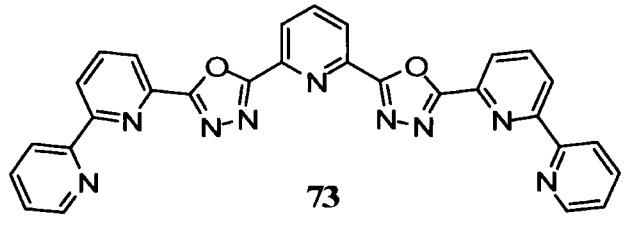

73

Their LUMO levels of 2.92 and 2.57 eV were low enough to easily accept electrons from the cathode and their HOMOs of 6.56 and 6.25 eV were low enough to suppress the passage of holes from the emissive layer. Devices comprising ITO/NPB/Alq_3/**72** or **73**/Mg:Ag were fabricated along with a reference device without the ET layer. Turn-on voltages (voltage required to reach 10 cd m^{-2}) decreased from 5.6 V with the reference device to 2.9 V for **72** and 2.7 V for **73**. A device containing OXD-7 turned on at 4.6 V. Incorporating an electron injecting buffer layer of LiF and an Al cathode with **72** dropped the turn-on voltage to 2.6 V and a luminance of 1,000 cd m^{-2} was obtained with a driving voltage of 3.8 V (5.5 V with Mg:Ag cathode). The authors speculated

that the use of an efficient hole injection layer should improve brightness and efficiencies.

Highly branched and starburst OXD compounds have been investigated for ET applications. The branched structure enhances their solubility and prevents intermolecular stacking. Several starburst molecules (**74** – **76**) using a central template have been reported.

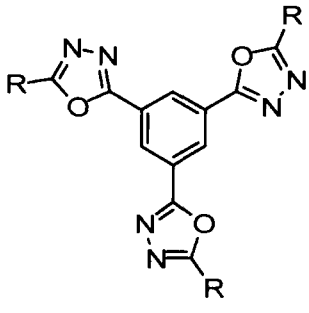

cpd	R
74	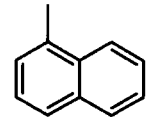
75	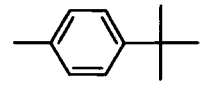
76	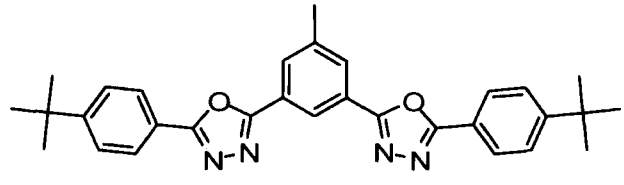

Compound **75** was incorporated into a device comprising ITO/PPV/**75**/Mg:Ag and gave an increase in EQE of two orders of magnitude over single layer devices.[53] This material was also used by Shirota *et al.* as an ET layer in devices with the emissive bis-{4-[bis(4-methylphenyl)amino]phenyl}thiophenes (BMA-*n*T, **77**).[54] Increasing the number of thiophene units shifted the colour of emission from light blue through to orange. Devices incorporating an ET layer of **75** showed improved efficiencies and brightnesses.

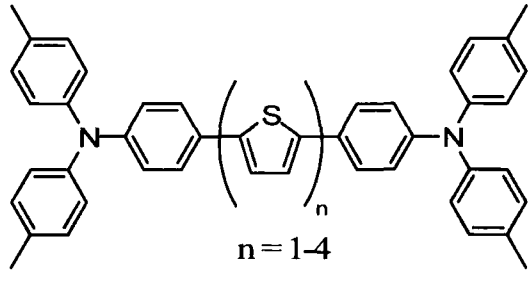

n = 1-4

77

The first generation dendrimer, **76**, possesses a very high T_g of 222 °C and bilayer devices with PPV again showed an EQE increase of two orders of magnitude.[55]

Tetraphenylmethane-based oxadiazole systems such as compounds **78** – **80**[56] share similar optical and electrochemical properties to PBD as conjugation is broken at the central carbon. These compounds are synthesised by reacting the relevant acid chloride with tetraphenyltetrazole in the Huisgen reaction.[43] The thermal properties are greatly enhanced due to the extra complexity of the molecules with T_gs ranging from 97 to 175 °C. Compound **80** was used as an electron-transport-hole-blocking (ETHB) layer in the device ITO/NPB/Alq_3/**80**/Mg:Ag giving rise to efficiencies between 0.75 and 1% at *ca.* 8 V. Yeh *et al.* also synthesised several bipolar compounds which will be discussed in Chapter 1.5.

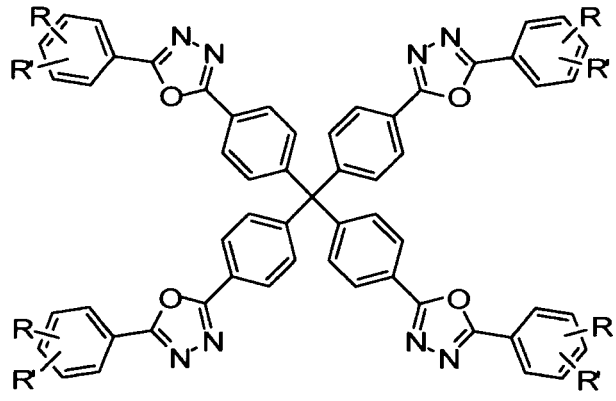

cpd	R	R'
78	3-^{t}Bu	5-^{t}Bu
79	3-OMe	4-OMe
80	3-CF_3	H

1.3.2.2 Blends

Our group has recently studied new OXD-containing fluorene systems for use as electron transporters in blended systems. Ahn *et al.* reported the use of 2,7-bis[2-(4-*tert*-butylphenyl)-1,3,4-oxadiazol-5-yl]-9,9-dihexylfluorene (DFD, **81**).[57] Blends with MEH-PPV incorporating between 20 and 95% of DFD were tested in ITO/MEH-PPV:**81**/Al devices. It was found that up to 70% loading with DFD resulted in higher light output, but above this threshold light output decreased. EQEs increased with increased concentrations of DFD with the 95% blend showing an improvement of two orders of magnitude over a pure MEH-PPV device. Phase separation in the films which can be detrimental to device operation was not seen in the blends by AFM studies. DFD itself is a blue emitter, but in the PL and EL spectra of the blends no emission due

to DFD was observed. The insertion of a PEDOT:PSS buffer layer between the ITO and blend improved efficiencies by a factor of three, but thermal annealing led to a decrease in efficiency, perhaps due to accelerated phase separation and crystallisation of DFD.

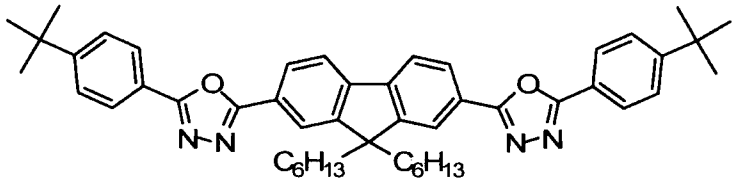

81

Further studies involved DFD analogues **82** – **88**.[58, 59]

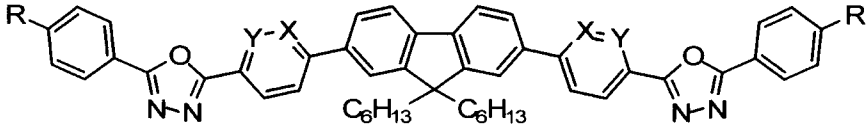

cpd	X	Y	R
82	CH	CH	$OC_{12}H_{25}$
83	CH	CH	^tBu
84	N	CH	$OC_{12}H_{25}$
85	CH	N	OCH_3

cpd	X'	Y'	R'
86	CH	CH	$OC_{12}H_{25}$
87	N	CH	$OC_{12}H_{25}$
88	CH	N	OCH_3

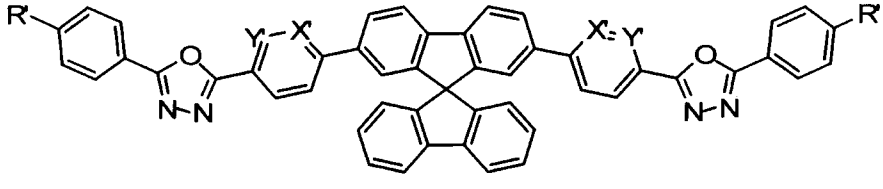

Initial studies compared blends of DFD, **84** and **86** comprising 70% of the ET material.[58] Single layer devices comprising ITO/blend/Al showed far greater light output and higher efficiencies compared to the pure MEH-PPV devices. Once again, the incorporation of a PEDOT:PSS layer increased efficiencies by a factor of three. There was no evidence of emission from the blue-emitting ET materials (**82** and **86** have λ_{max} values of 430 and 433 nm, respectively) and no shift in EL emission was

detected on changing the blend composition. However, whilst blends with DFD gave an EL spectrum identical to that of MEH-PPV, blends with **82** and **86** showed a significant red-shift to 590 nm compared to 570 nm for the pure MEH-PPV device. Both **82** and **86** feature long decyloxy chains at the periphery. A tertiary butyl analogue of **82** (i.e. **83**) was synthesised to investigate this effect. Blends of **83** gave an emission identical to that of pure MEH-PPV indicating that the long alkoxy chains of **82** and **86** were interacting with the MEH-PPV. Previously Schwartz and co-workers had shown that MEH-PPV emission is affected by the conformation of the chains.[60] In the study the PL spectrum of MEH-PPV was altered by varying the polarity of the solvent in which it was dissolved. Non-polar solvents gave rise to extended chains and a red-shifted emission.

Our group next introduced pyridine moieties into **82** and **86** to yield **84** and **87**.[59] The increased electron deficiency of the pyridine system compared to the phenyl ring was expected to further reduce the LUMO of these materials to more closely match the energy level of the cathode. Density functional theory (DFT) calculations showed that **84** and **87** were stronger electron accepters than their isomers **85** and **88** with the pyridine nitrogen adjacent to the oxadiazole ring. The calculations also showed that the pyridine containing species had LUMOs ~0.2 – 0.3 eV below their phenyl analogues. Device tests (again using an ITO/blend/Al configuration and 70% ET material in the blends) showed that the new pyridine analogues gave up to ten times the light output of the phenyl derivatives. Compound **87** showed an EQE of 0.25% compared with *ca.* 0.05% for **82** and **86** and 0.001% for the reference MEH-PPV device. Use of a PEDOT:PSS layer and calcium cathode improved the EQE of a 70% blend using **87** to 0.6%. Once again, ET materials containing long alkoxy chains showed a 20 nm red shift in emission compared to the reference MEH-PPV device. Phase separation could be controlled by spinning films from a single solvent, whilst mixed solvents gave rise to segregation. In these phase segregated devices, a small amount of emission from the ET material became apparent in the EL spectrum.

1.4 Emitters

For full commercialisation OLEDs must display the three primary colours of red, green and blue. The term "primary" comes from the response of the human retina to light rather than a physical concept. Cone photoreceptor cells are most responsive to light of yellow-green (long wavelength), blue-green (medium wavelength) and blue-violet (short wavelength). The difference in signals allows the brain to perceive a wide gamut of colours. For example, if orange light of wavelength 590 nm were to enter the eye it would stimulate both the long and medium wavelength receptors, but not equally. This difference in response can be interpreted by the brain. In 1931 the International Commission on Illumination (CIE) defined colour space by a mathematically derived diagram as shown in Figure 1.7.

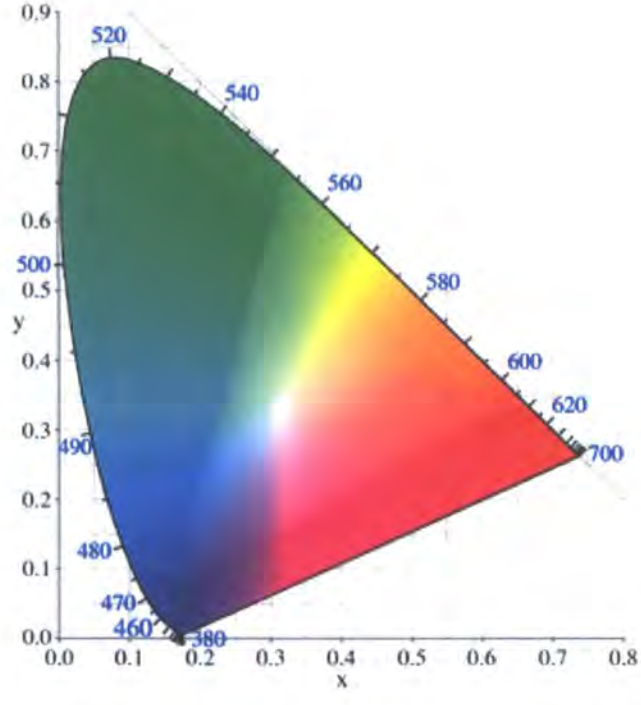

Figure 1.7 The 1931 CIE diagram

If X(λ), Y(λ) and Z(λ) are the responsivities of the long, medium and short wavelength receptors respectively, then the coordinates on the CIE diagram can be calculated from equations (5) and (6):

$$\bar{x} = \frac{x}{x+y+z} \qquad (5)$$

$$\bar{y} = \frac{y}{x+y+z} \qquad (6)$$

Where $\bar{x}$ and $\bar{y}$ are the coordinates for the CIE diagram and x, y and z are given by equations (7), (8) and (9) where $\phi(\lambda)$ is the spectral power distribution:

$$x = \int \phi(\lambda) X(\lambda) d\lambda \qquad (7)$$

$$y = \int \phi(\lambda) Y(\lambda) d\lambda \qquad (8)$$

$$z = \int \phi(\lambda) Z(\lambda) d\lambda \qquad (9)$$

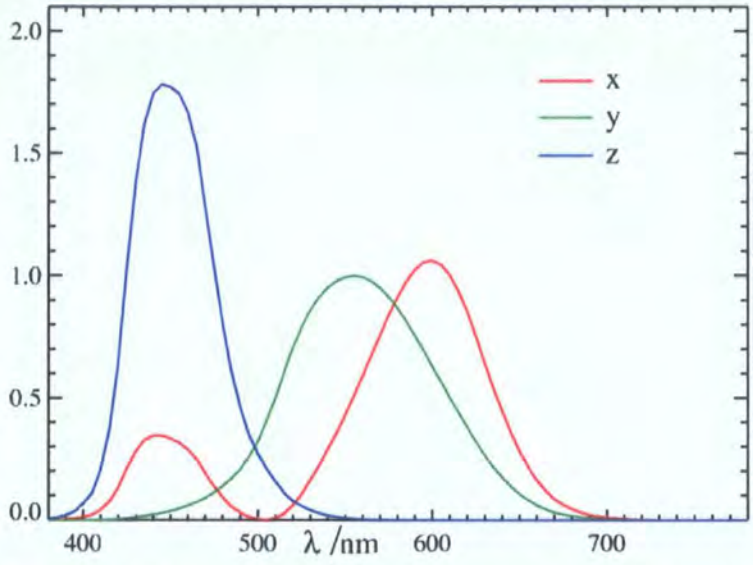

Figure 1.8 Relative sensitivities of the human eye to the primary colours

Different standards have slightly different definitions of colour. For example, the National Television Standards Committee (NTSC), whose television standards have been adopted in much of the Americas and Asia, have defined the colours as shown in Table 1.4.[18]

	Red	Green	Blue
wavelength /nm	625	520	460
x coordinate	0.67	0.21	0.14
y coordinate	0.33	0.71	0.08

Table 1.4 NTSC definitions of the primary colours

Much research has focused on getting molecules to emit as close to these values as possible. The use of colour dyes in front of white-light emitters has been explored.[61, 62] Common dyes include 1,1,4,4-tetraphenyl-1,3-butadiene (TPB, **89**) (blue), coumarin 6, **90**, (green) and DCM-1, **91**, (orange).

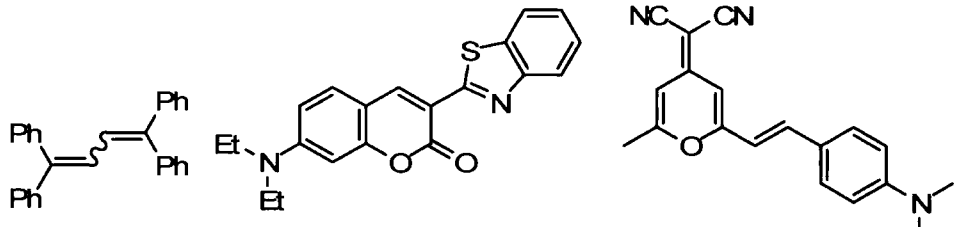

89 **90** **91**

1.4.1 Towards Blue Emission – Poly(*p*-Phenylenes)

In order to adjust colours, the band gap of the emitter must be finely tuned to deliver precise colours, so once again most interest is in the frontier molecular orbitals. Increasing conjugation leads to a lower band gap and red-shifted emission, while conversely short conjugation lengths favour large band gaps with blue-shifted emission. Stable red and green emitters are well known, but blue emitters have historically provided a challenge.[15] Blue-emitting inorganic semi-conductors were unknown until the discovery of GaN based diodes by Nakamura *et al.* in 1993.[63] The design of fluorescent blue-emitting compounds needs to incorporate interrupted conjugation to maintain a large band gap.

In 1992, Leising *et al.* reported blue electroluminescence from poly(*p*-phenylene) (PPP, **97**) – a polymer that was calculated to have a band gap of 2.7 eV.[64] Like PPV, PPP is very insoluble so for this initial study it was spin coated onto a device in a pre-polymer form and then converting to **97** by thermally annealing the device at 340 °C under vacuum (Scheme 1.7). The ITO/PPP/Al device produced similar efficiencies to PPV of *ca.* 0.01 – 0.05%.

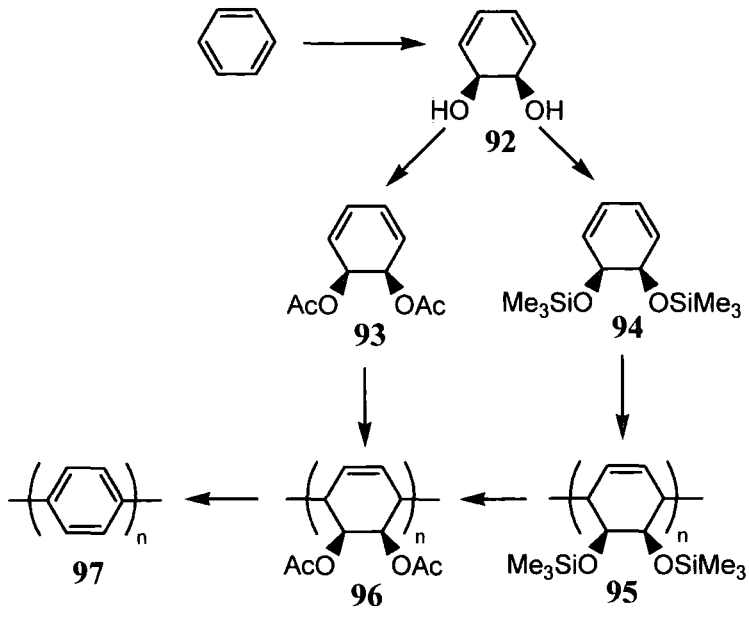

Scheme 1.7 Synthetic routes to PPP

Once again, alkoxy chains were added to improve solubility. An example of the synthetic route to these compounds is shown in Scheme 1.8.

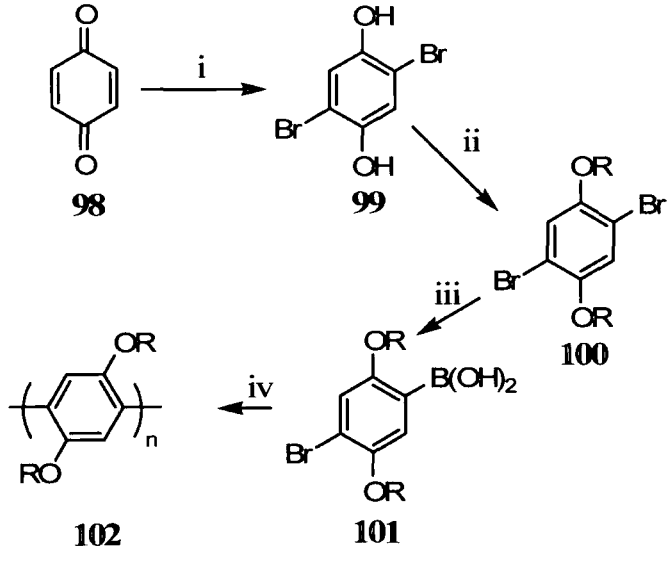

Figure 1.8 Synthetic route to a soluble alkoxy PPP derivative; i, HBr, Br_2; ii, KOH, RBr; iii, -78 °C, *n*BuLi, TIPB; $Pd(PPh_3)_4$, K_2CO_3, reflux

Poly(2-decyloxy-*p*-phenylene) (DO-PPP, **103**) provides a good example of this type of material, producing EQEs of up to 3% in double layer ITO/PVK/**103**/Ca devices where PVK is poly(vinylcarbazole).[65]

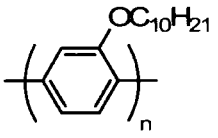

103

The alkoxy side chains of **103** also act to introduce more twisting between adjacent phenyl rings which reduces conjugation, blue shifting the emission and reducing the fluorescence quantum yield.[15] In order to avoid this problem, Scherf and Müllen developed ladder-type poly(*p*-phenylene)s (LPPPs) where the phenyl rings are held in the same plane by methylene bridges.[66] First the polymer backbone is formed by a Suzuki coupling reaction[67] followed by a reduction of **106** to **107** and finally a Friedel–Crafts ring-closure. The steric protection afforded to the alcohol is very important. If the R groups are too bulky then the final cyclisation is inefficient and the ladder structure is incomplete. If the R groups are too small then the cyclisation will be uncontrolled and competing intermolecular reactions will create insoluble networks.[68] A typical reaction pathway to ladder system **108** is shown in Scheme 1.9.

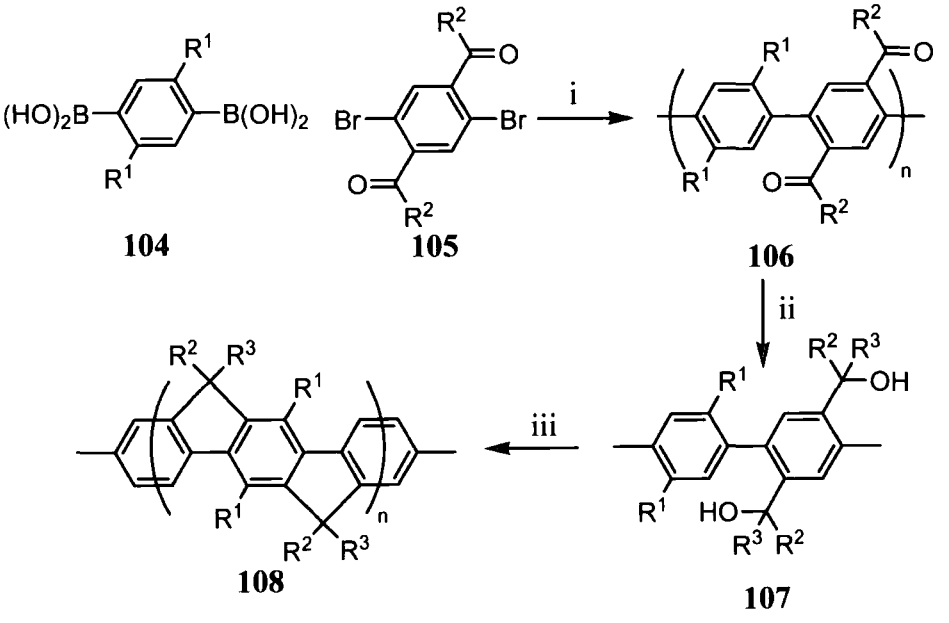

Scheme 1.9 Synthetic route to ladder systems; i, $Pd(PPh_3)_4$, K_2CO_3; ii, R^3Li; iii, BF_3

For **108** with R^1 = *n*-hexyl, R^2 = methyl and R^3 = *p*-decylphenyl (Me-LPPP) a device comprising ITO/Me-LPPP/Ca emitted blue-green light with an EQE of 4%.[69]

More recent ladder-type and indenofluorene type polymers have featured 9,9-diaryl units R^2 and R^3.[70-73]

1.4.2 Fluorenes

Research eventually afforded poly(9,9-dialkylfluorene), **34**, which has a structure intermediate between PPP and LPPPs. The fluorene moiety is well known for its thermal and chemical stability, high quantum yields and easy chemical modification – especially at the 9-position. In its polymeric form the twists between adjacent biphenyl groups give reduced conjugation and blue-emission. Initial syntheses of **34** were via ferric coupling of fluorene monomers.[74, 75] It was found that increasing the length of the alkyl chains at the 9-position decreased the T_g. Further syntheses involved Suzuki cross-couplings and Yamamoto-type couplings[76] which yielded polymers with M_n of several 10,000 and 100,000 respectively.[77]

Early polyfluorenes (PFs) synthesised by Pei and Yang introduced 2-(2-methoxyethoxy)ethane chains at the 9-position to give compound **112** (Scheme 1.10).[78]

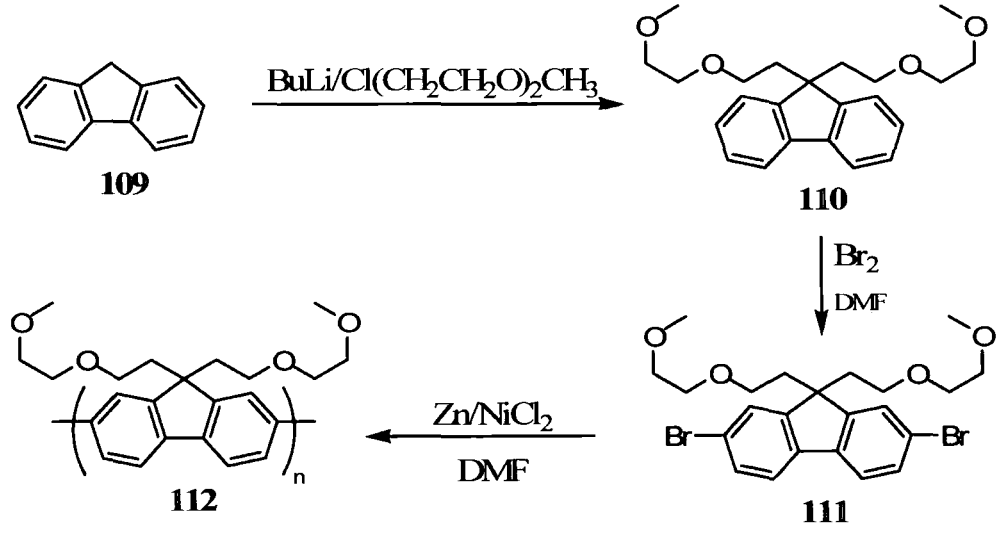

Scheme 1.10 Synthetic route to polyfluorene containing 2-(2-methoxyethoxy)ethane chains

An ITO/**112**/Ca device had a 0.3% EQE. When lithium triflate was added device performance improved to 4% EQE and 1,000 cd m^{-2} at 3.5V, but the sky blue luminescence changed to white emission during device operation.

Klärner *et al.* developed a novel method to avoid the complications associated with fabricating multilayer devices by end-capping with a styryl group to give compound **113**.[79]

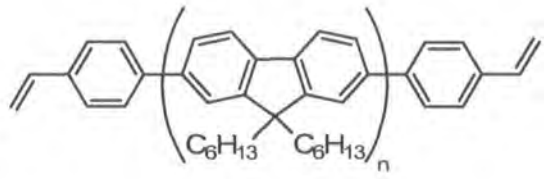

113

As synthesised, polymer **113** had similar solubility to other polyfluorenes. However, when spin-coated onto a device, thermal annealing caused the styryl units to autopolymerise leading to an insoluble network on which further layers could be deposited from solution without disrupting the PF layer.

The change in emission colour from fluorene-based materials became a common phenomenon. Most polymers initially showed deep blue emission, but after device operation or thermal annealing this changed to a blue-green emission which originated from the growth of a large green band in the PL and EL spectra. An example using **114** is shown in Figure 1.9.

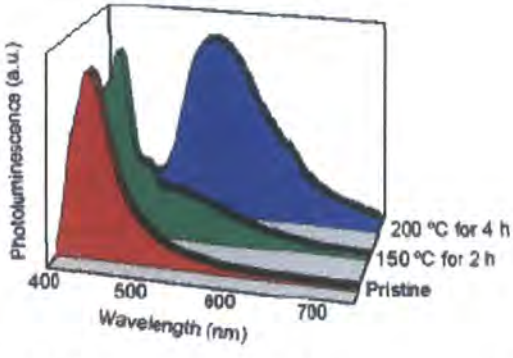

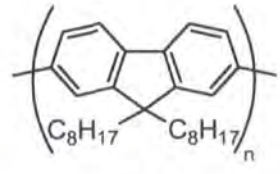

114

Figure 1.9 PL spectra of poly(9,9-alkylfluorene)s over time - reproduced from reference 95

Initially the green band was ascribed to aggregation and excimer formation caused by π-stacking and interactions between the alkyl chains[80, 81] and many efforts were made to reduce these interactions by introducing bulky substituents at the 9-position such as

the spiro-unit (**115**),[82] dendrons (**116**)[83] and incorporating 9,10-anthracyl units into the main chain (**117**).[84]

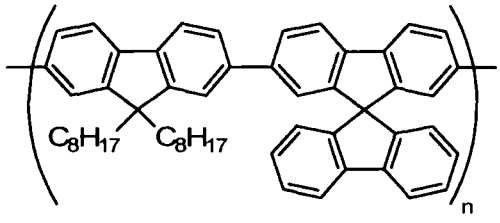

115

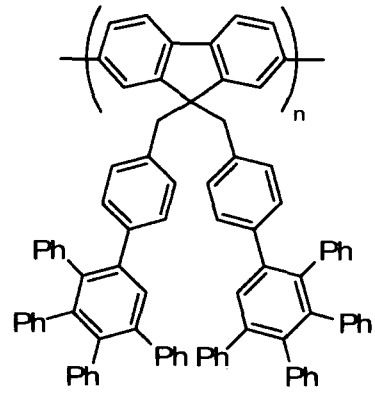

116

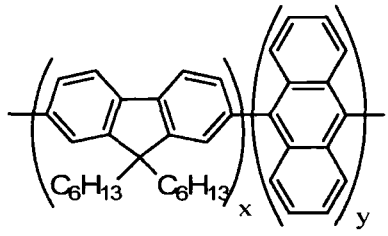

117

Recently, studies by several groups revealed that these green bands are due to keto-defects in the polymer chains.[77] List and Scherf introduced small amounts of 9-fluorenone, **118**, into the polymerisation of 9,9-dialkylfluorenes to produce well defined copolymers which display the green band.[85] These defect sites appear to arise from oxidation of monoalkylated fluorene units in the polymer. A mechanism for the proposed formation of these defects during reductive polymerisations (such as Yamamoto nickel-catalysed reactions) is shown in Scheme 1.11.[86]

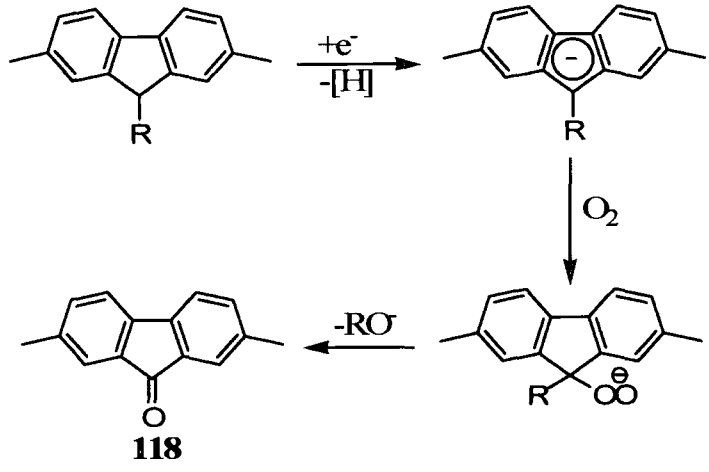

Scheme 1.11 Proposed mechanism for the generation of keto defects

Fluorene defects can also appear during photo- or electrooxidation of the device. This is seen as the gradual colour shift of devices from blue to green over time. Heeger's group showed that calcium was responsible for catalysing this oxidation and inserting a buffer layer such as CF_3OXD (**80**) between the polyfluorene layer and calcium cathode impeded this reaction.[87] With as little as 0.1 mol % of fluorenone in the polymer leading to a broad green emission in the EL spectrum,[77] it is clear that the starting monomers must be exceptionally pure.

Several groups have taken steps to remove the problem by using alternative groups at the 9-position in place of alkyl chains. The aforementioned spiro linkage ensures that there are no protons at the 9-position and also benefits from a second fluorene moiety in the unit. Spirobifluorene units such as compound **121** are synthesised from 2-halogenated biphenyls (**119**) via the carbinol (**120**) as shown in Scheme 1.12.[88]

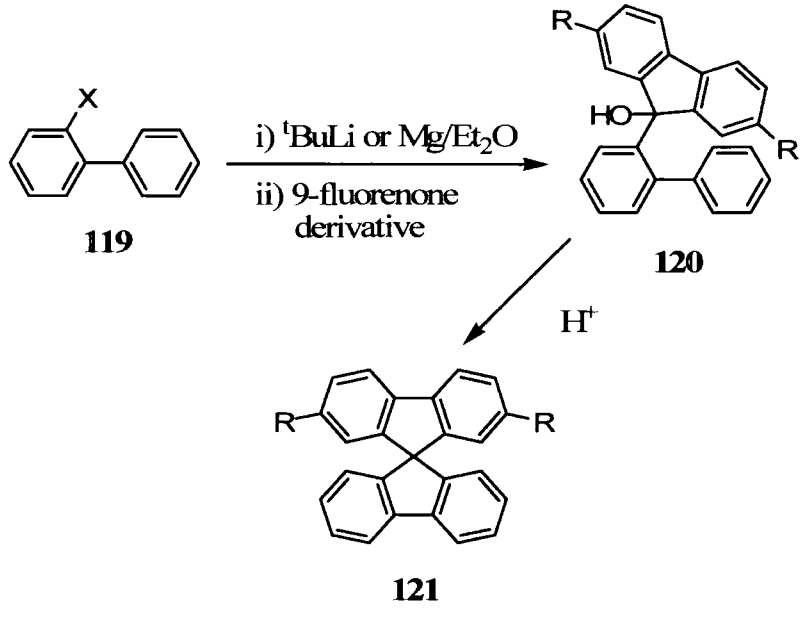

119 **120** **121**

Scheme 1.12 Synthetic route to 9,9-spirobifluorene derivatives

Marsitzky *et al.* developed amorphous networks based around 9,9'-spirobifluorene, **121**.[89] Brominating compound **121** with excess bromine and catalytic $FeCl_3$ gave 2,2',7,7'-tetrabromo-9,9'-spirobifluorene, **122**. This was then polymerised in the presence of 2,7-dibromo-9,9-dihexylfluorene, **123**, and 4-bromostyrene, **124**, in a Yamamoto coupling. The inclusion of 15 mol % end-capper, **124**, is important to prevent the formation of insoluble networks. The resultant polymer, shown in Scheme

1.13, retains the 4-phenylethenyl groups of **113** and once again, after thermal treatment, the polymer becomes cross-linked and insoluble. The optimal feed ratio was found to be 96:4 of **122**:**123** giving the resulting polymer a T_g of 144 °C. The multilayer device ITO/PEDOT:PSS/cross-linked poly(4-*n*-hexyl-triphenyl)amine/**125**/Ca:Al gave deep blue (λ_{max} = 424 nm) light at 3 V with an EQE of 0.08%. No change in colour during device operation was observed.

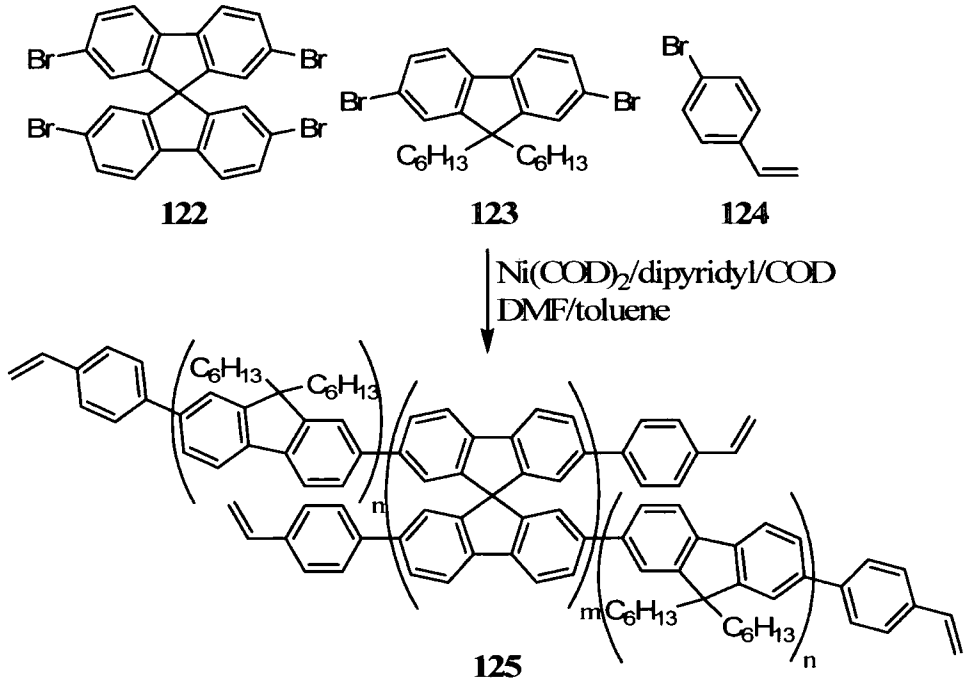

Scheme 1.13 Synthetic route to a 9,9-spirobifluorene-based polymer network

Work into 9,9'-spirobifluorene systems was reviewed in 2003.[90] Since then, several further systems have been investigated. A device comprising ITO/TPD/**126**/Alq_3/LiF/Al produced blue emission with an EQE of 2.8% at 100 cd m^{-2}.[91] The CIE coordinates for the emission were (0.14, 0.12).

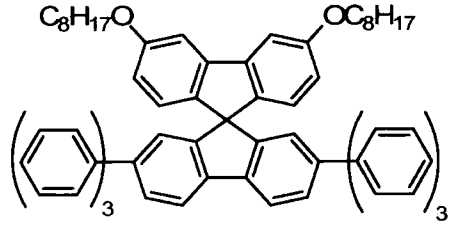

Wu *et al.* synthesised a series of 9,9-diarylterfluorenes and spiro-9,9'-bifluorenes (**127** and **128**).[92] The materials were expected to perform well as single layer devices as similar hole and electron mobilities had been reported for these types of molecules.[93] However, for devices comprising ITO/PEDOT:PSS/**127** or **128**/LiF/Al, the EQE was only 0.15% and only modest luminance values were obtained.

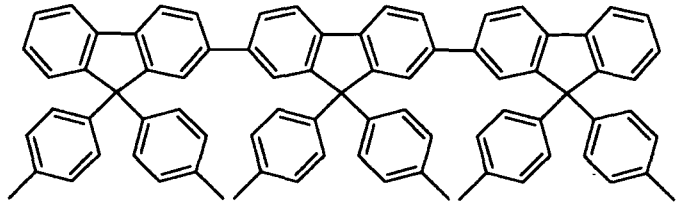

127

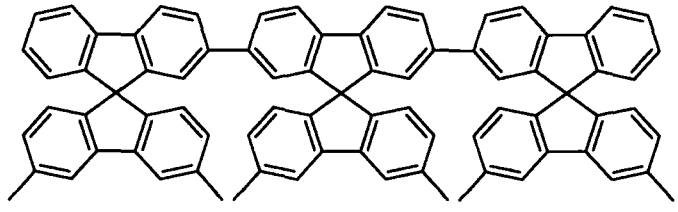

128

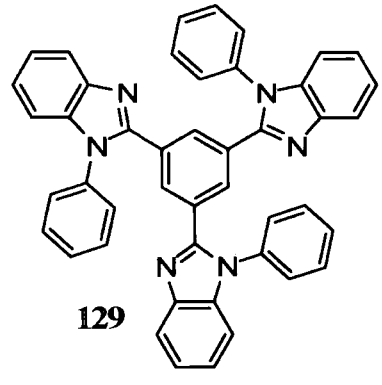

129

Incorporating TCTA, **25**, as a hole-transporting layer improved EQEs to *ca.* 0.7% and device luminance was substantially increased. A second device featuring a layer of the electron transport material TPBI, **129**, raised EQEs up to 2.5% with compound **128** as the emitter. Finally, multilayer structures incorporating both TCTA and TPBI were fabricated leading to very high EQEs of 5.3% and 4.1% when compounds **127** and **128**, respectively were used as the emitters. Turn-on voltages were *ca.* 3 V and luminances of up to 14,000 cd m^{-2} were observed. The deep blue colour emitted had CIE coordinates of (0.158, 0.041) and (0.160, 0.044) for **127** and **128**, respectively, giving a

deeper blue than that specified by the NTSC blue standard. In addition, thermal annealing of the films and continuous device operation showed no evidence of keto-defects. Further syntheses of 9,9-diarylterfluorenes have been reported by Wong *et al.*[94]

1.4.3 Introduction of a Heteroatom at C9

In the last two years alternative ways of dealing with the problem of keto-defects have been sought. Holmes and co-workers replaced the carbon at the C9 position with a silicon atom.[95] The resultant materials are very similar in emissive properties to polyfluorenes with all the emission peaks and shoulders being within 3 nm of those of poly(9,9-dioctylfluorene). In addition, the measured HOMO and LUMO levels for poly(2,7-dibenzosilole), **130**, were 0.1 eV below those of the fluorene analogue which has the effect of lowering the barrier to electron injection. Tests showed that even after thermally annealing films of **130** at 250 °C for 16 hours, no bands appeared in the green region unlike the polyfluorenes as shown in Figure 1.10.

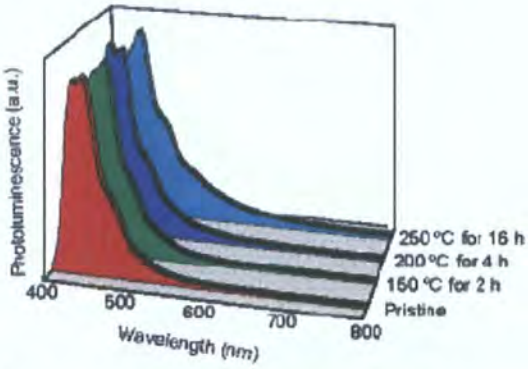

Figure 1.10 PL spectra of polymer 130 over time which shows no green band -reproduced from reference 95

The polymer **130** emits blue light with CIE coordinates of (0.15, 0.11).

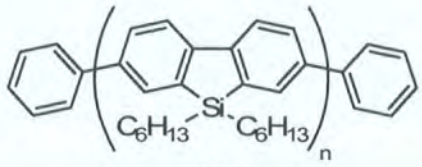

130

The dibutylgermanium analogue **131** has been synthesised.[96] Although insolubility is a problem, initial studies have given rise to devices emitting blue light with CIE coordinates (0.15, 0.07) – bluer than the silafluorenes.

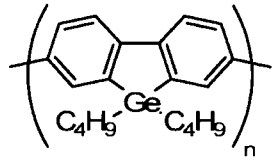

131

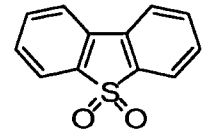

132

Perepichka *et al.* in our group have investigated the use of the dibenzothiophene-*S*,*S*-dioxide moiety, **132**, in blue-emitting materials.[97] The electron-accepting nature of the sulphone unit lowers the energy level of the frontier orbitals and dramatically lowers the barrier to electron injection. The band gap of dibenzothiophene-*S*,*S*-dioxide is only 0.1 eV less than that of fluorene, but the HOMO and LUMO are each about 1 eV lower in energy that those of fluorene. Synthesis and photophysical studies have been carried out on a range of fluorene co-oligomers **133** – **135**.

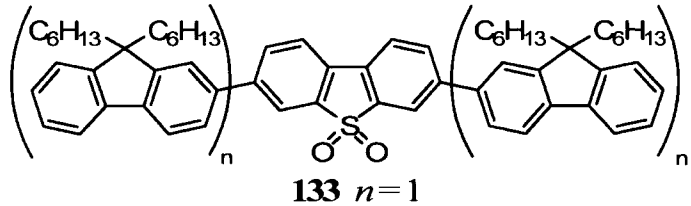

133 $n=1$
134 $n=2$

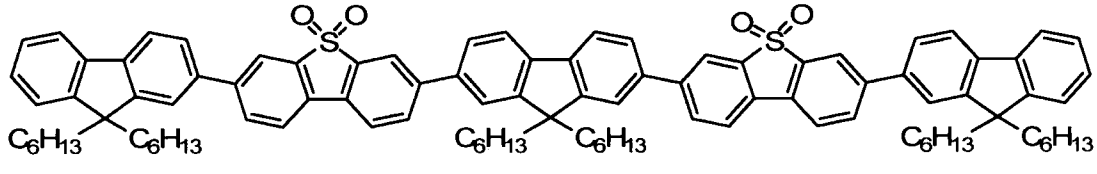

135

No evidence of the green band was seen after thermally annealing the films in the PL spectrum and no C=O stretch was observed in the IR spectrum. The PL emission maxima for **133**, **134** and **135** were 447, 457 and 462 nm, respectively. Initial device studies have given EQEs of up to 3% for co-polymers incorporating 30 mol % of the dibenzothiophene-*S*,*S*-dioxide unit in ITO/PEDOT/polymer/Ca:Al devices.[98]

Huang *et al.* have synthesised dibenzothiophene-*S*,*S*-dioxide derivatives **137** and **138** shown below in Scheme 1.14.[99]

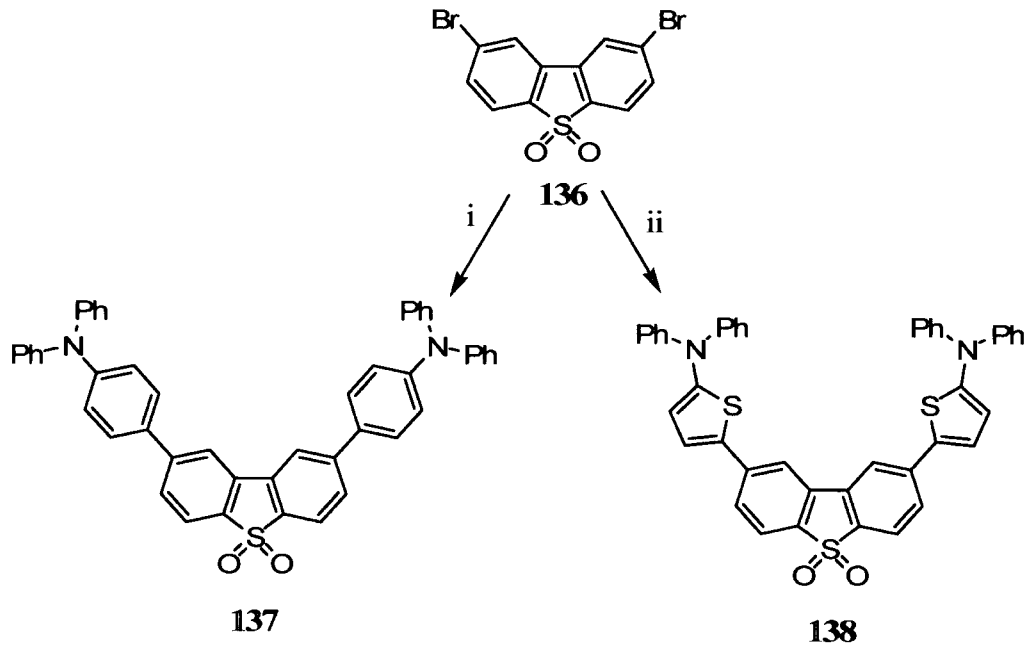

Scheme 1.14 Synthetic route to dibenzothiophene-*S*,*S*-dioxide derivatives; i, $Bu_3SnC_6H_4NPh_2$, $Pd(PPh_3)_2Cl_2$; ii, $Bu_3SnC_4H_2SNPh_2$, Pd $(PPh_3)_2Cl_2$

Devices comprising ITO/**137** or **138**/TPBI/LiF/Al were fabricated and tested. Compound **137** devices resulted in blue-green light (λ_{max} = 492 nm) and a high EQE of 4.9%. Devices containing **138** gave green-yellow light (λ_{max} = 540 nm) and EQE of 1.4%. Unoptimised single layer devices containing compound **137** gave EQEs of 3.1%.

1.5 Bipolar and Multifunctional Materials

So far we have mostly considered single function molecules – those that emit light or transport holes or electrons. However, it often makes sense to combine two or more functions in the same molecule. Common examples of this are materials which transport both holes and electrons – so called bipolar materials – or those combining charge transport with emission e.g. Alq_3 which is both an ET material and a green emitter.

Initial multifunctional materials were based around alterations to the MEH-PPV structure in an effort to improve the electron transporting ability of the polymer. Side groups with cyano or OXD functionality (e.g. **139** and **140**) were introduced.

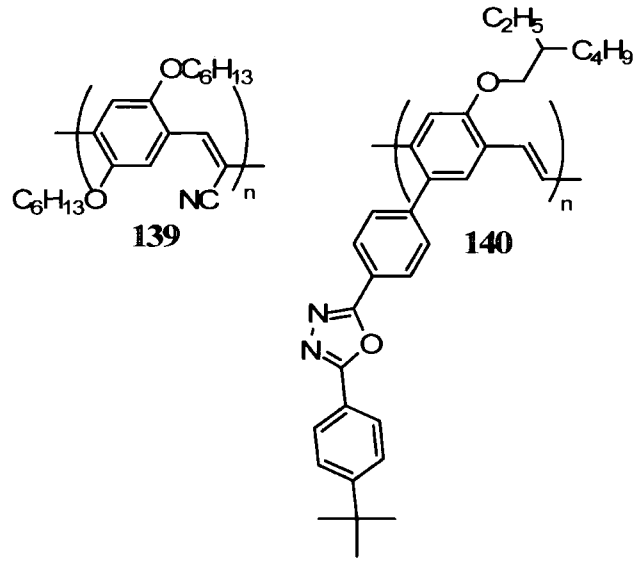

139 **140**

CN-PPV, **139**, gave red emission with an EQE of 0.2% in single layer devices utilising either Ca or Al cathodes. In a bilayer device comprising ITO/PPV/CN-PPV/cathode, efficiencies as high as 4% were achieved.[100, 101] Other electron-deficient substituents have been attached to the PPV framework. Compound **141** showed PL emissions at 580 nm and when used as an ET material for PPV increased device efficiency by two orders of magnitude.[102] Compound **142** with the substitution on the phenylene ring has low PL quantum yields suggesting that these materials act as poor emitters.[103]

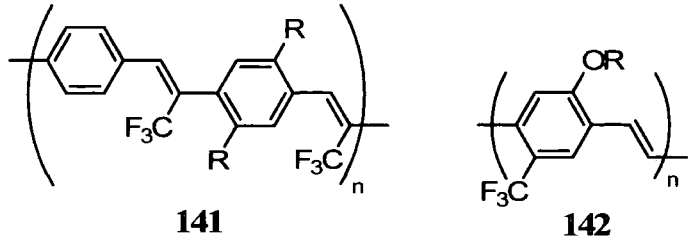

141 **142**

Other groups have synthesised polymers based on oxadiazole and fluorene. Sung and Lin studied alternating fluorene-based copolymers featuring various 2,5-diaryl-1,3,4-oxadiazoles as pendant groups such as compounds **143** and **144**.[104]

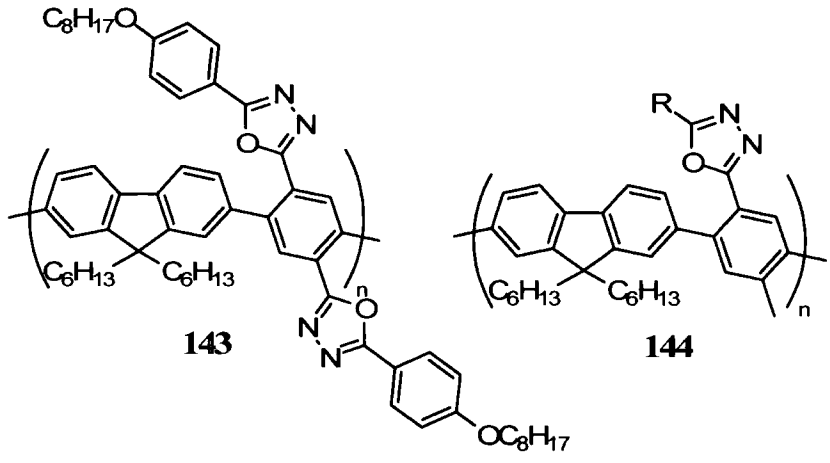

143 **144**

Devices comprising ITO/PEDOT:PSS/polymer/Ca:Al gave only modest light output (maximum of 482 cd m^{-2} for **144** with R = 1-naphthyl) but provided deep blue emission with λ_{max} ranging from 408 – 452 nm. Devices based on **143** showed broadened and red shifted emission upon increasing the voltages. The polymers based on **144** showed higher PL quantum yields and lower solution-state aggregation than symmetric materials based on **143**.

Ding *et al.* synthesised the alternating fluorene-oxadiazole polymers **145** – **148**[105] with band gaps of *ca.* 3 eV which is slightly less than that of polyfluorene (3.33 eV).[106]

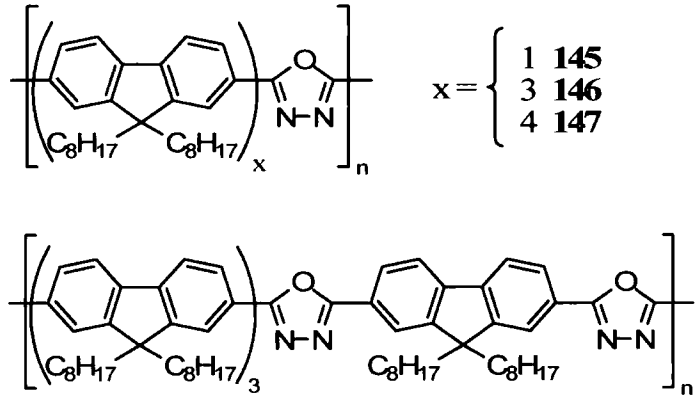

148

Thermal annealing of these materials under inert conditions revealed no green band in the PL spectra, but thermal annealing in air gave rise to the characteristic broad band of polyfluorene. Using an undisclosed HT layer the EL spectrum of the device ITO/HTL/**146**/LiF/Al closely matched the PL spectrum of **146.** Although the EL peaks

were broadened, there was no evidence of the green band even after 12 hours of device operation.

Shirota and co-workers synthesised polymers **149** – **152** containing pendant bipolar moieties on a PMMA backbone.[107]

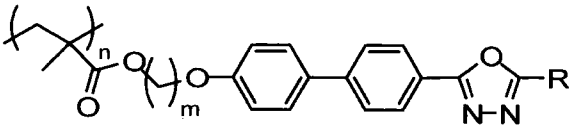

cpd	m	R
149-2, 149-6, 149-11	2, 6, 11	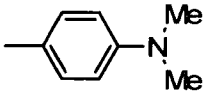
150-6, 150-11	6, 11	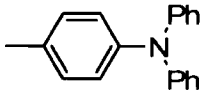
151	6	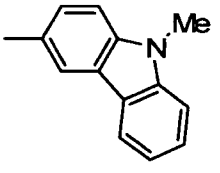
152	6	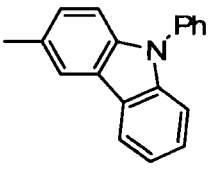

Compound **150-6**, which displayed the highest PLQY (0.82) was incorporated into a single-layer device comprising ITO/**150-6**/Mg:Ag which produced a bright blue emission (λ_{max} = 453 nm) which closely matched the PL spectrum. The device turned on at 10 V but only reached modest brightnesses of around 30 cd m^{-2} at 27 V. This low luminance is due to the lack of an active emitter in the structure.

Meng *et al.* synthesised the bipolar compound PCOPO, **153**, which emitted blue-green light from polymer films (λ_{max} = 475 nm).

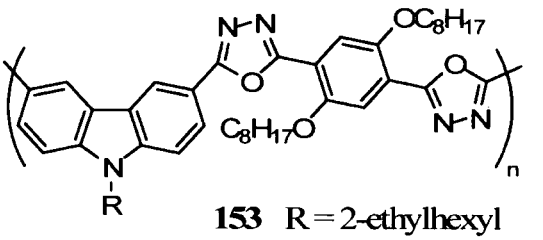

153 R = 2-ethylhexyl

A device comprising ITO/**153**/Al produced blue light at *ca.* 8 V. Cyclic voltammetric studies revealed that the polymer possesses a LUMO similar to that of MEH-PPV but a lower HOMO.

Zhang *et al.* recently synthesised the bipolar polymer **154** incorporating triphenylamine and oxadiazole in the main chain.[108] A derivative omitting the oxadiazole, **155**, was synthesized for comparison.

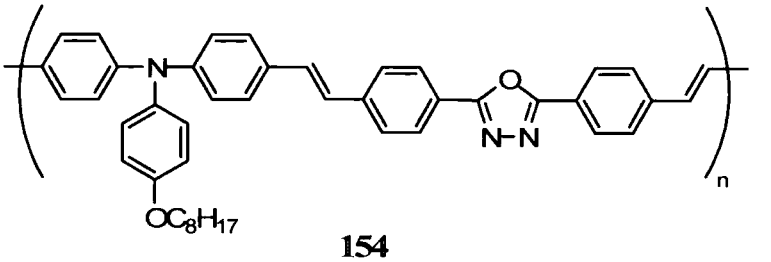

154

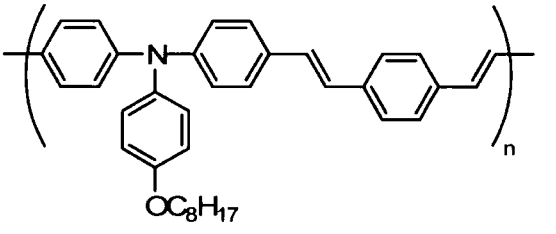

155

The inclusion of the OXD moiety red-shifted the PL emission by 10 nm as expected due to the increased conjugation. Devices comprising ITO/PEDOT:PSS/**154** or **155**/CsF/Al displayed blue electroluminescence. Bipolar polymer **154** turned on at 4 V and gave a brightness of 3,600 cd m^{-2} and an EQE of 0.3% whilst polymer **155** gave a much lower maximum brightness of 284 cd m^{-2} and a lower EQE.

Müllen and co-workers developed the HT blue emitting polymer poly[9,9-bis(triphenylamine)fluorene] (PTPAF, **156**).[109]

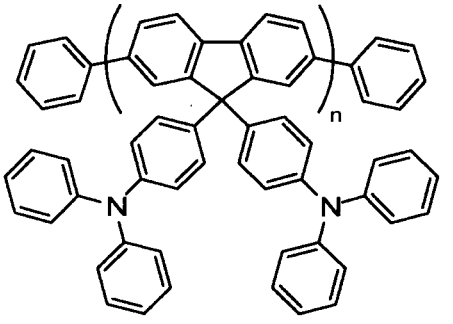

156

Two types of devices were fabricated: ITO/PEDOT:PSS/**156**/cathode and ITO/PEDOT:PSS/PVK/**156**/cathode. The best results were obtained by using a barium cathode. Both devices emitted blue light with the CIE coordinates of (0.184, 0.159) and (0.19, 0.181) and gave efficiencies of 1.05 cd A^{-1} and 0.65 cd A^{-1}, respectively. It was observed that the addition of the PVK layer only slightly increased efficiencies at the cost of higher operating voltages.

Wu *et al.* covalently bonded the charge-transporting 2,5-diaryl-1,3,4-oxadiazole units to the 9-position of fluorene units in copolymers to create copolymer **159** as shown in Scheme 1.15.[110]

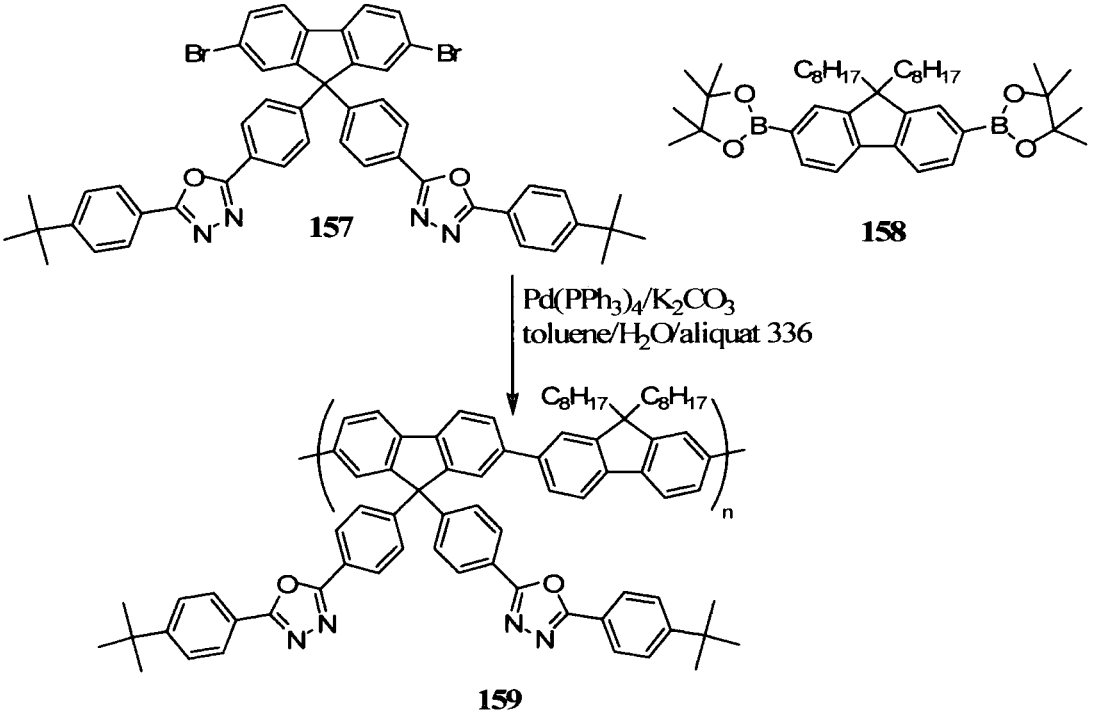

Scheme 1.15 Synthetic route to the alternating ET copolymer 162

The polymer demonstrated a high T_g of 213 °C and no melting transition was found up to 350 °C. Thermal annealing at 150 °C for 20 hours had almost no effect on the PL spectrum indicating that the oxidation at the 9-position of the fluorenes had been suppressed. Devices comprising ITO/PEDOT/**159**/Ca:Ag produced blue light (λ_{max} = 428 nm) with no evidence of longwave emissions. The voltage required to reach 1 cd m^{-2} was 5.3 V and the maximum brightness was 2,770 cd m^{-2} at 10.8 V. The maximum EQE was 0.52% at a luminance of 537 cd m^{-2} and bias of 7.4 V.

A second study by the group introduced an HT segment similar to **156** into the polymer chain to give polymer **160**.[111] This statistical copolymer had a T_g of 166 °C. Once again, thermal annealing yielded no changes to the PL spectrum. A device comprising ITO/PEDOT:PSS/**160**/Ca:Ag gave deep blue emission with CIE coordinates of (0.193, 0.141). The voltage required to reach 1 cd m^{-2} was 4.4 V and the maximum EQE was 1.23% which was at a luminance of 354 cd m^{-2} and bias of 7.6 V.

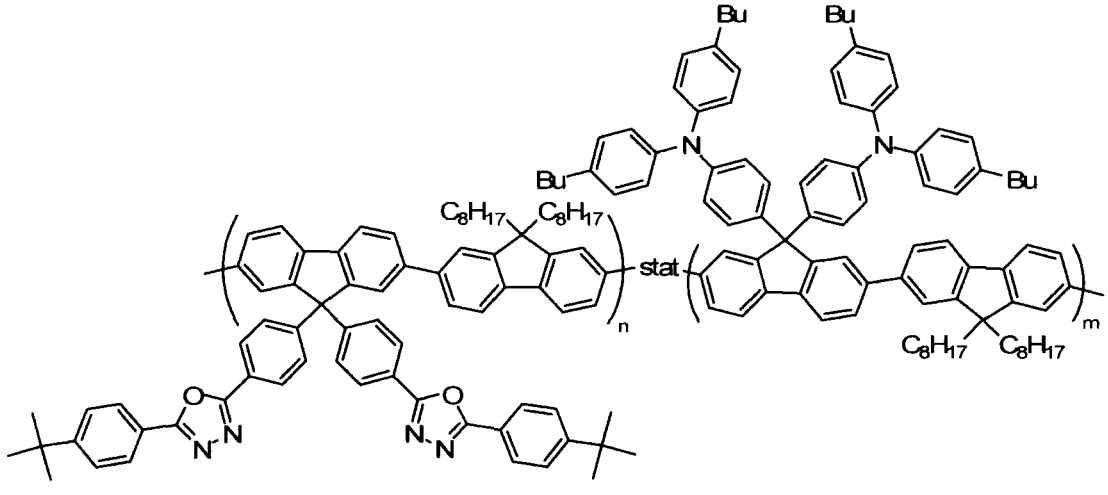

160

The higher efficiencies were attributed to the more balanced charge transport afforded by the triphenylamine and oxadiazole groups.

A further study, as shown in Scheme 1.16, moved the triphenylamine units into the main chain and removed the poly(9,9-dioctylfluorene) units. [112]

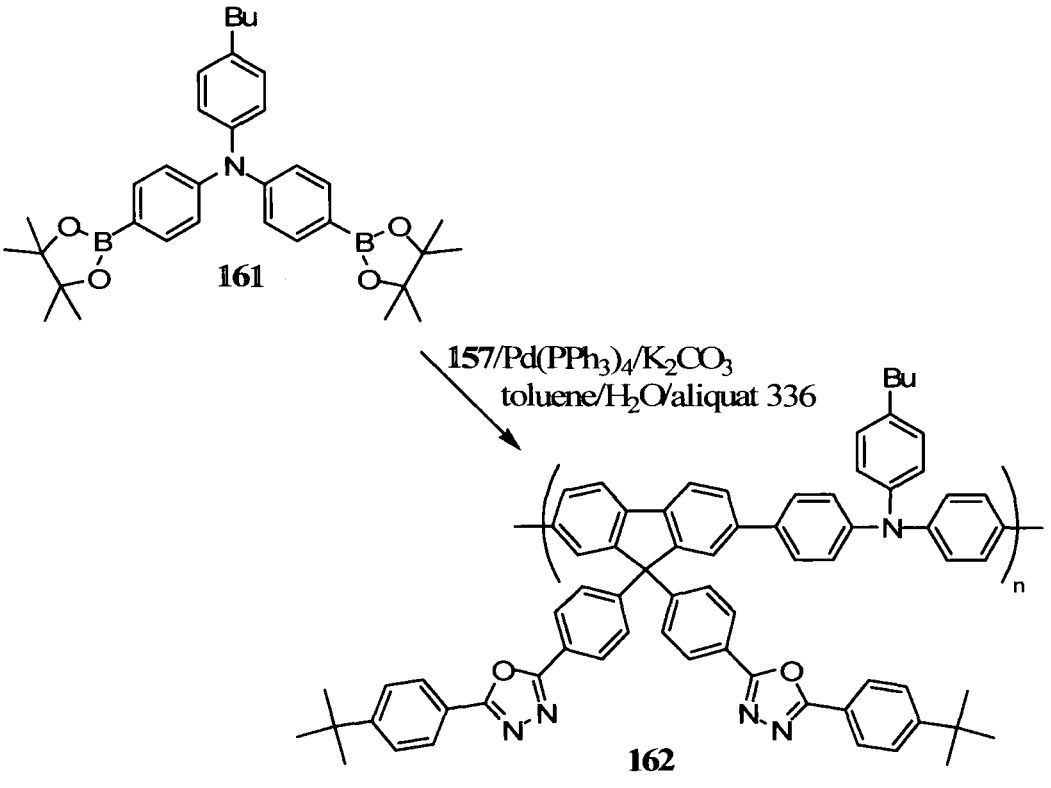

Scheme 1.16 Synthetic route to the bipolar polymer 165

The T_g of compound **162** was found to be 306 °C and no melting point was detected up to 370 °C. As before, thermal annealing yielded no extra bands at longer wavelengths. Bilayer devices comprising ITO/PEDOT/**162**/TBPI/Mg:Ag emitted blue EL (λ_{max} = 460 nm) with CIE coordinates of (0.14, 0.15). The driving voltage to produce 1 cd m^{-2} was lowered from previous materials to only 3.7 V and a maximum EQE of 1.59% was reached at 771 cd m^{-2} and a bias of 6.5 V.

1.6 Phosphorescent Emission from Heavy-Metal Complexes

As noted in Chapter 1.2.1, the incorporation of heavy metal atoms such as iridium or platinum can overcome selection rules and enable the harvesting of both singlet and triplet excited states.[18] This radiative decay of triplet states is allowed due to mixing of the singlet and triplet states such that the triplet state gains some singlet character and radiative decay is no longer forbidden. If the radiative rate of decay is faster than the non-radiative decay, then efficient phosphorescence can be observed. If the excited states are generated electrically the emission is known as electrophosphorescence. The

energy of a triplet exciton is lower than that of a singlet exciton so where singlet – triplet mixing occurs, intersystem crossing (ISC) from the singlet state to the triplet state will occur. The Jabłoński diagram shown in Figure 1.10 summarises the various transitions.

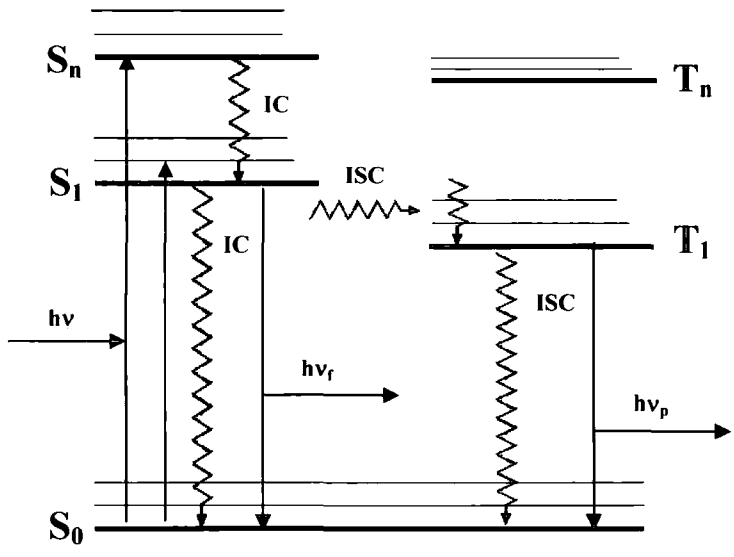

Figure 1.10 Jabłoński diagram showing the photophysical pathways that can occur on excitation

Due to self-quenching in homogeneous layers of phosphorescent materials, phosphors are normally blended into host materials. To ensure the phosphor acts as a charge trap the phosphor should possess an energy gap smaller than that of the host.

The first demonstration of electrophosphorescence used benzophenone, **163**, blended into a PMMA host.[113] Because the singlet – triplet mixing in benzophenone is very weak non-radiative decay is much more prevalent than radiative decay at room temperature. Although phosphorescence was detected at 100 K benzophenone was found to be a poor choice of phosphor for devices.

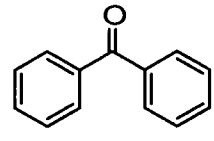

163

The doping concentration of the phosphor can affect the efficiencies of devices. If the concentration is too low then the increased lifetimes of triplet states can cause the low

number of phosphor sites to become saturated and recombination can start to occur on the host molecules, giving rise to emission not from the phosphor. If the concentration of phosphor is too high there is an increase in quenching processes such as triplet – triplet annihilation as shown in Figure 1.11.

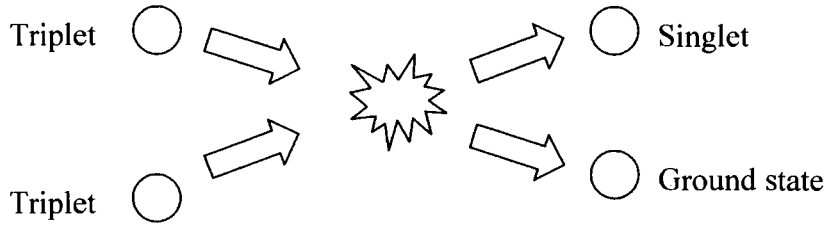

Figure 1.11 Triplet – triplet annihilation which can occur when phosphor concentration is too high

Recent interest has focused on electrophosphorescent materials based on complexes of iridium. In organometallic complexes the emissive state is a mixture of ligand centred (LC) excitons and metal-ligand charge transfer (MLCT) excitons. MLCT states have a larger overlap with the heavy metal atom and thus experience stronger spin-orbit coupling producing a greater mixing of singlet and triplet states. LC states undergo less mixing and have longer lifetimes making them more vulnerable to triplet – triplet annihilation (which increases with the square of triplet lifetime).[114] For strong spin-orbit coupling, the MLCT states can be lower in energy than the LC states so lifetimes and hence the amount of triplet – triplet annihilation are minimised

For the common complex *fac*-tris(2-phenylpyridine) iridium (*fac*-Irppy$_3$, **164**) the LC excited state energy is about 21700 cm^{-1} and the ^{3}MLCT state emits at 510 nm. The first testing of *fac*-Irppy$_3$ in OLED devices was reported in 1999 by Baldo *et al.* in the architecture ITO/α-NPD/CBP:**164**/BCP/Alq$_3$/Mg:Ag produced by high vacuum deposition.[20]

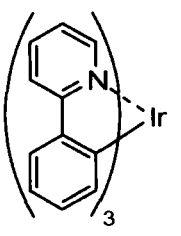

164

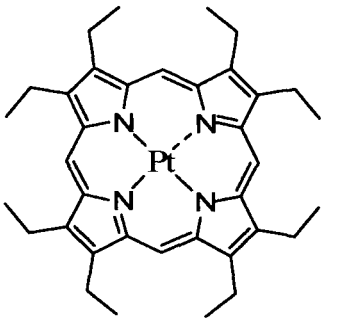

165

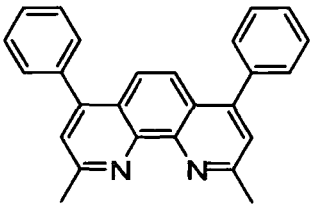

166

Devices based on a previously studied molecule, 2,3,7,8,12,13,17,18-ocatethyl-21*H*-23*H*-porphine platinum (PtOEP, **165**) had needed a layer of BCP (**164**) between the luminescent layer and the Alq_3 layer to prevent the diffusion of excitons out of the luminescent layer.[115] It was found that EQEs of 8% could be obtained at a doping level of 6 – 8% by mass of $Irppy_3$ in CBP. Lower doping levels (1%) led to reduced efficiencies as the lumophores lay beyond the Dexter transfer radius of excited Alq_3 molecules. Higher doping levels also showed lower efficiencies due to quenching. A device with a neat layer of $Irppy_3$ had a significantly reduced EQE of 0.8%. Similarly, doping $Irppy_3$ into Alq_3 or omitting the BCP layer produced devices with EQEs of < 1%. This information is summarised in Figure 1.12. The triplet lifetimes of $Irppy_3$ were found to be sufficiently short (in the order of 1 μs) to avoid saturation of the phosphorescent sites allowing maximum luminance values of *ca.* 100,000 cd m^{-2}. No evidence of emission from the blue-emitting CBP host was detected even at current densities as high as 100 mA cm^{-2} indicating complete energy transfer.

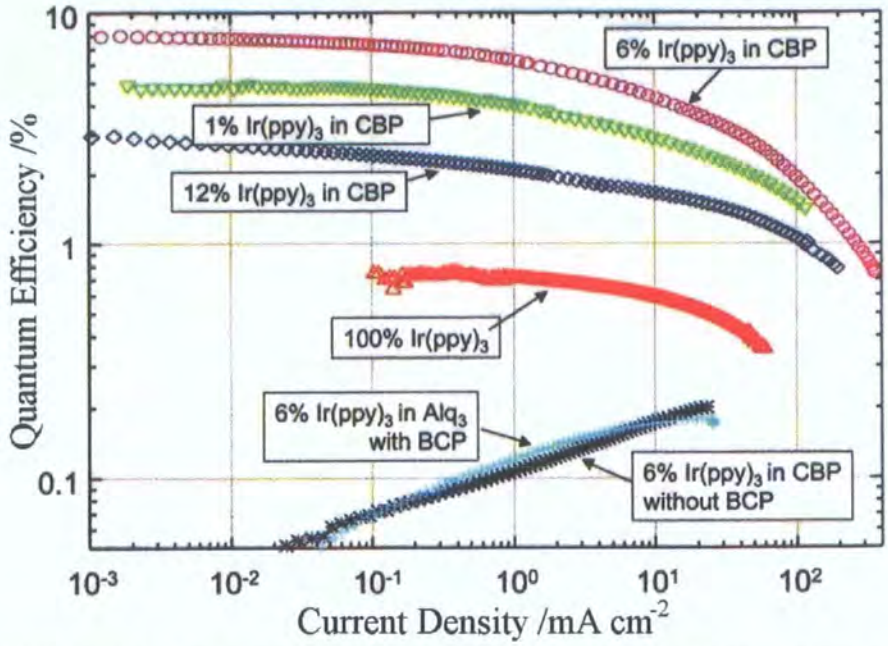

Figure 1.12 Efficiencies of varying doping concentrations of $Irppy_3$ - reproduced from reference 18

A further study by Adachi *et al.* blended $Irppy_3$ into 3-phenyl-4-(1'-napthyl)-5-phenyl-1,2,4-triazole (TAZ, **167**).[116] This time 4,4'-bis[*N,N'*-(3-tolyl)amino]-3,3'-dimethylbiphenyl (HMTPD, **168**) was used as the HT material in an ITO/HMTPD/$Irppy_3$:TAZ/Alq_3/Al:Li device.

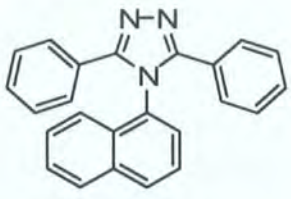

167

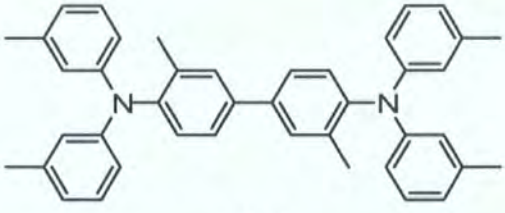

168

These devices showed a large improvement in EQE to 15.4% at a doping level of 7%. Increasing the brightness to 400 cd m^{-2} gave a still-impressive EQE of 10%. At lower doping levels, blue emission from the host was seen.

The same group reported the preparation of red-emitting phosphorescent materials based on benzothienylpyridine ligands in 2001.[117] Two types of device were fabricated with type 1 devices comprising ITO/α-NPD/**169** or **170**:CBP/DCP/Alq_3/Mg:Ag and type 2 devices comprising ITO/HMTPD/**169** or **170**:TBPI/Alq_3/Mg:Ag. In both devices the doping level was 7%. The $btp_2Ir(acac)$ type I device showed a maximum

EQE of 7%. By comparison the EQE of btpPt(acac) reached a maximum of 2.7%. This was ascribed to the much lower PL efficiency of 8% compared to 21% for the iridium compound.

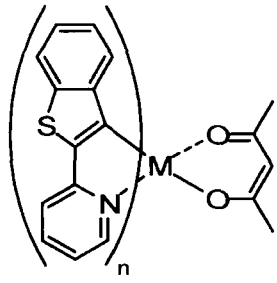

169 M = Ir, n = 2
170 M = Pt, n = 1

Both materials gave red emission with CIE coordinates (0.67, 0.33) which lie close to the NTSC recommended values.

The final primary colour was reported, again by Adachi *et al.* in 2001. By introducing electron-withdrawing fluorine atoms at the 4- and 6-positions on the phenyl ring to give compound **171** the emission was blue shifted by *ca.* 40 nm compared to $Irppy_3$.[118] Exchanging the acetylacetone ligand for picolinate resulted in a further *ca.* 20 nm blue-shift for FIrpic, **172**.

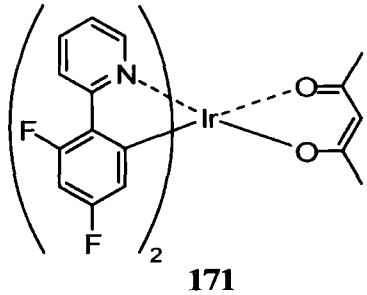

171

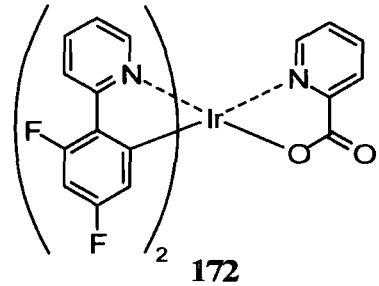

172

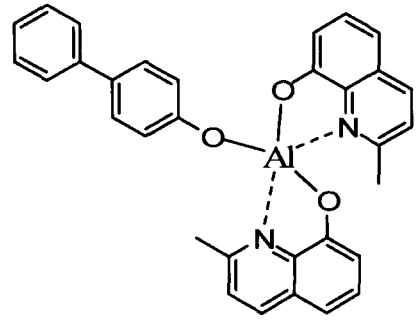

173

Devices with the structure ITO/CuPc/α-NPD/FIrpic:CBP/BAlq/Lif/Al (where BAlq is compound **173**) gave pale blue light of wavelength 475 nm and CIE coordinates of (0.16, 0.29). The maximum EQE was 5.7% and at a maximum brightness of 6,400 cd m^{-2} the EQE was 3.0%. The main difference with the blue emitter was that the triplet energy of the CBP host (2.56 eV)[119] was now lower than that of the FIrpic dopant (2.62 eV)[117] meaning that excited states are exothermically transferred from the dopant to the host and then transferred endothermically back to the dopant. This is seen in practice as a long decay time of *ca.* 10 ms. It was found that lowering the temperature below 200 K retarded the endothermic transfer, but at room temperature the transfer from FIrpic to CBP was very efficient.

1.6.1 Colour Tuning

Wang *et al.* published a detailed study of devices containing a wide range of tris-cyclometalated species based on 2-phenylpyridine.[120] By changing the substitutions on the aromatic rings emission was tuned from *ca.* 500 – 595 nm with both the electronic nature and position of the substituent groups affecting the colour.

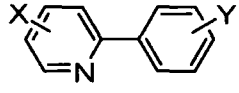

X = H, 5-NO_2, 5-CF_3, 3-Cl
Y = H, 4-F, 2-F, 3-CF_3, 3-MeO, 4-MeO, 4-CF_3O

In 2002, Thompson and co-workers carried out similar studies on platinum complexes with one C^N ligand and one ancillary ligand (either acac or dpm).[121] The complete list of ligands, their abbreviations, the structure of dpm and PL emission maxima at 77 K are shown in Figure 1.13.

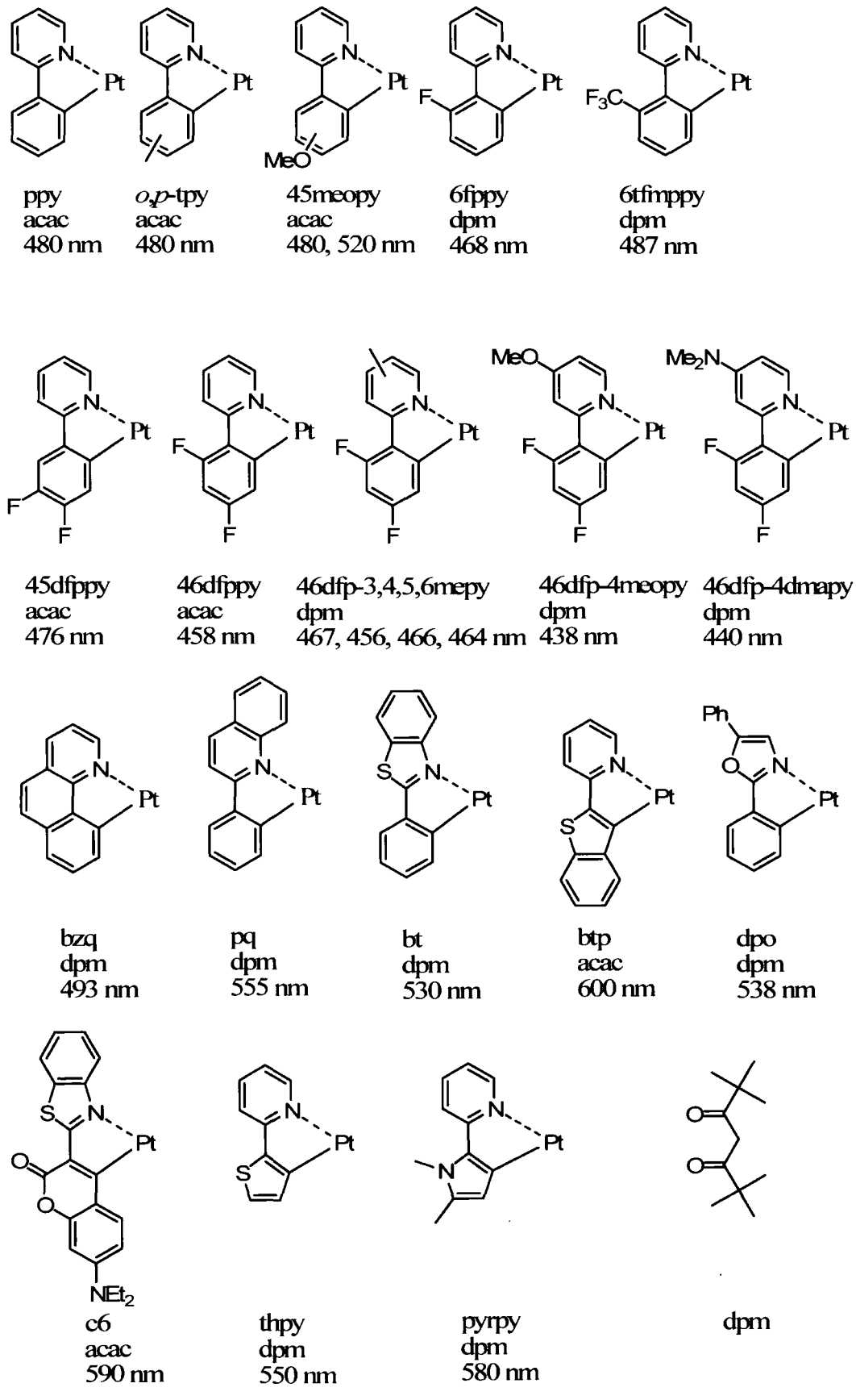

Figure 1.13 Structures and abbreviations for the ligands used by Thompson and co-workers

The emission was thereby tuned between 438 and 600 nm. DFT calculations were carried out on the ground and excited states. The results for all the ligands were all similar to the ones for ppyPt(acac) shown in Figure 1.14. Similar calculations were carried out by Hay on iridium complexes.[122]

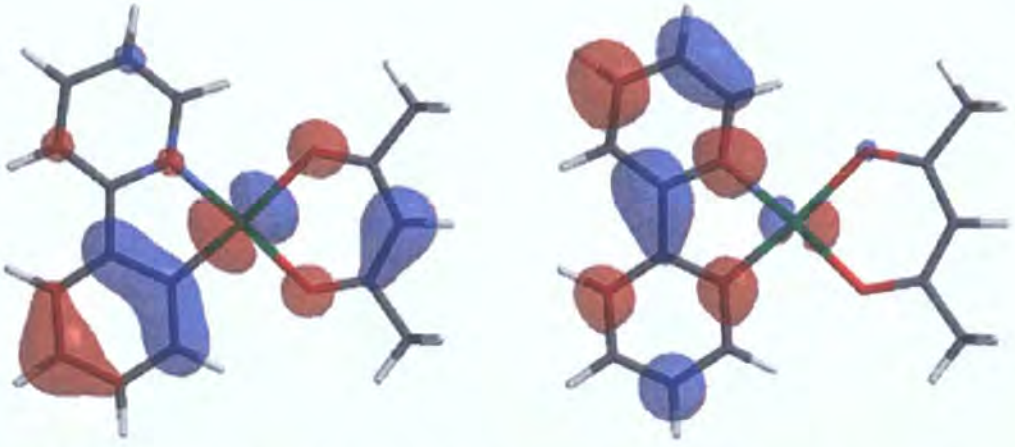

Figure 1.14 HOMO (left) and LUMO (right) of (ppy)Pt(acac) from DFT calculations - reproduced from reference 121

The HOMO consists of a mixture of phenyl, platinum and acac orbitals, whilst the LUMO is predominantly located on the 2-phenylpyridine ligand. Using these observations, the shift in emission observed upon changing ligand was rationalised. For example, difluoro substitution at the 4- and 6-positions gives a much more pronounced blue-shift (λ_{max} = 458 nm) compared to monofluoro substitution at the 6-position (λ_{max} = 468 nm), yet difluorosubstitution at the 4- and 5-positions leads to less blue-shift (λ_{max} = 476 nm). From the DFT calculations we can see that a large amount of electron density resides at the 5-position of the phenyl ring, whilst very little is centred at the 4- and 6-positions. It therefore follows that for 45dfppyPt(acac), weak π-donation from the 5-fluorine raises the HOMO level and lowers the band-gap leading to a redder emission. When this weak π donor is replaced by a stronger donor such as the methoxy group in 5meoppyPt(dpm), the HOMO is raised further and the resultant emission is at 520 nm. Methoxy substitution at the 4-position does not donate to the HOMO so the emission is bluer (λ_{max} = 480 nm). Similarly, the addition of electron-donating groups onto the LUMO-containing pyridine ring raises the level of the LUMO and blue shifts the emission further as seen in 46dpf-4mepyPt(dpm) (λ_{max} = 438 nm) and 46dpf-4dmapyPt(dpm) (λ_{max} = 440 nm).

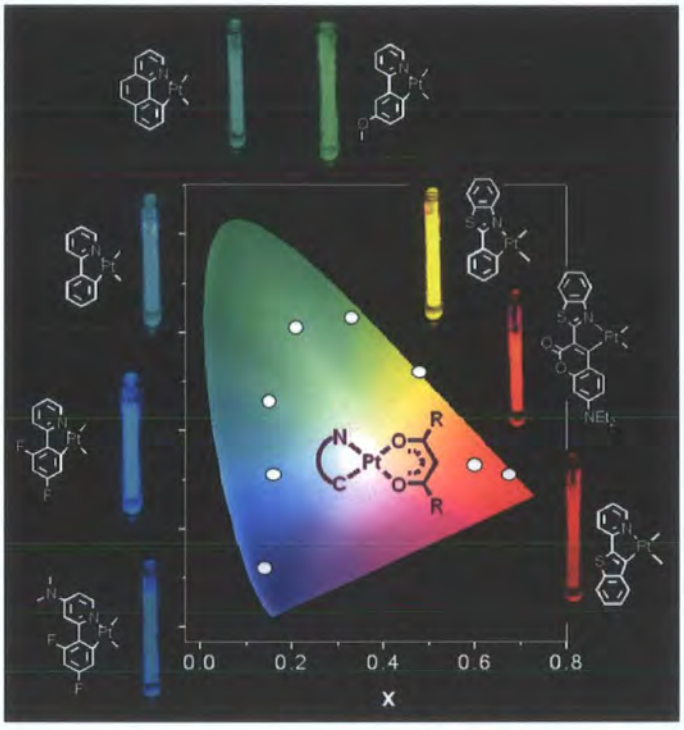

Figure 1.15 Selected complexes displayed as a function of their emission colour on a CIE diagram

These observations were backed up by Coppo *et al.* who synthesised a set of fluorine and trifluoromethyl containing complexes as shown below.[123] The emission varied between 461 nm (R = 4,6 F) and 511 nm (R = 4,6 CF_3).

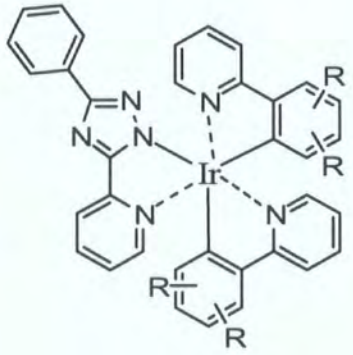

R = 4,6 F; 3,5 F; 4,6 CF_3; 3,5 CF_3

1.6.2 White Light Emission

By carefully choosing the host, phosphor dopant and doping level, it is possible to create white light. White light is defined as that of a black body emitter with a temperature between 2800 and 6500 K.[18] For example, a candle gives light with a colour temperature of *ca.* 1900 K, an incandescent bulb *ca.* 2800 K and daylight *ca.* 6500 K. The CIE coordinates for pure white light are (0.333, 0.333). Heeger and co-workers prepared two iridium systems.[124, 125] Type I systems blended 0.01-1% by weight of the red emitting complex $Ir(HFP)_3$, **174**,[126] into PFO, and type II systems blended the $Ir(HFP)_3$ into PFO and poly(9,9-dioctylfluorene) containing 1% fluorenone moieties (PFO-F, **175**).

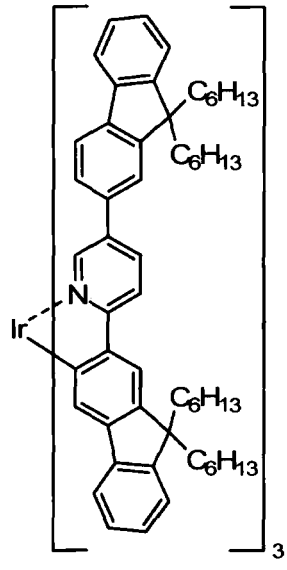

174

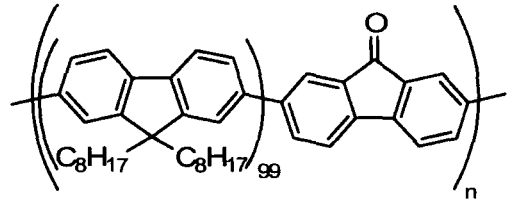

175

At doping levels above 0.1% red light from the $Ir(HFP)_3$ was observed. However, at low doping levels white light was observed made up from emission from red and green-blue emission in type I and red, green and green-blue emission in type II devices. Type I and type II devices produced light with CIE coordinates (0.329, 0.321) and (0.352, 0.388), respectively. These correspond to colour temperatures of *ca.* 6400 K for type I devices and 4600 K for type II devices and gave efficiencies of 4.3 and 3.0 cd A^{-1} respectively. Both devices were ITO/PEDOT:PSS/host:$Ir(HFP)_3$/Ca:Ag structures. A picture of one of these devices in operation is shown in Figure 1.15.

Figure 1.15 White light from a device - reproduced from reference 124

This approach was mirrored by Tavasli *et al.* from our group who doped diarylamine-capped poly[9,9-bis(2-ethylhexyl)fluorene-2,7-diyl] (PF2/6, **176**) with the orange emitting $Ir(Fl_3Py)_3$ iridium complex, **177**[127] to produce white-light emitting devices.[128]

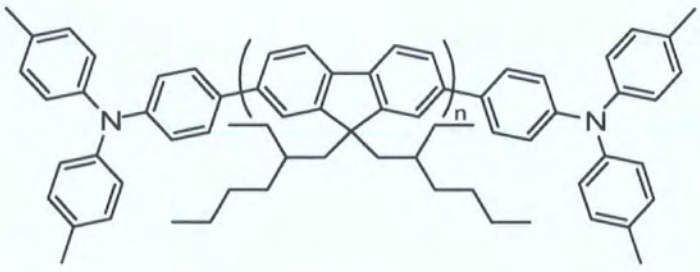

176

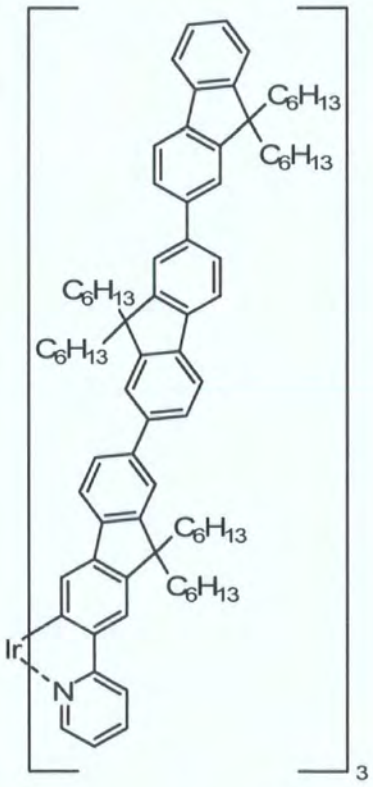

177

The devices once again comprised ITO/PEDOT:PSS/PF2/6:Ir($Fl_3Py)_3$/Ca:Al and at 2-3% doping levels white light was observed. Brightnesses reach 16,000 cd m^{-2} at 5 V, the maximum EQE was 2.8% and the CIE coordinates were (0.348, 0.367). Progress in white light emission has been recently reviewed.[129]

A very recent paper from Thompson, Forrest and co-workers uses a new device architecture to provide a very efficient white light device.[130] This device contains a blue fluorescent material, 4,4'-bis(9-ethyl-3-carbazovinylene)-1,1'-biphenyl (BCzVBi, **178**) and red and green phosphorescent materials (iridium bis(2-phenyl quinolyl-*N*,$C^{2'}$) acetylacetonate (PQIr, **179**) and $Irppy_3$ respectively) all doped into a CBP host.

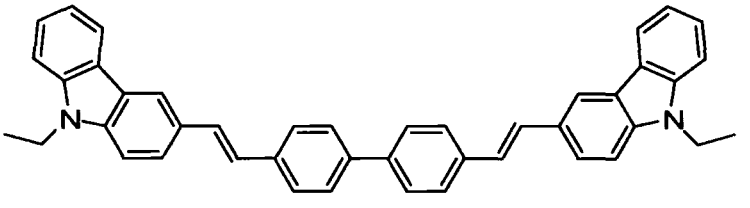

178

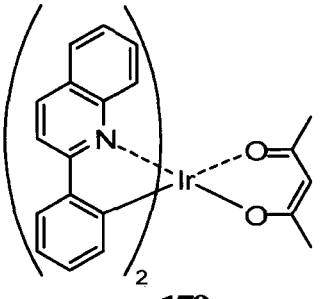

179

The unique multilayer structure comprising ITO/α-NPD/CBP:BCzVBi/CPB/CBP:PQIr/CBP:$Irppy_3$/CPB/CPB:BCzVBi/ETl/LiF/Al features extra undoped CBP encasing the phosphorescent dopants away from the fluorescent blue dopant. Upon device operation singlets and triplets are formed. The singlets formed are transferred quickly to the BCzVBi and cannot diffuse through to the iridium molecules at the centre of the device due to their short lifetimes. The triplet excited states, however, can diffuse through the device. The CBP spacer layers also prevent energy transfer from the blue emitter to the iridium molecules. Thus singlet and triplets are harvested in independent channels. In operation, the device gives an EQE of 18.4% at a high luminance of 500 cd m^{-2} and gives CIE coordinates of (0.38, 0.40). The authors have speculated that use of more efficient emitters could increase EQEs above 20%.

1.7 Conclusions

OLEDs represent one of the most intensively researched areas in recent years. Beginning with the initial work of Tang and VanSlyke there are now thousands of papers and patents in the area. OLED displays in the real world are now becoming more common in small displays. In the recent weeks a Samsung 17" panel with a UXGA resolution, response time of < 0.01 ms and panel thickness of just 1.2 mm was shown at the 2006 Korea Electronics Show.

This Chapter has reviewed recent progress in several fields including the use of triarylamines as HT materials, 1,3,4-oxadiazoles as ET materials and various bipolar materials. Progress in the recent field of electrophosphorescence, including the rapidly developing area of white-light emission has also been reviewed.

Chapter 2 – New Materials for Electron Transport

2.1 Introduction

As shown in Chapter 1.3, achieving a balanced injection of charges from the anode and cathode is essential to improve device performance. As previously discussed most emitting materials (such as polyfluorenes and MEH-PPV) are predominantly hole-transporting (p-dopable) and require extra materials to transport negative charge from the cathode. Our group has previously developed fluorene-containing 1,3,4-oxadiazole systems in an effort to create electron transporting materials. For example the work by Wang and Oyston has been mentioned in Chapter 1.3.2.2.[57-59] In conjunction with the

Department of Engineering, our approach involves blending our ET materials into MEH-PPV and creating single-layer devices that contain up to 95% by weight of the ET material and retain emission purely from MEH-PPV. In search of further improvements in device performance, novel fluorene-containing OXD materials were synthesised and their properties in devices tested.

The initial aim was to investigate new 2,5-diaryl-1,3,4-oxadiazole derivatives. Previous work by S. Oyston had shown that in compound **180** the bromide *para* to the oxadiazole could not be converted to the corresponding boronic acid or boronic ester.[131] A variety of methods shown in Scheme 2.1 had been attempted without success.

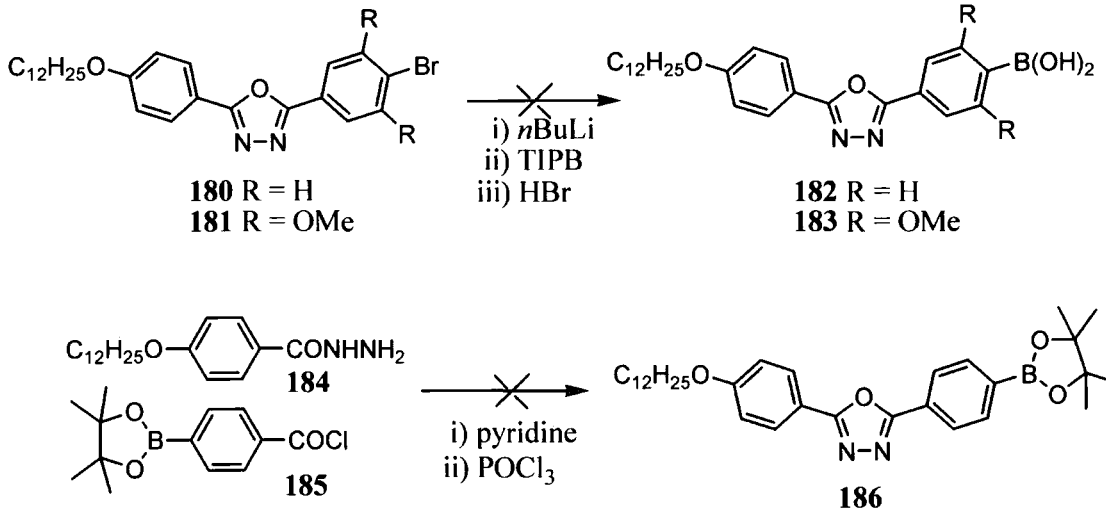

Scheme 2.1 Previous attempts in the group to generate the OXD-based boronic acid/ester

2.2 Results and Discussion

2.2.1 Synthesis

Previous 1,3,4-oxadiazole synthesis in the group had focused on the coupling of a hydrazide with an acid chloride followed by dehydration-cyclisation in $POCl_3$. From a carboxylic acid, conversion to the oxadiazole proceeded via the ester, hydrazide and diacyl hydrazine – four steps. For the present work the tetrazole-based Huisgen route was investigated.[43] This requires a cyano group which is converted via a tetrazole to

the oxadiazole – just two steps. 4-Bromobenzonitrile, **187**, was used as the starting material due to its ready availability. Conversion to the tetrazole was achieved with sodium azide in the presence of ammonium chloride in DMF as shown in Scheme 2.2.

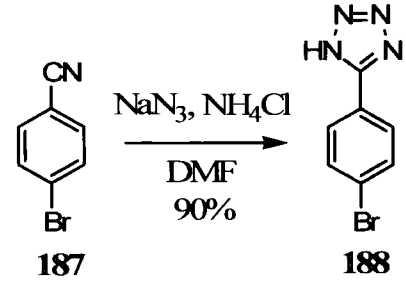

187 **188**

Scheme 2.2 Conversion from nitrile to tetrazole

The [3+2] cycloaddition proceeded cleanly and compound **188** was obtained by pouring the reaction mixture into water and acidifying the solution to precipitate out the tetrazole which can be purified by recrystallisation. To obtain the oxadiazole the tetrazole is reacted with an acid chloride in pyridine (Chapter 1.3.2.1). Several different commercially available acid chlorides were used to produce a small library of 1,3,4-oxadiazoles (**189 – 194)** as shown in Scheme 2.3.

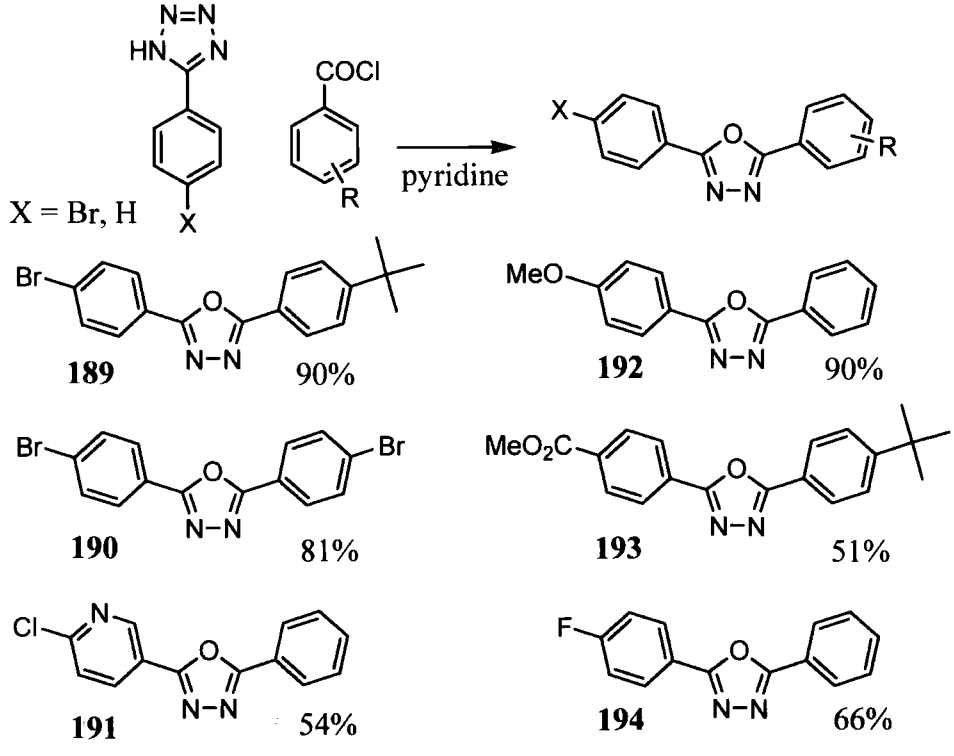

Scheme 2.3 Conversion of tetrazole to 1,3,4-oxadiazole derivatives

After refluxing the tetrazole in pyridine until the evolution of nitrogen ceases, the product can be precipitated by pouring the reaction mixture into water. Filtration and recrystallisation gave the pure product. The first OXD material synthesised was 2-(4-bromophenyl)-5-(4-*tert*-butylphenyl)-1,3,4-oxadiazole (**189**) which was obtained in 90% yield (81% from the original cyano compound). To test the benefits of this route a reaction was done between 4-bromophenylhydrazide (obtained from 4-bromobenzoic acid in 85% yield) and 4-*tert*-butylbenzoyl chloride as shown in Scheme 2.4.

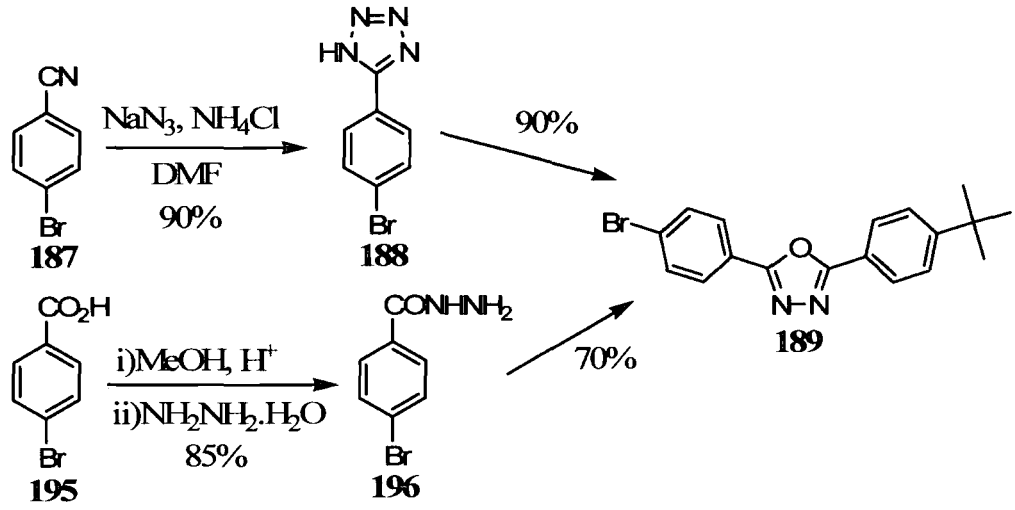

Scheme 2.4 Comparison of routes to OXD compound 189

The results clearly show the benefits of the tetrazole route – fewer steps and higher yields. The methyl ester derivative **193** can be converted to the hydrazide and then coupled to further acid chloride derivatives which can then be cyclised to form a second OXD heterocycle. This was demonstrated by coupling 4-bromobenzoyl chloride and 4-*tert*-butylbenzoyl chloride as shown in Scheme 2.5.

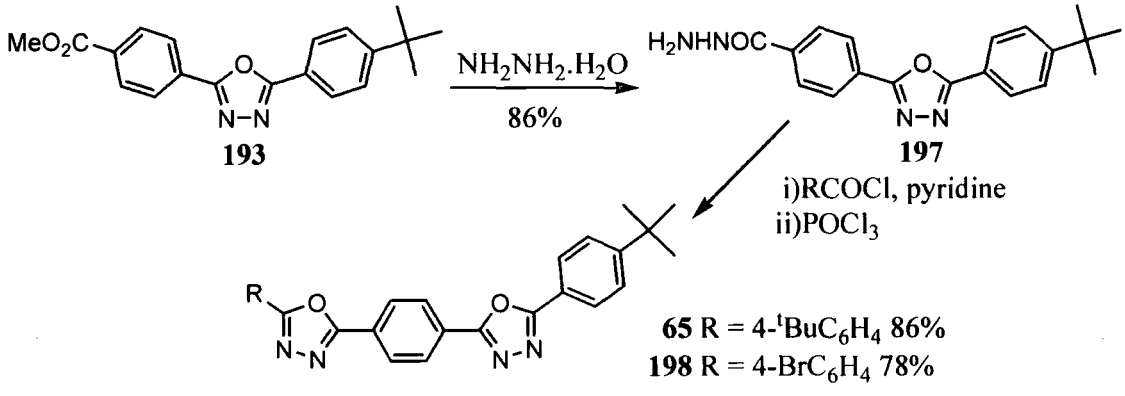

Scheme 2.5 Addition a second OXD ring

Compound **65** (PDPDP) has been made before in our group by a different route and compound **198** carries a bromide handle for further reactions. The two-step process gave yields of 86% and 78% for compounds **65** and **198**, respectively. Compound **198** was found to be fairly insoluble which hindered further reactions. If better solubilising groups were incorporated into the intermediates this strategy could be extended to create well-defined oligomeric oxadiazole compounds.

Dibromide compound **190** provided the possibility of functionalisation on both sides of the OXD. Previous ET materials from our group, such as DFD, had featured a fluorene core unit with two surrounding OXDs. Compound **190** offered the possibility to fabricate a molecule with a central oxadiazole molecule flanked by two fluorene moieties. The required fluorene boronic acid was obtained from commercially available 2-bromofluorene in 2 steps as shown in Scheme 2.6.

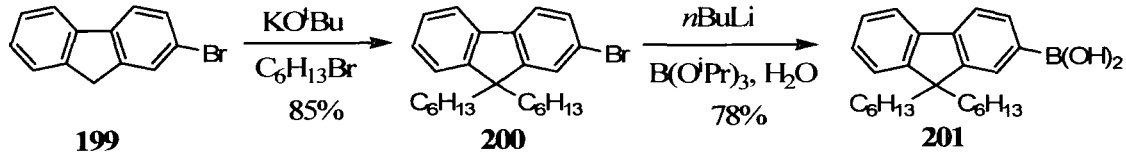

199 **200** **201**

Scheme 2.6 Synthesis of 9,9-dihexylfluoren-2-yl boronic acid

Following deprotonation of compound **199** at the benzylic C9-position with potassium *tert*-butoxide, nucleophilic attack on 1-bromohexane formed the desired dihexylated product, **200**, which was isolated as a pale yellow oil. The oil was dissolved in THF and lithiated with *n*-butyllithium at -78 °C before triisopropylborate (TIPB) was added. The product was hydrolysed with water and compound **201** was obtained after column chromatography as a foamy white solid (66% for both steps). The boronic acid was then reacted with the 2,5-di(bromoaryl)-1,3,4-oxadiazole compound **190** under Suzuki-Miyaura conditions[67] using 7.5 mol % of bis(triphenylphosphine)palladium dichloride as the catalyst as shown Scheme 2.7 to give the desired pure dicoupled product 2,5-bis[4-(9,9-dihexyl-9H-fluoren-2-yl)phenyl]-1,3,4-oxadiazole (**202**) in 43% yield.

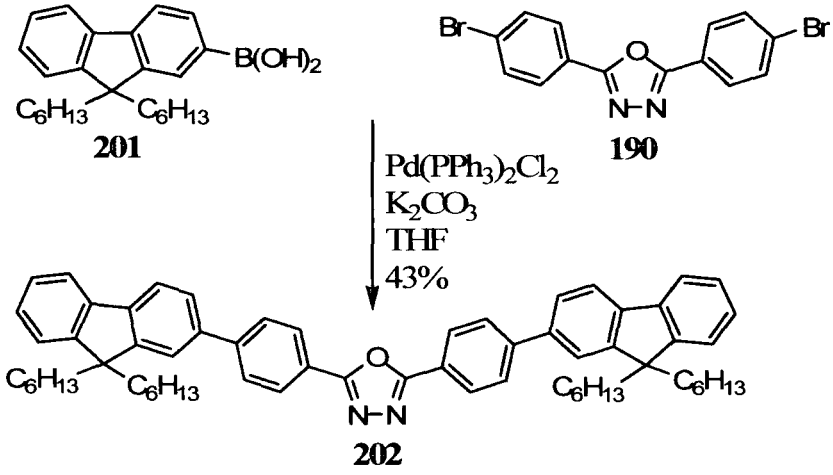

Scheme 2.7 Suzuki-Miyaura cross-coupling reaction

In addition to this dihexylfluorene based compound, we attempted to produce the 9,9'-spirobifluorene derivative. The synthesis of 9,9'-spirobifluorene and subsequent attempted monobromination to produce the needed precursor for the required boronic acid are shown in Scheme 2.8.

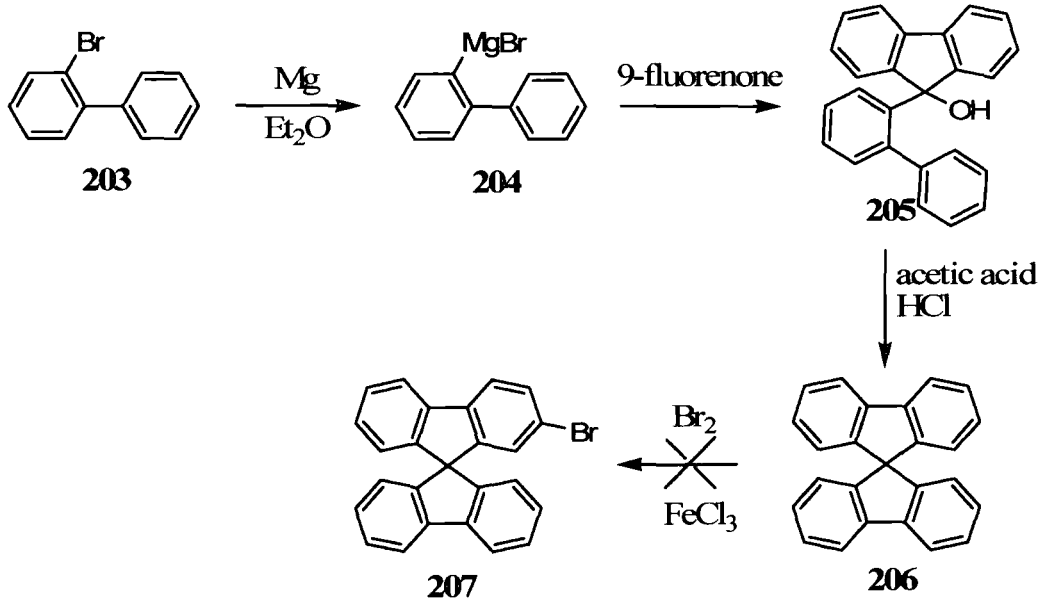

Scheme 2.8 Attempted synthesis of 2-bromo-9,9'-spirobifluorene

Commercially available 2-bromobiphenyl, **203**, was converted to the corresponding Grignard reagent, **204**, with magnesium in diethylether. A solution of 9-fluorenone was added and the mixture was refluxed before being hydrolysed with an ammonium chloride solution to yield the carbinol, **205**. The carbinol was dissolved in acetic acid

and refluxed with a few drops of hydrochloric acid to form the spirobifluorene, **206**, in a 60% yield from compound **203**. Reaction of compound **206** with bromine in DCM with a catalytic amount of iron(III) chloride gave a mixture of brominated products which could not be separated by column chromatography as the components ran together even in non-polar solvents such as hexane. A route to the desired mono-bromo compound was reported by Pei *et al.* and involved using 2-bromo-9-fluorenone in place of 9-fluorenone to construct the spiro framework with the desired bromide already in place.[88] 2-Bromo-9-fluorenone is a very expensive material (current price from Sigma-Aldrich is £46.20+VAT per 100 mg). The standard method employed to synthesise this material is an oxidation of 2-bromofluorene using chromium(VI) oxide as shown in Scheme 2.9 which yields hazardous chromium biproducts which must be disposed of properly and may explain the high retail price.

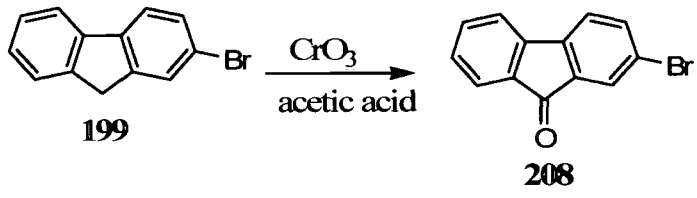

Scheme 2.9 Chromium-based oxidation of 2-bromofluorene

Thankfully a much more environmentally benign route exists. This route involves the bubbling of compressed air through a solution of 2-bromofluorene in pyridine and phase transfer agent tetra-*n*-butylammonium hydroxide. This route yields the desired product, **208**, in 82% yield and works on a 10 g scale.

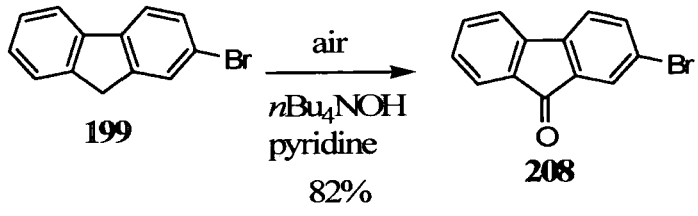

Scheme 2.10 Air-based oxidation of 2-bromofluorene

This material was incorporated into the established synthetic route to the spirobifluorene compound as shown in Scheme 2.11.

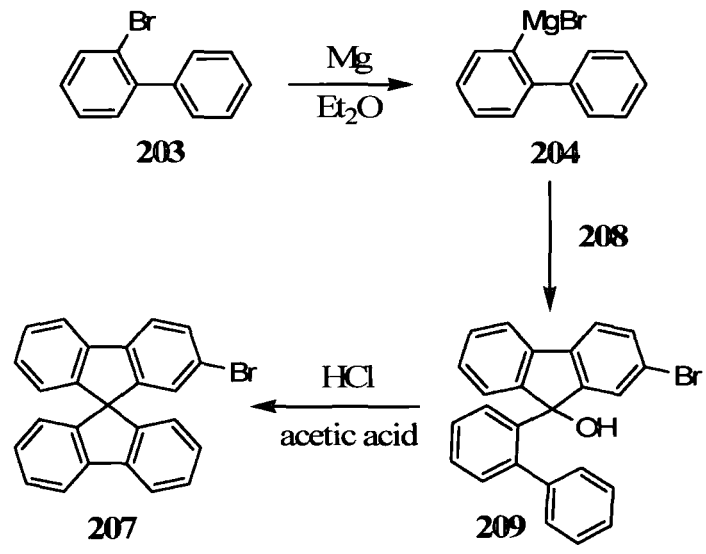

Scheme 2.11 Synthesis of 2-bromo-9,9'-spirobifluorene

Due to solubility problems of compound **208** in diethyl ether, the isolated yield was only 20%, but this reaction was not optimised. If it had been repeated with compound **208** in THF in place of diethyl ether, the solubility issues would have probably been overcome.

With compound **207** in hand, conversion to the boronic acid was achieved by lithiation of the bromide followed by quenching with TIPB to give the desired boronic acid **210** as a foamy white solid as shown in Scheme 2.12.

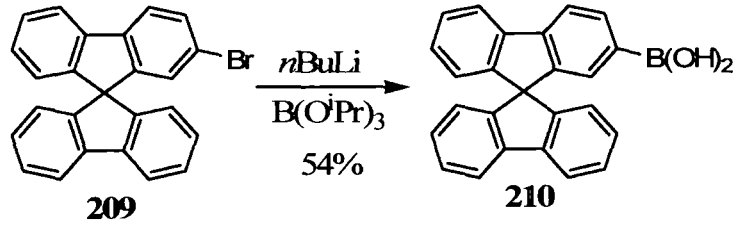

Scheme 2.12 Conversion to 9,9'-spirobifluoren-2-yl boronic acid

This boronic acid was reacted with compound **190** in another Suzuki-Miyaura cross-coupling reaction to yield the spiro-analogue of **202**, compound **211**, in 67% yield as shown in Scheme 2.13.

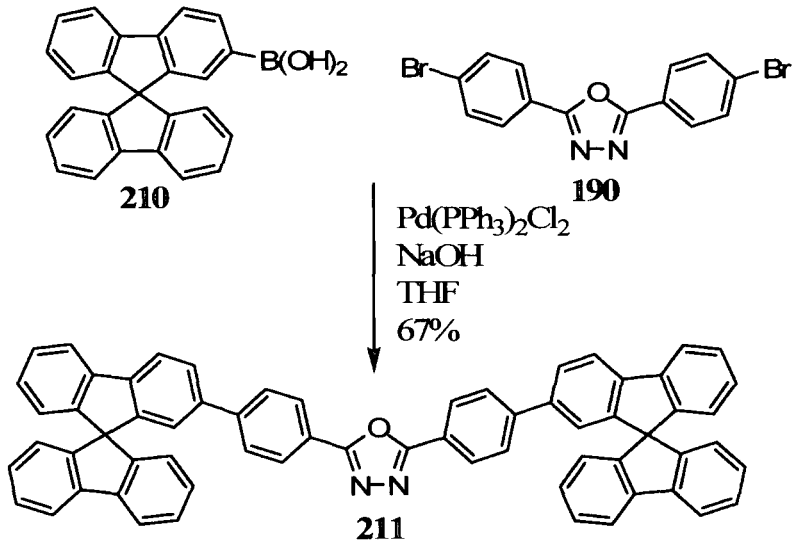

Scheme 2.13 Suzuki-Miyaura cross-coupling reaction to yield spirobifluorene compound 211

The synthesis of a copolymer was attempted as shown in Scheme 2.14. However, due to a lack of solubility, the material precipitated out after only a few hours of reflux and thus the desired polymer was not obtained.

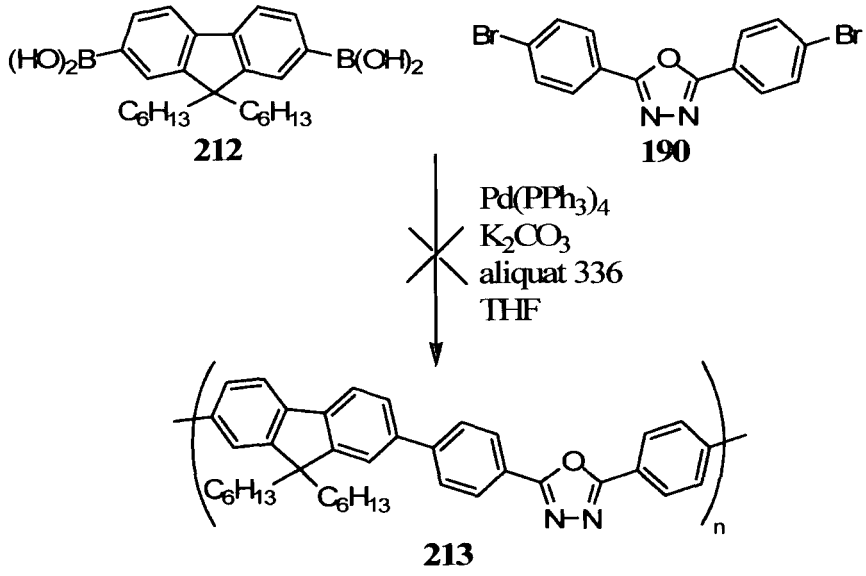

Scheme 2.14 Failed attempt to create a copolymer

The experiment was repeated using the diboronic ester **215** – synthesised as shown below in Scheme 2.15 – with the same result: insufficient solubility of the growing polymer chain leading to a mix of oligomers.

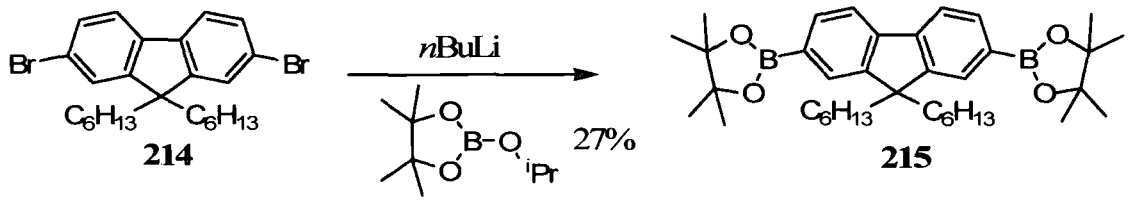

Scheme 2.15 Synthesis of the diboronic ester 215

Polymers were not the focus of this project so no further modifications to the monomers to improve solubility were made.

Our previous studies had shown that incorporation of the spiro unit into ET materials has no significant advantage over using 9,9-dihexylfluorene analogues.[58] The spiro unit improves colour purity in emissive materials, but for this study the materials are to be blended into MEH-PPV and function primarily as ET materials. Compound **202**, which was synthesised in larger quantities than the spiro analogue **211**, was the focus of device studies.

2.2.2 Theoretical Calculations

Density functional theory (DFT) calculations were carried out on compound **202** by Dr I. F. Perepichka in our group. Calculations were carried out on the molecule in both *syn* and *anti* configurations at the B3LYP/6-31G(d) level. In geometry optimisations both configurations gave nearly identical energy minima (with a difference of only 0.03 kcal mol^{-1}). The results of the calculations are shown below in Figure 2.1.

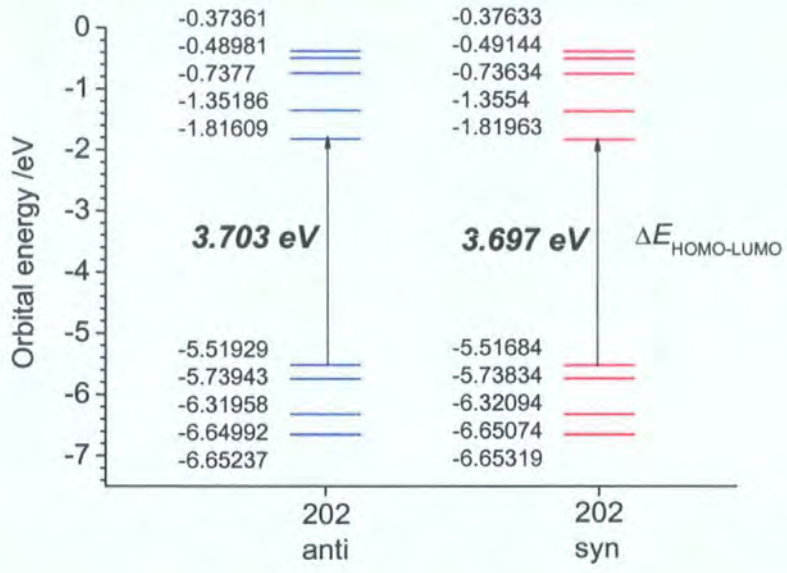

Figure 2.1 HOMO – LUMO levels of compound 202 from DFT calculations

The HOMOs and LUMOs of the *anti* configuration are shown below in Figure 2.2 and those of the *syn* configuration are shown in Figure 2.3. As with the energy, the locations of the HOMO and LUMO are very similar in both cases.

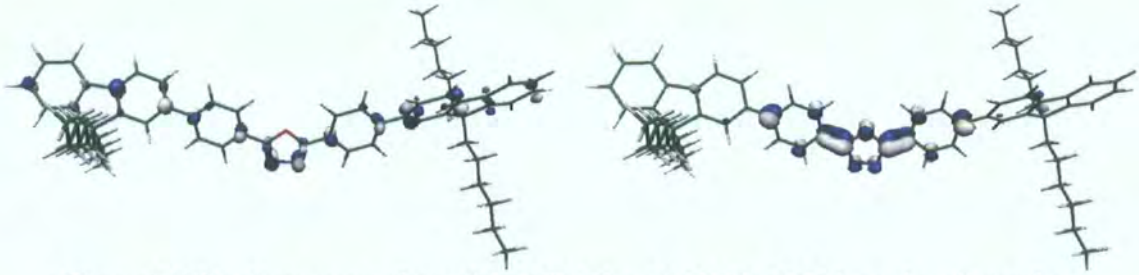

Figure 2.2 Visual representations of the HOMO and LUMO of 202 in *anti* configuration

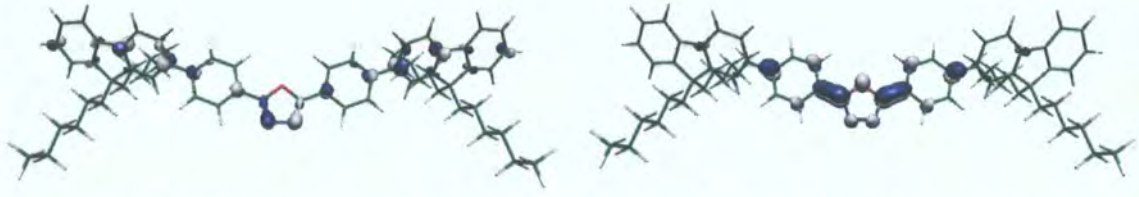

Figure 2.3 Visual representations of the HOMO and LUMO of 202 in *syn* configuration

2.2.3 Blended Device Studies

Devices were fabricated by N. E. Widdowson in the group of Prof. M. C. Petty in the School of Engineering, University of Durham. Devices consisted of **202**:MEH-PPV of 0:100, 20:80, 50:50, 70:30, 95:5 and 100:0 by weight and were capped with either a 100 nm aluminium cathode or a calcium (15 nm):Al (10 nm) cathode. A photograph of some of the devices is shown in Figure 2.4.

Figure 2.4 The devices (left to right) 100%, 80%, 50%, 30%, 5% MEH-PPV and pure 202

2.2.3.1 Blends with Aluminium Cathodes

The current-voltage (*I-V*) and photocurrent-voltage characteristics of the devices were measured and the data are shown in Figure 2.5. The greatest benefit afforded to the devices by incorporating compound **202** was an increase in light output by up to two orders of magnitude due to compound **202** allowing for a more balanced transporting of charge. The highest level of emission came from the 50% blend which provided a 100-fold increase over that of pure MEH-PPV devices. By comparison, there was just a 3-fold increase over the least emissive blend.

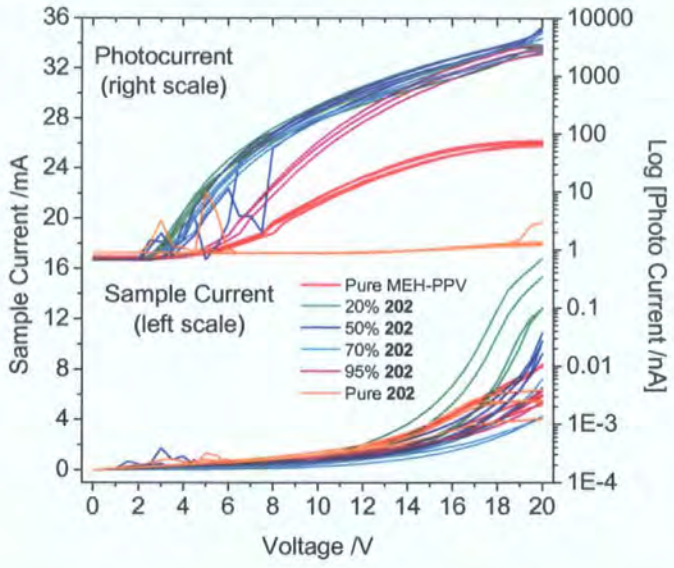

Figure 2.5 *I-V* and photocurrent data for the devices of configuration ITO/PEDOT:PSS/202:MEH-PPV/Al

As with previous fluorene-OXD molecules studied in blends,[58] increasing the blend ratio to 95% **202** did not adversely affect the light emission from the devices. By comparison, studies of PDPyDP (**67**) showed that 95% blends emitted two orders of magnitude less light than lower blend ratios.

Devices containing 100% **202** were found to be electrically conductive but no visible light was emitted which suggests that the current in these devices was due to the flow of electrons from the cathode to the anode.

Turn-on voltages were reduced from 6 V in the pure MEH-PPV devices to between 2.5 V and 3.5 V for the 20%, 50% and 70% blends. Although the LUMO levels of compound **202** and MEH-PPV are similar, the lower turn-on voltages exhibited by the blends suggest that the LUMO of compound **202** lies between the LUMO of MEH-PPV and the cathode's work function helping to lower the barrier to electron injection.

The EQEs for the devices are shown in Figure 2.6. The 50% and 70% blends showed the highest EQEs of approximately 0.1% representing a 65-fold increase over that shown by the pure MEH-PPV device.

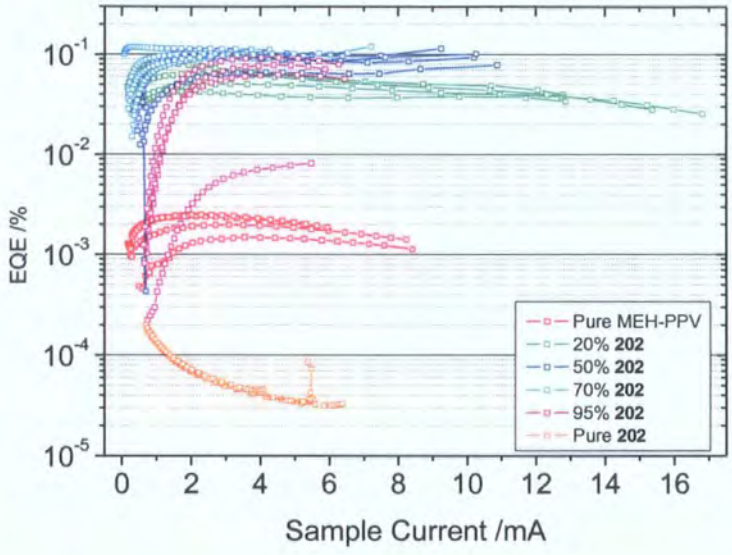

Figure 2.6 EQE data for the devices of configuration ITO/PEDOT:PSS/202:MEH-PPV/Al

Stability tests were performed at a constant current of 0.56 mA. The photocurrents and voltages are shown as a function of time in Figures 2.7a and 2.7b.

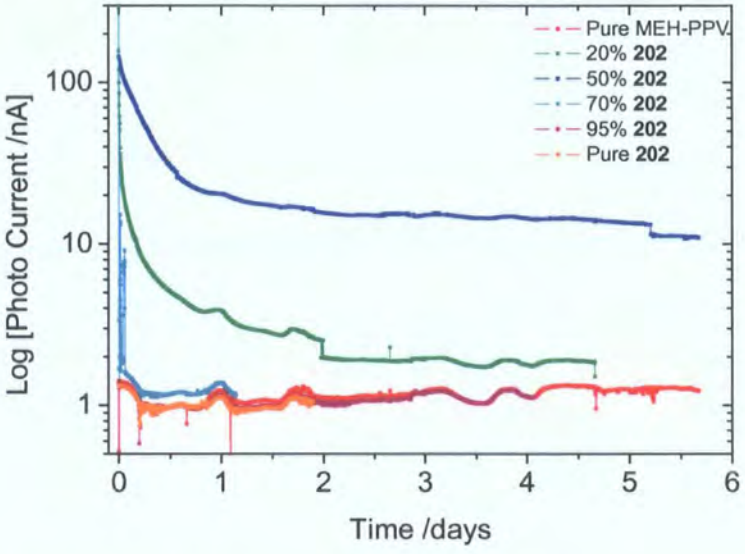

Figure 2.7a Stability data for devices of configuration ITO/PEDOT:PSS/202:MEH-PPV/Al: photocurrent vs time

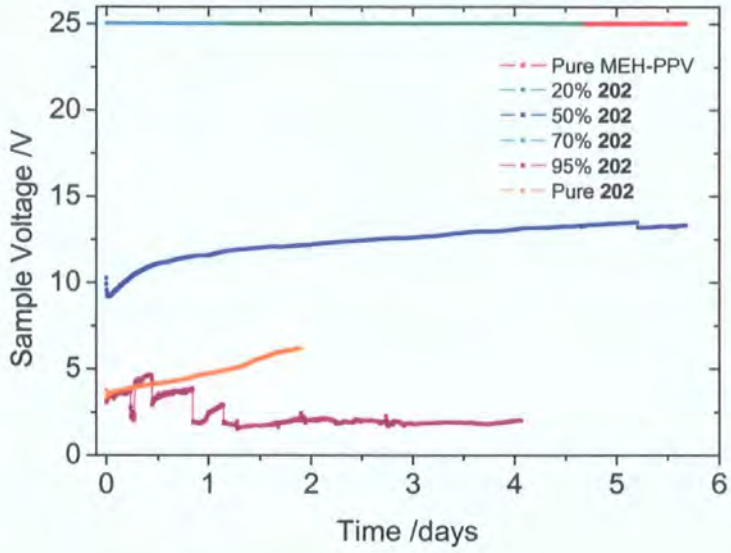

Figure 2.7b Stability data for devices of configuration ITO/PEDOT:PSS/202:MEH-PPV/Al: sample voltage vs time

The 50% device was found to be the most stable and it was also the only blend with visible light not to immediately reach the 25 V threshold immediately. The other blends reached 25 V as a result of the measurement apparatus trying to maintain a constant current and it is unlikely that the 0.56 mA current was maintained at 25 V. Increasing the amount of compound **202** in the devices results in an increased probability of molecularly encapsulating the MEH-PPV chains resulting in higher stability over pure MEH-PPV devices. However, above 50% it appears that any decay which affects the small amount of MEH-PPV in the blend could significantly affect the balance of charge flow through the device as demonstrated by the lack of visible light emitted from the 100% **202** device.

2.2.3.2 Blends with Calcium Cathodes

A second batch of devices featuring the same blend ratios and a 15 nm layer of calcium between the blend and aluminium were fabricated and tested. The *I-V* and photocurrent characteristics are shown in Figure 2.8. With the addition of calcium the pure MEH-PPV now emitted more light than the blends and the voltages and currents required to generate a set level of light emission were lower than those required for the devices

with aluminium cathodes. For example a 50% blend with a calcium cathode required 7.5 V and 0.5 mA to achieve a photocurrent of 1 mA whilst the same blend with an aluminium cathode required 14 V and 2 mA to achieve the same photocurrent.

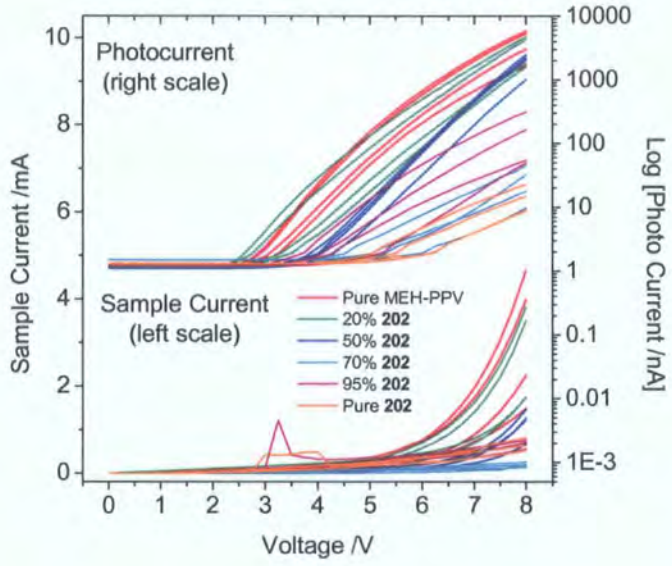

Figure 2.8 *I-V* and photocurrent data for devices of configuration ITO/PEDOT:PSS/202:MEH-PPV/Ca:Al

Whereas the aluminium cathodes led to increased light output as the amount of compound **202** in the blend increased, the calcium cathode devices showed the opposite trend. A 70% blend emitted light averaging 25 nA with a calcium cathode whilst the 20% blend emitted light averaging 2.5 mA. This lowering of light output with increasing incorporation of compound **202** is attributed to electrons outnumbering holes in the device caused by the increasing amount of compound **202** present.

The EQEs for the calcium cathode devices are shown in Figure 2.9. The greatest EQE of 0.25% was from the 50% blend device although this was only slightly greater than the value of 0.20% obtained for the pure MEH-PPV device. Increasing the incorporation of compound **202** above 50% led to an imbalance of charge carriers and therefore lowered the EQE of the 70% and 95% blends.

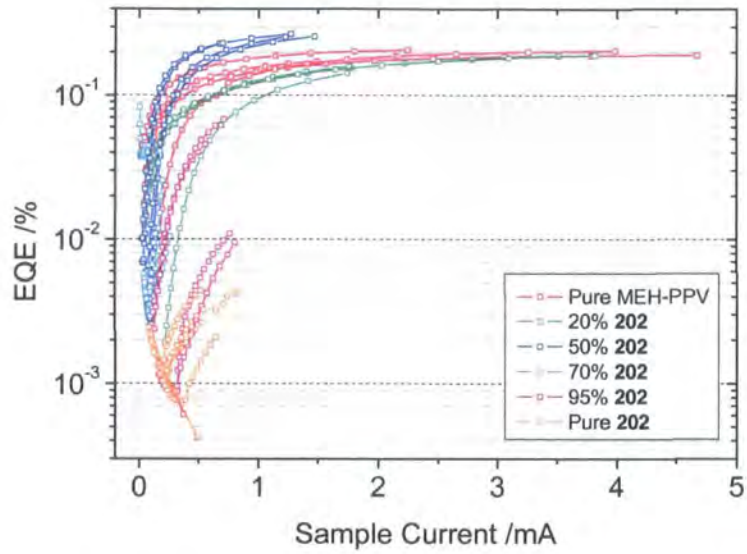

Figure 2.9 EQE data for the devices of configuration ITO/PEDOT:PSS/202:MEH-PPV/Ca:Al

Stability tests were again performed at a constant current of 0.56 mA. The photocurrents and voltages are shown as a function of time in Figure 2.10a and 2.10b.

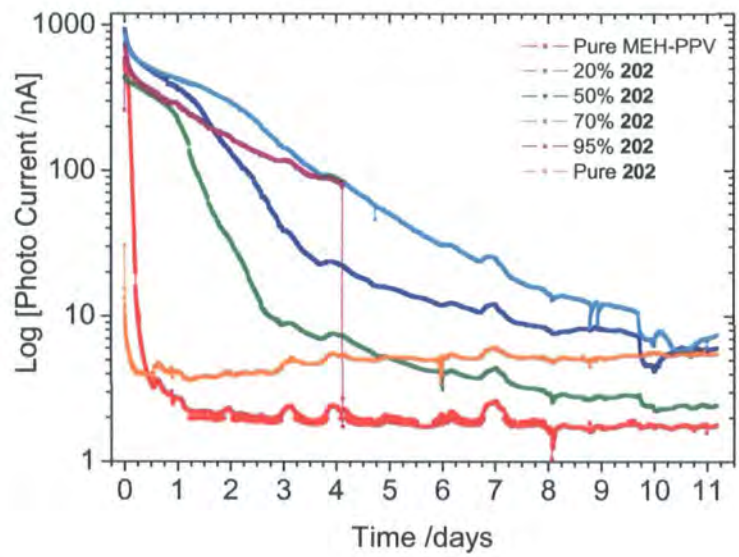

Figure 2.10a Stability data for the devices of configuration ITO/PEDOT:PSS/202:MEH-PPV/Ca:Al: photocurrent vs time

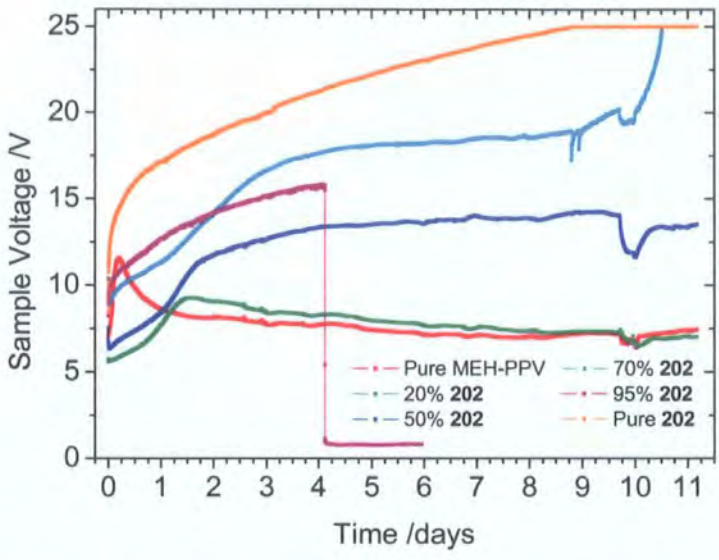

Figure 2.10b Stability data for the devices of configuration ITO/PEDOT:PSS/202:MEH-PPV/Ca:Al: sample voltage vs time

The calcium cathode devices were more stable than the aluminium cathode devices. This can be attributed to the lower voltages and currents found in the calcium cathode devices which in turn mean that the calcium cathode devices experience smaller electric fields and lower current densities which are known to accelerate device decay. Whilst most of the aluminium cathode devices reached the 25 V threshold almost immediately, only one of the calcium cathode devices reached it over the eleven day testing period. After three days, only one of the aluminium cathode devices still emitted visible light, but three of the calcium cathode devices continued to emit visible light after the same amount of time.

The half-lives of the calcium cathode devices are shown in Figure 2.11. There appears to be a relationship between the blend ratio and stability. The 95% blend showed the highest stability with a half life of 63 hours.

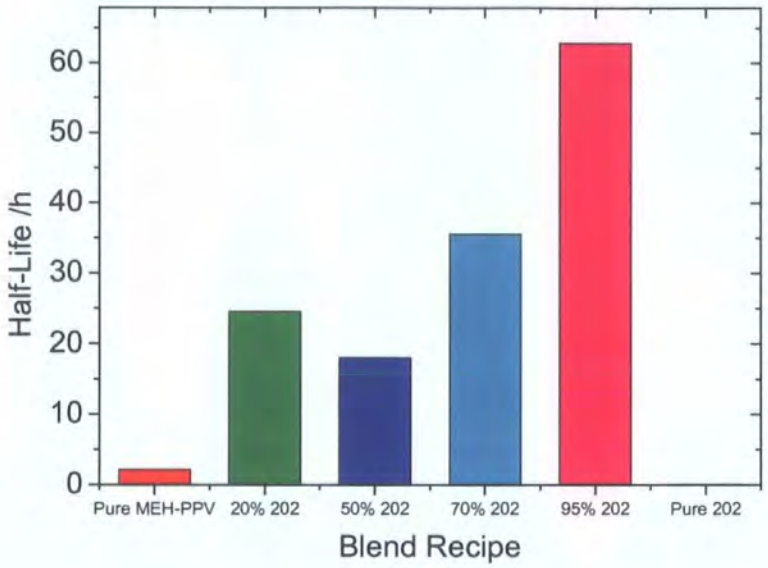

Figure 2.11 Half lives of the devices of configuration ITO/PEDOT:PSS/202:MEH-PPV/Ca:Al

Unlike previous fluorene-OXD studies[58] the EL spectrum of the blended devices had the same peaks as pure MEH-PPV devices (λ_{max} = 580 nm and 615 nm). The only variations were in the relative peak height and width of the shoulder as shown in Figure 2.12.

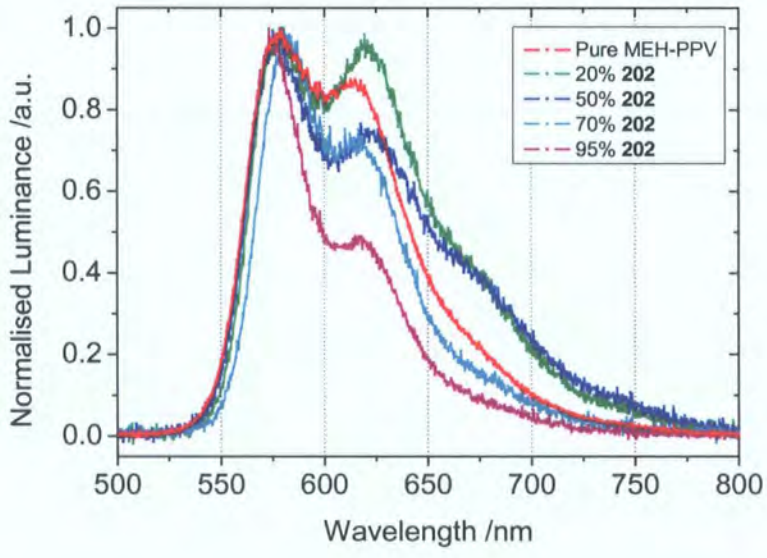

Figure 2.12 EL spectra for the devices of configuration ITO/PEDOT:PSS/202:MEH-PPV/Ca:Al

Further studies of the devices, including AFM analysis of anode degradation in the devices, are discussed in the thesis of N. E. Widdowson.[132]

2.3 Conclusions

The benefits of the tetrazole route to OXD materials have been demonstrated – a lower number of steps and generally higher-yielding reactions compared to the hydrazide route. Using this methodology, the known compound PDPDP (**65**) has been synthesised, a potential route to well-defined oligomeric 1,3,4-oxadiazole compounds has been identified and a small library of OXD materials has been synthesised. One of these compounds has been used to synthesise the new fluorene-containing OXD materials **202** and **211**. With previous studies indicating no advantage in using 9,9-spirobifluorene-containing moieties over 9,9-dialkylfluorene-containing moieties in ET materials, compound **202** was tested as an ET material in blends with MEH-PPV. Devices with both aluminium and calcium cathodes were fabricated. It has been shown that the light output, EQE and stability of the devices can be influenced by varying not only the blend compositions but also the nature of the cathode used. The maximum light output was obtained from a pure MEH-PPV device with a calcium cathode, the highest EQE was obtained from the 50% blend with a calcium cathode and the most stable device was produced with the 95% blend and a calcium cathode. The 50% and 70% blends with calcium cathodes gave the best overall balance of light output, EQE and stability.

Chapter 3 – New Bipolar Triad Molecules for Balanced Charge-Transport

3.1 Introduction

As reviewed in Chapter 1 the ideal OLED would contain materials which facilitate balanced charge injection and transport. In Chapter 2 ET molecules were designed and synthesised that could be blended into emitters which transport holes to provide balanced charge transport. While this approach has successfully produced films with little evidence of phase segregation in MEH-PPV blends, an alternative approach is to

combine the emitting, ET and HT units into one molecule. This strategy negates the possibility of phase segregation whilst still allowing for single-layer devices which are easier to fabricate than those with multilayer structures. Bipolar diad molecules have been discussed in Chapter 1.5, however, very little work has been carried out on bipolar triad materials that also incorporate the emitter in the structure. Tamoto *et al.* synthesised five bipolar emitting materials based on 1,3,4-oxadiazole and triphenylamines (**216** – **220**)[133] which emit blue-green EL with wavelengths ranging from 450 – 490 nm.

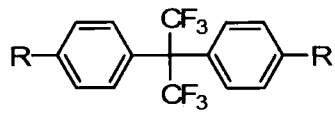

216

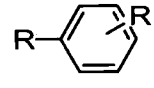

217 = *para*
218 = *meta*
219 = *ortho*

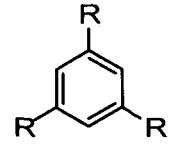

220

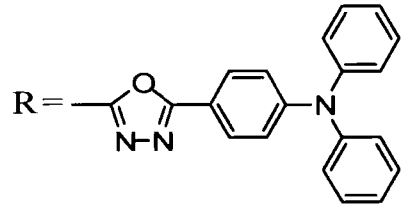

Antoniadis *et al.* synthesised a range of fluorene-oxadiazole-amine molecules with general structure **221** that were used in multilayered structures.[134] Rapid degradation of the devices was ascribed to exciplex formation at the organic interfaces.

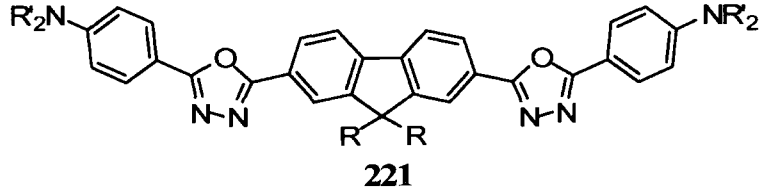

221

Yeh *et al.* furthered their work on tetraphenylmethanes by again incorporating 1,3,4-oxadiazole and triphenylamine units into the *para* and *meta* isomers of **222**.[56]

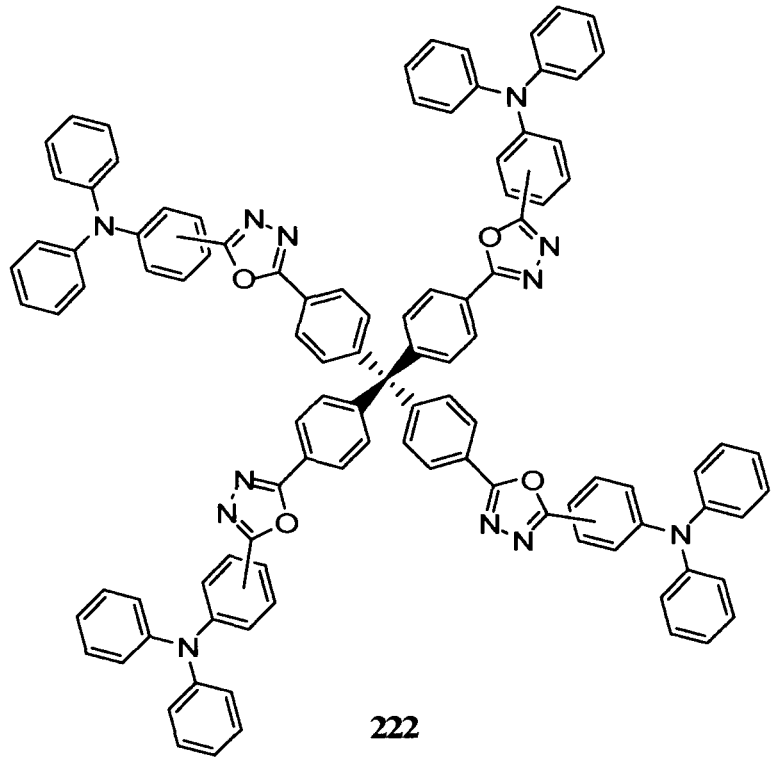

222

The *para* isomer was incorporated into a single-layer device that emitted blue-green light (λ_{max} ~485 nm) with a turn-on voltage of 8 V and a peak current efficiency of 0.7 cd A^{-1}.

Thomas *et al.* produced a series of bipolar triad materials incorporating 1,3,4-oxadiazole and quinoxaline as ET segments and triphenylamine and carbazole as HT segments including the fluorene containing compound **223**.[135, 136] Devices with this material turned-on at 3.0 V and gave efficiencies of up to 4.2%.

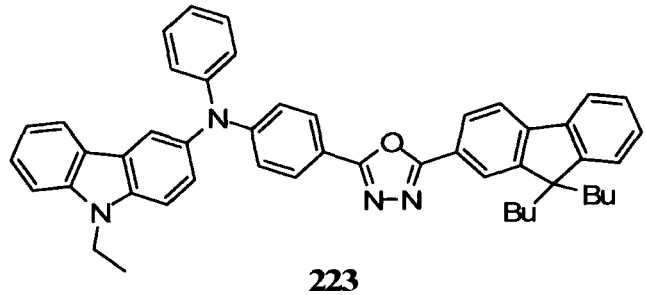

223

Chien *et al.*, Pudzich and Salbeck and Shen *et al.* produced bipolar 9,9'-spirobifluorene-based materials including **224**,[137] **225**[138] and **226**.[139] Device studies for the first two molecules have not been reported whilst an ITO/**226**/TBPI/Mg:Ag device

turned on at 3.3 V and displayed blue light (λ_{max} = 450 nm) with an EQE of 4.2% and maximum luminance of 8,390 cd m^{-2}.

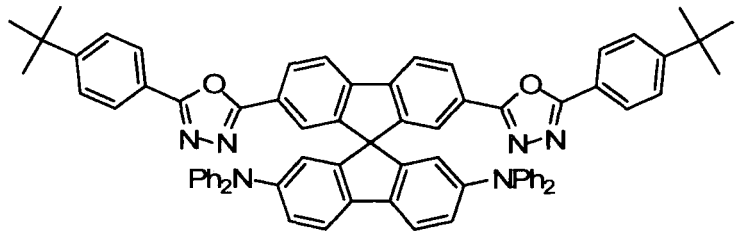

224

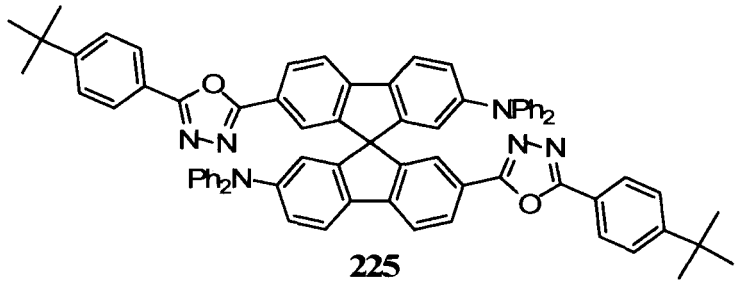

225

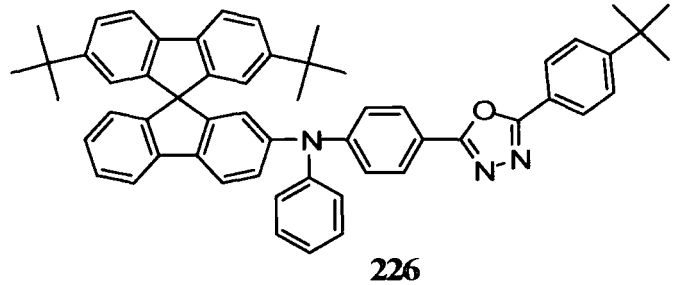

226

Finally Guan *et al.* reported blue-green emission from 2-(4-biphenylyl)-5-(4-carbazol-9-yl)phenyl-1,3,4-oxadiazole, **227**, with the device ITO/TPD/**227**/Alq_3/Mg:Ag producing blue light (0.14, 0.19) with a luminous efficiency of 2.25 lm W^{-1}.[140]

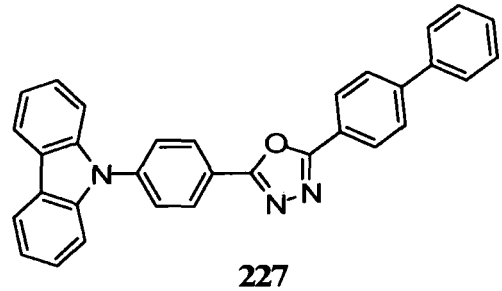

227

3.2 Results and Discussion

In our group the bipolar materials (**228** – **230**) had already been synthesised by Dr C. Wang.

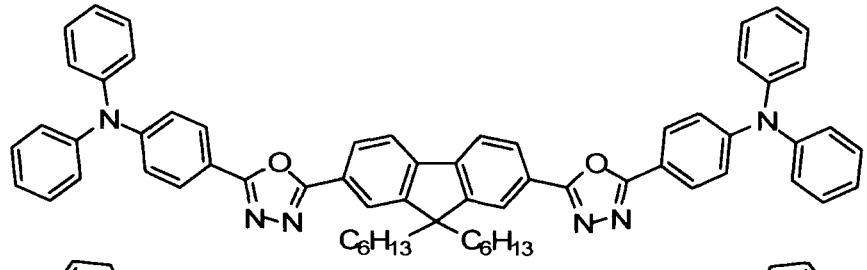

228

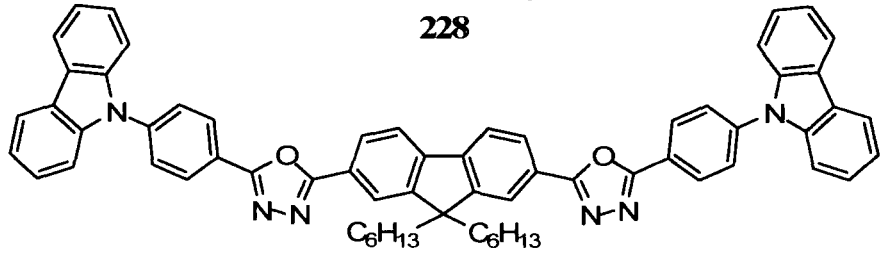

229

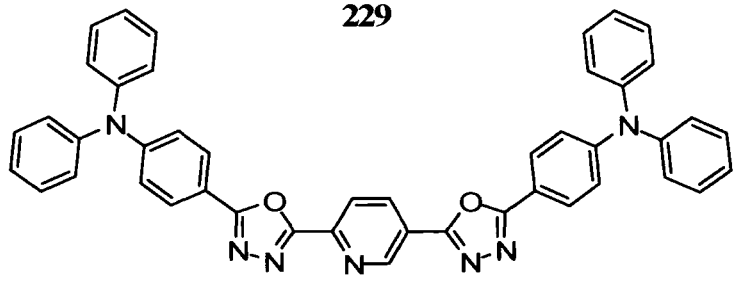

230

Initial device studies had focused on performance as charge transporting units in blends with MEH-PPV. These are symmetrical systems so to vary the optoelectronic properties we opted to synthesise an unsymmetrical "push-pull" system with the oxadiazole on one side of the fluorene unit and the triphenylamine on the other in a similar approach to that adopted by Patra *et al.*[141] To facilitate the attachment of different moieties at the 2 and 7-positions of fluorene it was necessary that one of these positions was reversibly blocked. Geng *et al.* had used a trimethylsilyl protecting group on monodisperse fluorene oligomers[142] which is easy to add to 2,7-dibromo-9,9-dihexylfluorene following careful monolithiation. The TMS group is stable to further lithiations and cross-coupling reactions. Deprotection to either the bromide[71] or

iodide[142] in high yields is then possible. Tavasli *et al.* in our group have utilised this strategy to synthesise fluorene oligomers up to pentamers.[127]

3.2.1 Synthesis

Reaction of commercially available 2,7-dibromofluorene with potassium *tert*-butoxide in the presence of an excess of 1-bromohexane afforded 2,7-dibromo-9,9-dihexylfluorene, **114**, in 86% yield as shown in Scheme 3.1.[57]

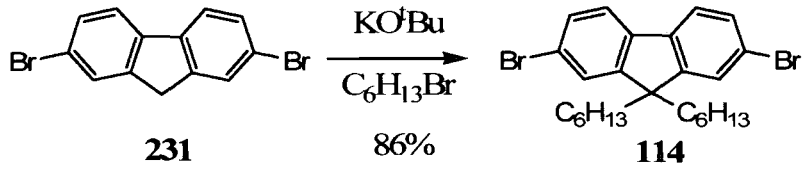

231 **114**

Scheme 3.1 Synthetic route to 2,7-dibromo-9,9-dihexylfluorene

Careful monolithiation of compound **114** followed by quenching with trimethylsilylchloride afforded 2-bromo-7-trimethylsilyl-9,9-dihexylfluorene, **232**, as a colourless oil. Compound **232** was then lithiated again, quenched with TIPB and hydrolysed with water to afford the TMS-protected fluoreneboronic acid, **233** (42% for both steps). When 2-isopropyl-4,4,5,5-tetramethyl-1,3,2-dioxaborolane was used instead of TIPB, the resultant boronic ester, **234**, was obtained cleanly and in higher yield (69% for both steps) than the boronic acid. These reactions are shown in Scheme 3.2.

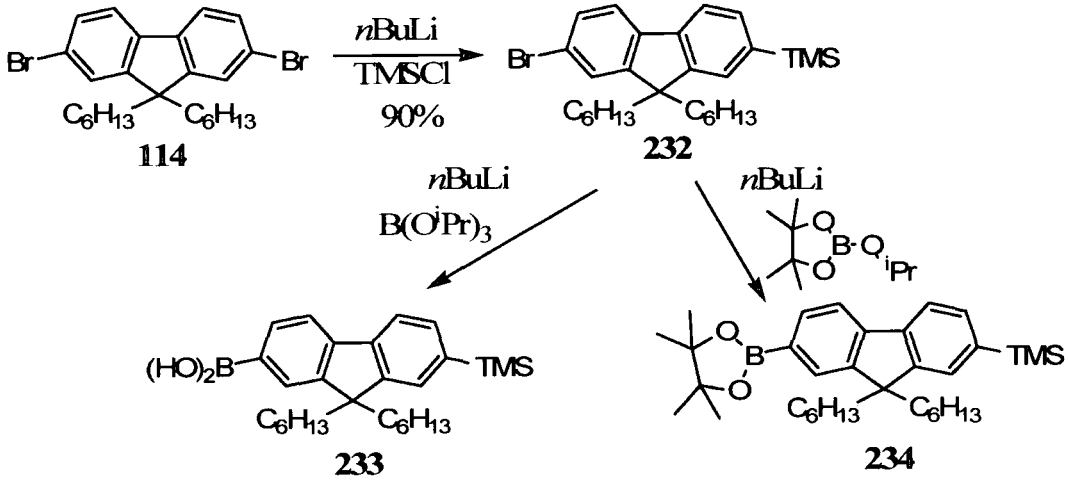

114 **232** **233** **234**

Scheme 3.2 Synthetic routes to TMS protected fluorene boronates

Suzuki-Miyaura cross coupling of compounds **189** and **234** afforded the fluorene-oxadiazole fragment **235** in 78% yield. Reaction of compound **235** with iodine monochloride in DCM gave the deprotected iodo-compound **236** in 90% yield as shown in Scheme 3.3.[142]

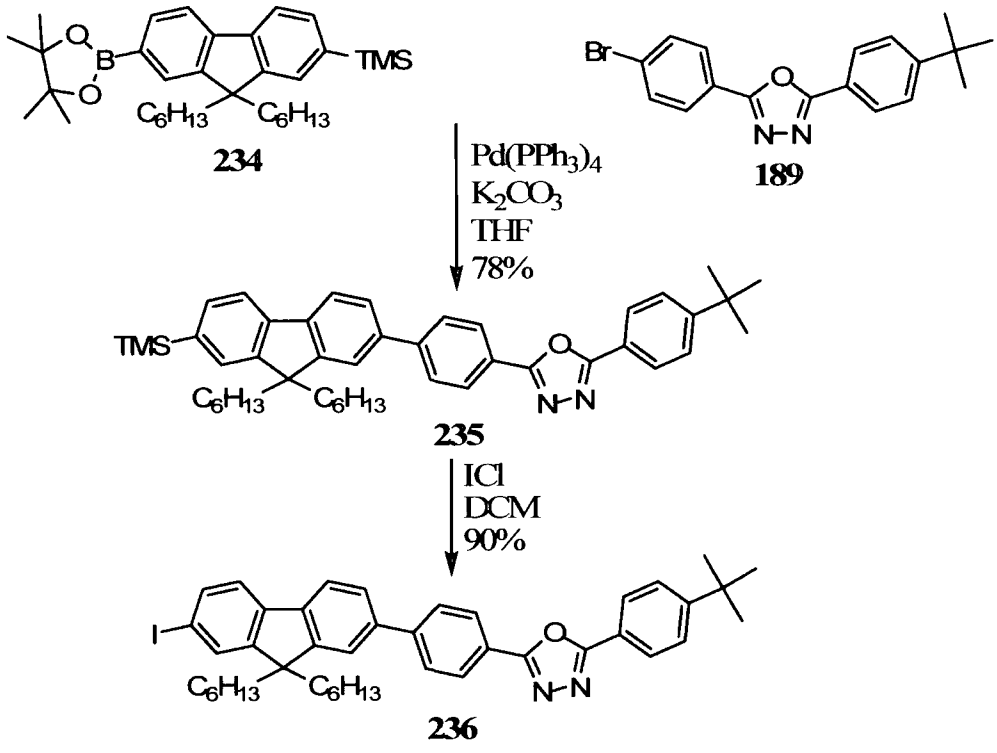

Scheme 3.3 Use of compound 235 as a masked halide

With compound **236** in hand Ullmann copper-catalysed C-N bond-forming conditions[143] were employed with diphenylamine to complete the synthesis of the target material **237** as shown in Scheme 3.4.

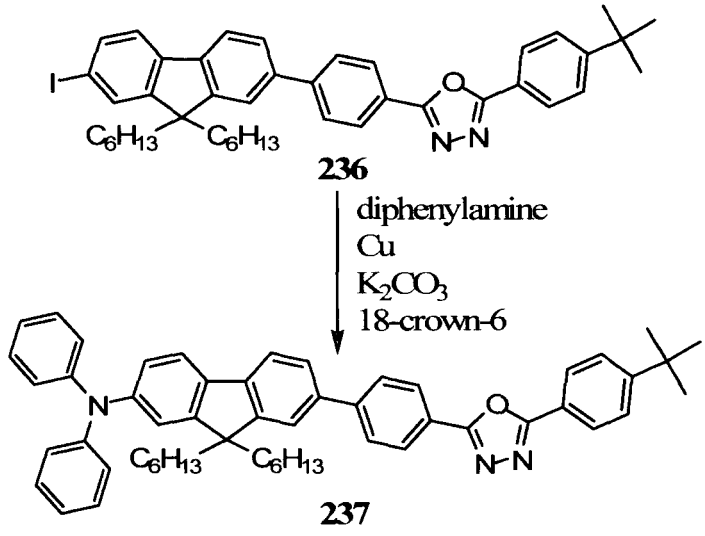

Scheme 3.4 Attempted Ullmann coupling of compound 236

Purification was effected through column chromatography. However, even though the ^{1}H and ^{13}C NMR and mass spectrum were correct, CHN elemental analysis consistently reported that the material contained 1% less carbon than expected. Repeated columns did not improve the purity. Dr C. Wang's compound **228** also had this problem – in this case though, recrystallisation from cyclohexane afforded the pure product **228**, but compound **237** does not crystallise due to the triphenylamine end cap, instead forming thin films.

Returning to the TMS protected material, compound **235**, conversion to the bromide in the presence of bromine and sodium acetate formed compound **238** in 93% yield as shown in Scheme 3.5.

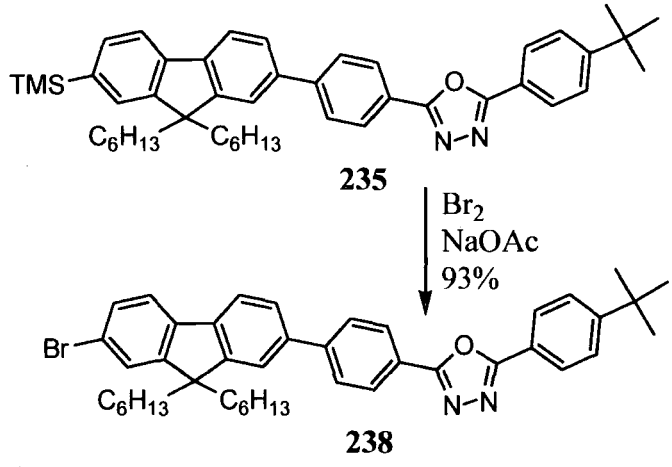

Scheme 3.5 Deprotection to yield the bromide derivative

Utilising the Buchwald-Hartwig palladium-catalysed cross-coupling reaction[144-146] diphenylamine was attached to the fluorene-OXD unit in 90% yield as shown in Scheme 3.6. The catalyst system used was tris(dibenzylideneacetone)dipalladium with a tri-*tert*-butylphosphine ligand. After running the crude product through one column, elemental analysis and NMR data confirmed the high purity of 2-(4-*tert*-butylphenyl)-5-[4-(9,9-dihexyl-2-bromofluoren-7-yl)phenyl]-1,3,4-oxadiazole, **237**, which is a yellow, highly fluorescent solid.

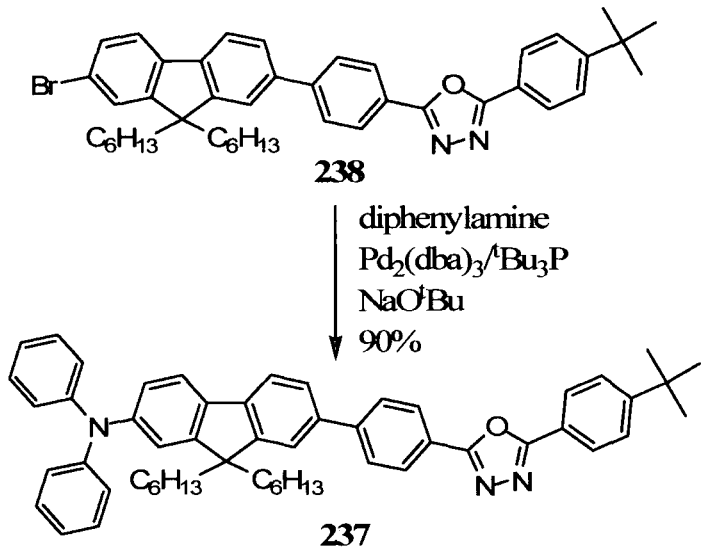

Scheme 3.6 Buchwald-Hartwig cross-coupling

Due to the nature of the final step – the addition of diphenylamine – the use of aniline should allow further groups to be attached. Initially, it was planned to react two equivalents of compound **238** with aniline to create the long symmetrical molecule **240** as shown in Scheme 3.7. However the reaction yielded no products.

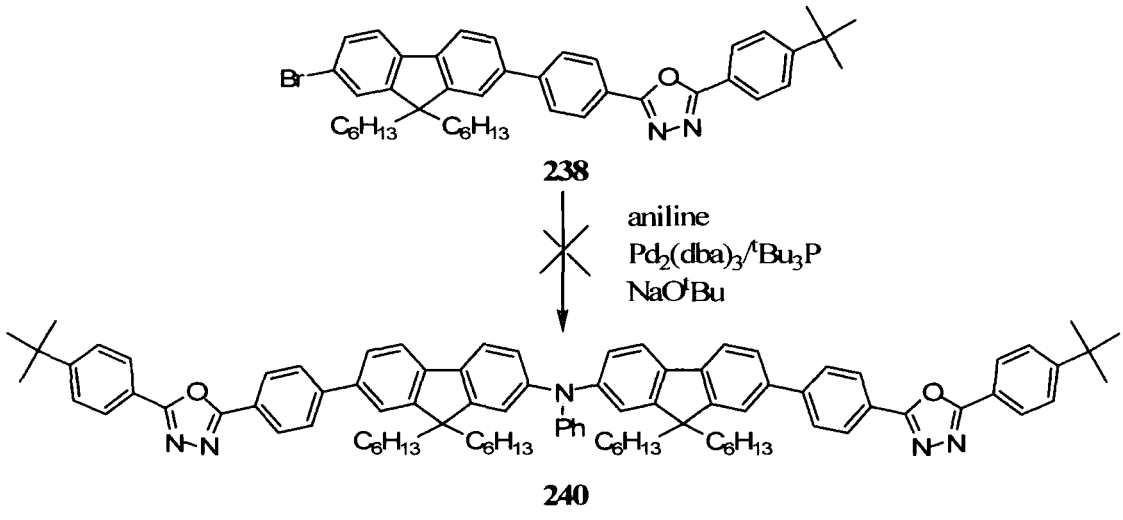

Scheme 3.7 Attempted bicoupling of 238 to aniline

Instead, reaction of compound **238** with an excess of aniline resulted in the secondary amine **239** being cleanly obtained in 81% yield and coupling of a further equivalent of compound **238** produced the desired compound, **240**, in 71% yield as shown in Scheme 3.8.

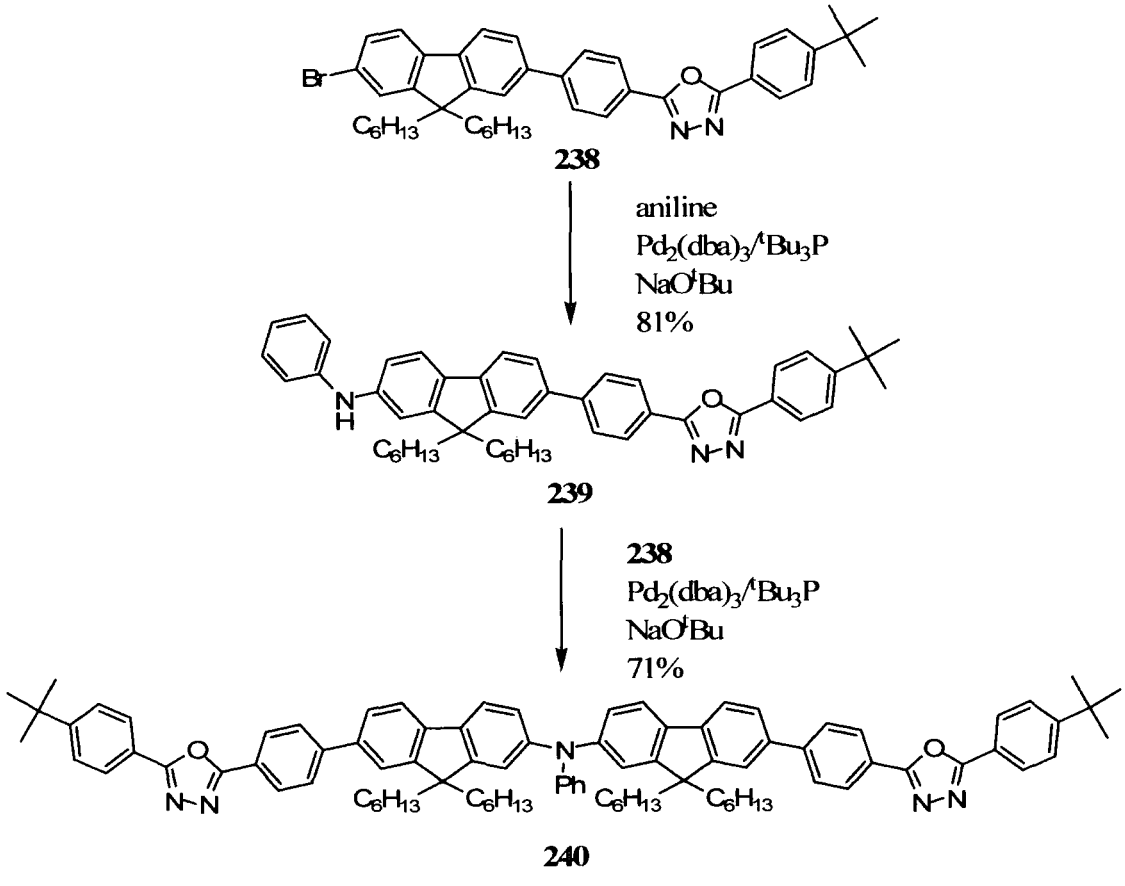

Scheme 3.8 Two step synthetic route to compound 240

3.2.2 X-Ray Analysis

The crystal structures of **235**, **238** (crystals grown by Dr S. L. Bettington) and **189** were solved by Dr A. Batsanov and are shown in Figures 3.1 – 3.3. None of the molecules have crystallographic symmetry. In **238**, the *tert*-butyl group is disordered between two orientations which differ by a rotation of *ca.* 170 ° around the C(phenyl)–CMe_3 bond and a tilt of this bond by *ca.* 19 ° (the tilt may involve the benzene ring also, but that was too small to resolve). The terminal methyl group of one of the *n*-hexyl chains is also disordered between two positions, which form short intermolecular contacts with the disordered *tert*-butyl group; hence both disorders must be correlated. The refinement of occupancy factors converged at 82.0(2)% and 18.0(2)% for the major and minor orientations, respectively. In both **235** and **238** the fluorene system is planar.

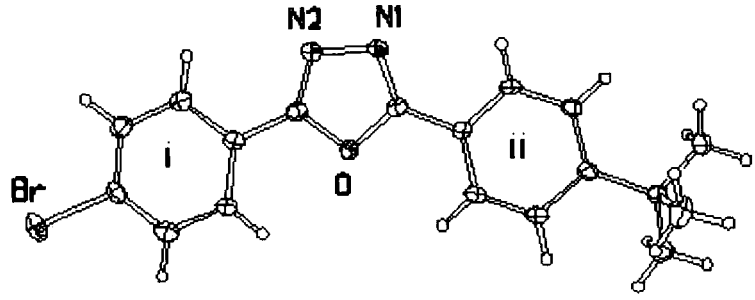

Figure 3.1 X-ray crystal structures of compound 189

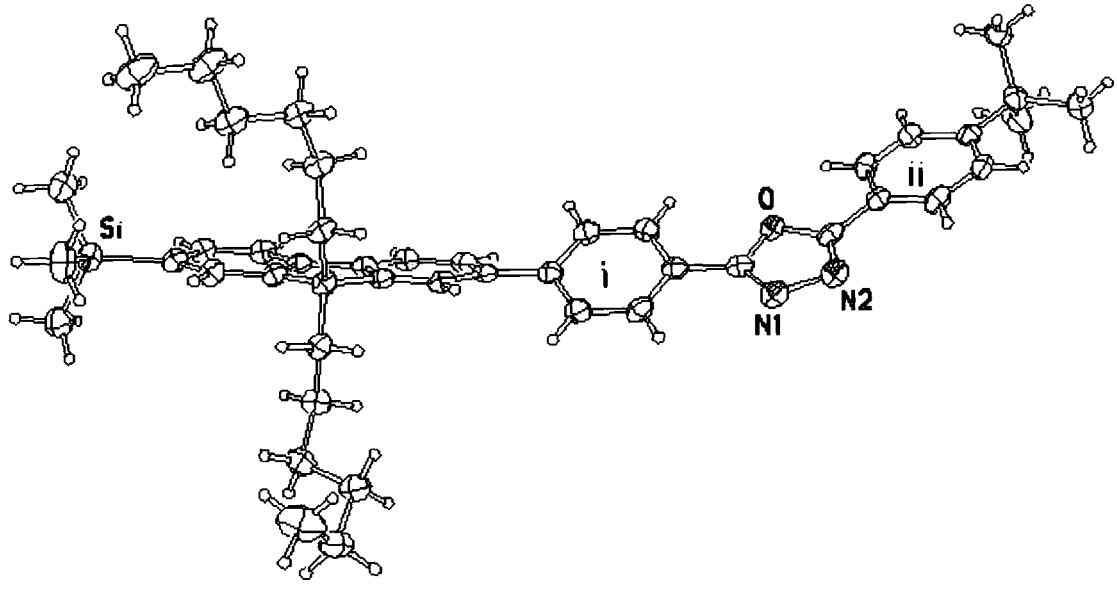

Figure 3.2 X-ray crystal structure of compound 235

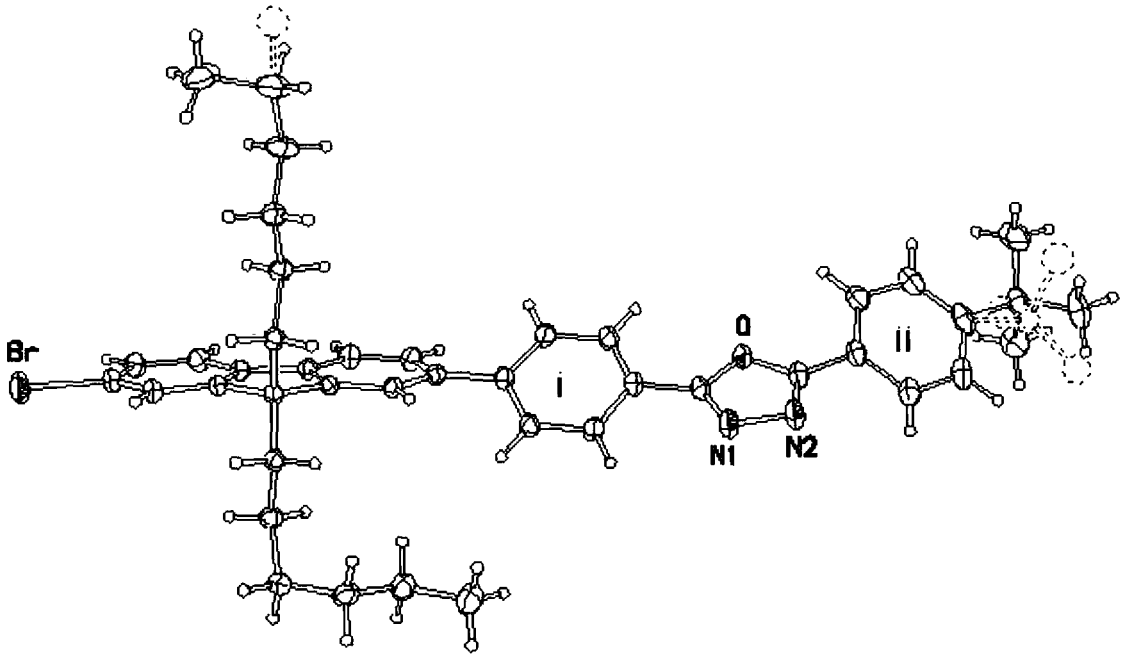

Figure 3.3 X-ray crystal structure of compound 238

3.2.3 Thermal Properties

Compounds **237** and **240** did not appear to display melting points up to 300 °C so differential scanning calorimetry (DSC) was used to probe their properties. The T_gs of compounds **237** and **240** are 76 and 146 °C respectively and no melting points were found up to 400 °C. Thermal gravimetric analysis (TGA) revealed that the molecules were stable up to 500 °C with a weight loss of < 5%.

3.2.4 Theoretical Calculations

Density Functional Theory (DFT) calculations were carried out on compounds **228**, **229**, **230**, **237** and **240** by Dr I. F. Perepichka in our group. As a comparison, the common ET material OXD-7 (**61**) was included in the calculations. To decrease the time taken for the calculations to run, the hexyl groups in compounds **228**, **229**, **237** and **240** were replaced by ethyl groups in the model compounds **228a**, **229a**, **237a** and **240a**. The results of the calculation at the B3LYP/6-311G(2d,p)//B3LYP/6-31G(2d) level are shown below in Figure 3.4.

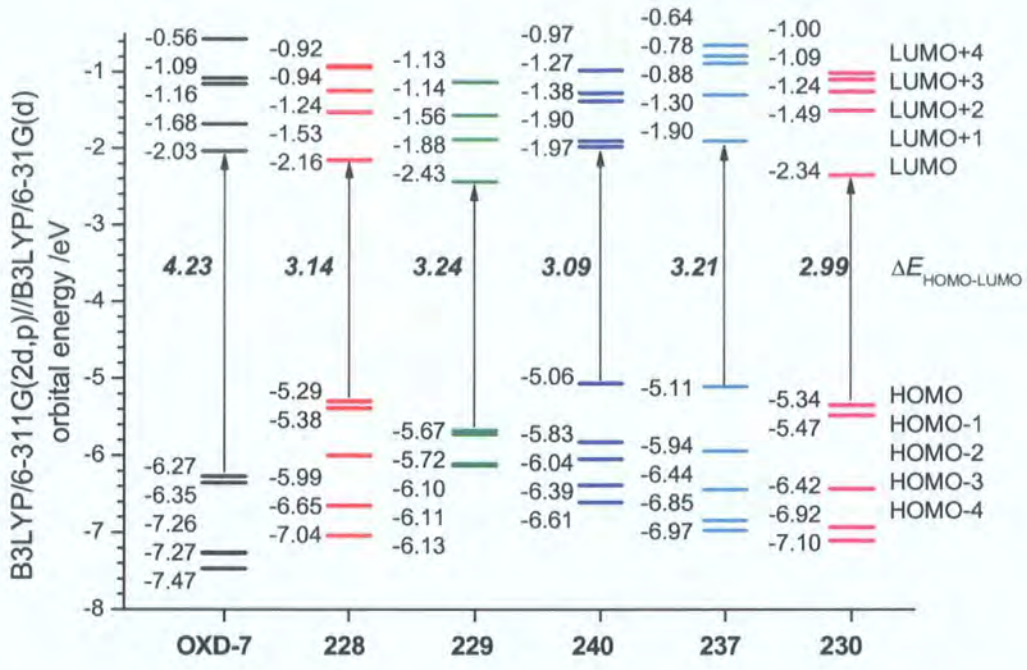

Figure 3.4 DFT calculated energy levels for compounds 228, 229, 240, 237, 230 and OXD-7

The calculations show that **228, 229** and **230** possess lower LUMO levels than OXD-7 indicating a better ET ability by facilitating easier injection of electrons from a calcium cathode (at energy level -2.87 eV).[27] Compound **230** has the lowest lying LUMO due to the substitution of the central fluorene core for a more electron-deficient pyridine. All the new compounds show HOMOs above that of OXD-7 by 0.6 – 1.02 eV. This is expected due to the bipolar nature of the new triarylamine-containing compounds. Compound **229** shows the lowest lying HOMO of all the compounds in this series and is the furthest from the energy level of ITO which is *ca.* -4.7 eV. This suggests that this molecule will have the worst performance in single-layer devices as although it has an excellent ET ability, its poor HT ability will hinder balanced injection and transport of charges. Visualisations of the HOMOs and LUMOs are in Appendix A.

3.2.5 Electrochemical Studies

The electrochemical properties of the compounds were investigated with assistance from Dr I. F. Perepichka by performing cyclic voltammetry (CV) in benzonitrile solution using tetrabutylammonium hexafluorophosphate (Bu_4NPF_6) as the supporting electrolyte. Compounds **237** and **240** undergo reversible single-electron oxidation to

form radical cations followed by a second non-reversible oxidation process. The extended conjugation of **240** compared to **237** lowers the first oxidation potential from +0.60 to +0.57 V, which is in good agreement with the theoretical calculations. Reduction of both compounds occurs at high negative potentials (< -2 V) and are irreversible processes. Compounds **228, 229** and **230** all possess two triarylamine groups and their oxidation processes are irreversible or only partly reversible.

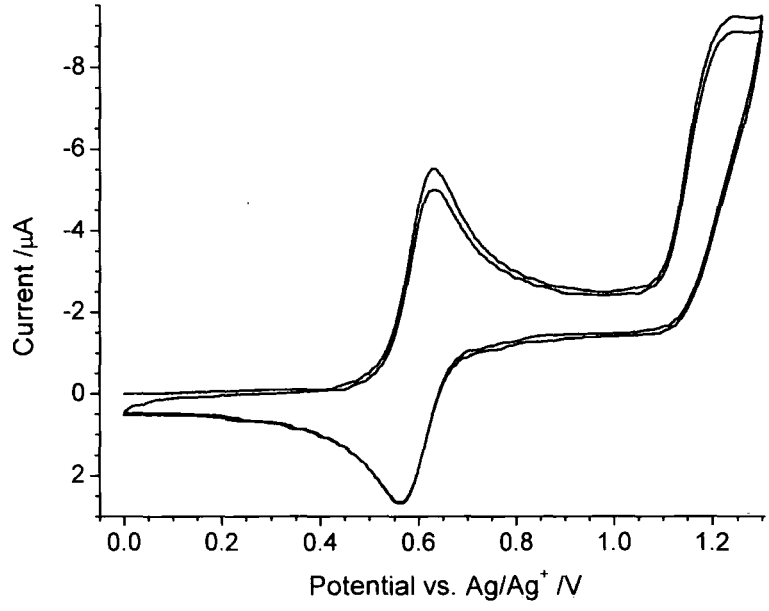

Figure 3.5 CV of compound 237 at 100 mV s^{-1}

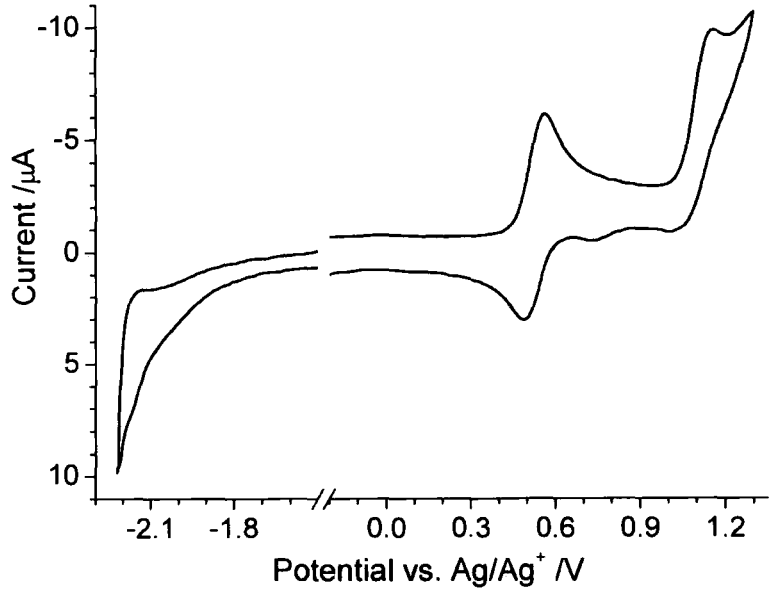

Figure 3.6 CV of compound 240 at 100 mV s^{-1}

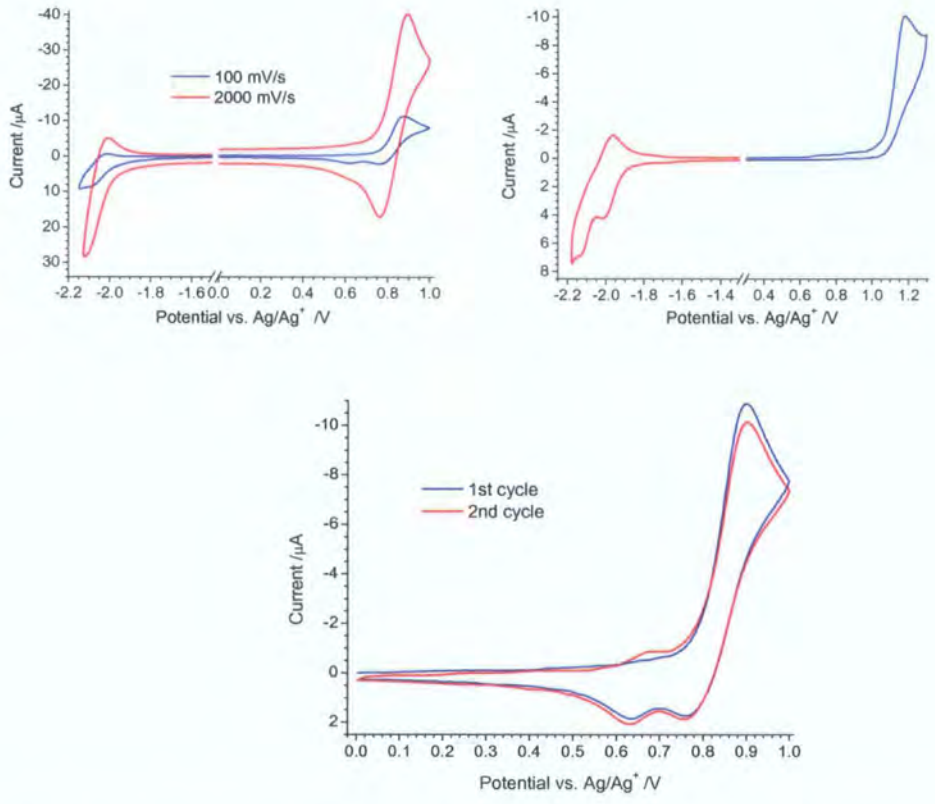

Figure 3.7 CVs of (clockwise from top left) compound 228 at 100 and 2000 mV s^{-1}, compound 229 at 100 mV s^{-1} and compound 230 at 100 mV s^{-1}

At scan rates of *ca.* 100 mV s^{-1} an additional peak grew at potentials lower than those of the oxidation of the compounds **228**, **229** and **230**. Further studies revealed this was due to the electropolymerisation of the bifunctional triarylamines and subsequent deposition of the polymer films on the electrode surface. These investigations are detailed in the literature.[147] The CV data are displayed in Table 3.1.

cpd	E^{ox1} /V	E^{ox2} /V	E^{red} /V	E_g /V
228	E_{pa} = 0.88 E_{pc} = 0.77		E_{pc} ~ -2.06	2.71
229	E_{pa} = 1.13		$E_{1/2}$ = -1.99 (50 mV)	2.93
237	$E_{1/2}$ = 0.60 (60 mV)	E_{pa} = 1.24	-2.15	2.55
240	$E_{1/2}$ = 0.53 (81 mV)	E_{pa} = 1.18	-2.02, -2.16	2.37
230	E_{pa} = 0.89 E_{pc} = 0.78		$E_{1/2}$ = -1.76 (62 mV)	2.48

Table 3.1 Summary of the CV data – run at 298K in benzonitrile. Values in parentheses are peak-to-peak separations

3.2.6 Photophysical Studies

The UV-Vis absorption (shown in Figure 3.8) and photoluminescence spectra (shown in Figure 3.9) of the compounds in chloroform solution show an incremental red-shift in the sequence: λ_{max} (abs): **229**, 361; **237**, 380; **228**, 385; **240**, 399; **230**, 402 nm; λ_{max} (PL): **229**, 416; **228**, 452; **237**, 478; **240**, 483, **230**, 533 nm. The PL values for **228**, **237** and **240** fall within 30 nm of each other.

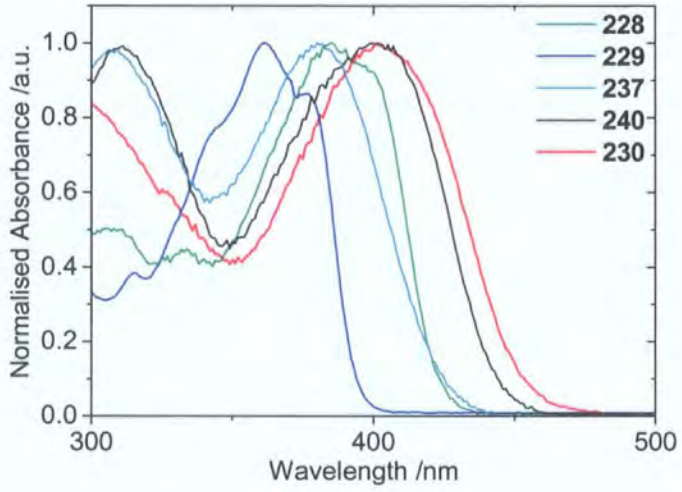

Figure 3.8 UV-Vis absorption for the compounds

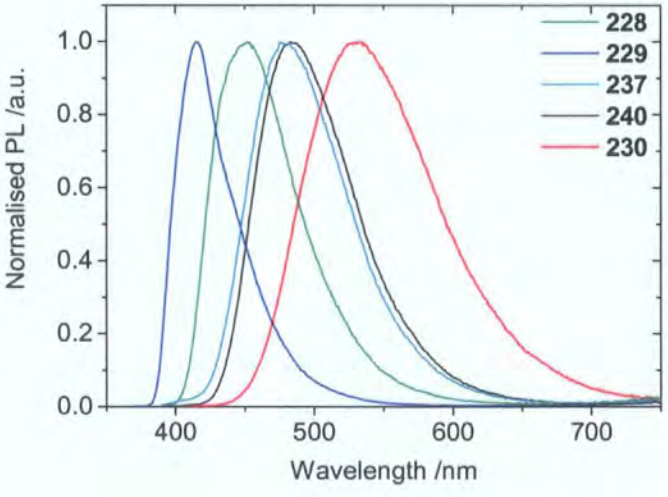

Figure 3.9 PL spectra for the compounds

Fluorescence quantum yields were measured in DCM solution against quinine sulphate and fluorescein standards. The fluorene-containing compounds possess very high

values, ranging from 0.86 – 0.93 whilst the pyridine containing compound **230** gave a value of 0.55. All the photophysical data are summarised in Table 3.2.

cpd	λ_{max} abs /nm	λ_{max} PL /nm	ϕ_f
228	385	452	0.86
229	361	416	0.87
237	380	478	0.92
240	399	483	0.93
230	402	533	0.55

Table 3.2 Summary of the photophysical data – run at 298K in chloroform

During the preparation of samples of **240** and **237** for NMR analysis it was noted that the materials displayed solvatochromatic behaviour. Further photoluminescence studies were undertaken in solvents of differing polarities. The results are shown in Figures 3.10 (compound **240**) and 3.11 (compound **237**).

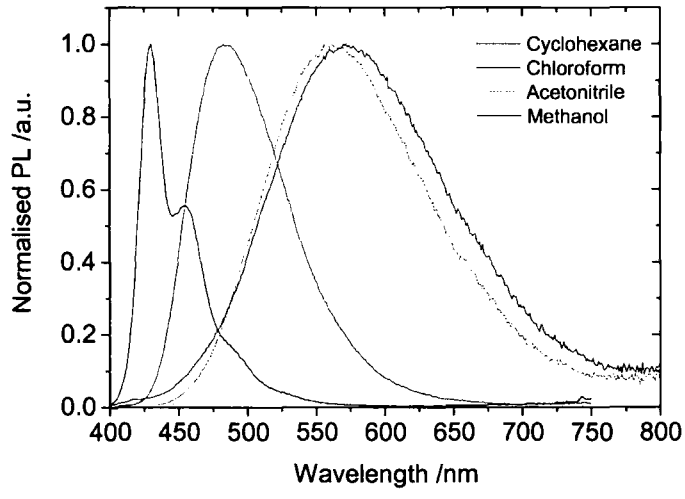

Figure 3.10 PL spectra of compound 240 in solvents of varying polarities

Compound **240** shows a 142 nm shift in PL between cyclohexane (λ_{max} = 430 nm, with a shoulder at 455 nm) and methanol (λ_{max} = 572 nm) with the λ_{max} values in chloroform and acetonitrile occurring at 483 nm and 562 nm respectively.

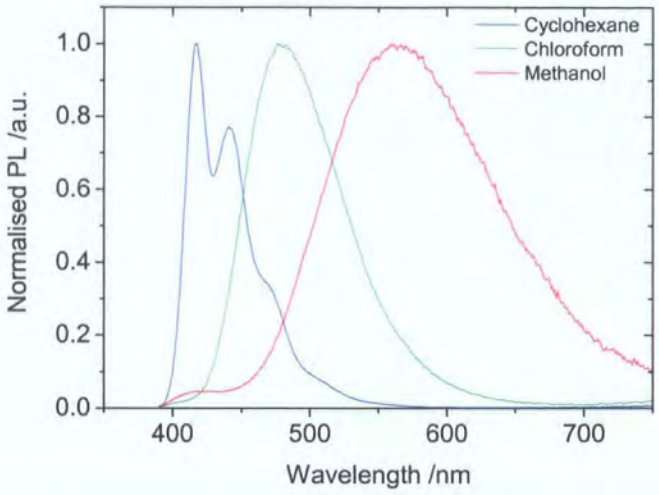

Figure 3.11 PL spectra of compound 237 in solvents of varying polarities

Compound **237** shows a 144 nm shift between cyclohexane (λ_{max} = 417 nm, with a shoulder at 440 nm) and methanol (λ_{max} = 561 nm) with λ_{max} in chloroform at 476 nm. The red-shift in increasing the solvent polarity indicates that the excited state is stabilised more by more polar solvents which leads to a reduction of the band gap and redder emission.

Although the spectra of the compounds in further solvents were not recorded, solutions of compound **237** in a range of solvents (hexane, toluene, DCM, IPA and DMSO) are shown under 365 nm wavelength UV light in Figure 3.12.

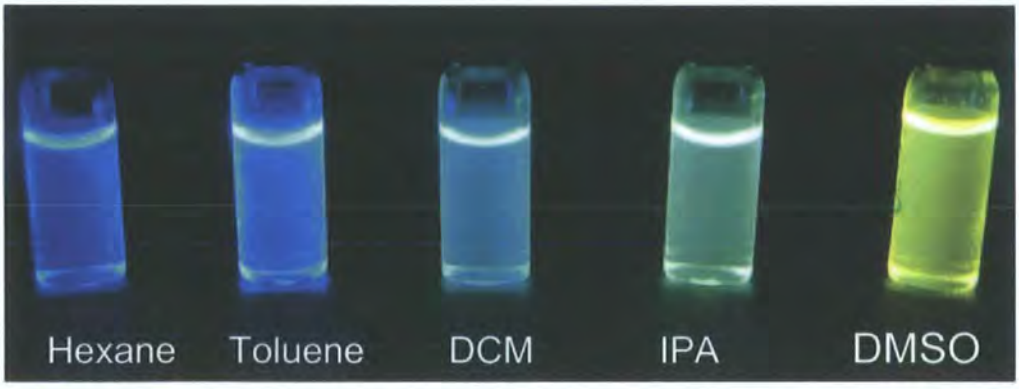

Figure 3.12 Compound 237 in various solvents under 365 nm UV light

3.2.7 Device Performance Studies

3.2.7.1 Triad Devices

Devices were fabricated by Dr J. H. Ahn in the group of Prof. M. C. Petty in the School of Engineering, University of Durham. Previous work (Chapter 1.3.2.2) has shown that incorporating a layer of PEDOT:PSS between the rough ITO surface and the organic layer can improve efficiencies by up to a factor of four.[58] The devices fabricated comprised ITO/PEDOT:PSS/compound/Ca:Al. The current versus voltage (*I-V*) and photocurrent versus voltage characteristics of these devices are shown in Figures 3.13 – 3.14.

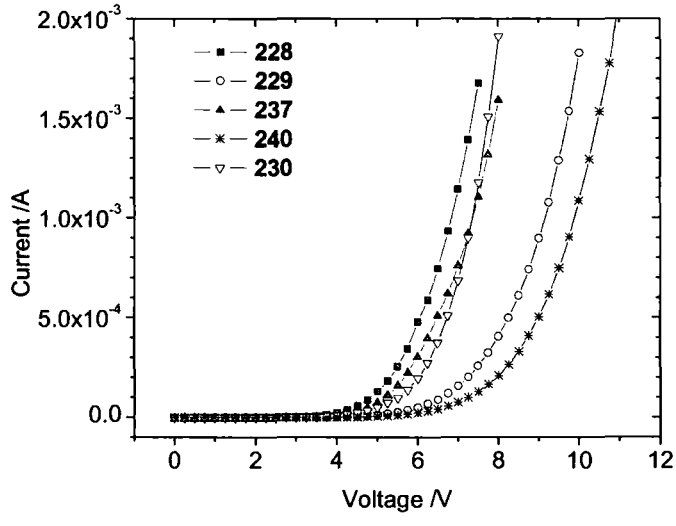

Figure 3.13 *I-V* characteristics of the devices

Compounds **228**, **237** and **230** show similar currents to each other. The currents of **229** and **240** were lower at the same bias. The voltage required for a current of 30 mA cm^{-2} was *ca.* 7 V for **228**, **237** and **230**, 9 V for **229** and 10 V for **240**.

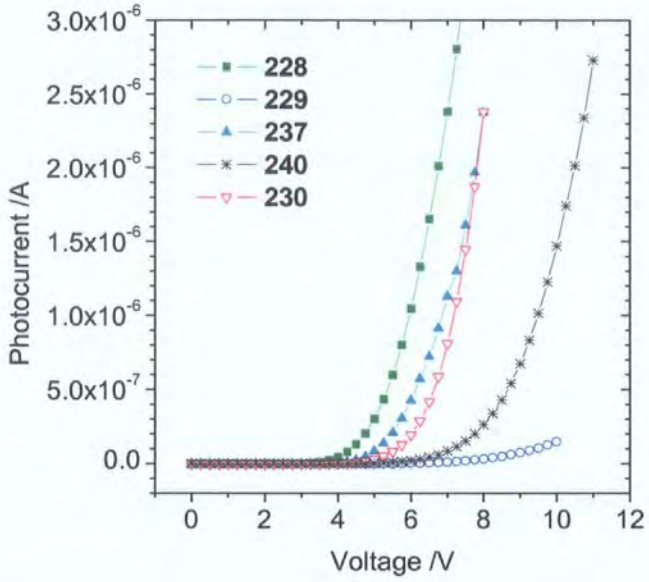

Figure 3.14 photocurrent characteristics of the devices

Light emission from the **240** device was noticeably lower than the other devices. The relative light emission at 7 V normalised to **240** was 157, 89, 7 and 64 for **228**, **237**, **229** and **230** respectively. The EQE versus current data for the devices is shown in Figure 3.15.

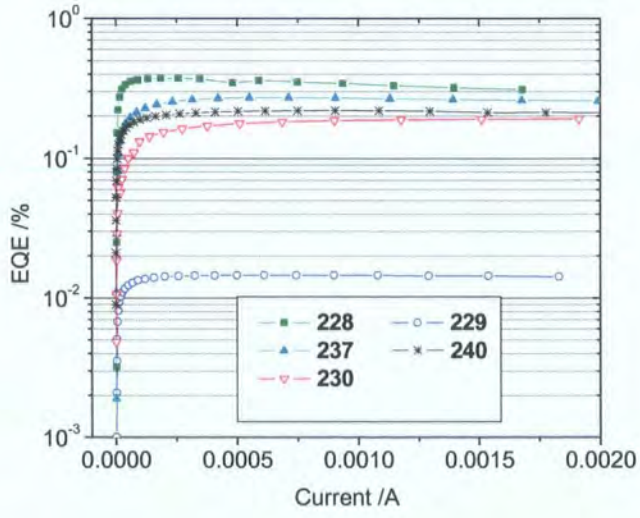

Figure 3.15 EQEs of the devices

The EQE of the **229** device was more than an order of magnitude lower than the values obtained for devices containing the other materials. This low efficiency results from

the very low light emission shown in Figure 3.14. The low light emission can be explained by the large energy barrier to hole injection as seen from the DFT calculations. Compound **240** also emits a low level of light but this is compensated for by the lower current in the device, so overall the devices made with this material have an EQE similar to the others.

Figure 3.16 compares the operating voltages of each device. Turn-on voltage was defined as the bias required to achieve a brightness of 0.1 cd m^{-2}. Due to the bipolar nature of the materials the turn-on voltages were low, *viz.* 2.9, 5.5, 3.6, 4.5 and 3.4 V for devices incorporating **228**, **229**, **237**, **240** and **230**, respectively. For devices containing compounds **228**, **237** and **230** voltages required to reach 200 cd m^{-2} (typical operating brightness of a screen) were < 8 V.

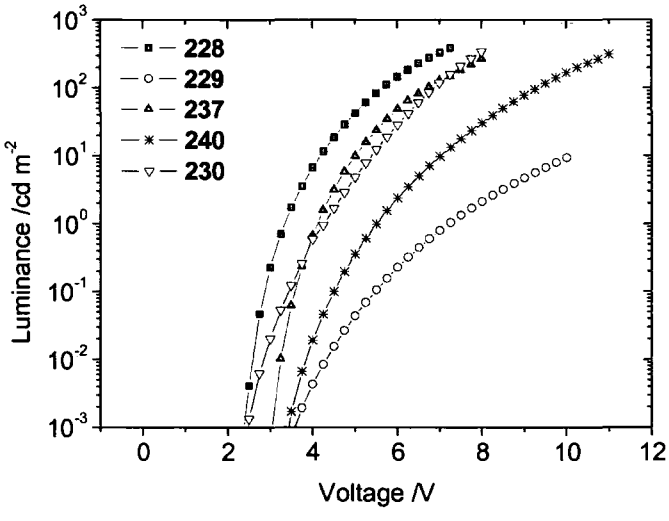

Figure 3.16 *L-V* characteristics of the devices

The EL spectra of the devices are shown in Figure 3.17.

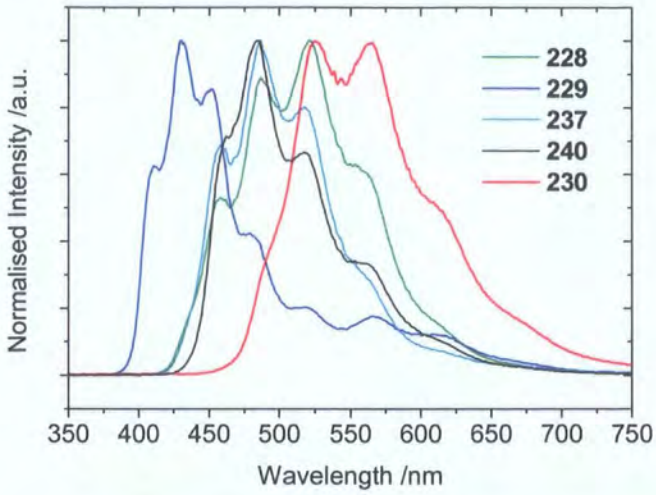

Figure 3.17 EL spectra of the devices

The λ_{max} (EL) values are as follows: **229**, 430 nm (2.89 eV); 487 nm (2.55 eV), **237**; 487 nm (2.55 eV), **240**; 521 nm (2.38 eV), **228**. Compound **230** showed peaks at 521 nm (2.38 eV) and 564 nm (2.20 eV). The CIE coordinates were (0.235, 0.432), (0.214, 0.160), (0.191, 0.532), (0.213, 0.358) and (0.393, 0.549) for compounds **228**, **229**, **237**, **240** and **230** respectively. These are shown on a CIE diagram in Figure 3.18.

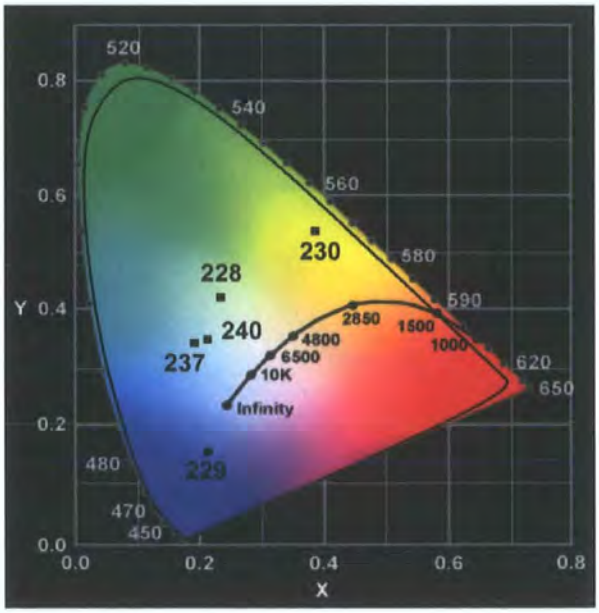

Figure 3.18 Colours of the devices displayed on a CIE diagram

3.2.7.2 Blended Devices

Compound **237** was also tested as a charge-transporting material by blending it with MEH-PPV at 50% and 95% by weight of **237**. Using the device configuration ITO/PEDOT:PSS/MEH-PPV:**237**/Al EQEs of 0.04% and 0.26% were obtained for the 50% and 95% blends, respectively. These values are up to two orders of magnitude higher than undoped MEH-PPV devices. Current and light output behaviours were also similar to those reported before for these types of blends with other ET additives.[57, 58] Light output was solely from the MEH-PPV for the 50% device whilst an additional peak in the emission spectrum for the 95% device can be assigned to compound **237**. The spectra for these devices are shown in Figures 3.19 and 3.20. Once again, this implies that the two components (MEH-PPV and **237**) are intimately mixed and there is very efficient energy transfer to the MEH-PPV.

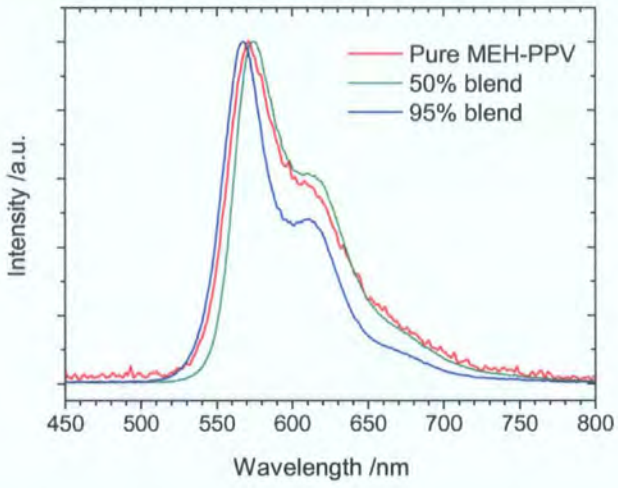

Figure 3.19 EL spectra of blended layer devices incorporating 237 and MEH-PPV

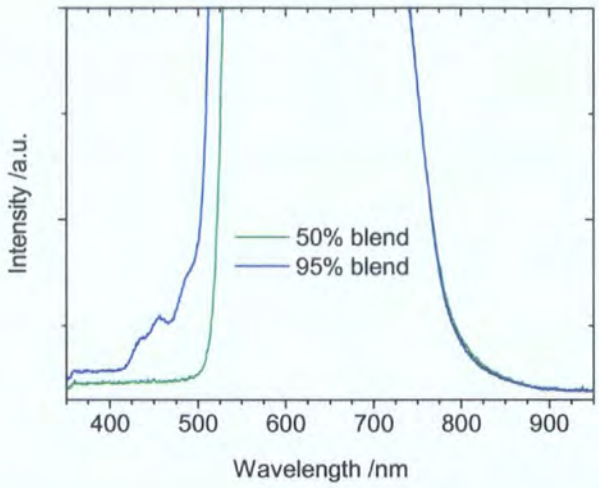

Figure 3.20 Light output from 237 visible at high doping levels

Using a device configuration of ITO/PEDOT:PSS/MEH-PPV:**237**/Ca:Al a blend of 70% **237** with MEH-PPV produced an EQE of 0.4%. With the PEDOT layer removed this fell to 0.1%. As expected, the light output was solely from the MEH-PPV as shown in Figure 3.21.

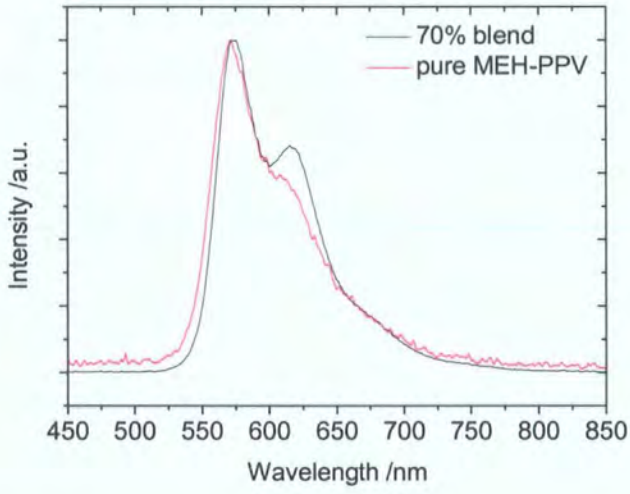

Figure 3.21 EL spectrum of the blended device compared to a pure MEH-PPV device

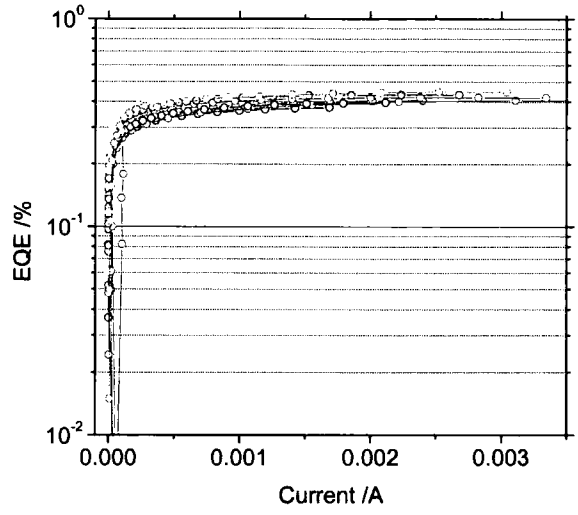

Figure 3.22 EQEs of the blended layer devices with 70% 237

3.3 Conclusions

Several novel bipolar compounds have been synthesised using a variety of synthetic approaches. The key compound 9,9-dihexyl-7-trimethylsilyl-fluoren-2-yl-2-boronic acid, **233**, that has been used before by our group has been modified to the boronic ester derivative which is obtained in higher yields and can be more easily purified and characterised. Difficulties encountered using Ullmann copper-catalysed couplings were overcome by using Buchwald-Hartwig palladium coupling conditions leading to compounds **237** and **240** in good yields. DFT, photophysical and cyclic voltammetric studies have been carried out on **237** and **240** as well as the similar materials **228**, **229** and **230** which all possess linearly π-extended systems with 1,3,4-oxadiazole moieties for electron transport and triarylamines for hole transport. The studies reveal that all the compounds possess a higher HOMO energy level than that of OXD-7 (by 0.60 – 1.02 eV) due to the presence of the electron-donating triarylamines which give rise to more balanced charge transport. Simple devices have been fabricated using solution-based spin-coating techniques using these new compounds as light-emitting materials. The low turn-on voltages (as low as 2.9 V and not higher than 5.5 V) indicate that all the compounds display balanced charge transport. Compounds **228** and **237** provided the best performance with EQEs of 0.36% (1.00 cd A^{-1}) and 0.26% (0.60 cd A^{-1}),

respectively. The colour of emitted light varies from blue through to green by chemical modification within the series. The comparatively low efficiencies are offset by the high chemical and thermal stability (**240** and **237** show no melting point up to 400 °C) and simplicity of the device structure. In addition, compound **237** has been shown to perform well as a charge-transporter in blended layer devices with MEH-PPV. This range of materials shows promise for a wide range of future OLED applications.

Chapter 4 – Oxadiazole-Containing Ligands for Phosphorescent Materials

4.1 Introduction

As shown in Chapter 1.6 complexes of heavy metal atoms such as iridium can lead to very efficient OLEDs due to their ability to harvest both the singlet and triplet excited states formed within devices. Most studies have focused on alteration of the ligand systems to tune the colour of emitted light. To date the OXD moiety has not been attached to an iridium centre and there are very few reports of OXDs being

components of any metal complexes. Examples include a 2,5-diaryl-1,3,4-oxadiazole which is tethered by a saturated alkyl chain to a 2-(2-pyridyl)benzimidazole (PyBM) system which is a ligand in europium complex **241**.[148] An ITO/PBD/**241**/LiF/Al device produced red light (λ_{max} = 612 nm) with a maximum luminance of 322 cd m^{-2} and maximum EQE of 1.7%. By comparison a test device incorporating an *N*-alkyl PyBM ligand displayed very poor results.

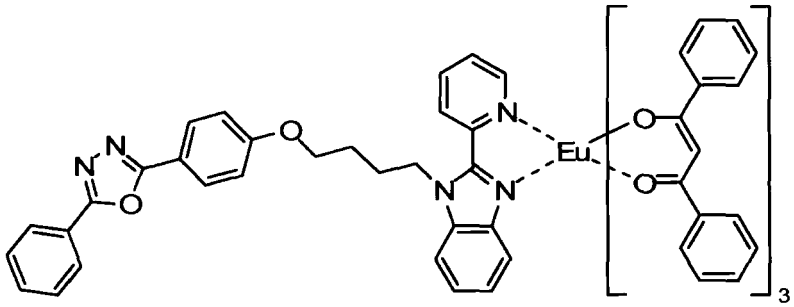

241

A further example was reported by Wong *et al.* in which an oxadiazole-containing ligand was bound to platinum to form the complex **242**.[149] A bilayer device comprising ITO/CuPc/**242**/Ca:Al displayed orange light (λ_{max} = 538 nm, 578 nm) with CIE coordinates (0.52, 0.47) and a turn-on voltage of *ca.* 6 V. The luminance reached 1,065 cd m^{-2} and luminous efficiencies up to 1.2 cd A^{-1} were reported.

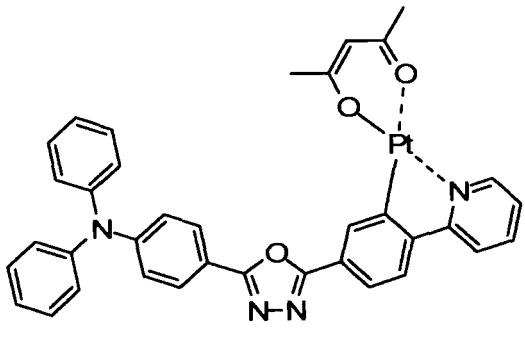

242

This Chapter will report the synthesis of OXD-containing ligands and attempts to bind them to iridium metal centres by cyclometalation reactions.

4.2 Results and Discussion

The synthesis of triscyclometalated iridium compounds was discussed by Thompson and co-workers in a recent review.[150] Three methods for their preparation were outlined as shown below.

Method A

$$Ir(acac)_3 + 3HC\hat{}N \xrightarrow[\text{heat, } N_2]{\text{glycerol}} Ir(C\hat{}N)_3 + 3acacH$$

Method B

$$(C\hat{}N)_2Ir(O\hat{}O) + HC\hat{}N \xrightarrow[\text{heat, } N_2]{\text{glycerol}} Ir(C\hat{}N)_3 + O\hat{}OH$$

Method C

$$(C\hat{}N)_2Ir(\mu\text{-}Cl)_2Ir(C\hat{}N)_2 + 2HC\hat{}N \xrightarrow[\text{heat, } N_2]{\text{glycerol, } K_2CO_3} Ir(C\hat{}N)_3 + 2KCl + H_2O + CO_2$$

In order to produce the desired facial isomer, reaction temperatures of > 200 °C need to be employed, although any meridional isomer can be removed (by recrystallisation or column chromatography) or converted to the facial isomer by refluxing in glycerol at high temperatures.

4.2.1 Synthesis of Conjugated Ligands

Initial work was carried out to determine whether 2,5-diaryl-1,3,4-oxadiazoles themselves bind to iridium centres. For this purpose 2,5-diphenyl-1,3,4-oxadiazole, **244**, was synthesised from the reaction of benzoyl chloride with hydrazine monohydrate followed by cyclisation in $POCl_3$. Subsequent reaction with $IrCl_3.xH_2O$ failed to yield any products demonstrating that the OXD moiety itself apparently doesn't bind to the metal centre under standard cyclometalating conditions.

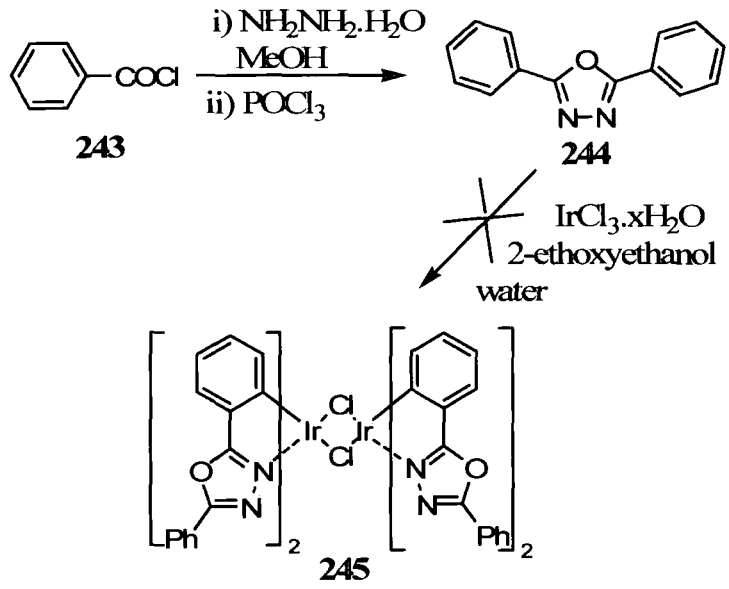

Scheme 4.1 Synthesis of 2,5-diphenyl-1,3,4-oxadiazole and trial reaction with $IrCl_3.H_2O$

The first potential ligand we synthesised was structurally the most simple: 2-[4-(1,3,4-oxadiazol-2-yl)phenyl]pyridine, **247**. Commercially available 4-bromobenzhydrazide was converted to the terminal OXD material **247** by refluxing in ethylorthoformate.[44] The product **247** was obtained in 83% yield and then reacted under Stille cross-coupling conditions[151] with 2-(tributylstannyl)pyridine to yield **247** in 53% yield as shown in Scheme 4.2.

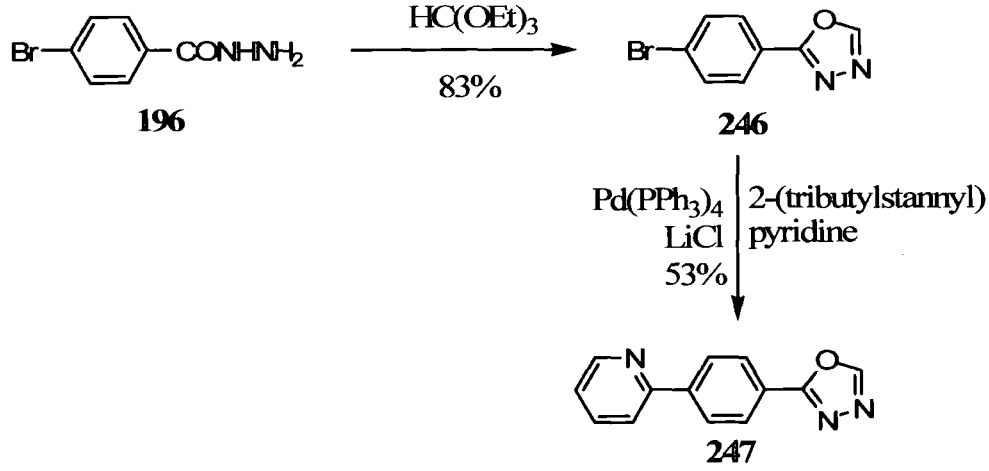

Scheme 4.2 Synthesis of a potential OXD ligand 247

The related 2,5-diaryl-1,3,4-oxadiazole derivative was synthesised using an alternative approach as shown in Scheme 4.3.

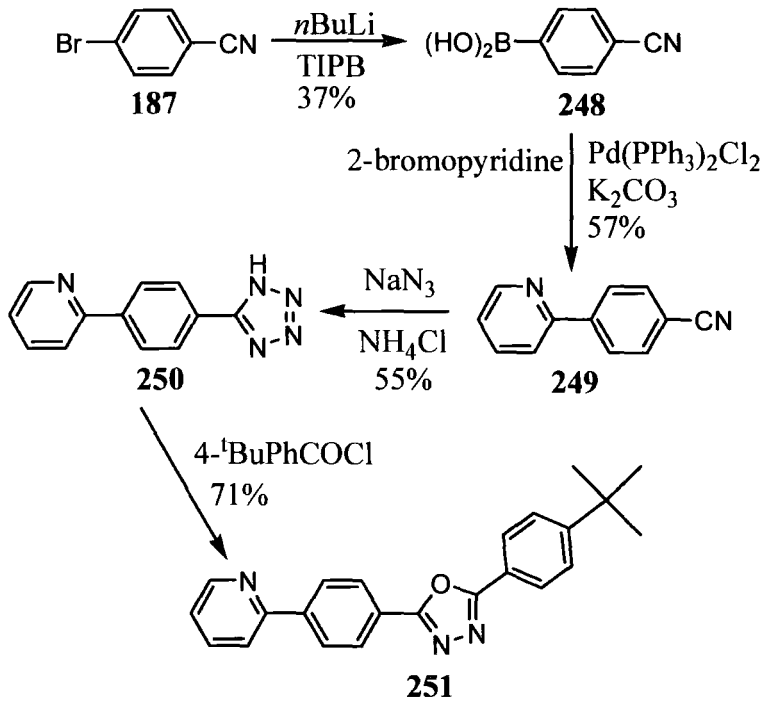

Scheme 4.3 Synthesis of 2,5-diaryl derivative of 251

4-Bromobenzonitrile was converted to the boronic acid derivative **248** in 37% yield with *n*-butyllithium and TIPB. Suzuki-Miyaura cross-coupling of compound **248** with 2-bromopyridine produced the 2-phenylpyridine derivative **249** and the subsequent [3+2] cycloaddition with sodium azide yielded the tetrazole **250**. The final step was the formation of the OXD derivative **251** by refluxing compound **250** with 4-*tert*-butylbenzoyl chloride in pyridine which gave the product in 71% yield. The yields were lower than expected as previous tetrazole routes to OXDs had given much higher yields (e.g. compounds **189** – **194**). An alternative route which was not explored makes use of the previously utilised high-yielding tetrazole reaction to form compound **189** followed by Stille cross-coupling. Even allowing for a low yield in the Stille reaction, the complete synthesis as outlined in Scheme 4.4 is only two steps.

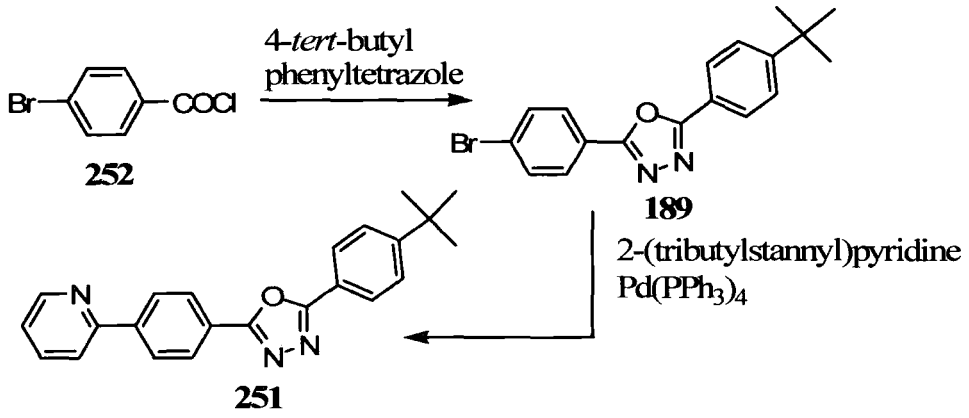

Scheme 4.4 Alternative synthesis of compound 251

With these two simple ligands **247** and **251** in hand, attention turned to adapting the previously made compound **237** to potentially function as a ligand. It is known that fluorenyl pyridines such as **253** can be bound to metal centres[127] so by using the previously synthesised compound **236**, Stille cross-coupling with 2-(tributylstannyl)pyridine would yield a derivative with the desired 2-phenylpyridine moiety.

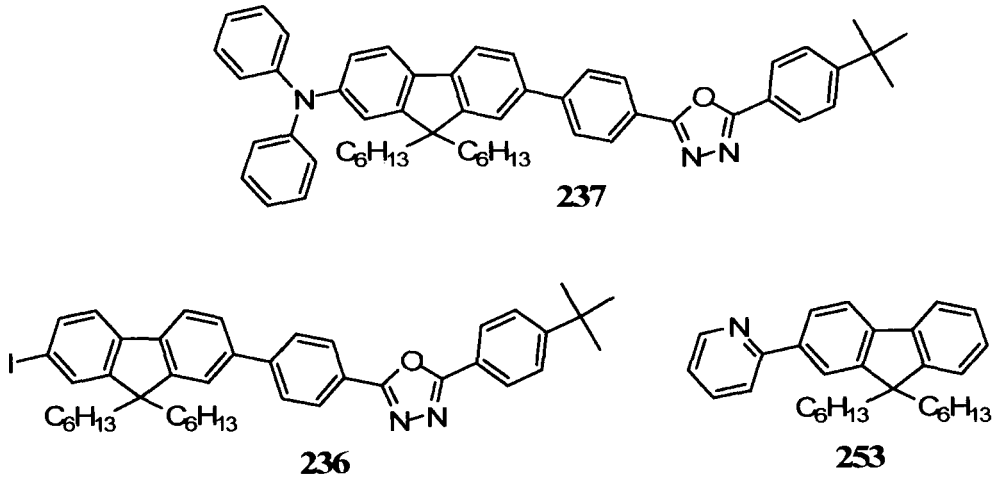

Stille cross-coupling of **236** on a 100 mg scale reaction led to a low 43% yield. The reaction was repeated with the bromo analogue **238** but the yield remained similar at 44% as shown in Scheme 4.5.

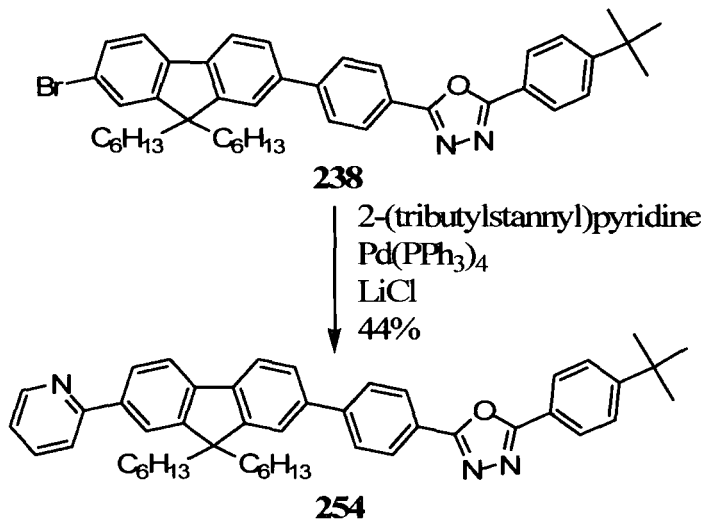

Scheme 4.5 Synthesis of the fluorene-OXD ligand 254

A second modification to compound **237** was envisioned by replacing the phenyl unit between the fluorene and OXD unit with the pyridyl moiety. Synthesis of this molecule started with the pyridine unit. Initial plans to start the synthesis from 2-bromo-5-methylpyridine and oxidise the methyl group to a carboxylic acid[152] followed by conversion to methyl ester and then hydrazide led to the discovery that refluxing the methyl ester in hydrazine monohydrate also substitutes hydrazine at the 2-position of pyridine to give compound **258** as shown in Scheme 4.6.

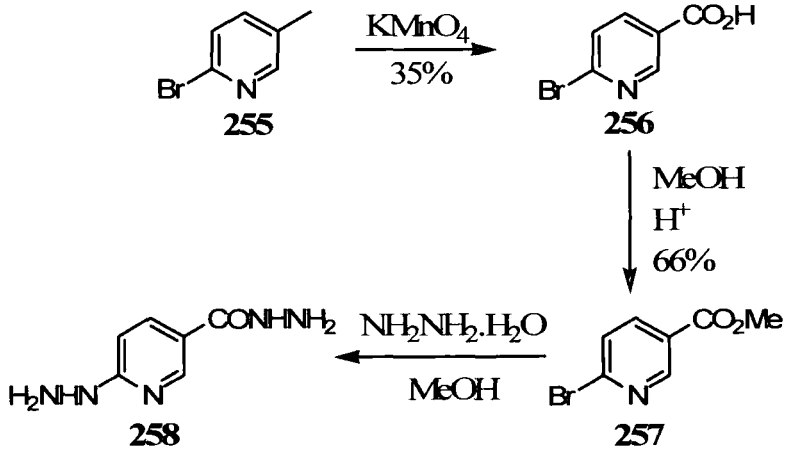

Scheme 4.6 Failed route to 2-bromopyridine-5-hydrazide

A second proposed route used 6-chloronicotinoyl chloride as the starting pyridine unit which would allow the hydrazide to be built onto a phenyl unit, thus leaving the halide at the 2-position of the pyridine ring unchanged. 4-*tert*-Butylbenzoic acid was

converted through the methyl ester to the hydrazide **260** (90% for two steps) before being coupled with 6-chloronicotinoyl chloride and cyclised to form the oxadiazole **264** as shown in Scheme 4.7.

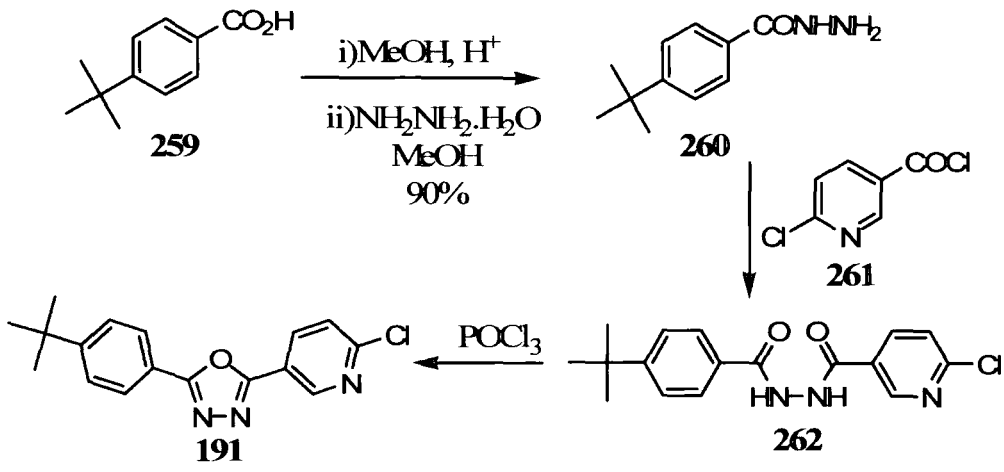

Scheme 4.7 Attempted synthesis of OXD-pyridyl fragment 191

The resultant purple solid was very insoluble and NMR analysis was only possible in hot DMSO-d_6. This also meant that the material could not be dissolved for purification by column chromatography. Elemental analysis failed to prove the purity of the compound so the decision was made to carry out the final Suzuki-Miyaura cross-coupling on **191** anyway and attempt to fully purify the final compound. However, the reaction failed to produce any products instead giving back starting materials.

Once again it was decided to use the tetrazole route as the OXD compound **191** could be synthesised in one step from commercially available 5-phenyltetrazole and 6-nicotinoyl chloride as shown in Scheme 4.8 instead of the two step hydrazide route. The reaction was carried out with the standard conditions of stirring in refluxing pyridine for 15 hours before pouring into water to precipitate the product. The pink solid was recrystallised from ethanol to give the product **191** in 54% yield. This time the solid dissolved in DMSO-d_6 at room temperature and NMR and elemental analysis confirmed the structure as being the desired OXD compound **191**.

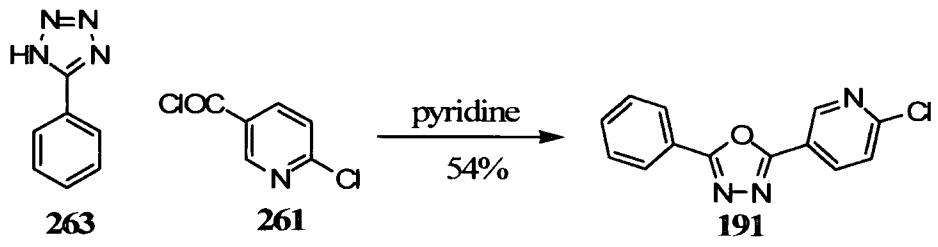

Scheme 4.8 Synthesis of the OXD fragment 191

Previous work has shown that although chloro groups are normally poor cross-coupling partners in Suzuki-Miyaura reactions, when they are adjacent to a ring nitrogen they are activated towards coupling.[153] Thus compound **191** was reacted directly with the fluorene boronic acid **201** to give the desired compound **264** in 73% yield as shown in Scheme 4.9.

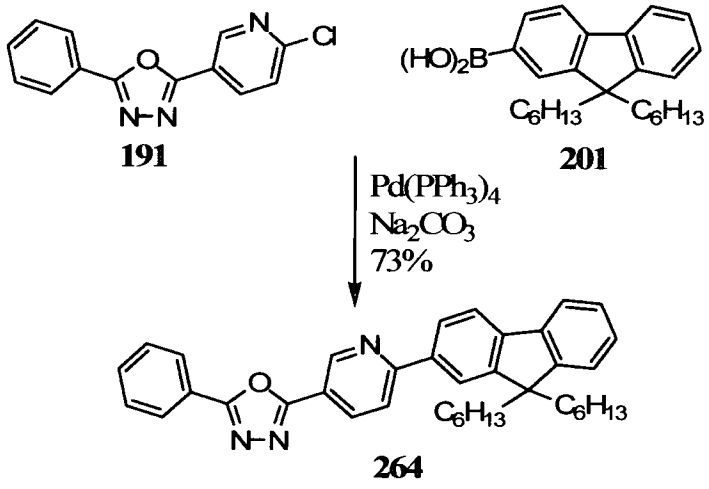

Scheme 4.9 Successful synthesis of ligand 264

4.2.2 Attempted Cyclometalation of the Ligands

With four novel OXD-containing ligands in hand, attempts were made to bind them to an iridium metal centre. As discussed previously, the main methods for achieving this are (i) reaction with iridium chloride in 2-ethoxyethanol to yield the bridged chlorine dimer followed by reaction with further ligand in the presence of a chloride scavenger such as silver(I) triflate or (ii) by reaction with iridium acetonylacetate in glycerol at high temperature. In addition, recent developments in the use of microwave-assisted heating have led to increased heating rates and greatly reduced reaction times. The

optimisation of microwave conditions for the cyclometalation of 2-phenylpyridine is discussed in Chapter 5.

Each of the four ligands **247**, **251**, **254** and **264** was reacted with iridium chloride. Unlike the reaction with 2,5-diaryl-1,3,4-oxadiazole, **244**, all four reaction mixtures changed colour indicating that a reaction was taking place. Unfortunately, in each case the resulting crude product proved to be inseparable from the mixture of by-products. In the case of 2-phenylpyridine, the bridged dimer sticks to silica requiring a polar solvent (such as ethyl acetate in DCM) to elute the product from a column. The desired OXD compounds stick to the silica and only co-elute with the other baseline products making it impossible to accurately characterise the product. Reaction of the crude product with more ligand in the presence of silver(I) triflate failed to produce any of the desired tris-cyclometalated products.

Reaction of the ligands with iridium acetonylacetate in glycerol at high temperature also failed to produce any of the cyclometalated products. Thin layer chromatography showed the presence of iridium acetonylacetate and ligand starting materials as the major products.

Finally, reaction of the ligands with both iridium acetonylacetate and iridium chloride in glycerol using microwave-assisted heating was attempted. The reactions were done with ten equivalents of ligand which resulted in some solubility issues when using 5 ml of solvent. Even with 10 ml of glycerol, the ligands did not fully dissolve but after the reactions had been run there were no signs of undissolved ligand suggesting that all the ligand dissolved once heating had been initiated. As with the thermal iridium acetonylacetate reactions the two major compounds in the reaction mixtures were the ligands and the iridium starting material.

Chemical reactions are controlled by sterics and electronics. Whilst the smaller ligands should cause no problems sterically, the larger ligands **254** and **264** might encounter some steric resistance to forming tris-cyclometalated compounds. Compound **254** with the pyridine unit at the end of the molecule is a smaller ligand than some others which are known to form tris-cyclometalated iridium complexes such as the penta-fluorene ligand reported by our group.[127] Compound **264** has conjugated units either side of the

pyridine ring, but once again, similar sized fluorenyl complexes have been reported.[126] From this it would appear that sterics are not the reason for these reactions failing.

In order for heterocyclic ligands to *ortho*-metalate the C-H bond *ortho* to the heterocycle must be broken in order to bond with the metal atom. This can be aided by incorporating a lone-pair donor to bind to the metal and hold it in close proximity to the *ortho* carbon.[154] In the case of 2-phenylpyridine ligands this donor is the nitrogen in the pyridine ring. The failure of the reaction with the OXD-containing ligands is likely due to the electron withdrawing nature of the OXD moiety affecting the ability of the ligand to bind to the metal centre through removing electron density by mesomeric and inductive effects through the π and σ frameworks respectively.

Another possibility is that despite the apparent failure trying to bind compound **244**, OXD does in fact bind to the iridium which could then block the binding of the 2-phenylpyridine moieties and inhibit the cyclometalation of compounds **247**, **251**, **254** and **264**.

4.2.3 Attempted Synthesis of Non-conjugated Ligands

With the ligands containing an OXD unit included in the conjugation having failed to bind to iridium centres, attention turned to the synthesis of molecules containing the OXD unit tethered to the binding group via a non-conjugated chain. The OXD unit was similar to that included in the europium complex **241** synthesised by Liang *et al.*[148] The synthesis of the precursor 4-(5-phenyl-1,3,4-oxadiazol-2-yl)phenol, **266**, was achieved by reaction of 5-phenyltetrazole and *p*-anisoyl chloride and reduction of the subsequent methyl ether **192** to the hydroxide as shown in Scheme 4.10.

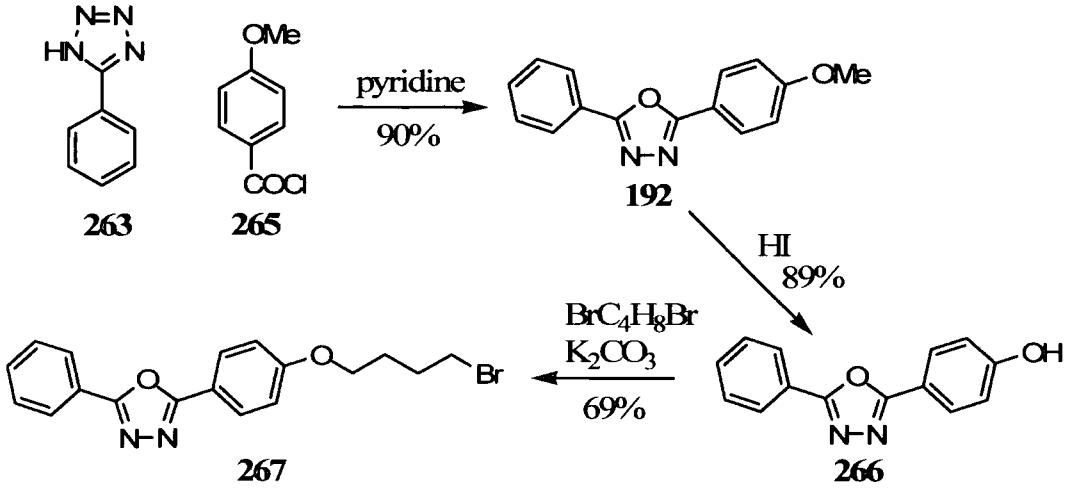

Scheme 4.10 Synthesis of OXD tether 266

The literature features several ways of accomplishing the demethylation of **192** to **266** including the use of boron tribromide, hydriodic acid[155] or aluminium chloride.[156] Refluxing **192** in HI for 5 hours allowed the desired product to be obtained by diluting and filtering the resultant suspension. The hydroxide group was reacted with 1,4-dibromobutane under basic conditions[157] to afford the OXD tether **267**.

The 2-phenylpyridine derivatives remained as the preferred choice for the binding group and we planned to link the two units (i.e. 2-phenylpyridine and OXD) via nucleophilic attack of an amine on the pyridine ring in compound **270** on the terminal bromide of compound **267**. This compound, **270**, was prepared by the Suzuki-Miyaura cross-coupling of 4-amino-2-chloropyridine with benzene boronic acid as shown in Scheme 4.11.[158]

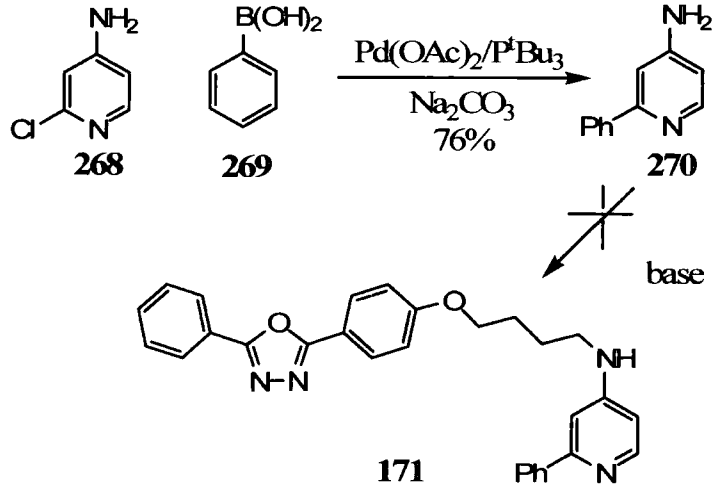

Scheme 4.11 Attempted synthesis of OXD material 271

Attempts to join the two molecules as shown in Scheme 4.11 failed despite the use of several different types of base and solvent reported from the literature for related reactions. These included sodium hydroxide and DMF, triethylamine and DMF, *n*-butyllithium and THF, potassium hydroxide and acetonitrile, no base and ethanol and potassium butoxide and THF. All these reactions simply gave back the starting materials. Finally a literature method for monoalkylation of pyridine-4-amine in the presence of a catalytic amount of potassium iodide using microwave-assisted heating[159] was tried and also failed to yield any product.

The failure of this reaction can be ascribed to the various resonance forms of 4-amino-2-phenylpyridine. The lone pair of electrons in the amine nitrogen can be delocalised to various positions throughout not only the pyridine ring, but also the adjacent phenyl ring. In addition they can be delocalised to the pyridine nitrogen which creates a stable canonical form as shown in Scheme 4.12. This means that the lone pair is much less available to attack the alkyl bromide of the OXD tether.

Scheme 4.12 Two resonance forms of compound 270

As expected from this assumption, the reaction between **268** or **270** and 1,4-dibromobutane shown in Scheme 4.13 failed to give any product.

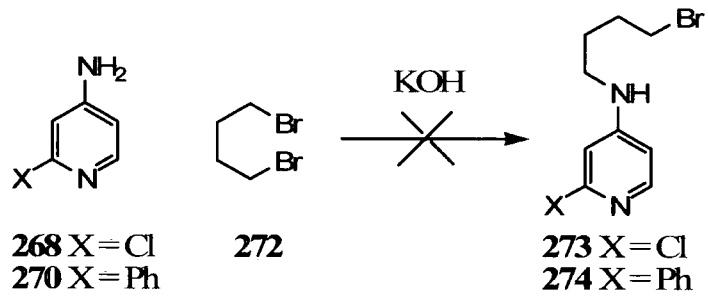

268 X=Cl **272** **273** X=Cl
270 X=Ph **274** X=Ph

Scheme 4.13 Failed reaction between 4-aminopyridines and 1,4-dibromobutane

Previous work in our group had added an alkyl chain to the methyl group of 4-methylpyridines by deprotonating the benzylic protons of the methyl group with lithium diisopropylamide (LDA) and subsequent reaction with an alkyl bromide.[160] In preparation, two 2-phenyl-4-methylpyridine derivatives **276** and **277** were synthesised as shown in Scheme 4.14.

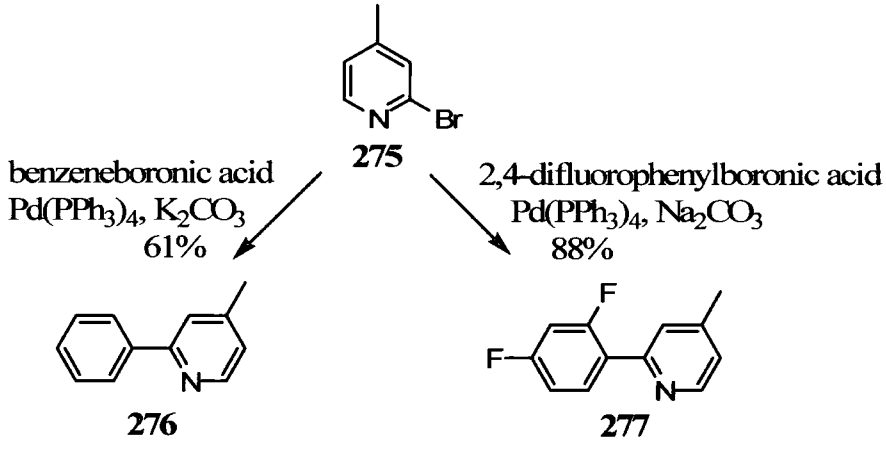

276 **277**

Scheme 4.14 Synthesis of two 4-methyl-2-phenylpyridine derivatives

Both compounds **276** and **277** were obtained purified by Kugelrohr distillation and then solidified on standing. Treatment of compound **276** with LDA followed by quenching with deuterium oxide successfully transformed the CH_3 group to a CH_2D group based on ^1H NMR evidence, but treatment with the OXD fragment **167** or 1,4-dibromobutane failed to yield the desired products as shown in Scheme 4.15, instead giving back starting materials. This implies that there is another, more reactive target for the generated nucleophile than the alkyl bromide in the reaction.

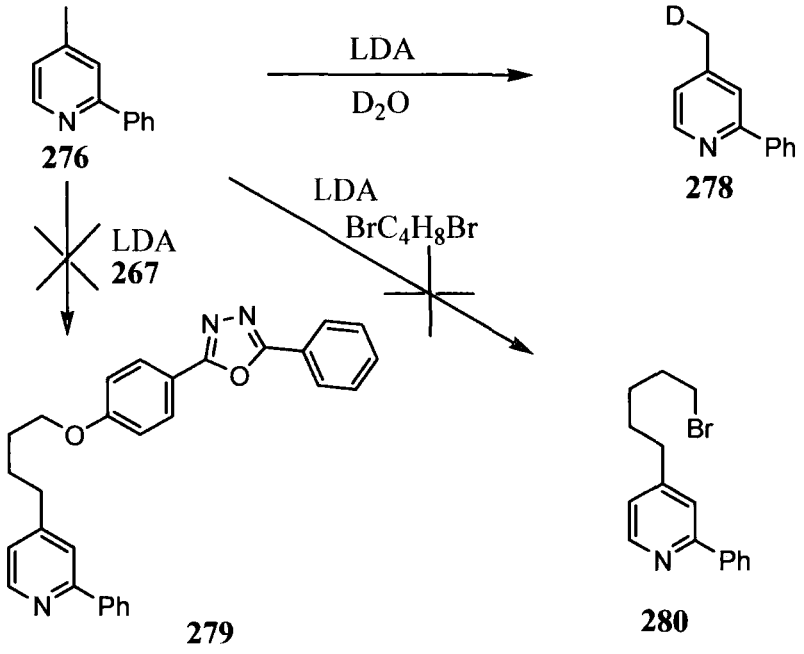

Scheme 4.15 Reactions of compound 276 with LDA and electrophiles

Unfortunately, due to time constraints, reactions to add the OXD tether to the phenyl ring were not carried out.

4.3 Conclusions

Several new 1,3,4-oxadiazole-containing 2-phenylpyridine systems have been synthesised using a variety of approaches. Once again, the tetrazole-route to 1,3,4-oxadiazoles has proved useful, *viz.* the synthesis of compound **264**. Despite the success in synthesising the ligands, efforts to bind them to an iridium metal centre using a range of literature procedures, including the use of the relatively new method of microwave-assisted heating, failed to produce the desired complexes. The fluorene-containing ligands (**254** and **264**) may prove interesting to study as ET blend and/or ET/emitter materials in their own right due to their unsymmetrical nature. Shen *et al.* reported several spirobifluorene-containing devices. Devices with unsymmetrical compounds such as compound **281** outperformed devices fabricated with analogous symmetrical compounds such as **282** (with EQEs of 4.2% and 1.2%, brightnesses of 8,390 cd m^{-2} and 3,853 cd m^{-2} and CIE coordinates of (0.15, 0.09) and (0.15, 0.16) respectively).[139]

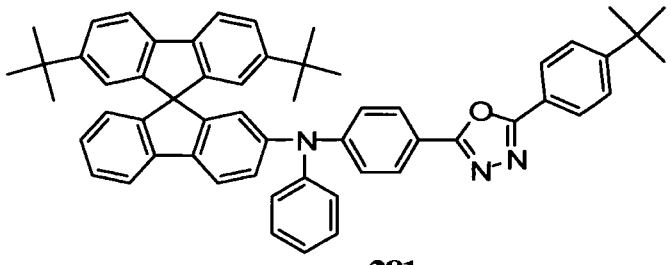

281

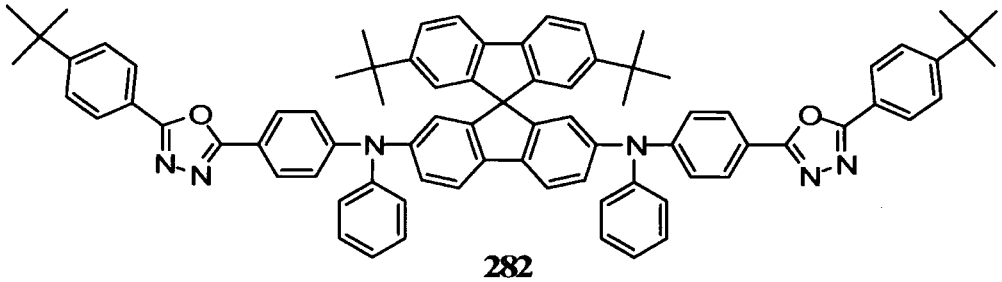

282

By slightly altering the reaction Scheme to use the literature compound **284**[133] instead of 5-phenyltetrazole as the starting material it should be straightforward to produce compound **285** which can be used as an unsymmetrical diad/emitter.

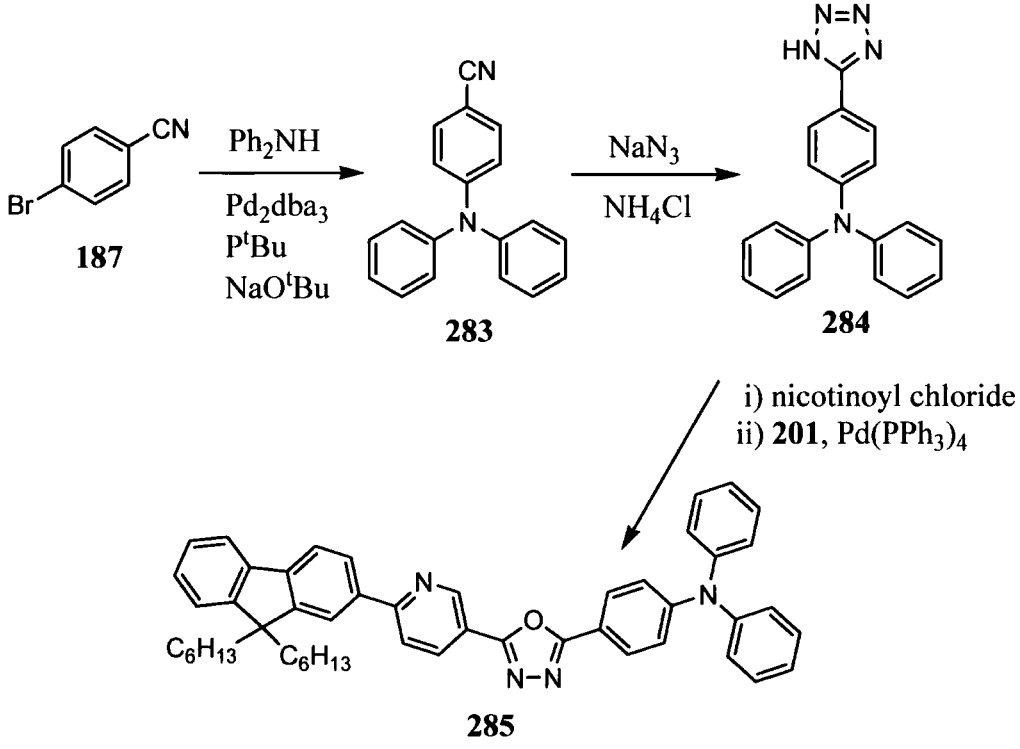

Scheme 4.18 Potential synthetic route to an unsymmetrical bipolar material

Attempts to synthesise a non-conjugated 1,3,4-oxadiazole-containing 2-phenylpyridine-based ligand by linking compound **267** to several 2-phenylpyridine compounds (**270**, **276** and **277**) failed due to issues with deprotonation. Further studies could investigate the attachment of OXD unit **267** to the phenyl ring instead of the pyridine ring.

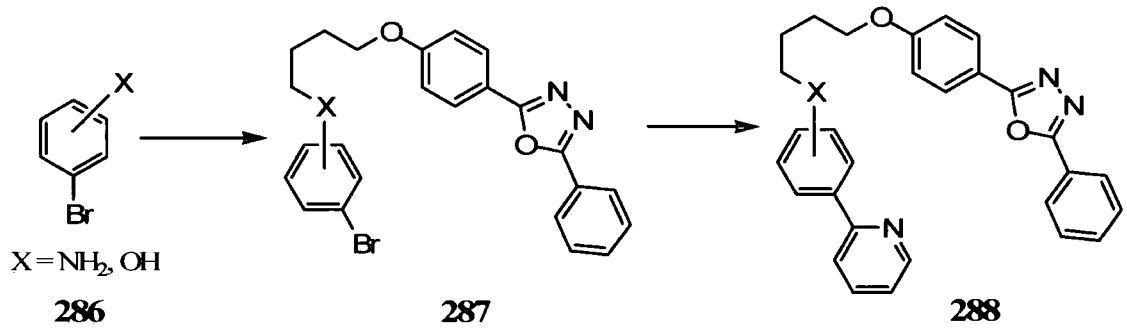

286 **287** **288**

Scheme 4.18 Potential route to compounds with OXD tethered to the phenyl ring

Most 2-phenylpyridine complexes produce green-yellow light. As shown in Chapter 1.6.1, the emission colour can be fine-tuned by manipulating the nature and position of any peripheral groups. Addition of the electron donating OR or NHR at the 5-position of the phenyl ring as shown in Scheme 4.18 will red-shift the emission by raising the level of the HOMO. Replacement of the pyridine group with an isoquinoline group should further red-shift the emission by lowering the LUMO potentially leading to a novel electron-transporting red emitter.

Chapter 5 – Synthesis of Tris(2-phenylpyridine) Iridium Using Microwave Reactions

5.1 Introduction

The first devices that could reproducibly generate fixed frequency microwaves were developed by Randall and Booth during World War II. The interest was due to the use of microwaves in radar transmitters. It was already known that IR and UV radiation were capable of inducing chemical reactions, so it was no surprise to find that microwaves were also suitable. It was soon discovered that the heating effects seen in

foods were due to the efficient conversion of microwaves into thermal energy in the water molecules contained within foods. With this knowledge, early industrial uses of microwaves included the drying of nylon by DuPont. Once the water had been removed, the heating would stop as the microwaves did not interact with the nylon and thus the product could avoid being scorched.

Initial work by Gedye[161] and then Majetich[162] and co-workers showed that reactions in organic solvents could be greatly accelerated by microwave heating. Early papers described synthesis using domestic microwave appliances, adapted for laboratory use. This led to speculation about the mechanism by which the reaction mixtures were heated and also led to reproducibility and safety problems.

Although the microwave region of the electromagnetic spectrum spans 1 cm to 1 m, (30 GHz to 300 MHz), domestic and chemical microwaves operate at 12.2 cm (2.45 GHz). The best solvents possess a strong dipole due to their increased interaction with microwaves. Because the interaction is with the bulk solvent, heating is very rapid compared to the slow convection-based heating in conventional heating methods. A full discussion of the mechanisms by which microwaves can enhance chemical reactions and the theory behind microwave dielectric heating can be found in recent reviews.[163-165]

In recent years interest in microwaves for chemical synthesis has greatly increased and there are now over 2,000 papers describing such research.[165] By superheating polar solvents above their normal boiling points, microwaves allow reactions that normally take many hours to be completed in minutes and allow alterations of thermally heated reactions. For example, the Suzuki-Miyaura cross-coupling reaction usually requires a ligand-containing palladium catalyst, organic solvent (such as THF, toluene or 1,4-dioxane), inert conditions and long reaction times.[67] Kabalka *et al.* reported a microwave cross-coupling reaction that used ligand-less palladium powder, potassium fluoride on alumina and no solvent other than a small amount of water as shown in Scheme 5.1.[166]

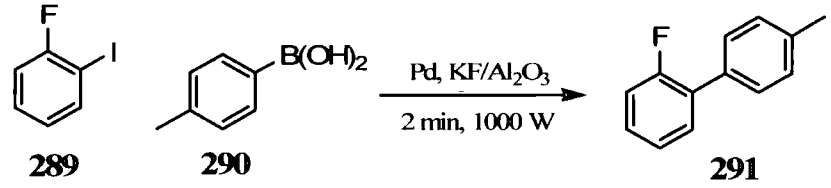

289 290 291

Scheme 5.1 Microwave assisted Suzuki-Miyaura coupling using a ligand-less Pd catalyst

In addition to using the cheapest form of palladium, the reaction produced a 79% yield after only 2 minutes heating. The products could be isolated via a simple filtration as the catalyst remains bound to the alumina. The addition of more potassium fluoride allowed the catalyst to be reused.

Leadbeater and Marco produced biaryls that had been coupled without any transition-metal additives as shown in Scheme 5.2.[167] Tetrabutylammonium bromide (TBAB) was used as a solvating and activating agent and the reaction was again carried out in water. After only 5 minutes heating at 150 °C a 73% yield of biaryl **293** was produced.

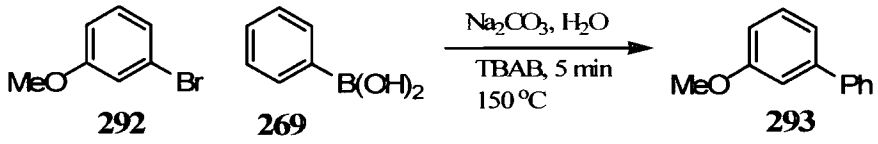

292 269 293

Scheme 5.2 Catalyst free Suzuki-Miyaura coupling

Similarly, improvements to many classical organic reactions have been made utilising dielectric heating and many laboratories – both industrial and academic – contain specialist chemical microwave equipment.

Several groups have utilised microwaves in the synthesis of tris-cyclometalated iridium complexes. Konno and Sasaki demonstrated that the use of microwaves could vastly improve the reaction time and simplicity of the reaction of iridium chloride with 2-phenylpyridine and 2-(4-methylphenylpyridine) as shown in Scheme 5.3.[168] By conventional heating, the major product obtained is the bridged dichloro dimer **297**. By incorporating a dehalogenating agent such as silver(I) triflate and refluxing for 24 hours this bridged species generated the desired tris-cyclometalated product. By reacting 100 equivalents of ligand in ethylene glycol solution with iridium chloride, 75% yield was obtained after heating in the microwave for just 1 minute.

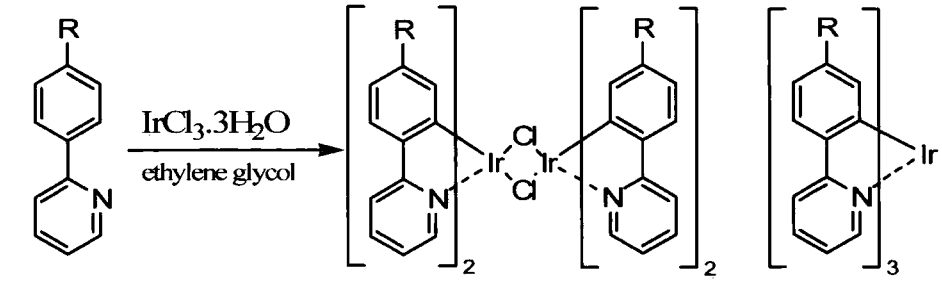

294 R = H
295 R = Me

296 R = H
297 R = Me

164 R = H
298 R = Me

Scheme 5.3 Tris-cyclometalation using microwave-assisted heating

If less than 50 equivalents of ligand were used, 45-100% of **297** remained even after heating for longer periods. This suggested that the excess arylpyridine was acting as a base to help deprotonate the phenyl ring. In the presence of Na_2CO_3, only 30 equivalents of ligand were required to produce the desired tris-cyclometalated product selectively.

Saito *et al.* reported that the use of iridium acetonylacetate ($Ir(acac)_3$) as the source of iridium required only 3.5 equivalents of ligand and 30 minutes heating time to yield the tris-cyclometalated product.[169] $Ir(ppy)_3$, Ir(2-[4-methylphenyl]pyridine)$_3$ and $Ir(46dfp)_3$ were obtained in 37%, 36% and 20%, respectively. It was further reported that whilst conventional heating gives only trace amounts of tris(2-phenyl-1-quinoline)iridium ($Ir(phq)_3$, **300**), microwave heating for just 20 minutes allows isolation of this compound in 10% yield.

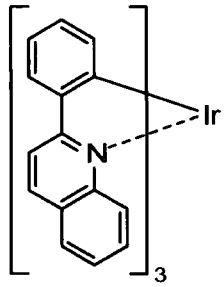

300

5.2 Results and Discussion

5.2.1 Initial Reactions

Most reports are very unspecific about the heating conditions. Reactions carried out in converted domestic microwaves had no way to accurately control the temperature, so only the wattage used in the reaction was reported. Many of these reactions used traditional flasks and condensers, while today's custom microwaves make use of sealed thick-walled pyrex tubes leading to reaction pressures of up to 20 bar. We set out to perform a series of cyclometalation reactions using the simple 2-phenylpyridine ligand to investigate the optimum conditions for the reaction shown in Scheme 5.4. The source of iridium ($IrCl_3.xH_2O$ and $Ir(acac)_3$), length of heating, temperature, solvent and presence of base were all varied.

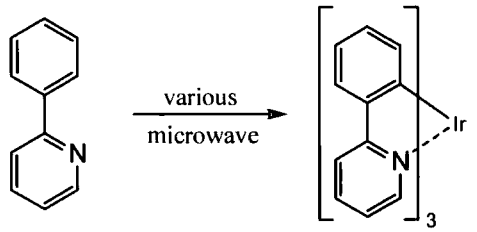

294 **164**

Scheme 5.4 Synthesis of $Ir(ppy)_3$

The following reactions were undertaken in conjunction with Dr S. L. Bettington from our group and were carried out in 10 ml pyrex microwave vessels and sealed prior to heating in an Emrys Optimiser microwave oven. For this set of reactions 50 mg of $IrCl_3.xH_2O$ (0.142 mmol) or 20 mg of $Ir(acac)_3$ (0.041 mmol) and four equivalents of 2-phenylpyridine (88 mg and 25 mg respectively) were used. Following the observations of Saito *et al.* a base was included in the iridium chloride reactions. This was sodium carbonate (two equiv.) and the total volume of solution was 5 ml. All the reaction vessels were degassed before heating. The pre-heating stirring time was 2 s. The work-up for all the experiments in this Chapter is described in Chapter 6.

Iridium Source	Base	Ethylene Glycol /ml	Water /ml	Temperature /°C	Time /s	Yield /%
$IrCl_3.3H_2O$	yes	5	0	200	600	17
$IrCl_3.3H_2O$	yes	5	0	220	600	30
$IrCl_3.3H_2O$	yes	4	1	230	600	25
$IrCl_3.3H_2O$	yes	4	1	240	600	22
$IrCl_3.3H_2O$	yes	4	1	220	1800	15
$Ir(acac)_3$	no	5	0	200	600	0
$Ir(acac)_3$	no	5	0	220	1800	0
$Ir(acac)_3$	yes	5	0	220	600	0
$Ir(acac)_3$	yes	5	0	220	1800	0

Table 5.1 Results from the first set of microwave reactions

The results from these initial experiments, shown in Table 5.1, suggest that for the iridium chloride systems the optimal heating temperature is 220 °C, however, the yield of 30% could not be repeated. The addition of water to the solvent and increasing the reaction temperature to 230 °C and 240 °C did not improve the yield but allowed the results to be repeated. The increased temperature led to some failed reactions where the pressure in the reaction tube reached to the microwave's cut-out limit of 20 bar. Increasing the length of the reaction to 30 minutes reduced the yield to 15%.

It is clear that $Ir(acac)_3$ did not produce any tris-cyclometalated product with or without base and increasing the heating times had no effect.

5.2.2 $Ir(acac)_3$ Reactions

Further investigations into the use of $Ir(acac)_3$ were carried out. $Ir(acac)_3$ (25 mg) was used exclusively as the source of iridium and ligand (ten equiv.) and a glycerol solvent was used. The results are shown in Table 5.2.

Base	Glycerol /ml	Water /ml	Temp /°C	Time /s	Yield /%
no	3	0	220	1800	26
yes (10 eq)	3	0	220	1800	trace
yes (10 eq)	2	1	220	1800	57
no	3	0	230	1800	28
no	3	0	240	1800	15
no	3	0	250	1800	6
yes (10 eq)	2	1	230	1800	60
yes (10 eq)	2	1	225	1800	58

Table 5.2 Results from microwave reactions using $Ir(acac)_3$ as the source of iridium

The results show that the switching from ethylene glycol to glycerol permits the reaction to proceed. Reproducible yields approaching 60% could be obtained in the presence of base in a mixture of glycerol and water. From the first three entries it is seen that the presence of undissolved base (in glycerol-only solution) yields virtually no product whilst the addition of water and base greatly increases the yield.

5.2.3 Optimising Conditions

A final set of reactions was carried out involving both $IrCl_3.xH_2O$ (50 mg, 0.14 mmol) and $Ir(acac)_3$ (70 mg, 0.14 mmol). Ten equivalents of both ligand and sodium carbonate were used and the reaction temperature was fixed at 220 °C. The solvent and heating times were varied. The results are shown in Table 5.3.

Iridium	Ethylene glycol /ml	Glycerol /ml	Water /ml	Time /s	Yield /%
$IrCl_3.xH_2O$	4	0	0	600	15
$IrCl_3.xH_2O$	4	0	0	1800	15
$IrCl_3.xH_2O$	3	0	1	600	18
$IrCl_3.xH_2O$	0	3	1	600	32
$Ir(acac)_3$	0	3	1	600	2
$Ir(acac)_3$	0	3	1	1800	51

Table 5.3 Results from microwave reactions where the reaction temperature was 220 °C

From these results there is confirmation that a repeat of the $IrCl_3.xH_2O$ reaction with no base in ethylene glycol failed to reproduce the 30% yield obtained in the original set of results. However, the use of glycerol in place of ethylene glycol as the solvent in the $IrCl_3.xH_2O$ reactions did reproducibly increase the yield of the reaction to > 30%. The $Ir(acac)_3$ reactions only produced very low yields (2%) when heated for only 10 minutes. Upon increasing the reaction time to 30 minutes, the yields increased to give > 50% yields - in agreement with the earlier results.

5.3 Conclusions

The microwave-assisted synthesis of tris(2-phenylpyridine)iridium has been explored. Optimum yields were obtained when 2-phenylpyridine, $Ir(acac)_3$, sodium carbonate (ten equiv.) and a glycerol-water solvent was used with a heating time of 30 min. Seemingly the most important feature was using a mixture of glycerol and water as the solvent as ethylene glycol failed to yield any product and glycerol without water gave much reduced yields. This improvement can be prescribed to better dissolution of the inorganic base in the reaction mixture. Increasing the temperature seemed to make small improvements to the yields. However, it also increased the pressure in the reaction tubes and led to some reactions failing to run.

The $IrCl_3.xH_2O$ reactions also benefit from the use of glycerol and water solvents, with this solvent combination increasing the yields to a maximum of 32%. Increasing the reaction time did not increase the yields.

There remains much more to investigate in this field – there are many types of inorganic base that can be tested and extra additives such as the chloride-scavenging silver(I) triflate. However, it has been shown that yields comparable to those obtained by conventional heating can be obtained in vastly reduced times due to the dielectric heating afforded by the microwave.

Chapter 6 – Experimental Procedures

This Chapter details the experimental procedures and analytical data for each of the novel compounds presented in this thesis. This Chapter also includes the experimental procedures for some compounds which were already known in the literature and were synthesised in the course of this work.

6.1 General Methods

All reactions that required inert or dry atmospheres were carried out under a blanket of argon which was dried by passage through a column of phosphorus pentoxide and blue indicating silica gel. All reagents employed (with the exception of 2-(tributylstannyl)pyridine where 90% tech-grade was used) were of standard reagent grade and purchased from Aldrich, Lancaster, Avocado or Alfa Aesar and were used without further purification unless otherwise stated. Dichloromethane, diethyl ether, chloroform, methanol, tetrahydrofuran, hexane, toluene, *N*,*N*-dimethylformamide, petroleum ether (bp 40 – 60 °C) and acetonitrile were dried by an Innovative Technology Inc. solvent purification system and degassed before use. Pyridine was dried by standing over potassium hydroxide before use. All other chemicals were used as purchased.

Column chromatography was carried out using Davisil silica (40 – 63 μm). Solvents for chromatography were used without purification. Analytical thin layer chromatography was performed on Merck DC-Alufolien silica gel precoated on to aluminium plates (60 F_{254}, 0.2 mm thickness) precoated plates.

Solution ^{1}H NMR and ^{13}C NMR spectra were recorded on Mercury 200, Varian Unity 300, Bruker Avance 400 and Varian Inova 500 spectrometers operating at (^{1}H) 199.99, 299.91, 400.13, 499.99 and (^{13}C) 50.29, 75.42, 100.62, 124.99 MHz, respectively. Chemical shifts are reported in ppm downfield of tetramethylsilane (TMS), using TMS or the residual solvent as an internal reference. The following abbreviations are used in the listing of NMR spectra: s = singlet, d = doublet, dd = doublet of doublets, dt = doublet of triplets, t = triplet, q = quartet and m = multiplet. Splitting constants are reported in Hertz.

Mass spectra were obtained on a VG7070E instrument operating in EI mode at 70 eV, a Thermoquest Trace GCMS system or a Micromass LCT (TOF). Elemental analyses were obtained on an Exeter Analytical CE-440 elemental analyser. Melting points were determined in open-end capillaries using a Stuart Scientific SMP3 melting point apparatus at a maximum ramp rate of 5 °C min^{-1} without calibration.

UV-Vis spectra were recorded using a Varian Cary 5 spectrophotometer at ambient temperatures. PL spectra were recorded using a Jobin-Yvon Horiba Flurolog 3-22 Tau-3 spectrofluorimeter with a 0.5 – 2 nm bandpass using a Xenon lamp. Spectra were recorded using conventional 90 ° geometry. Solution-state PLQYs were measured against quinine sulphate and fluorescein standards.

Cyclic voltammetry experiments were carried out with a BAS-CV50W electrochemical workstation in a three-electrode cell equipped with a platinum disk (∅ 1.6) as working electrode, platinum wire as a counter electrode and a non-aqueous Ag/Ag^+ reference electrode (0.01 M $AgNO_3$ in dry MeCN), with *iR* compensation. CV of compounds **228**, **229**, **230, 237** and **240** were measured in dry benzonitrile with 0.1 M tetrabutylammonium hexafluorophosphate (Bu_4NPF_6) as a supporting electrolyte, under argon atmosphere. The potential of the reference electrode in benzonitrile (0.1 M Bu_4NPF_6) was checked against the ferrocene/ferrocenium couple (Fc/Fc^+), which showed the average potential against the reference electrode of +0.187 V.

The *ab initio* computations of the geometries were carried out with the Gaussian 03[170] package of programs at density functional theory (DFT) level using Pople's 6-31G split valence basis set supplemented by *d*-polarisation functions on heavy atoms. DFT calculations were carried out using Becke's three-parameter hybrid exchange functional[171, 172] with Lee-Yang-Parr gradient-corrected correlation functional (B3LYP).[173] Thus, the geometries were optimised with a B3LYP/6-31G(d) level of theory and the electronic structures were then calculated for a single point at B3LYP/6-311G(2d,p)// B3LYP/6-31G(d) level. The HOMO and LUMO orbital energies calculated at B3LYP/6-311G(2d,p)//B3LYP/6-31G(d) level are *ca.* 0.17 – 0.23 eV lower than that for B3LYP/6-31G(d) optimized geometries. The HOMO-LUMO gaps are quite similar, showing a deviation of only 0.01 – 0.03 eV. Space-filled structures for optimised geometries and contours of HOMO and LUMO orbitals were visualised using Molekel v.4.3 program.[174]

MEH-PPV was purchased from Aldrich. Indium-tin-oxide (ITO) coated glass from Merck with sheet resistance of 9 $\Omega\ \square^{-1}$ was used as the anode. The ITO coated glass was cleaned by ultrasonification in acetone and isopropyl alcohol for 30 minutes each and dried with a nitrogen gun. For the hole injection layer, poly(3,4-

ethylenedioxythiophene) was doped with polystyrene sulphonated acid (PEDOT:PSS, purchased from Bayer AG) and spin-coated onto the ITO prior to the deposition of the organic materials. The PEDOT:PSS layer (40 nm in thickness) was dried for 12 h in nitrogen at room temperature to remove residual solvent. For the blended devices, compounds **202** and **237** were blended with MEH-PPV and dissolved in chloroform (in solutions of up to 16 mg cm^{-3}) to provide the blended solutions and were spin-coated (at 750 or 1000 rpm) onto the ITO. For the single layer devices the bipolar compounds (**228**, **229**, **230**, **237** and **240**) were dissolved in chloroform (15 mg cm^{-3}) and were spin-coated onto the ITO to make 110 nm thick layers. Following the spin-coating, Ca (15 – 40 nm) and/or Al (100 nm) electrodes with 1 mm radius were thermally evaporated at a pressure of *ca.* 10^{-6} mbar.

Electrical measurements were conducted in a vacuum chamber (10^{-1} mbar). A D.C. bias was applied and the current was measured by a Keithley 2400 source measure unit and the light emitted from the device was collected by a large area photodiode (1.5 cm diameter) connected to a Keithley 485 digital picoammeter. For external quantum efficiency measurements, the light power was calculated using the photocurrent and the conversion factor (wavelength dependent) of the photodiode (ampere/watt). Electroluminescence (EL) spectra were measured using an Ocean Optics USB2000 Miniature Fibre Optic Spectrometer.

6.2 Experimental Procedures for Chapter 2

5-(4-Bromophenyl)-tetrazole (188)[175]

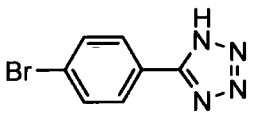

An argon-purged flask was charged with 4-bromobenzonitrile (6.00 g, 33.0 mmol), sodium azide (2.60 g, 39.9 mmol), ammonium chloride (2.30 g, 40.6 mmol) and degassed *N*,*N*-dimethylformamide (DMF) (100 ml). The solution was refluxed overnight producing a yellow solution with a suspension of undissolved base. The solution was cooled and water added before the solution was acidified to precipitate **188** which was filtered and recrystallised from a methanol and water solution to yield a white solid (6.69 g, 90%);

mp: 265.0 – 266.8 °C; Anal. Calcd. for $C_7H_5BrN_4$: C, 37.36; H, 2.24; N, 24.90, Found: C, 37.33; H, 2.21; N, 25.08; δ_H ($CDCl_3$) 7.84 (d, J = 8.4, 2H), 7.99 (d, J = 8.4, 2H).

2-(4-Bromophenyl)-5-(4-*tert*-butylphenyl)-1,3,4-oxadiazole (189)[176]

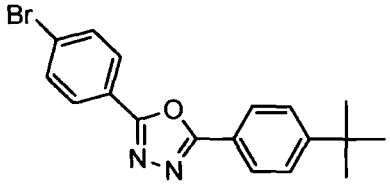

Method A

A flask was charged with 4-bromophenylhydrazide (3.31 g, 15.4 mmol) and pyridine (40 ml). 4-*tert*-Butyl benzoylchloride (3.9 ml, 20.8 mmol) was added and the solution was stirred at 80 °C for 1 h. The pyridine was removed by distillation yielding a yellow oil which was recrystallised from ethanol to produce a white solid (4.05 g, 70%). δ_H (DMSO-d_6) 1.33 (s, 9H), 7.54 (m, 2H), 7.84 (m, 6H), 10.48 (s, 1H), 10.61 (s, 1H); δ_c (DMSO-d_6) 30.88, 34.66, 125.24, 125.60, 127.29, 129.51, 129.73, 131.56, 131.70, 154.72, 164.93, 165.68.

This solid (3.14 g) was dissolved in phosphorous oxychloride ($POCl_3$) (35 ml) and refluxed overnight. The $POCl_3$ was removed by distillation to leave a white solid. This was recrystallised from ethanol to yield **189** as white needles (1.87 g, 63%); mp: 145.5 – 146.9 °C; Anal. Calcd. for $C_{18}H_{17}BrN_2O$: C, 60.52; H, 4.80; N, 7.84, Found: C, 60.46; H, 4.81; N 7.96; δ_H ($CDCl_3$) 1.38 (s, 9H), 7.58 (m, 2H), 7.68 (m, 2H), 8.02 (m, 4H); δ_c ($CDCl_3$) 31.11, 35.12, 120.92, 123.01, 126.09, 126.82, 128.29, 132.41, 155.56, 163.66, 164.87; MS (EI) *m/z*: 341 (M^+ - CH_3, ^{79}Br, 99%), (M^+ - CH_3, ^{81}Br, 100%), 356 (M^+, ^{79}Br, 70%), 368 (M^+, ^{81}Br, 69%).

Method B

An argon-purged flask was charged with 5-(4-bromophenyl)-tetrazole, **188**, (6.65 g, 29.5 mmol) and pyridine. 4-*tert*-Butyl benzoyl chloride (8.0 ml, 37.6 mmol) was added and the solution was refluxed until the emission of nitrogen stopped (~2 h). The solution was cooled and poured into water to precipitate the product, which was filtered and recrystallised from ethanol to yield **189** as shiny white needles (9.59 g, 90%). Analysis consistent with that obtained by Method A.

2,5-Bis(4-bromophenyl)-1,3,4-oxadiazole (190)[177]

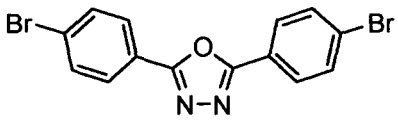

An argon-purged flask was charged with 5-(4-bromophenyl)-tetrazole, **188**, (1.00 g, 4.44 mmol), 4-bromobenzoyl chloride (1.07 g, 4.9 mmol) and pyridine (25 ml). The mixture was stirred at 120 °C overnight. After cooling, water was added to precipitate the product which was isolated by suction filtration and recrystallised from ethanol to yield **190** as a white solid (1.36 g, 81%); mp: 256.4 – 258.7 °C; Anal. Calcd. for $C_{14}H_8Br_2N_2O$: C, 44.25; H, 2.12; N, 7.37. Found: C, 44.18; H, 2.09; N, 7.39; δ_H (DMSO-d_6) 7.85 (d, J = 7.5, 4H), 8.07 (d, J = 7.5, 4H); MS (EI) *m/z*: 378 (M^+, ^{79}Br, ^{79}Br, 54%), 380 (M^+, ^{79}Br, ^{81}Br, 100%), 382 (M^+, ^{81}Br, ^{81}Br, 53%).

2-Chloro-5-(5-phenyl-1,3,4-oxadiazol-2-yl)pyridine (191)

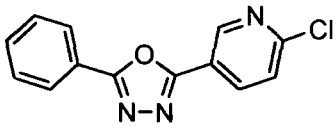

An argon-purged flask was charged with 5-phenyltetrazole (2.00 g, 13.7 mmol), 6-chloronicotinoyl chloride (2.41 g, 13.7 mmol) and pyridine (50 ml). The solution was stirred at 100 °C for 3 h. After cooling, the solution was poured into water and the precipitate was isolated by suction filtration and recrystallised from ethanol and then ethyl acetate to yield **191** as a pink solid (1.90 g, 54%); mp: 178.0 – 178.5 °C; Anal. Calcd. for $C_{13}H_8ClN_3O$: C, 60.60, H, 3.13; N, 16.31. Found: C, 60.62; H, 3.10; N, 16.42; δ_H (DMSO-d_6) 7.67 (m, 3H), 7.82 (d, J = 8.4, 1H), 8.18 (m, 2H), 8.56 (dd, ^1J = 8.4, ^2J = 2.8, 1H), 9.17 (m, 1H); δ_C (DMSO-d_6) 119.51, 123.02, 125.11, 126.85, 129.42, 132.29, 137.59, 147.84, 153.03, 161.58, 164.52.

2-(4-Methoxyphenyl)-5-phenyl-1,3,4-oxadiazole (192)

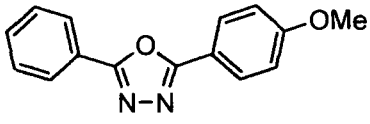

An argon-purged flask was charged with phenyl tetrazole (7.50 g, 51.3 mmol), 4-methoxybenzoyl chloride (7.10 ml, 51.5 mmol) and pyridine (100 ml). The solution was stirred at 120 °C overnight. After cooling, the suspension was poured

into water. The white precipitate was isolated by suction filtration and washed with water before being recrystallised from ethanol to yield **192** as white needles (11.71 g, 90%); mp: 148.2 – 149.9 °C; Anal. Calcd. for $C_{15}H_{12}N_2O_2$: C, 71.42; H, 4.79; N, 11.10. Found: C, 71.43; H, 4.80; N, 11.12; δ_H ($CDCl_3$) 3.89 (s, 3H), 7.04 (d, J = 8.8, 2H), 7.54 (m, 3H), 8.08 (m, 2H), 8.13 (m, 2H); δ_C ($CDCl_3$) 55.47, 114.53, 116.52, 124.16, 126.84, 128.71, 129.02, 131.50, 162.37, 164.15, 164.55; MS (EI) *m/z*: 252 (M^+, 100%).

4-(Tetrazol-5-yl)-benzoic acid methyl ester[43]

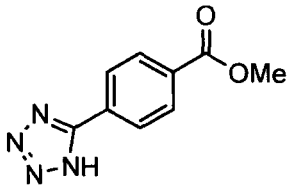

An argon-purged flask was charged with 4-cyanobenzoic acid methyl ester (1.35 g, 8.4 mmol), sodium azide (0.65 g, 10.1 mmol), ammonium chloride (0.54 g, 10.1 mmol) and degassed DMF (40 ml). The mixture was refluxed for 48 h. After cooling, the solution was acidified with ~2 M HCl to pH 1, precipitating out a white solid. This was filtered and recrystallised from a methanol and water solution to yield the product as a white solid (1.52 g, 89%); mp: 230.8 – 232.5 °C; Anal. Calcd. for $C_9H_8N_4O_2$: C, 52.94; H, 3.95; N, 27.44. Found: C, 52.74; H, 3.96; N, 27.34; δ_H (DMSO-d_6) 3.91 (s, 3H), 8.17 (m, 4H).

4-[5-(4-*tert*-Butylphenyl)-1,3,4-oxadiazol-2-yl]-benzoic acid methyl ester (193)

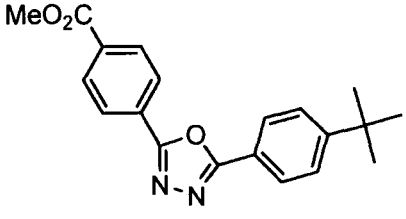

An argon-purged flask was charged with 4-(tetrazol-5-yl)-benzoic acid methyl ester (0.51 g, 2.5 mmol) and degassed pyridine (20 ml). 4-*tert*-Butylbenzoyl chloride (0.9 ml, 4.9 mmol) was added and the solution was refluxed overnight. The pyridine was removed by distillation and the resulting orange solid was diluted with methanol (20 ml). Water was added to precipitate the crude product which was filtered. The solid was dissolved in ethyl acetate and filtered through a silica plug to remove impurities. The ethyl acetate was removed *in vacuo* and the crude product recrystallised from a methanol and water solution twice to give **193** as a shiny white solid (0.43 g, 51%); mp: 212.6 – 214.3 °C;

Anal. Calcd. for $C_{20}H_{20}N_2O_3$: C, 71.41; H, 5.99; N, 8.33. Found: C, 70.92; H, 5.98; N, 8.33; δ_H ($CDCl_3$) 1.39 (s, 9H), 3.98 (s, 3H), 7.57 (d, J = 6.8, 2H), 8.09 (d, J = 6.8, 2H), 8.22 (m, 4H); δ_C ($CDCl_3$) 31.11, 35.14, 52.45, 120.84, 126.14, 126.81, 126.92, 127.87, 130.27, 132.74, 155.71, 163.63, 165.19, 166.16; MS (EI) *m/z*: 321 (M^+ - CH_3, 100%), 336 (M^+, 69%).

2-(4-Fluorophenyl)-5-phenyl-1,3,4-oxadiazole (194)[178]

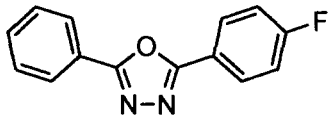

A flask was charged with 4-fluorobenzoyl chloride (3.0 ml, 25.4 mmol), phenyltetrazole (3.60 g, 24.6 mmol) and pyridine (60 ml). The mixture was stirred for 15 h at 120 °C. After cooling, the mixture was poured into water (150 ml). The precipitate was isolated by suction filtration and recrystallised from ethanol to yield **194** as white needles (3.90 g, 66%); mp: 155.0 – 155.7 °C; Anal. Calcd. for $C_{14}H_9FN_2O$: C, 69.99; H, 3.78; N, 11.66. Found: C, 69.91; H, 3.79; N, 11.38; δ_H ($CDCl_3$) 7.16 (m, 2H), 7.47 (m, 3H), 8.06 (m, 4H); δ_C ($CDCl_3$) 116.70 (d, $^2J_{CF}$ = 21.9), 120.65 (d, $^3J_{CF}$ = 3.7), 124.20, 127.26, 132.12, 163.89, 164.13, 166.41 (d, $^1J_{CF}$ = 229.1), 164.96; δ_F ($CDCl_3$) - 107.23; MS (EI) *m/z*: 183 (M^+ - C_3H_2F, 100%), 240 (M^+, 74%).

4-Bromobenzoic acid hydrazide (196)[179]

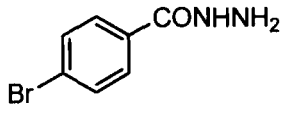

A flask was charged with 4-bromobenzoic acid (5.02 g, 25.0 mmol), methanol (50 ml) and a few drops of *conc.* H_2SO_4. The solution was refluxed overnight before the excess methanol was distilled off and water added to precipitate out the product which was filtered and recrystallised from a methanol and water solution to yield a white solid. This was dissolved in methanol (50ml), hydrazine monohydrate (25 ml) was added and the solution refluxed overnight. After cooling, water was added to precipitate out **196** which was isolated as a white solid (4.54 g, 85%); δ_H (DMSO-d_6) 4.53 (s, 2H), 7.74 (dd, ^1J = 29.6, ^2J = 8.4, 4H), 9.87 (s, 1H); δ_c (DMSO-d_6) 39.76, 129.02, 131.30.

4-[5-(4-*tert*-Butylphenyl)-1,3,4-oxadiazol-2-yl]-benzoic acid hydrazide (197)

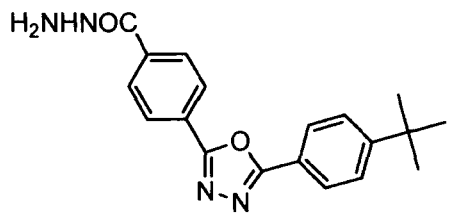

A flask was charged with 4-[5-(4-*tert*-butyl-phenyl)-1,3,4-oxadiazol-2-yl]-benzoic acid methyl ester, **193**, (250 mg, 0.74 mmol) and methanol (40 ml). Hydrazine monohydrate (25 ml) was added and the solution was refluxed overnight. After cooling, the solution was poured into water to precipitate **197** which was isolated by suction filtration as a white solid (220 mg, 88%); mp: 233.0 – 234.7 °C; Anal. Calcd. for $C_{19}H_{20}N_4O_2$: C, 67.84; H, 5.99; N, 16.66. Found: C, 67.71; H, 5.93; N, 16.83; δ_H ($CDCl_3$) 1.39 9 (s, 9H), 4.19 (s, 2H), 7.48 (s, 1H), 7.57 (d, J = 8.4, 2H), 7.93 (d, J = 8.4, 2H), 8.08 (d, J = 8.4, 2H), 8.24 (d, J = 8.4, 2H); MS (EI) *m/z*: 305 (M^+ - N_2H_3, 100%), 336 (M^+, 15%).

2-(4-*tert*-Butylphenyl)-5-{4-[5-(4-*tert*-butylphenyl)-1,3,4-oxadiazol-2-yl]phenyl}-1,3,4-oxadiazole (65)

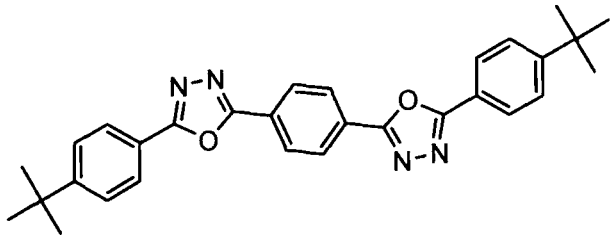

A flask was charged with 4-[5-(4-*tert*-butylphenyl)-1,3,4-oxadiazol-2-yl]-benzoic acid hydrazide, **197**, (300 mg, 0.89 mmol) and dry pyridine (25 ml). 4-*tert*-Butylbenzoyl chloride (0.25 ml, 1.37 mmol) was added and the mixture was stirred for 15 h at 40 °C. The pyridine was removed by distillation and the residue was recrystallised from a methanol and water solution. The white precipitate was isolated by suction filtration. After thorough drying, the solid was combined with $POCl_3$ (15 ml) and stirred at 120 °C for 15 h. The $POCl_3$ was removed by distillation and the residual solid was recrystallised from ethanol to yield **65** as a white powder (365 mg, 86%); mp: 321.2 – 322.8 °C; δ_H ($CDCl_3$) 1.38 (s, 18H), 7.57 (d, J = 7.9, 4H), 8.09 (d, J = 7.9, 4H), 8.32 (s, 4H); δ_C ($CDCl_3$) 31.12, 35.16, 120.79, 126.17, 126.66, 126.94, 127.49, 155.79, 163.55, 165.18; MS (EI) *m/z* 479 (M^+, 100%).

2-(4-*tert*-Butylphenyl)-5-{4-[5-(4-bromophenyl)-1,3,4-oxadiazol-2-yl]phenyl}-1,3,4-oxadiazole (198)

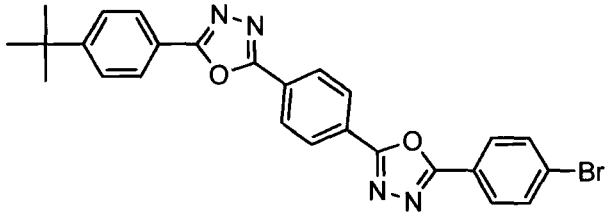

A flask was charged with 4-[5-(4-*tert*-butyl-phenyl)-1,3,4-oxadiazol-2-yl]-benzoic acid hydrazide, **197**, (1.00 g, 2.98 mmol) and dry pyridine (25 ml). 4-Bromobenzoyl chloride (1.00 g, 4.56 mmol) was added and the mixture was stirred at room temperature for 15 h. The pyridine was removed by distillation and the residue was recrystallised from ethanol to yield a white solid that was isolated by suction filtration. After thorough drying, the solid was combined with $POCl_3$ (30 ml) and stirred for 15 h at 120 °C. The $POCl_3$ was removed by distillation and the residue was recrystallised from ethanol to yield **198** as a white powder (1.16 g, 78%); mp 327.6 – 328.9 °C; Anal. Calcd. for $C_{26}H_{21}BrN_4O_2$: C, 62.28; H, 4.22; N, 11.17. Found: C, 62.17; H, 4.15; N, 11.10; δ_H ($CDCl_3$) 1.38 (s, 9H), 7.57 (d, J = 8.2, 2H), 7.71 (d, J = 8.2, 2H), 8.04 (d, J = 8.2, 2H), 8.09 (s, 4H); δ_C ($CDCl_3$) 31.12, 35.16, 120.79, 122.58, 126.17, 126.31, 126.81, 126.94, 127.53, 127.53, 127.56, 128.44, 132.56, 155.80, 163.95, 164.36, 165.23; MS (EI) *m/z*: 501 (M^+, ^{79}Br, 100%), 503 (M^+, ^{81}Br, 100%).

2-Bromo-9,9-dihexylfluorene (200)[180]

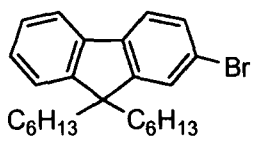

An argon-purged flask was charged with 2-bromofluorene (12.49 g, 51.0 mmol), 1-bromohexane (36 ml, 0.26 mol) and dry THF (150 ml). The colourless solution was cooled with stirring to 0 °C. Potassium *tert*-butoxide (5.72 g, 51.0 mmol) was added in one portion turning the solution red, then pink. After 2 h another portion of potassium *tert*-butoxide (5.72 g, 51.0 mmol) was added again turning the solution red. After 1 h, a final portion of potassium *tert*-butoxide (5.72 g, 51.0 mmol) was added and the solution was stirred overnight at room temperature. The mixture was filtered to give a light green inorganic solid. The filtrate was concentrated *in vacuo* to yield a colourless oil. This was purified by column chromatography on silica, eluting with petroleum ether (40 – 60 °C). The product **200** was isolated as a colourless oil (17.98 g, 85%); δ_H ($CDCl_3$) 0.59 (m, 4H),

0.77 (t, J = 7.2, 6H), 1.03 (m, 12H), 1.96 (m, 4H), 7.32 (m, 3H), 7.45 (m,2H), 7.54 (m, 1H), 7.66 (m, 1H); δ_C ($CDCl_3$) 13.99, 22.57, 23.66, 29.64, 31.47, 40.29, 55.37, 119.73, 120.94, 121.01, 122.87, 126.91, 127.45, 129.86, 140.02, 140.14, 150.31, 152.97

9,9-Dihexylfluoren-2-yl boronic acid (201)[181]

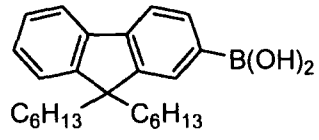

An argon-purged flask was charged with 2-bromo-9,9-dihexylfluorene, **200**, (12.13 g, 29 mmol) and dry THF (100 ml). The solution was cooled to -78 °C with stirring and *n*-butyllithium (2.5 M solution, 15 ml, 38 mmol) was slowly added and the solution was stirred for 1.5 h. Triisopropyl borate (10 ml, 43 mmol) was added and the solution was stirred for a further 1 h at -78 °C before being allowed to warm to room temperature. HCl (7 ml) was added and the solution was stirred overnight. The THF was removed *in vacuo* and diethyl ether and water were added. The layers were separated and the aqueous layer was extracted with diethyl ether and the combined organic extracts were washed with water, dried ($MgSO_4$), filtered and concentrated to yield a white foamy solid. This was purified by column chromatography on silica, eluting with 0 – 50% ethyl acetate in DCM to afford **201** as a white foamy solid (8.62 g, 78%); mp 69.5 – 70.9 °C; Anal. Calcd. For $C_{25}H_{35}BO_2$: C, 83.33; H, 9.23. Found: C, 82.97; H, 9.25; δ_H ($CDCl_3$) 0.71 – 0.78 (m, 10H), 1.10 (m, 12H), 2.10 (m, 4H), 7.41 (m, 3H), 7.82 (m, 1H), 7.91 (d, J = 7.2, 1H), 8.24 (s, 1H), 8.32 (d, J = 7.2, 1H); δ_C ($CDCl_3$) 13.97, 22.54, 23.81, 29.73, 40.39, 55.06, 119.25, 120.38, 122.97, 123.05, 126.83, 127.90, 129.69, 134.59, 140.74, 145.57, 150.13, 151.66.

2,5-Bis[4-(9,9-dihexyl-9H-fluoren-2-yl)phenyl]-1,3,4-oxadiazole (202)

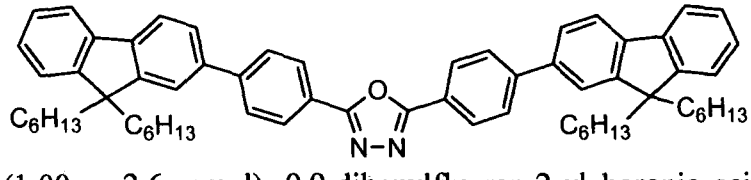

A flask was charged with 2,5-bis(4-bromophenyl)-1,3,4-oxadiazole, **190**, (1.00 g, 2.6 mmol), 9,9-dihexylfluoren-2-yl boronic acid, **201**, (2.00 g, 5.3 mmol), potassium carbonate (0.5 M solution, 40 ml) and THF (100 ml). The mixture was

degassed for 1 h before bis(triphenylphosphine)palladium dichloride (0.14 g, 7.5 mol %) was added and the mixture was heated to 75 °C for 3 days. After cooling, the THF was removed *in vacuo* and DCM added. The layers were separated and the aqueous layer was extracted with DCM. The combined organic layers were dried ($MgSO_4$), filtered and concentrated yielding a dark oil. This was purified by column chromatography on silica eluting with petroleoum ether (40 – 60 °C) then DCM. The product was recrystallised from ethanol to yield **202** as a white solid (1.01 g, 43%); mp: 180.5 – 181.4 °C; Anal. Calcd. for $C_{64}H_{74}N_2O$: C, 86.63; H, 8.41; N, 3.16. Found: C, 86.86; H, 8.46; N, 3.20; δ_H ($CDCl_3$) 0.70 – 0.78 (m, 20H), 1.07 (m, 24H), 2.05 (m, 8H), 7.37 (m, 6H), 7.65 (m, 4H), 7.75 (d, J = 6.6, 2H), 7.80 (d, J = 7.6, 2H), 7.86 (d, J = 8.4, 4H), 8.27 (d, J = 8.4, 4H); δ_C ($CDCl_3$) 13.98, 22.56, 23.78, 29.69, 31.48, 40.39, 55.26, 119.93, 120.13, 121.43, 122.50, 122.97, 126.09, 126.89, 127.38, 127.42, 127.74, 138.56, 140.47, 141.43, 145.03, 151.08, 151.68, 164.59; MS (EI) *m/z*: 886 (M^+, 100%).

9,9'-Spirobifluorene (206)[88]

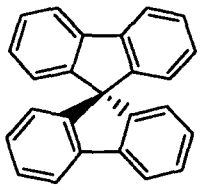

An argon-purged flask was charged with magnesium turnings (1.30 g, 53.5 mmol), 2-bromobiphenyl (8.5 ml, 50.2 mmol) and dry diethyl ether (45 ml). The mixture was refluxed for 3 h at 40 °C forming the brown-coloured Grignard solution. A separate argon-purged flask was charged with 9-fluorenone (9.10 g, 50.5 mmol) and dry diethyl ether (50 ml). The Grignard solution was added via a cannular and the solution was refluxed for 15 h. The cooled suspension was filtered and the yellow solid was added to an ice-cold saturated NH_4Cl solution (100 ml) and stirred for 2 h. The pale yellow solid was isolated by suction filtration and recrystallised from ethanol to yield the white carbinol, **205**. The carbinol was dissolved in acetic acid and refluxed with a few drops of conc. HCl for 10 min. After cooling, the product precipitated out and was isolated by suction filtration and washed with ethanol to give **206** (9.60 g, 60%).

Carbinol 205: δ_H ($CDCl_3$) 2.23 (s, 1H), 6.00 (d, J = 7.6, 2H), 6.60 (t, J = 12, 2H), 6.81 (t, J = 8.0, 1H), 6.89 (d, J = 12, 1H), 7.17 (m, 8H), 7.31 (m, 1H), 7.53 (m, 1H), 8.45

(d, J = 8.0, 1H); δ_C ($CDCl_3$) 82.5, 120.1, 124.3, 125.1, 126.1, 126.3, 126.9, 127.1, 127.9, 128.7, 128.9, 131.3, 139.6, 140.2, 140.3, 141.0, 150.6.

9,9'-Spirobifluorene 206: mp: 203.7 – 205.0 °C; δ_H ($CDCl_3$) 6.73 (d, J = 7.6, 2H), 7.10 (t, J = 8.4, 2H), 7.37 (t, J = 7.6, 2H), 7.84 (d, J = 6.8, 2H); δ_C ($CDCl_3$) 120.0, 124.0, 127.7, 127.8, 141.8, 148.8.

2-Bromo-9-fluorenone (208)[88]

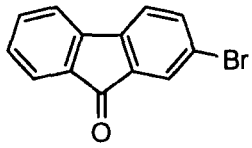

A flask was charged with 2-bromofluorene (14.99 g, 61.2 mmol), pyridine (150 ml) and tetrabutylammonium hydroxide (2 ml). The solution was stirred overnight with a stream of air passed through it. The resulting suspension was poured into water (300 ml) and acidified with acetic acid. The resulting solid was isolated by suction filtration and recrystallised from ethanol to yield **208** as yellow needles (13.06 g, 82%); mp 147.4 – 148.5 °C; Anal. Calcd. For $C_{13}H_7BrO$: C, 60.26; H, 2.72. Found: C, 59.98; H, 2.68; δ_H ($CDCl_3$) 7.30 – 7.34 (m, 1H), 7.38 (d, J = 8.0, 1H), 7.50 (dd, ^1J = 5.2, ^2J = 0.8, 2H), 7.59 (dd, ^1J = 7.6, ^2J = 1.6, 1H), 7.64(dt, ^1J = 7.6, ^2J = 0.8, 1H), 7.50 (d, J = 2.0, 1H); δ_C ($CDCl_3$) 120.43, 121.70, 122.93, 124.60, 127.56, 129.42, 133.72, 135.01, 135.80, 137.08, 143.01, 143.68, 192.33; MS (EI) *m/z*: 151 (M^+ - COBr, 100%), 258 (M^+, ^{79}Br, 50%), 260 (M^+, ^{81}Br, 50%).

2-Bromo-9,9'-spirobifluorene (207)[88]

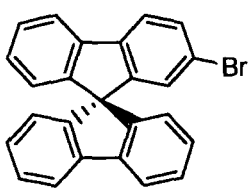

An argon-purged flask was charged with magnesium (0.47 g, 19.3 mmol). A solution containing 2-bromobiphenyl (3.0 ml, 17.4 mmol) in dry diethyl ether (50 ml) was slowly added via a dropping funnel. The mixture was gently heated for 2h. A separate argon-purged flask was charged with 2-bromo-9-fluorenone (4.60 g, 17.8 mmol) in dry THF (75 ml). The Grignard solution was transferred by a canular to the fluorenone solution which was gently refluxed overnight. After cooling, the precipitate

was isolated by suction filtration and then stirred in a saturated ammonium chloride solution (100 ml) for 2 h. The resulting solid was isolated by suction filtration and was recrystallised from ethanol and water to yield the white carbinol, **209**. This was dissolved in acetic acid before 2 drops of conc. HCl were added and the solution refluxed for 10 min. After cooling, water was added and the product precipitated out. After being isolated by suction filtration it was recrystallised from ethanol to yield **207** as a white solid (1.36 g, 20%); Anal. Calcd. for $C_{25}H_{15}Br$: C, 75.96; H, 3.82. Found: C, 75.86; H, 3.79; δ_H ($CDCl_3$) 6.72 (m, 3H), 6.85 (d, J = 1.6, 1H), 7.13 (t, J = 7.6, 3H), 7.38 (q, J = 7.2, 3H), 7.49 (dd, ^1J = 8.0, ^2J = 1.6, 1H), 7.70 (d, J = 7.6, 1H), 7.81 – 7.86 (m, 3H); δ_C ($CDCl_3$) 65.84, 120.05, 120.13, 121.31, 121.42, 124.06, 124.11, 127.30, 127.91, 127.95, 127.99, 128.26, 130.91, 140.66, 140.78, 141.75, 147.94, 148.58, 150.85. The compound was used without further analysis.

9,9'-Spirobifluoren-2-ylboronic acid (210)

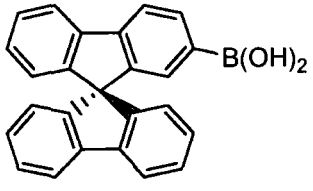

An argon-purged flask was charged with 2-bromo-9,9'-spirobifluorene, **207**, (1.20 g, 3.03 mmol) and dry THF (50 ml). The solution was cooled to -78 °C and *n*-butyllithium (2.5 M solution, 1.90 ml, 4.75 mmol) was added dropwise. The slurry was stirred for a further 2 h at -78 °C before triisopropylborate (1.40 ml, 6.07 mmol) was added. The mixture was allowed to warm to room temperature overnight. Water was added to quench the reaction and the solution was stirred for a further 0.5 h. The layers were separated and the aqueous layer was extracted with diethyl ether. The combined organic extracts were washed with water, dried ($MgSO_4$), filtered and concentrated to yield a white solid. This was purified by column chromatography on silica eluting with DCM followed by 3:7 DCM:ethyl acetate to yield **210** as a white foamy solid (0.59 g, 54%); mp 187.0 – 187.7 °C. This compound was used without further analysis.

2,5-Bis[4-(9,9-spirobifluoren-2-yl)phenyl]-1,3,4-oxadiazole (211)

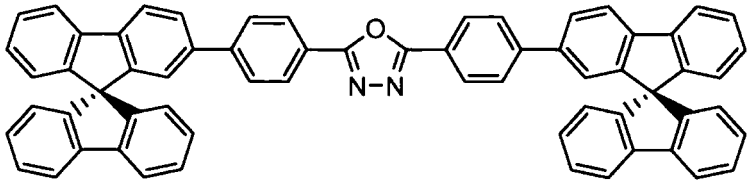

A flask was charged with 9,9-spirobifluoren-2-ylboronic acid, **210**, (0.48 g, 1.3 mmol), 2,5-bis(4-bromophenyl)-1,3,4-oxadiazole, **190**, (0.20 g, 0.53 mmol), sodium hydroxide (2 M solution, 20 ml) and THF (50 ml). The solution was degassed for 1 h before bis(triphenylphosphine)palladium dichloride (18 mg, 5 mol %) was added and the mixture was stirred at 75 °C for 3 days. After cooling, the layers were separated and the aqueous layer was extracted with diethyl ether. The combined organic extracts were washed with brine, dried ($MgSO_4$), filtered and concentrated. The product was purified by column chromatography on silica eluting with 0 – 10% ethyl acetate in DCM. The product was recrystallised from ethanol to yield **211** as a white solid (300 mg, 67%); mp > 370 °C; δ_H ($CDCl_3$) 6.74 (d, J = 7.6, 2H), 6.79 (d, J = 7.2, 4H), 7.00 (s, 2H), 7.13 (t, J = 7.6, 6H), 7.39 (t, J = 7.6, 6H), 7.58 (d, J = 8.4, 4H), 7.78 (dd, ^1J = 7.6, ^2J = 1.6, 2H), 7.88 (m, 6H), 7.95 (d, J = 8.0, 2H), 8.05 (d, J = 8.8, 4H); δ_C ($CDCl_3$) 66.07, 120.10, 120.22, 120.48, 122.50, 122.63, 124.09, 124.12, 127.00, 127.18, 127.58, 127.86, 127.93, 128.17, 139.45, 141.06, 141.83, 142.02, 144.14, 148.53, 149.30, 149.75, 164.39; MS (ES) *m/z*: 851 (M^+ + H, 100%); HRMS calcd. for $C_{64}H_{39}N_2O$ (M^+ + H): 851.3057. Found: 851.3068.

2-[9,9-Dihexyl-2-(4,4,5,5-tetramethyl-1,3,2-dioxaborolan-2-yl)-9H-fluoren-7-yl]-4,4,5,5-tetramethyl-1,3,2-dioxaborolane (215)[180]

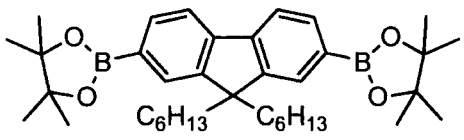

An argon-purged flask was charged with 2,7-dibromo-9,9-dihexylfluorene, **214**, (3.00 g, 6.1 mmol) and dry THF (70 ml) and the solution was cooled to -78 °C. *n*-Butyllithium (2.5 M solution, 7.3 ml, 18.3 mmol) was added dropwise and the resulting white slurry was stirred for 1h at -78 °C. 2-Isopropoxy-4,4,5,5-tetramethyl-1,3,2-dioxaborolane (4.1 ml, 20.1 mmol) was added in one portion and the mixture was slowly warmed to room temperature. Water was added to the

yellow solution to quench the reaction. The THF was removed *in vacuo* and the product was extracted into diethyl ether. The combined organic extracts were washed with brine, dried ($MgSO_4$), filtered and concentrated to yield a white solid. The product was purified by passing the crude product through a silica plug initially using petroleum ether (40 – 60 °C) to wash out the impurity and then DCM to elute the product. The product was recrystallised from ethanol to yield **215** as white needles (0.98 g, 27%); δ_H ($CDCl_3$) 0.55 (m, 4H), 0.75 (t, J = 7.0, 6H), 1.06 (m, 12H), 1.40 (s, 24H), 2.00 (m, 4H), 7.70 (d, J = 7.1, 2H), 7.75 (m, 2H), 7.79 (d, J = 7.1, 2H); δ_C ($CDCl_3$) 13.98, 22.54, 23.57, 24.93, 29.61, 31.42, 40.07, 55.17, 83.70, 119.36, 128.93, 133.64, 143.92, 150.47.

6.3 Experimental Procedures for Chapter 3

2,7-Dibromo-9,9-dihexylfluorene (214)[182]

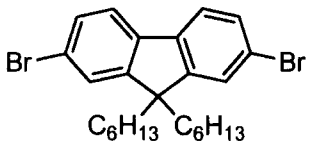

An argon-purged flask was charged with 2,7-dibromofluorene (12.96 g, 40 mmol), 1-bromohexane (28 ml, 0.2 mol) and dry THF (100 ml). The mixture was heated until all the solids had dissolved and then cooled to 0 °C. 1. Potassium *tert*-butoxide (1.0 M solution, 40 ml, 40 mmol) was added and the solution immediately changed to a dark red colour. After 0.5 h of stirring at 0 °C, more potassium *tert*-butoxide (40 ml) was added and the solution was stirred overnight. Filtering through a celite plug gave a purple inorganic solid. The solvents were removed from the filtrate *in vacuo* leaving a green oil. This was recrystallised from ethanol yielding large off-white crystals of **214**, which were filtered and washed thoroughly with ethanol (17.27 g, 88%); δ_H ($CDCl_3$) 0.57 (m, 4H), 0.79 (t, J = 7.2, 6H), 1.05 (m, 12H), 1.93 (t, J = 16.8, 4H), 7.47 (t, J = 1.2, 4H), 7.52 (d, J = 8.8, 2H); δ_C ($CDCl_3$) 14.0, 22.6, 23.6, 29.6, 31.5, 40.2, 55.7, 121.1, 121.5, 126.2, 130.2, 139.1, 152.6.

(7-Bromo-9,9-dihexylfluoren-2-yl) trimethyl silane (232)[180]

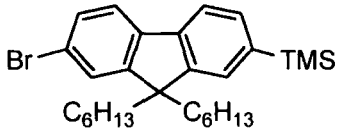

An argon-purged flask was charged with 2,7-dibromo-9,9-dihexylfluorene, **214**, (5.99 g, 12.2 mmol) and dry THF (100 ml) and cooled with stirring to -78 °C. *n*-Butyllithium (2.5 M solution, 4.9 ml, 12.2 mmol) was added slowly over 0.5 h and the solution was stirred for a further 1 h at -78 °C. Trimethylsilylchloride (2.4 ml, 18.9 mmol) was added and the solution was allowed to slowly warm to room temperature before being quenched with water. The layers were separated and the aqueous layer was extracted with petroleum ether. The combined organic extracts were washed with brine, dried ($MgSO_4$), filtered and concentrated to yield a yellow oil. This was purified by column chromatography on silica, eluting with petroleum ether (40 – 60 °C) to give **232** as a colourless oil (5.27 g, 89%); δ_H ($CDCl_3$) 0.31 (s, 9H), 0.61 (m, 4H), 0.78 (m, 6H), 1.05 (m, 12H), 1.93 (m, 4H), 7.44 (m, 4H), 7.58 (m, 1H), 7.65 (m, 1H); δ_c ($CDCl_3$) 0.00, 14.88, 23.47, 24.51, 30.42, 32.25, 40.95, 56.24, 119.91, 122.02, 127.83, 128.36, 128.47, 131.07, 132.86, 140.58, 141.05, 141.04, 150.40, 154.10.

(2-Trimethylsilyl-9,9-dihexylfluoren-7-yl) boronic acid (233)[127]

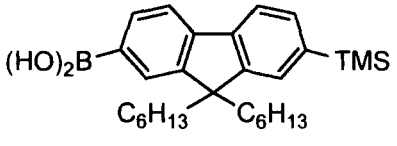

An argon-purged flask was charged with (7-bromo-9,9-dihexylfluoren-2-yl) trimethyl silane, **232**, (5.00 g, 10.3 mmol) and dry THF (75 ml) and cooled with stirring to -78 °C. *n*-Butyllithium (2.5 M solution, 4.9 ml, 12.3 mmol) was slowly added and the solution was stirred for a further 2 h before triisopropyl borate (3.8 ml, 16.5 mmol) was added and the solution was allowed to warm to room temperature. Water was added and the solution was stirred for a further 0.5 h. DCM was added and the layers were separated and the aqueous layer was extracted with DCM. The combined organic layers were washed with water, dried ($MgSO_4$), filtered and concentrated to yield a yellow oil. This was purified by column chromatography on silica, eluting with a mixture of petroleum ether (40 – 60 °C):ethyl acetate (7:3 v/v). The product, **233**, was isolated as a crunchy white solid anhydride (2.17 g, 47%); Anal. Calcd. for $C_{28}H43BO_2Si$: C, 77.75; H, 9.55. Found: C, 78.12; H, 9.53; δ_H ($CDCl_3$) 0.35

(s, 9H), 0.76 (m, 10H), 1.10 (m, 12H), 2.11 (m, 4H), 7.45 (m, 2H), 7.81, (d, J = 7.8, 1H), 7.90 (d, J = 7.8, 1H), 8.23 (s, 1H), 8.31 (d, J = 7.5); δ_c ($CDCl_3$) 0.00, 14.85, 23.35, 24.62, 30.49, 31.78, 32.26, 41.02, 55.85, 120.23, 120.49, 128.63, 130.65, 132.71, 135.44, 141.09, 142.20, 146.41, 151.20, 151.67.

4,4,5,5-Tetramethyl-2-(9,9-dihexyl-2-(trimethylsilyl)-fluoren-7-yl)-1,3,2-dioxaborolane (234)[180]

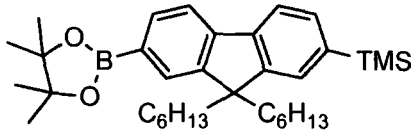

An argon-purged flask was charged with 2,7-dibromo-9,9-dihexylfluorene, **214**, (9.00 g, 18.3 mmol) and dry THF (70 ml) and cooled to -78 °C. *n*-Butyllithium (2.5 M solution, 7.3 ml, 18.3 mmol) was added dropwise and the resulting green solution was stirred at -78 °C for 0.5 h. Trimethylsilyl chloride (3.4 ml, 26.8 mmol) was added in one portion and the solution was stirred at -78 °C for a further 0.5 h before being allowed to warm to room temperature for 1 h. The reaction was quenched with brine and layers were separated. The aqueous layer was extracted with diethyl ether and the combined organic extracts were dried ($MgSO_4$), filtered and concentrated to yield a yellow oil. The crude product was purified by column chromatography on silica eluting with petroleum ether (bp 40 – 60 °C) to yield a colourless oil which was used without further purification.

The oil was dissolved in dry THF (50 ml) under argon and cooled to -78 °C. *n*-Butyllithium (2.5 M solution, 7.4 ml, 18.5 mmol) was added dropwise and the solution stirred at -78 °C for a further 0.5 h. 2-Isopropyl-4,4,5,5-tetramethyl-1,3,2-dioxaborolane (4.2 ml, 20.6 mmol) was added in one portion and the reaction was slowly allowed to warm to room temperature overnight. Brine was added and the mixture was stirred for a further 3 h. The product was extracted into diethyl ether and the combined organic extracts were washed with water, dried ($MgSO_4$), filtered and concentrated to yield a white solid. This was purified by column chromatography on silica eluting with 5% ethyl acetate in DCM to yield **234** as a white solid (6.76 g, 69%); mp: 113.2 – 115.1 °C; Anal. Calcd. for $C_{34}H_{53}BO_2Si$: C, 76.66; H, 10.03. Found: C, 76.73; H, 10.05; δ_H ($CDCl_3$) 0.30 (s, 9H), 0.60 (m, 4H), 0.76 (t, J = 6.7, 6H), 1.03

(m, 12H), 1.39 (s, 12H), 1.98 (t, J = 8.4, 4H), 7.47 (s, 1H), 7.48 (d, J = 8.5, 1H), 7.77 (d, J = 8.5, 2H), 7.75 (s, 1H), 7.80 (d, J = 8.5, 1H); δ_C ($CDCl_3$) 0.00, 14.86, 23.36, 24.48, 25.72, 25.84, 30.43, 32.22, 40.87, 55.91, 84.58, 119.96, 120.23, 128.58, 129.84, 132.58, 134.56, 140.50, 142.46, 145.00, 151.01, 151.35.

2-(4-*tert*-Butylphenyl)-5-[4-(9,9-dihexyl-7-trimethylsilylfluoren-2-yl)-phenyl]-1,3,4-oxadiazole (235)

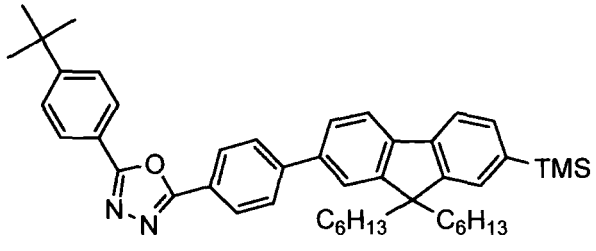

Method A

A flask was charged with 2-trimethylsilyl-9,9-dihexylfluorenyl-7-boronic acid, **233**, (3.38 g, 7.5 mmol), 2-(4-bromophenyl)-5-(4-*tert*-butylphenyl)-1,3,4-oxadiazole, **189**, (3.50 g, 9.8 mmol), sodium hydroxide (0.84 g in 100 ml water) and THF (200 ml). The solution was degassed for 2 h and purged with argon before bis(triphenylphosphine)palladium dichloride (500 mg, 8 mol %) was added and the solution was refluxed for 48 h. The solution was cooled and water and DCM were added. The layers were separated and the aqueous layer was extracted with DCM (3 x 50 ml portions). The combined organic extracts were dried ($MgSO_4$), filtered and concentrated to yield a black sludge. This was purified by column chromatography on silica, eluting with DCM and then 10% ethyl acetate in DCM. The product was obtained as a yellow oil which was recrystallised from ethanol to yield **235** as a shiny white crystalline solid (4.52 g, 70%); mp: 144.0 – 144.7 °C; Anal. Calcd. for $C_{46}H_{58}N_2OSi$: C, 80.89; H, 8.56; N, 4.10. Found: C, 81.11; H, 8.57; N, 4.10; δ_H ($CDCl_3$) 0.34 (s, 9H), 0.75 (m, 4H), 0.78 (t, J = 6.4, 6H), 1.09 (m, 12H), 1.40 (s, 9H), 2.03 (m, 4H), 7.52 (m, 2H), 7.58 (d, J = 8.8, 2H), 7.63 (m, 2H), 7.73 (d, J = 7.6, 1H), 7.81 (d, J = 8.0, 1H), 7.84 (d, J = 8.4, 2H), 8.11 (d, J = 8.4, 2H), 8.24 (d, J = 8.4, 2H); δ_c ($CDCl_3$) 0.00, 14.85, 23.35, 24.59, 30.44, 32.03, 32.23, 36.00, 41.02, 56.07, 120.07, 121.11, 122.09, 122.39, 123.46, 126.96, 127.71, 128.24, 128.53, 128.58, 132.79, 139.59, 140.40, 141.95, 142.25, 145.81, 151.11, 152.76, 156.24, 165.27, 165.57; MS (EI) *m/z*: 682 (M^+, 100%).

Method B

A flask was charged with 4,4,5,5-tetramethyl-2-[9,9-dihexyl-2-(trimethylsilyl)-fluoren-7-yl]-1,3,2-dioxaborolane, **234**, (3.00 g, 5.6 mmol), 2-(4-bromophenyl)-5-(4-*tert*-butylphenyl)-1,3,4-oxadiazole **189** (2.01 g, 5.6 mmol), potassium carbonate (1 M solution, 30 ml) and THF (50 ml). The mixture was degassed for 1 h before tetrakis(triphenylphosphine)palladium (330 mg, 5 mol %) was added and the mixture was refluxed under argon at 80 °C for 65 h. After cooling to room temperature, the layers were separated and the aqueous layer was extracted with ethyl acetate. The combined organic extracts were washed with brine, dried ($MgSO_4$), filtered and concentrated to yield a dark oil. This was purified by column chromatography on silica eluting with DCM. The product was recrystallised from ethanol to yield **235** as a white crystalline solid (3.00 g, 78%). Analysis was in agreement with the product produced by Method A.

2-(4-*tert*-Butylphenyl)-5-[4-(9,9-dihexyl-7-iodofluoren-2-yl)-phenyl]-1,3,4-oxadiazole (236)

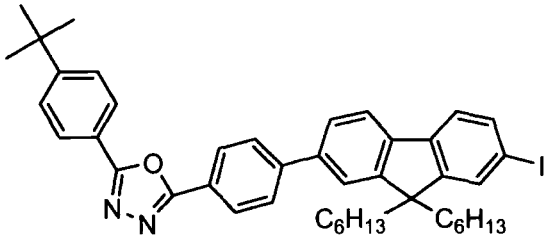

A flask was charged with 2-(4-*tert*-butylphenyl)-5-[4-(9,9-dihexyl-7-trimethylsilanylfluoren-2-yl)-phenyl]-1,3,4-oxadiazole, **235**, (1.75 g, 2.5 mmol) and DCM (25 ml). The solution was cooled to 0 °C before iodine monochloride (1.0 M solution, 3.0 ml, 3.0 mmol) was added dropwise and the orange solution was stirred for 1.5 h. The solution was poured into a 5% sodium thiosulphate solution (50 ml) and stirred until the orange colour disappeared. The layers were separated and the aqueous layer was extracted with DCM. The combined organic layers were washed with brine, dried ($MgSO_4$), filtered and concentrated to yield the crude product which was recrystallised from ethanol to yield **236** as a shiny white solid (1.70 g, 90%); mp: 139.5 – 140.9 °C; Anal. Calcd. for $C_{43}H_{49}IN_2O$: C, 70.10; H, 6.70; N, 3.80. Found: C, 70.34; H, 6.77; N, 3.72; δ_H ($CDCl_3$) 0.66 (m, 4H), 0.79 (t, J = 6.8, 6H), 1.08 (m, 12H), 2.01 (m, 4H), 7.49 (d, J = 7.6, 1H), 7.58 (d, J = 8.8, 2H), 7.66 (m, 1H), 7.70 (m, 2H), 7.78 (d, J = 8.0, 1H), 7.83 (d, J =

8.4, 2H), 8.11 (d, J = 8.4, 2H), 8.25 (d, J = 8.4, 2H); δ_C ($CDCl_3$) 13.99, 22.56, 23.73, 29.61, 31.15, 31.44, 35.12, 40.24, 55.54, 92.91, 120.30, 121.17, 121.39, 121.62, 122.76, 126.08, 126.29, 126.83, 127.38, 127.72, 132.17, 136.00, 139.29, 140.15, 140.32, 144.65, 151.10, 153.47, 155.39, 164.31, 164.72; MS (EI) *m/z*: 736 (M^+, 100%).

2-(4-*tert*-Butylphenyl)-5-[4-(9,9-dihexyl-2-bromofluoren-7-yl)phenyl]-1,3,4-oxadiazole (238)

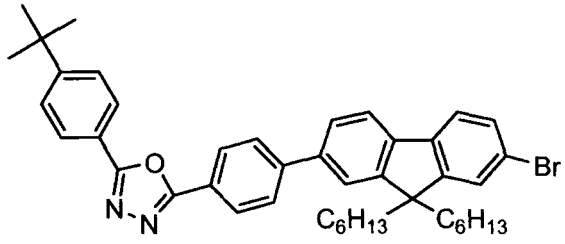

An argon-purged flask was charged with 2-(4-*tert*-butylphenyl)-5-{4-[9,9-dihexyl-2-(trimethylsilyl)-fluoren-7-yl]phenyl}-1,3,4-oxadiazole, **235**, (3.00 g, 4.4 mmol), sodium acetate (0.75 g, 9.0 mmol) and dry THF (40 ml) and cooled in the dark to 0 °C in an ice bath. Bromine (0.90 ml, 17.5 mmol) was added and the solution was stirred for 2 h with the ice bath removed. The reaction was then quenched with triethylamine (4.9 ml, 8 equiv.) producing a white precipitate. A saturated sodium thiosulphate solution was then added to quench the excess bromine. The product was extracted with diethyl ether and the combined organic extracts were washed with water, dried ($MgSO_4$), filtered and concentrated. The resulting solid was recrystallised from ethanol to yield **238** as shiny white crystals (2.82 g, 93%); mp: 133.9 – 134.8 °C; Anal. Calcd. for $C_{43}H_{49}BrN_2O$: C, 74.87; H, 7.16; N, 3.97. Found: C, 74.91; H, 7.22; N, 4.02; δ_H ($CDCl_3$) 0.74 (m, 10H), 1.04 (m, 12H), 1.37, (s, 9H), 2.00 (m, 4H), 7.49 (m, 2H), 7.59 (m, 5H), 7.82 (m, 3H), 8.08 (d, J = 7.9, 2H), 8.22 (d, J = 7.9, 2H); δ_C ($CDCl_3$) 13.96, 22.54, 23.73, 29.61, 31.14, 31.44, 35.11, 40.28, 55.61, 120.24, 121.18, 121.26, 121.40, 121.45, 122.76, 126.08, 126.27, 126.31, 126.82, 127.38, 127.72, 130.11, 139.12, 139.52, 140.26, 144.65, 151.30, 153.30, 155.40, 164.32, 164.73; MS (ES) *m/z*: 689 (M^+ + H, ^{79}Br, 100%), 691 (M^+ + H, ^{81}Br, 100%).

2-(4-*tert*-Butylphenyl)-5-[4-(9,9-dihexyl-2-bromofluoren-7-yl)phenyl]-1,3,4-oxadiazole (237)

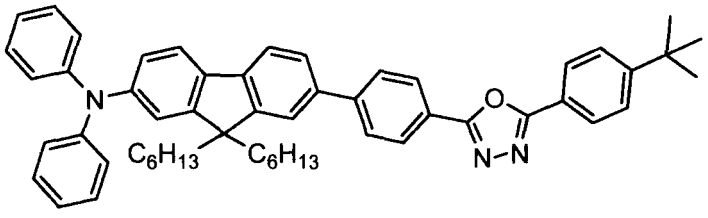

An argon-purged flask was charged with 2-(4-*tert*-butylphenyl)-5-[4-(9,9-dihexyl-2-bromofluoren-7-yl)phenyl]-1,3,4-oxadiazole, **238**, (300 mg, 0.4 mmol), diphenylamine (74 mg, 0.4 mmol), sodium *tert*-butoxide (58 mg, 0.6 mmol), tris(dibenzylideneacetone)dipalladium (5 mg), tri-*tert*-butylphosphine (~2 mg) and dry toluene (25 ml). The dark red solution was heated to 80 °C with stirring for 16 h. After cooling to room temperature water was added and the layers were separated. The aqueous layer was extracted with diethyl ether and the combined organic extracts were washed with brine, dried ($MgSO_4$), filtered and concentrated to yield a yellow oil. The product was purified by column chromatography on silica eluting with DCM to yield **237** as a yellow solid which was dried under vacuum (306 mg, 90%). Anal. Calcd. for $C_{55}H_{59}N_3O$: C, 84.90; H, 7.64; N, 5.40. Found: C, 84.68; H, 7.66; N, 5.12; δ_H ($CDCl_3$) 0.71 (s, 4H), 0.80 (t, J = 7.2, 6H), 1.07 (m, 12H), 1.39 (s, 9H), 1.90 (m, 4H), 7.03 (m, 3H), 7.14 (m, 4H), 7.24 (m, 5H), 7.58 (m, 5H), 7.70 (d, J = 8.0, 1H), 7.83 (d, J = 8.8, 2H), 8.10 (d, J = 8.4, 2H), 8.23 (d, J = 8.8, 2H); δ_C ($CDCl_3$) 14.01, 22.54, 23.82, 29.62, 31.15, 31.51, 35.11, 40.26, 55.25, 119.27, 119.53, 120.62, 121.24, 122.47, 122.60, 123.52, 123.92, 126.07, 126.12, 126.82, 127.35, 127.60, 127.70, 129.19, 135.58, 137.79, 141.24, 144.91, 147.49, 147.98, 151.60, 152.51, 155.34, 164.40, 164.67; MS (ES) *m/z*: 779 (M^+ + H, 100%).

7-{4-[5-(4-*tert*-Butylphenyl)-1,3,4-oxadiazol-2-yl]phenyl}-9,9-dihexyl-*N*-phenyl-fluoren-2-amine (239)

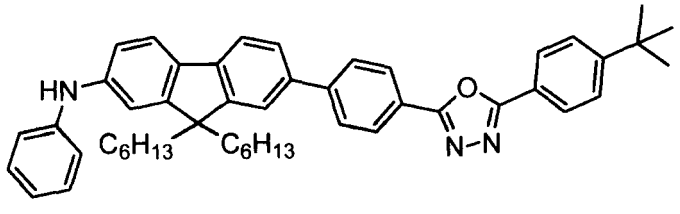

An argon-purged flask was charged with 2-(4-*tert*-butylphenyl)-5-[4-(9,9-dihexyl-2-bromofluoren-7-yl)phenyl]-

1,3,4-oxadiazole **238** (500 mg, 0.72 mmol), aniline (0.13 ml, 1.4 mmol), sodium *tert*-butoxide (80 mg, 0.83 mmol), tris(dibenzylideneacetone)dipalladium (35 mg 5 mol %), tri-*tert*-butylphosphine (~15 mg) and dry toluene (30 ml) and was heated at 80 °C for 16 h. After cooling to room temperature, water was added and the layers were separated. The aqueous layer was extracted with diethyl ether and the combined organic extracts were washed with brine, dried ($MgSO_4$), filtered and concentrated to yield a brown oil. This was purified by column chromatography on silica eluting with DCM. The product was recrystallised from ethanol to yield **239** as a yellow crystalline solid (0.41 g, 81%); mp; 169.2 – 170.2 °C; Anal. Calcd. for $C_{49}H_{55}N_3O$: C, 83.84; H, 7.90; N, 5.99. Found: C, 83.79; H, 7.90; N, 5.79; δ_H (DMSO-d_6) 0.70 (m, 10H), 1.05 (m, 12H), 1.36 (s, 9H), 2.00 (m, 4H), 6.86 (t, J = 7.1, 1H), 7.12 (m, 4H), 7.26 (t, J = 8.2, 2H), 7.68 (d, J = 8.2, 2H), 7.73 (m, 2H), 7.80 (2H), 8.01 (d, J = 8.2, 2H), 8.10 (d, J = 8.2, 2H), 8.22 (d, J = 8.2, 2H), 8.38 (s, 1H); δ_C (DMSO-d_6) 13.74, 21.88, 23.43, 28.88, 30.81, 30.86, 34.83, 38.30, 54.64, 111.88, 116.61, 117.33, 119.85, 120.41, 121.38, 121.53, 121.77, 122.42, 126.51, 126.98, 127.29, 127.90, 128.03, 129.90, 132.87, 136.64, 142.11, 143.89, 144.15, 144.54, 151.28, 152.75, 155.71, 164.51, 164.72.

7-{4-[5-(4-*tert*-Butylphenyl)-1,3,4-oxadiazol-2-yl]phenyl}-*N*-{2-[4-(5-(4-*tert*-butylphenyl)-1,3,4-oxadiazol-2-yl)phenyl]-9,9-dihexyl-fluoren-7-yl}-9,9-dihexyl-*N*-phenyl-9H-fluoren-2-amine (240)

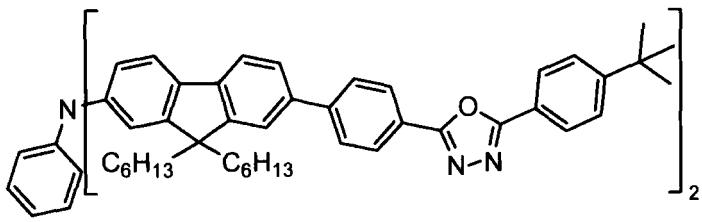

An argon-purged flask was charged with 7-{4-[5-(4-*tert*-butylphenyl)-1,3,4-oxadiazol-2-yl]phenyl}-9,9-dihexyl-*N*-phenyl-fluoren-2-amine, **239**, (360 mg, 0.51 mmol), 2-(4-*tert*-butylphenyl)-5-[4-(9,9-dihexyl-2-bromofluoren-7-yl)phenyl]-1,3,4-oxadiazole, **238**, (360 mg, 0.52 mmol), sodium *tert*-butoxide (80 mg, 0.83 mmol), tris(dibenzylideneacetone)dipalladium (25 mg 5 mol %), tri-*tert*-butylphosphine (~15 mg) and dry toluene (30 ml) and was heated at 80 °C for 16 h. After cooling to room temperature, brine was added and the layers were separated. The

aqueous layer was extracted with diethyl ether and the combined organic extracts dried ($MgSO_4$), filtered and concentrated to yield a brown oil. This was purified by column chromatography on silica eluting with 5% ethyl acetate in DCM. The product was recrystallised from ethanol to yield **240** as a powdery yellow solid (0.48 g, 71%); Anal. Calcd. for $C_{92}H_{103}N_5O_2$: C, 84.30; H, 7.92; N, 5.34. Found: C, 84.10; H, 7.94; N, 5.35; δ_H ($CDCl_3$) 0.77 (m, 20H), 1.70, (m, 24H), 1.39 (s, 18H), 1.95 (m, 8H), 7.07 (m, 3H), 7.20 (m, 4H), 7.28 (m, 2H), 7.60 (m, 10H), 7.72 (d, J = 8.9, 2H), 7.84 (d, J = 8.9, 2H), 8.10 (d, J = 8.9, 2H), 8.23 (d, J = 8.9, 2H); δ_C ($CDCl_3$) 14.34, 22.85, 24.12, 29.92, 31.40, 31.83, 35.37, 40.56, 55.51, 119.03, 119.77, 120.88, 121.41, 121.50, 122.68, 122.85, 123.53, 123.96, 126.34, 126.40, 127.06, 127.60, 127.85, 129.47, 135.75, 138.02, 141.49, 145.13, 147.64, 148.35, 151.76, 152.73, 155.61, 164.64, 164.93; MS (ES) *m/z*: 1312 (M^+ + 2H, 100%).

6.4 Experimental Procedures for Chapter 4

2,5-Diphenyl-1,3,4-oxadiazole (244)[183]

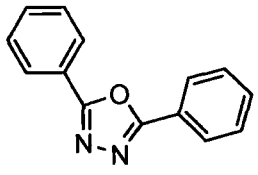

Benzoyl chloride was added to a solution of hydrazine monohydrate in methanol. A white solid formed immediately. Water was added, the solid was isolated by suction filtration and the solid was dried. The solid was then dissolved in $POCl_3$ (25 ml) and refluxed overnight. The $POCl_3$ was distilled off yielding a viscous red oil. Recrystallisation from ethanol yielded **244** as white crystals (yield not recorded); δ_H ($CDCl_3$) 7.55 (m, 6H), 8.15 (m, 4H); δ_c ($CDCl_3$) 126.96, 129.10, 131.75.

2-(4-Bromophenyl)-1,3,4-oxadiazole (246)

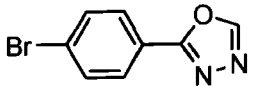

A flask was charged with 4-bromobenzhydrazide (2.00 g, 9.3 mmol) and triethyl orthoformate (15 ml). The mixture was stirred for 15 h at 150 °C. The solvent was removed *in vacuo* and the residue was recrystallised from ethanol to yield **246** as white needles (1.73 g, 83%); mp: 146.4 –

148.2 °C; Anal. Calcd. for $C_7H_7BrN_2O$: C, 42.70; H, 2.24; N, 12.45. Found: C, 42.63; H, 2.20; N, 12.36; δ_H ($CDCl_3$) 7.67 (d, J = 8.6, 2H), 7.95 (d, J = 8.6, 2H), 8.48 (s, 1H); δ_C ($CDCl_3$) 122.44, 126.78, 128.51, 132.51, 152.69, 164.09; MS (EI) *m/z*: 223 (M^+, ^{79}Br, 100%), 225 (M^+, ^{81}Br, 100%).

2-[4-(1,3,4-oxadiazol-2-yl)phenyl]pyridine (247)

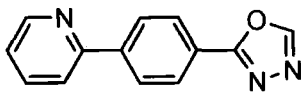

An argon-purged flask was charged with 2-(4-bromophenyl)-1,3,4-oxadiazole, **246**, (1.50 g, 6.7 mmol), 2-(tributylstannyl)pyridine (3.50 g, 8.6 mmol), lithium chloride (1.00 g, crushed), bis(triphenylphosphine)palladium dichloride (240 mg, 5 mol %) and dry toluene (40 ml). The mixture was stirred for 72 h at 115 °C. The toluene was removed *in vacuo* and DCM and water added. The layers were separated and the organic layer extracted with DCM. The combined organic layers were washed with brine and dried ($MgSO_4$), filtered and concentrated. The crude product was purified by column chromatography on silica eluting with EtOAc:DCM (1:9 v/v changing to 2:3 v/v). The product was recrystallised from ethanol to yield **247** as white needles (0.79 g, 53%); mp: 147.7 – 149.0 °C; Anal. Calcd. for $C_{13}H_9N_3O$: C, 69.95; H, 4.06; N, 18.82. Found: C, 69.99; H, 4.01; N, 18.94; δ_H ($CDCl_3$) 7.29 (q, J = 4.6, 1H), 7.79 (d, J = 3.5, 2H), 8.17 (m, 4H), 8.49 (s, 1H), 8.73 (d, J = 4.3, 1H); δ_C ($CDCl_3$) 120.81, 122.95, 123.72, 127.51, 127.54, 136.97, 142.69, 149.94, 152.67, 155.88, 164.60; MS (EI) *m/z* 223 (M^+, 100%).

4-Cyanophenylboronic acid (248)[184]

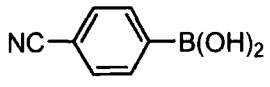

An argon-purged flask was charged with 4-bromobenzonitrile (1.00 g, 5.5 mmol), triisopropyl borate (1.60 ml, 6.9 mmol) and dry THF (50 ml). The solution was cooled to -78 °C before *n*-butyllithium (2.5 M solution, 2.40 ml, 6.0 mmol) was added dropwise. The solution was stirred at -78 °C for a further 0.5 h before being allowed to warm to -10 °C when HCl (1 ml) in water (4 ml) was added and the mixture was stirred overnight at room temperature. The THF was removed *in vacuo* and DCM and water were added. The layers were separated and

the aqueous layer was extracted with DCM. The combined organic extracts were dried ($MgSO_4$), filtered and concentrated to yield pale yellow needles. These were recrystallised from acetonitrile to yield **248** as white needles (0.30 g, 37%); mp: 109.6 – 111.4 °C; δ_H ($CDCl_3$) 7.52 (d, J = 8.4, 2H), 7.64 (d, J = 8.4, 2H); δ_C ($CDCl_3$) 111.28, 118.02, 128.02, 132.65, 133.40.

4-(Pyridin-2-yl)benzonitrile (249)[185]

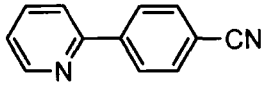

A flask was charged with 4-cyanophenylboronic acid, **248**, (2.26 g, 15.4 mmol), 2-bromopyridine (1.60 ml, 16.8 mmol), potassium carbonate (2 M solution, 20 ml) and THF (40 ml). The solution was degassed for 1 h before bis(triphenylphosphine)palladium dichloride (0.54 g, 5 mol %) was added and the mixture stirred at 80 °C for 4 days. The layers were separated and the aqueous layer was extracted with DCM. The combined organic extracts were washed with water, dried ($MgSO_4$), filtered and concentrated to yield a dark red solid. This was purified by column chromatography on silica eluting with DCM followed by ethyl acetate. The product was recrystallised from a toluene and hexane solution to yield **249** as a yellow solid (1.59 g, 57%); mp: 100.0 – 101.4 °C; Anal. Calcd. for $C_{12}H_8N_2$: C, 79.98; H, 4.47; N, 15.55. Found: C, 79.41; H, 4.44; N, 15.49; δ_H ($CDCl_3$) 7.60 (m, 1H), 7.75 – 7.72 (m, 4H), 8.12 (d, J = 8.0, 2H), 8.73 (m, 1H); δ_C ($CDCl_3$) 112.52, 118.78, 120.96, 123.33, 127.46, 132.56, 137.11, 143.43, 150.03, 155.21; MS (EI) *m/z*: 180 (M^+, 100%).

2-[4-(1H-tetrazol-5-yl)phenyl]pyridine (250)

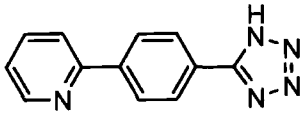

An argon-purged flask was charged with 4-(pyridin-2-yl)benzonitrile, **249**, (1.25 g, 6.94 mmol), sodium azide (0.54 g, 8.3 mmol), ammonium chloride (0.45 g, 8.3 mmol) and DMF (30 ml). The mixture was stirred at 105 °C overnight. After cooling, the mixture was poured into water and acidified with HCl to pH 6. The resulting precipitate was isolated by suction filtration and recrystallised from methanol to yield **250** as a white

solid (0.85 g, 55%); mp: 272.3 – 273.3 °C; δ_H (DMSO-d_6) 7.74 (m, 1H), 8.31 – 8.36 (m, 6H), 8.85 (d, J = 5.2, 1H); δ_C (DMSO-d_6) 122.91, 124.47, 125.75, 127.57, 128.26, 137.51, 141.37, 146.60, 152.77, 154.54.

2-{4-[5-(4-*tert*-Butylphenyl)-1,3,4-oxadiazol-2-yl]phenyl}pyridine (251)

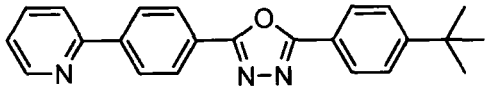

A flask was charged with 2-[4-(1H-tetrazol-5-yl)phenyl]pyridine, **250**, (0.75 g, 3.4 mmol) and pyridine (20 ml). 4-*tert*-Butylbenzoyl chloride (0.73 ml, 4.0 mmol) was added and the reaction was stirred at 100 °C overnight. After cooling, the solution was poured into water and the resulting precipitate was isolated by suction filtration and recrystallised from ethanol to yield **251** as white needles (0.85 g, 71%); mp: 181.9 – 182.9 °C; Anal. Calcd. for $C_{23}H_{21}N_3O$: C, 77.72 H, 5.96; N, 11.82, Found: C, 77.55; H, 5.92; N, 11.87; δ_H ($CDCl_3$) 1.37 (s, 9H), 7.28 (m, 1H), 7.55 (d, J = 8.4, 2H), 7.79 (m, 2H), 8.08 (d, J = 8.4, 2H), 8.17 (d, J = 8.8, 2H), 8.24 (d, J = 8.8, 2H), 8.73 (d, J = 4.8, 1H); δ_C ($CDCl_3$) 31.13, 35.11, 120.80, 121.10, 122.87, 124.31, 126.07, 126.84, 127.29, 127.48, 136.98, 142.23, 149.89, 155.41, 155.99, 164.20, 164.80; MS (EI) *m/z*: 355 (M^+, 100%).

2-{2-[4-(5-(4-*tert*-Butylphenyl)-1,3,4-oxadiazol-2-yl)phenyl]-9,9-dihexylfluoren-7-yl}pyridine (254)

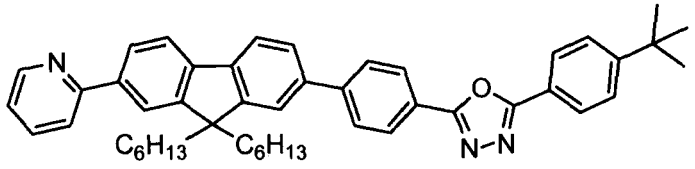

An argon-purged flask was charged with 2-(4-*tert*-butylphenyl)-5-[4-(9,9-dihexyl-2-bromofluoren-7-yl)phenyl]-1,3,4-oxadiazole, **238**, (1.03 g, 1.5 mmol), 2-(tributylstannyl)pyridine (0.90 g, 2.4 mmol), lithium chloride (0.50 g, crushed) and dry toluene (50 ml). Tetrakis(triphenylphosphine)palladium (90 mg, 5 mol %) was added and the mixture stirred at 80 °C for 48 h. After cooling, a saturated potassium fluoride solution (10 ml) was added and the mixture stirred for a further 1 h. The toluene was removed *in vacuo* and DCM and a sodium hydrogen carbonate solution (75 ml) was

added. The layers were separated and the aqueous layer extracted with DCM. The combined organic extracts were dried ($MgSO_4$), filtered and concentrated to yield a yellow oil. This was purified by column chromatography on silica eluting with 0 – 5% ethyl acetate in DCM. The product was recrystallised from ethanol to yield **254** as a white crystalline solid (0.55 g, 54%); mp: 172.7 – 174.8 °C; Anal. Calcd. for $C_{48}H_{53}N_3O$: C, 83.80; H, 7.77; N, 6.11. Found: C, 83.76; H, 7.74; N, 6.13; δ_H ($CDCl_3$) 0.74 (m, 10H), 1.07 (m, 12H), 1.39 (s, 9H), 2.08 (m, 4H), 7.25 (t, J = 6.6, 1H), 7.57 (d, J = 8.4, 2H), 7.66 (m, 2H), 7.77 – 7.86 (m, 6H), 8.03 (m, 2H), 8.10 (d, J = 8.4, 2H), 8.24 (d, J = 8.4, 2H), 8.74 (d, J = 6.1, 1H); δ_C ($CDCl_3$) 14.25, 22.83, 24.08, 29.94, 31.40, 31.75, 35.37, 40.67, 55.81, 120.53, 120.80, 121.24, 121.40, 121.64, 121.73, 122.35, 122.89, 126.35, 126.41, 126.48, 127.07, 127.63, 128.00, 137.66, 139.26, 141.02, 142.04, 145.03, 149.40, 152.08, 152.53, 155.63, 157.66, 164.61, 164.96; MS (EI) *m/z* 688 (M^+, 100%).

6-Bromopyridine-3-carboxylic acid (256)[59]

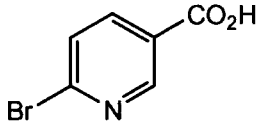

A flask was charged with 2-bromo-5-methylpyridine (5.00 g, 22.8 mmol), potassium permanganate (3.60 g, 22.8 mmol) and water (100 ml). The mixture was refluxed for 4 h before another portion of potassium permanganate (3.60 g, 22.8 mmol) was added and the mixture refluxed for a further 20 h. After cooling, the mixture was filtered through celite and the solid residue was washed with ethyl acetate. The layers of the filtrate were separated and the aqueous layer was acidified with conc. HCl to precipitate the product which was isolated by suction filtration and washed with water and then DCM yielding shiny white crystals of **256** (2.07 g, 35%); δ_H (DMSO-d_6) 7.82 (d, J = 8.0, 1H), 8.18 (dd, ^1J = 8.4, ^2J = 2.4, 1H), 8.86 (d, J = 2.4, 1H), 13.66 (s, 1H); δ_C (DMSO-d_6) 126.36, 128.26, 139.88, 145.58, 151.12, 165.50.

Methyl 6-bromopyridine-3-carboxylate (257)[186]

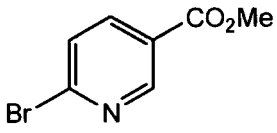

A flask was charged with 6-bromopyridine-3-carboxylic acid, **256**, (1.69 g, 8.3 mmol), methanol (50 ml) and conc. sulphuric acid (0.5 ml). The solution was stirred at 80 °C for 15 h. The excess methanol was removed *in vacuo* and water was added. The precipitated product **257** was isolated by suction filtration as a white solid (1.20 g, 66%); δ_H ($CDCl_3$) 3.96 (s, 3H), 7.59 (d, J = 8.4, 1H), 8.13 (dd, ^1J = 8.4, ^2J = 2.4, 1H), 8.96 (d, J = 2.4, 1H); δ_C ($CDCl_3$) 52.60, 125.35, 128.06, 139.15, 146.82, 151.41, 165.02.

4-*tert*-Butylbenzohydrazide (259)[187]

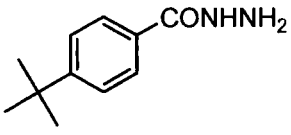

A flask was charged with 4-*tert*-butylbenzoic acid (10.00 g, 56.1 mmol), methanol (100 ml) and conc. sulphuric acid (0.5 ml). The solution was stirred at 80 °C for 20 h before the excess methanol was removed *in vacuo* to yield a colourless oil which was dried *in vacuo*. The oil was dissolved in methanol (65 ml) and hydrazine monohydrate (40 ml) and stirred at 90 °C for 15 h. The methanol was removed *in vacuo* and water was added to precipitate out the product **259** which was isolated by suction filtration as shiny white crystals (9.71 g, 90%); mp: 130.3 – 131.1 °C; δ_H (DMSO-d_6) 4.47 (s, 2H), 7.47 (d, J = 8.4, 2H), 7.77 (d, J = 6.8, 2H), 9.70 (s, 1H); δ_C (DMSO-d_6) 30.90, 34.53, 125.00, 126.74, 130.55, 153.74, 165.85.

2-(9,9-Dihexylfluoren-2-yl)-5-(5-phenyl-1,3,4-oxadiazol-2-yl)pyridine (264)

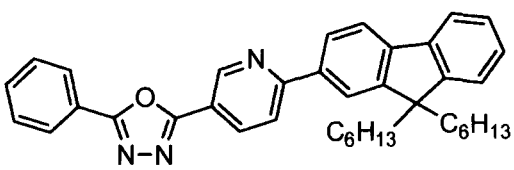

A flask was charged with 2-chloro-5-(5-phenyl-1,3,4-oxadiazol-2-yl)pyridine, **191**, (1.00 g, 3.9 mmol), 9,9-dihexylfluoren-2-yl boronic acid, **201**, (1.50 g, 4.0 mmol), sodium carbonate (2 M solution, 50 ml) and toluene (150 ml). The mixture was degassed for 1 h before tetrakis(triphenylphosphine)palladium (0.23 g, 0.19 mmol) was added and the mixture

was stirred at 90 °C for 44 h. After cooling, the layers were separated and the aqueous layer was extracted with ethyl acetate. The combined organic extracts were washed with brine, dried ($MgSO_4$), filtered and concentrated to yield an orange solid. This was purified by column chromatography on silica eluting with hexane:ethyl acetate (4:1 v/v). The product was recrystallised from ethanol to yield **264** as a white solid (1.57 g, 73%); mp: 130.2 – 132.2 °C; Anal. Calcd. For $C_{38}H_{41}N_3O$: C, 82.12; H, 7.44; N, 7.56. Found: C, 82.07; H, 7.41; N, 7.41; δ_H ($CDCl_3$) 0.72 (m, 10H), 1.07 (m, 12H), 2.08 (m, 4H), 7.36 (m, 3H), 7.58 (m, 3H), 7.76 (m, 1H), 7.82 (d, J = 8.4, 1H), 8.00 (d, J = 8.4, 1H), 8.10 (m, 2H), 8.18 (m, 2H), 8.50 (dd, ^1J = 8.4, ^2J = 2.4, 1H), 9.44 (m, 1H); δ_C ($CDCl_3$) 13.96, 22.55, 23.79, 29.69, 31.49, 40.38, 55.35, 118.25, 120.08, 120.21, 120.33, 121.49, 123.01, 123.72, 126.26, 126.91, 127.07, 127.71, 129.19, 131.99, 134.82, 136.74, 140.34, 143.29, 147.79, 151.46, 151.60, 160.29, 162.85, 164.93; MS (EI) *m/z*: 470 (M^+ - C_6H_{13}, 100%), 555 (M^+, 97%).

4-(5-Phenyl-1,3,4-oxadiazol-2-yl)phenol (266)[156]

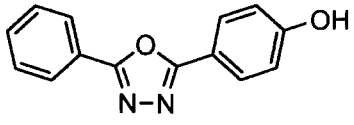

An argon-purged flask was charged with 2-(4-methoxyphenyl)-5-phenyl-1,3,4-oxadiazole, **192**, (2.00 g, 7.9 mmol) and 57% hydroiodic acid (70 ml). The mixture was refluxed at 130 °C for 5 h. After cooling, water was added and the precipitate was isolated by suction filtration, washed with water and dried on *in vacuo* to yield **266** as a pale yellow solid (1.69 g, 89%); mp: 256.3 – 257.9 °C; Anal. Calcd. for $C_{14}H_{10}N_2O_2$: C, 70.58; H, 4.23; N, 11.76. Found: C, 70.50; H, 4.20; N, 11.77; δ_H (DMSO-d_6) 7.00 (d, J = 8.8, 2H), 7.64 (m, 3H), 7.98 (d, J = 8.8, 2H), 8.11 (m, 2H), 10.38 (s, 1H); δ_C (DMSO-d_6) 114.06, 116.17, 123.53, 126.45, 128.66, 129.35, 131.74, 160.86, 163.27, 164.22.

2-[4-(4-Bromobutoxy)phenyl]-5-phenyl-1,3,4-oxadiazole (267)

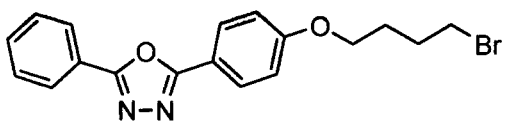

An argon-purged flask was charged with 4-(5-phenyl-1,3,4-oxadiazol-2-yl)phenol, **266**,

(1.65 g, 6.9 mmol), 1,4-dibromobutane (2.5 ml, 21.0 mmol), potassium carbonate (9.60 g, 69.0 mmol) and DMF (50 ml). The mixture was stirred for 24 h. The solvent was removed *in vacuo* and DCM and water were added. The layers were separated and the aqueous layer was extracted with DCM. The combined organic extracts were dried ($MgSO_4$), filtered and concentrated. The crude product was purified by column chromatography on silica eluting with 10% ethyl acetate in DCM. The product **267** was isolated as a white solid (1.79 g, 69%); mp: 134.1 – 134.9 °C; Anal. Calcd. for $C_{18}H_{17}BrN_2O_2$: C, 57.92; H, 4.59; N, 7.51. Found: C, 57.77; H, 4.53; N, 7.36; δ_H ($CDCl_3$) 1.99 (m, 2H), 2.10 (m, 2H), 3.51 (t, J = 6.4, 2H), 4.09 (t, J = 6.4, 2H), 7.02 (d, J = 8.8, 2H), 7.54 (m, 3H), 8.06 – 8.14 (m, 4H); δ_C ($CDCl_3$) 27.79, 29.38, 33.21, 67.15, 114.97, 116.57, 124.16, 126.84, 128.73, 129.03, 131.51, 161.65, 164.16, 164.53; MS (ES) *m/z*: 372 (M^+, ^{79}Br, 31%), 769 ($2M^+ + Na$, ^{79}Br, ^{81}Br, 100%)

4-Amino-2-phenylpyridine (270)[188]

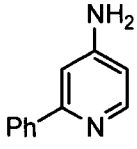

A flask was charged with 4-amino-2-chloropyridine (2.00 g, 15.6 mmol), benzeneboronic acid (2.10 g, 17.0 mmol), sodium carbonate (1 M solution, 20 ml) and dioxane (50 ml). The mixture was degassed for 1.5 h before palladium acetate (190 mg, 5 mol %) and tri-*tert*-butylphosphine (~5 mol %) were added and the mixture was stirred at 105 °C for 48 h. After cooling, the dioxane was removed *in vacuo* and ethyl acetate and water were added. The layers were separated and the aqueous layer was extracted with ethyl acetate. The combined organic extracts were washed with brine, dried ($MgSO_4$), filtered and concentrated to yield a yellow oil. Hot toluene was added and the solution was filtered hot to remove the yellow precipitate. Upon cooling, the product **270** precipitated and was isolated by suction filtration as white plates (2.02 g, 76%); mp: 129.2 – 130.7 °C; Anal. Calcd. for $C_{11}H_{10}N_2$: C, 77.62; H, 5.92; N, 16.46. Found: C, 77.65; H, 5.90; N, 16.25; δ_H (DMSO-d_6) 6.09 (s, 2H), 6.48 (dd, ^1J = 5.6, ^2J = 2.0, 1H), 7.02 (d, J = 2.0, 1H), 7.38 – 7.47 (m, 3H), 7.93 (d, J = 7.2, 2H), 8.11 (d, J = 5.6, 1H); δ_C (DMSO-d_6) 104.98, 107.85, 126.16, 128.32, 128.41, 139.77, 149.47, 155.09, 156.20.

4-Methyl-2-phenylpyridine (276)[189]

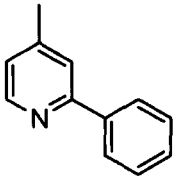

A flask was charged with 2-bromo-4-methylpyridine (2.6 ml, 23.4 mmol), benzeneboronic acid (3.00 g, 24.6 mmol), sodium carbonate (1M solution, 30 ml) and dioxane (50 ml). The mixture was degassed for 1 h before $Pd(PPh_3)_4$ (475 mg, 2 mol %) was added and the mixture was stirred for 65 h at 105 °C. The solvent was removed *in vacuo* and ethyl acetate and water were added. The layers were separated and the aqueous layer was extracted with ethyl acetate. The combined organic layers were washed with brine, dried ($MgSO_4$), filtered and concentrated. The crude product was purified by column chromatography on silica eluting with DCM and then distillation in Kugelrohr apparatus at 150 °C and 25 mbar to yield **276** as a colourless oil which solidified on standing (2.41 g, 61%); mp: 49.0 – 50.7 °C; Anal. Calcd. for $C_{12}H_{11}N$: C, 85.17; H, 6.55; N, 8.28. Found: C, 84.98; H, 6.54; N, 8.29; δ_H ($CDCl_3$) 2.39 (s, 3H), 7.03 (d, J = 4.9, 1H), 7.41 (m, 1H), 7.47 (m, 1H), 7.54 (m, 1H), 7.99 (d, J = 7.0, 2H), 8.55 (d, J = 4.9, 1H); δ_C ($CDCl_3$) 21.19, 121.49, 123.123, 126.942, 128.68, 128.80. 139.562, 147.70, 149.44, 157.38; MS (EI) *m/z*: 169 (M^+, 100%).

2-(2,4-Difluorophenyl)-4-methylpyridine (277)

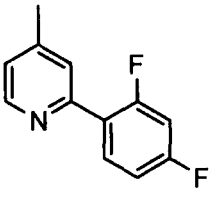

A flask was charged with 2,4-difluorophenylboronic acid (1.50 g, 9.5 mmol), 4-methyl-2-bromopyridine (0.9 ml, 8.1 mmol), sodium carbonate (1M solution, 20 ml) and THF (40 ml). The mixture was degassed for 1 h before $Pd(PPh_3)_4$ (190 mg, 2 mol %) was added and the mixture was stirred for 65 h at 80 °C. Upon cooling, the layers were separated and the aqueous layer was extracted with ethyl acetate. The combined organic layers were washed with brine and dried ($MgSO_4$), filtered and concentrated. The crude product was purified by column chromatography on silica eluting with 10% ethyl acetate in DCM and then by distillation in Kugelrohr apparatus at 145 °C and 26 mbar to yield **277** as a pale pink oil that solidified to a white solid on standing (1.47 g, 88%); mp: 34.2 – 35.7 °C; δ_H ($CDCl_3$) 2.42 (s, 3H), 6.91 (td, J_{HH} = 8.9, J_{HF} = 2.6, 1H), 6.99 (td, J_{HH} = 8.9, J_{HF} = 2.7, 1H), 7.09 (d, J = 5.8, 1H), 7.56 (s, 1H), 7.96 (m, 1H), 8.56 (d,

J = 5.1, 1H); δ_C ($CDCl_3$); 21.21, 104.31 (m, $^2J_{CF}$ = 27.1, $^2J_{CF'}$ = 24.9), 111.79, (dd, $^2J_{CF}$ = 21.2, $^4J_{CF}$ = 3.7), 123.47, 125.15 (d, $^2J_{CF}$ = 8.8), 132.20 (dd, $^3J_{CF}$ = 9.6, $^3J_{CF'}$ = 4.4), 147.78, 149.34, 152.34, 157.97, 159.32 & 161.70 (d, $^1J_{CF}$ = 240.1), 161.96 & 161.38 (dd, $^1J_{CF}$ = 251.0, $^3J_{CF}$ = 12.5); δ_F ($CDCl_3$) -113.27 (1F), -109.86 (1F); MS (EI) *m/z*: 205 (M^+, 100%)

6.5 Experimental Procedures for Chapter 5

General procedure for microwave reactions to make tris(2-phenylpyridine)iridium (164)

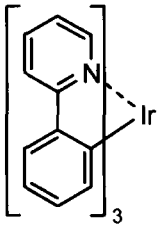

A 2 – 5 ml microwave vial was charged with either $IrCl_3.3H_2O$ (50 mg, 0.14 mmol) or $Ir(acac)_3$ (70 mg, 0.14 mmol) and varying amounts of 2-phenylpyridine, sodium carbonate, ethylene glycol, glycerol and water. The mixtures were degassed, sealed and reacted in an Emry Optimiser microwave for either 600 s or 1800 s. Upon completion of heating, the mixtures were cooled to 50 °C by compressed air. If the pressure had not fallen below 4 bar, a syringe needle was used to depressurise the vial. The mixture was poured into DCM/water and the product extracted several times with DCM. The combined organic layers were washed with water, dried ($MgSO_4$), filtered and concentrated before being purified by column chromatography on silica eluting with DCM. The product was dried under vacuum. δ_H ($CDCl_3$) 6.83-6.90 (m, 4H), 7.53 (d, J = 6.0, 1H), 7.58 (t, J = 7.6, 1H), 7.65 (d, J = 7.6, 1H), 7.87 (d, J = 8, 1H) which is in agreement with literature data.[150]

6.6 X-Ray Crystal Data

The accompanying data for the X-ray crystal structures shown in Chapter 3 is shown in Tables 6.1 and 6.2.

Compound	**189**	**235**	**238**
Formula	$C_{18}H_{17}BrN_2O$	$C_{46}H_{58}N_2OSi$	$C_{43}H_{49}BrN_2O$
M	357.25	683.03	689.75
Temp., K	120	120	120
Crystal system	monoclinic	monoclinic	triclinic
Space group	$P2_1/n$ (#14)	$C2/c$ (#15)	$P\bar{1}$ (#2)
a /Å	7.357(1)	14.695(2)	10.945(5)
b /Å	6.139(1)	13.330(1)	12.714(3)
c /Å	34.909(6)	41.182(5)	13.128(4)
α /°	90	90	96.10(1)
β /°	91.43(2)	94.32(1)	93.84(1)
γ /°	90	90	94.38(1)
V /Å^3	1576.2(4)	8044(2)	1806(1)
Z	4	8	2
D_{calc} /g cm^{-3}	1.505	1.128	1.268
μ /mm^{-1}	2.61	0.09	1.17
Reflections total	14799	34477	32533
-- unique	3504	7093	10531
-- , with $I \geq 2\sigma(I)$	3114	4312	7932
R_{int} /%	6.7	7.8	4.2
Refined parameters	203	467	447
$R(F)$, $I \geq 2\sigma(I)$ /%	7.6	4.5	3.5
w$R(F^2)$, all data /%	17.1	11.8	9.4

Table A.1 Crystal data

Angle	**189**	**235**	**238**
fluorene / benzene i	-	37.3	40.1
benzene i / oxadiazole	5.7	6.7	13.8
oxadiazole / benzene ii	7.4	7.5	28.9
pyridine / oxadiazole			
benzene i / N(4)C(14)C(21)C(31)			
N(4)C(14)C(21)C(31) / phenyl ii			
N(4)C(14)C(21)C(31) / phenyl iii			

Table A.2 Dihedral angles (°) between planar fragments

Chapter 7 – References

1 J. K. Borchardt, *Materials Today*, 2004, **7**, 42.
2 M. Pope, H. P. Kallman, and P. Magnante, *J. Chem. Phys.*, 1963, **38**, 2042.
3 W. Helfrich and W. G. Schneider, *Phys. Rev. Lett.*, 1965, **14**, 229.
4 M. Schadt and W. Helfrich, *Appl. Phys. Lett.*, 1971, **18**, 127.
5 P. S. Vincett, W. A. Barlow, R. A. Hann, and G. G. Roberts, *Thin Solid Films*, 1982, **94**, 171.
6 C. W. Tang and S. A. VanSlyke, *Appl. Phys. Lett.*, 1987, **51**, 913.
7 C. Adachi, T. Tsutsui, and S. Salto, *Appl. Phys. Lett.*, 1989, **55**, 1489.
8 J. M. Burroughes, D. D. C. Bradley, A. R. Brown, A. N. Marks, K. Mackay, R. H. Friend, P. L. Burn, and A. B. Holmes, *Nature*, 1990, **347**, 539.
9 W. A. Hartman and H. L. Armstrong, *J. Appl. Phys.*, 1967, **38**, 2393.
10 D. Braun and A. J. Heeger, *Appl. Phys. Lett.*, 1991, **58**, 1982.
11 S. Doi, M. Kuwabara, T. Noguchi, and T. Ohnishi, *Synth. Met.*, 1993, **57**, 4174.
12 H. G. Gilch and W. L. Wheelwright, *J. Polym. Sci. A1*, 1966, **4**, 1337.
13 G. Yu, *Synth. Met.*, 1996, **80**, 143.

14 M. R. Andersson, G. Yu, and A. J. Heeger, *Synth. Met.*, 1997, **85**, 1275.
15 A. Kraft, A. C. Grimsdale, and A. B. Holmes, *Angew. Chem. Int. Ed.*, 1998, **37**, 402.
16 M. Wohlgennant, X. M. Jiang, Z. V. Vardeny, and R. A. J. Janssen, *Phys. Rev. Lett.*, 2002, **88**, 197401.
17 D. Beljonne, A. J. Ye, Z. Shuai, and J. L. Bredas, *Adv. Funct. Mater.*, 2004, **14**, 684.
18 Z. Kafafi, 'Organic Electroluminescence', Taylor & Francis Group, 2005.
19 S. R. Forrest, D. D. C. Bradley, and M. E. Thompson, *Adv. Mater.*, 2003, **15**, 1043.
20 M. A. Baldo, S. Lamansky, P. E. Burrows, M. E. Thompson, and S. R. Forrest, *Appl. Phys. Lett.*, 1999, **75**, 4.
21 Y. Shirota, *J. Mater. Chem.*, 2000, **10**, 1.
22 G. Hughes and M. R. Bryce, *J. Mater. Chem.*, 2005, **15**, 94.
23 U. Mitschke and P. Bäuerle, *J. Mater. Chem.*, 2000, **10**, 1471.
24 S. A. VanSlyke, C. H. Chen, and C. W. Tang, *Appl. Phys. Lett.*, 1996, **69**, 2160.
25 E. I. Haskal, M. Büchel, P. C. Duineveld, A. Sempel, and P. van de Weijer, *MRS Bulletin*, 2002, **27**, 864.
26 B.-Y. Oh, M.-C. Jeong, T.-H. Moon, W. Lee, and J.-M. Myoung, *J. Appl. Phys.*, 2006, **99**, 124505.
27 M. T. Bernius, M. Inbasekaran, J. O' Brien, and W. Wu, *Adv. Mater.*, 2000, **12**, 1737.
28 C. Adachi, T. Tsutsui, and S. Saito, *Appl. Phys. Lett.*, 1990, **56**, 799.
29 J. Salbeck, N. Yu, J. Bauer, F. Weissörtel, and H. Bestgen, *Synth. Met.*, 1997, **91**, 209.
30 W. Ishikawa, K. Noguchi, Y. Kuwabara, and Y. Shirota, *Adv. Mater.*, 1993, **5**, 559.
31 H. Inada and Y. Shirota, *J. Mater. Chem.*, 1993, **3**, 319.
32 Y. Kuwabara, H. Ogawa, H. Inada, N. Noma, and Y. Shirota, *Adv. Mater.*, 1994, **6**, 677.
33 D. F. O'Brien, P. E. Burrows, S. R. Forrest, B. E. Koene, D. E. Loy, and M. E. Thompson, *Adv. Mater.*, 1998, **10**, 1108.
34 B. E. Koene, D. E. Loy, and M. E. Thompson, *Chem. Mater.*, 1998, **10**, 2235.
35 Y. Shirota, K. Okumoto, and H. Inada, *Synth. Met.*, 2000, **111-112**, 387.
36 K. Okumoto and Y. Shirota, *Chem. Lett.*, 2000, 1034.
37 A. P. Kulkarni, C. J. Tonzola, A. Babel, and S. A. Jenekhe, *Chem. Mater.*, 2004, **16**, 4556.
38 C. J. Abshire and C. S. Marvel, *Makromol. Chem.*, 1961, **44**, 388.
39 M. Gillo, P. Iannelli, P. Laurienzo, M. Malinconico, A. Roviello, P. Mormile, and L. Petti, *Chem. Mater.*, 2002, **14**, 1539.
40 S. Janietz and S. Anlauf, *Macromol. Chem. Phys.*, 2002, **203**, 427.
41 B. Schulz, M. Bruma, and L. Brehmer, *Adv. Mater.*, 1997, **9**, 601.
42 F. N. Hayes, B. S. Rogers, and D. G. Ott, *J. Am. Chem. Soc.*, 1955, **77**, 1850.
43 R. Huisgen, J. Sauer, and H. J. Sturm, *Chem. Ber.*, 1960, **93**, 2106.
44 C. Ainsworth, *J. Am. Chem. Soc.*, 1955, **77**, 1148.
45 Y. Cao, I. D. Parker, G. Yu, C. Zhang, and A. J. Heeger, *Nature*, 1999, **397**, 414.
46 S. Hoshino, K. Ebata, and K. Furukawa, *J. Appl. Phys.*, 2000, **87**, 1968.
47 T. Tsutsui, E.-I. Aminaka, Y. Fujita, Y. Hamada, and S. Saito, *Synth. Met.*, 1993, **57**, 4157.

[48] G. Y. Jung, C. Wang, C. Pearson, M. R. Bryce, I. D. W. Samuel, and M. C. Petty, Proceedings of the 45th SPIE Annual Meeting, San Diego, 2000, p. 307.

[49] C. Wang, G. Y. Jung, Y. Hua, C. Pearson, M. R. Bryce, M. C. Petty, A. S. Batsanov, A. E. Goeta, and J. A. K. Howard, *Chem. Mater.*, 2001, **13**, 1167.

[50] C. Wang, G. Y. Jung, A. S. Batsanov, M. R. Bryce, and M. C. Petty, *J. Mater. Chem.*, 2002, **12**, 173.

[51] H. Aziz, Z. Popovic, S. Xie, A. M. Hor, N. X. Hu, and G. Xu, *Appl. Phys. Lett.*, 1998, **72**, 2642.

[52] M. Ichikawa, T. Kawaguchi, K. Kobayoshi, T. Miki, K. Furukawa, T. Koyama, and Y. Taniguchi, *J. Mater. Chem.*, 2006, **16**, 221.

[53] J. Bettenhausen, P. Strohriegl, W. Brütting, H. Tokuhisa, and T. Tsutsui, *J. Appl. Phys.*, 1997, **82**, 4957.

[54] T. Noda, H. Ogawa, N. Noma, and Y. Shirota, *J. Mater. Chem.*, 1999, **9**, 2177.

[55] J. Bettenhausen, M. Greczmiel, M. Jandke, and P. Strohriegl, *Synth. Met.*, 1997, **91**, 223.

[56] H.-C. Yeh, R.-H. Lee, L.-H. Chan, T.-Y. Lin, J., C.-T. Chen, E. Balasubramaniam, and Y.-T. Tao, *Chem. Mater.*, 2001, **13**, 2788.

[57] J. H. Ahn, C. S. Wang, C. Pearson, M. R. Bryce, and M. C. Petty, *Appl. Phys. Lett.*, 2004, **85**, 1283.

[58] S. Oyston, C. Wang, G. Hughes, A. S. Batsanov, I. F. Perepichka, M. R. Bryce, J. H. Ahn, C. Pearson, and M. C. Petty, *J. Mater. Chem.*, 2005, **15**, 194.

[59] S. Oyston, C. Wang, I. F. Perepichka, A. S. Batsanov, M. R. Bryce, J. H. Ahn, and M. C. Petty, *J. Mater. Chem.*, 2005, **15**, 5164.

[60] T.-Q. Nguyen, V. Doan, and J. Schwartz, *J. Chem. Phys.*, 1999, **110**, 4068.

[61] J. Kido, K. Hongawa, K. Okuyama, and K. Nagei, *Appl. Phys. Lett.*, 1994, **64**, 815.

[62] J. Kido, H. Shionoya, and K. Nagai, *Appl. Phys. Lett.*, 1995, **67**, 2281.

[63] S. Nakamura, M. Senoh, and T. Mukai, *Appl. Phys. Lett.*, 1993, **62**, 2390.

[64] G. Leising, B. Ullrich, G. Grem, and G. Leditzky, *Adv. Mater.*, 1992, **4**, 36.

[65] Y. Yang, Q. Pei, and A. J. Heeger, *J. Appl. Phys.*, 1996, **79**, 934.

[66] U. Scherf and K. Müllen, *Macromolecules*, 1992, **25**, 3546.

[67] N. Miyaura and A. Suzuki, *Chem. Rev.*, 1995, **95**, 2457.

[68] U. Scherf, *J. Mater. Chem.*, 1999, **9**, 1853.

[69] S. Tasch, A. Niko, G. Leising, and U. Scherf, *Appl. Phys. Lett.*, 1996, **68**, 1090.

[70] J. Jacob, S. Sax, T. Poiok, E. J. W. List, A. C. Grimsdale, and K. Müllen, *J. Am. Chem. Soc.*, 2004, **126**, 6987.

[71] J. Jacob, J. Zhang, A. C. Grimsdale, and K. Müllen, *Macromolecules*, 2003, **36**, 8240.

[72] J. Jacob, S. Sax, M. Gaal, E. J. W. List, A. C. Grimsdale, and K. Müllen, *Macromolecules*, 2005, **38**, 9933.

[73] A. K. Mishra, M. Graf, F. Grasse, J. Jacob, E. J. W. List, and K. Müllen, *Chem. Mater.*, 2006, **18**, 2879.

[74] M. Fukuda, K. Sawada, and K. Yoshino, *Jpn. J. Appl. Phys.*, 1989, **28**, L1433.

[75] M. Fukuda, K. Sawada, and K. Yoshino, *J. Polym. Sci. Polym. Chem.*, 1993, **31**, 2465.

[76] T. Yamamoto, Y. Hayashi, and Y. Yamamoto, *Bull. Chem. Soc. Jpn.*, 1978, **51**, 2091.

[77] U. Scherf and E. J. W. List, *Adv. Mater.*, 2002, **14**, 477.

[78] Q. Pei and Y. Yang, *J. Am. Chem. Soc.*, 1996, **118**, 7416.

[79] G. Klärner, J. I. Lee, E. Chan, J. P. Chen, A. Nelson, D. Markiewicz, R. Siemens, J. C. Scott, and R. D. Miller, *Chem. Mater.*, 1999, **11**, 1800.

[80] U. Lemmer, S. Heun, R. F. Mahrt, U. Scherf, M. Hopmeier, U. Siegner, E. O. Göbel, K. Müllen, and H. Bässler, *Chem. Phys. Lett.*, 1995, **240**, 373.

[81] E. Conwell, *Trends Polym. Sci.*, 1997, **5**, 218.

[82] W.-L. Yu, J. Pei, W. Huang, and A. J. Heeger, *Adv. Mater.*, 2000, **12**, 828.

[83] S. Setayesh, A. C. Grimsdale, T. Weil, V. Enkelmann, K. Müllen, F. Meghdadi, E. J. W. List, and G. Leising, *J. Am. Chem. Soc.*, 2001, **123**, 946.

[84] G. Klärner, M. H. Davey, W.-D. Chen, J. Campbell Scott, and R. D. Miller, *Adv. Mater.*, 1998, **10**, 993.

[85] L. Romaner, A. Pogantsch, P. S. de Freitas, U. Scherf, M. Gaal, E. Zojer, and E. J. W. List, *Adv. Funct. Mater.*, 2003, **13**, 597.

[86] E. J. W. List, R. Guentner, P. S. de Freitas, and U. Scherf, *Adv. Mater.*, 2002, **14**, 374.

[87] X. Gong, P. K. Iyer, D. Moses, G. C. Bazan, A. J. Heeger, and S. S. Xiao, *Adv. Funct. Mater.*, 2003, **13**, 325.

[88] J. Pei, J. Ni, X. H. Zhou, X. Y. Cao, and Y. H. Lai, *J. Org. Chem.*, 2002, **67**, 4924.

[89] D. Marsitzky, J. Murray, J. Campbell Scott, and K. R. Carter, *Chem. Mater.*, 2001, **13**, 4285.

[90] T. Spehr, R. Pudzich, T. Fuhrmann, and J. Salbeck, *Org. Electron.*, 2003, **4**, 61.

[91] H. Lee, J. Oh, H. Y. Chu, J. I. Lee, S. H. Kim, Y. S. Yang, G. H. Kim, L. Do, T. Zyung, J. I. Lee, and Y. Park, *Tetrahedron*, 2003, **59**, 2773.

[92] C.-C. Wu, Y.-T. Lin, K.-T. Wong, R.-T. Chen, and Y.-Y. Chien, *Adv. Mater.*, 2004, **16**, 61.

[93] C.-C. Wu, T.-L. Liu, W.-Y. Hung, Y.-T. Lin, K.-T. Wong, R.-T. Chen, Y.-M. Chen, and Y.-Y. Chien, *J. Am. Chem. Soc.*, 2003, **123**, 3710.

[94] K.-T. Wong, Y.-Y. Chien, R.-T. Chen, C.-F. Wang, Y.-T. Lin, H.-H. Chiang, P.-Y. Hsieh, C.-C. Wu, C. H. Chou, Y. O. Su, G. H. Lee, and S.-M. Peng, *J. Am. Chem. Soc.*, 2002, **124**, 11576.

[95] K. L. Chan, M. J. McKiernan, C. R. Towns, and A. B. Holmes, *J. Am. Chem. Soc.*, 2005, **127**, 7662.

[96] A. B. Holmes, 7th International Symposium on Functional Pi-Electron Systems, Osaka, Japan, 2006.

[97] I. I. Perepichka, I. F. Perepichka, M. R. Bryce, and L.-O. Pålsson, *Chem. Commun.*, 2005, 3397.

[98] I. I. Perepichka, I. F. Perepichka, M. R. Bryce, S. King, and A. P. Monkman, 2006.

[99] T.-H. Huang, J. T. Lin, L.-Y. Chen, Y.-T. Lin, and C.-C. Wu, *Adv. Mater.*, 2006, **18**, 602.

[100] N. C. Greenham, F. Cacialli, D. D. C. Bradley, R. H. Friend, S. C. Moratti, and A. B. Holmes, *Mater. Res. Soc. Symp. Proc.*, 1996, **328**, 351.

[101] S. C. Moratti, D. D. C. Bradley, R. H. Friend, N. C. Greenham, and A. B. Holmes, *Mater. Res. Soc. Symp. Proc.*, 1994, **413**, 13.

[102] A. Lux, A. B. Holmes, R. Cervini, J. E. Davies, S. Moratti, J. Grüner, F. Caciallo, and R. H. Friend, *Synth. Met.*, 1997, **84**, 293.

[103] A. C. Grimsdale, F. Cacialli, J. Grüner, X.-C. Li, A. B. Holmes, S. Moratti, and R. H. Friend, *Synth. Met.*, 1996, **76**, 165.

[104] H.-H. Sung and H.-C. Lin, *Macromolecules*, 2004, **37**, 7945.

[105] J. Ding, M. Day, G. Robertson, and J. Roovers, *Macromolecules*, 2002, **35**, 3474.

[106] J. Ding, Y. Tao, M. Day, J. Roovers, and M. D'Iorio, *J. Opt. A: Pure Appl. Opt.*, 2002, **4**, 267.

[107] H. Mochizuki, T. Hasui, M. Kawamoto, T. Ikeda, C. Adachi, Y. Taniguchi, and Y. Shirota, *Macromolecules*, 2003, **36**, 3457.

[108] Y. Zhang, Y. Hu, H. Li, L. Wang, X. Jing, F. Wang, and D. Ma, *J. Mater. Chem.*, 2003, **13**, 773.

[109] C. Ego, A. C. Grimsdale, F. Uckert, G. Yu, S. G., and K. Müllen, *Adv. Mater.*, 2002, **14**, 809.

[110] F. Wu, S. Reddy, and C. Shu, *Chem. Mater.*, 2003, **15**, 269.

[111] C. Shu, R. Dodda, F. Wu, M. S. Liu, and A. K. Jen, *Macromolecules*, 2003, **36**, 6698.

[112] F.-I. Wu, P.-I. Shih, C.-F. Shu, Y.-T. Tung, and Y. Chi, *Macromolecules*, 2005, **38**, 9028.

[113] S. Hoshino and H. Suzuki, *Appl. Phys. Lett.*, 1996, **69**, 224.

[114] M. A. Baldo, C. Adachi, and S. R. Forrest, *Phys. Rev. B*, 2000, **62**, 10967.

[115] D. F. O'Brien, M. A. Baldo, M. E. Thompson, and S. R. Forrest, *Appl. Phys. Lett.*, 1999, **74**, 442.

[116] C. Adachi, M. A. Baldo, S. R. Forrest, and M. E. Thompson, *Appl. Phys. Lett.*, 2000, **77**, 904.

[117] C. Adachi, M. A. Baldo, S. R. Forrest, S. Lamansky, M. E. Thompson, and R. C. Kwong, *Appl. Phys. Lett.*, 2001, **78**, 1622.

[118] C. Adachi, R. C. Kwong, P. Djurovich, V. Adamovich, M. A. Baldo, M. E. Thompson, and S. R. Forrest, *Appl. Phys. Lett.*, 2001, **79**, 2082.

[119] M. A. Baldo and S. R. Forrest, *Phys. Rev. B*, 2000, **62**, 10958.

[120] V. V. Grushin, N. Herron, D. D. LeCloux, W. J. Marshall, V. A. Petrov, and Y. Wang, *Chem. Commun.*, 2001, 1494.

[121] J. Brooks, Y. Babayan, S. Lamansky, P. I. Djurovich, I. Tsyba, R. Bau, and M. E. Thompson, *Inorg. Chem.*, 2002, **41**, 3055.

[122] P. J. Hay, *J. Phys. Chem. A*, 2002, **106**, 1634.

[123] P. Coppo, E. A. Plummer, and L. De Cola, *Chem. Commun.*, 2004, 1774.

[124] X. Gong, W. M. Jacek, J. C. Ostrowski, G. C. Bazan, D. Moses, and A. J. Heeger, *Adv. Mater.*, 2004, **16**, 615.

[125] X. Gong, D. Moses, A. J. Heeger, and S. Xiao, *J. Phys. Chem. B*, 2004, **108**, 8601.

[126] J. C. Ostrowski, M. R. Robinson, A. J. Heeger, and G. C. Bazan, *Chem. Commun.*, 2002, 784.

[127] M. Tavasli, S. L. Bettington, M. R. Bryce, H. A. Al Attatar, F. B. Dias, S. King, and A. P. Monkman, *J. Mater. Chem.*, 2005, **15**, 4963.

[128] H. A. Al Attar, A. P. Monkman, M. Tavasli, S. Bettington, and M. R. Bryce, *Appl. Phys. Lett.*, 2005, **86**, 121101.

[129] B. W. D'Andrade and S. R. Forrest, *Adv. Mater.*, 2004, **16**, 1585.

[130] Y. Sun, N. C. Giebink, H. Kanno, B. Ma, M. E. Thompson, and S. R. Forrest, *Nature*, 2006, **440**, 908.

[131] S. Oyston, 'Synthesis and Optoelectronic Properties of New Fluorene-2,5,-diaryl-1,3,4-oxadiazole Hybrid Materials', University of Durham, Durham, 2005.

[132] N. E. Widdowson, 'Electroluminescent devices based on blended polymeric thin films', University of Durham, Durham, 2006.

133 N. Tamoto, C. Adachi, and K. Nagai, *Chem. Mater.*, 1997, **9**, 1077.

134 H. Antoniadis, M. Inbasekaran, and E. P. Woo, *Appl. Phys. Lett.*, 1998, **73**, 3055.

135 K. R. J. Thomas, J. T. Lin, Y.-T. Tao, and C.-H. Chien, *Chem. Mater.*, 2002, **14**, 3852.

136 K. R. J. Thomas, J. T. Lin, Y.-T. Tao, and C.-H. Chuen, *Chem. Mater.*, 2004, **16**, 5437.

137 Y. Chien, K. Wong, P. Chou, and T. Cheng, *Chem. Commun.*, 2002, 2874.

138 R. Pudzich and J. Salbeck, *Synth. Met.*, 2003, **138**, 21.

139 J. Y. Shen, C. Y. Lee, T.-H. Huang, J. T. Lin, Y.-T. Tao, C.-H. Chien, and C. Tsai, *J. Mater. Chem.*, 2005, **15**, 2455.

140 M. Guan, Z. Q. Bian, Y. F. Zhou, F. Y. Li, Z. J. Li, and C. H. Huang, *Chem. Commun.*, 2003, 1708.

141 A. Patra, M. Pan, C. S. Friends, T.-C. Lin, A. N. Cartwright, and P. N. Prasad, *Chem. Mater.*, 2002, **14**, 4044.

142 Y. Geng, A. Trajkovska, D. Katsis, J. J. Ou, S. W. Culligan, and S. H. Chen, *J. Am. Chem. Soc.*, 2002, **124**, 8337.

143 F. Ullmann and J. Bielecki, *Chem. Ber.*, 1901, **34**, 2174.

144 F. Paul, J. Patt, and J. F. Hartwig, *J. Am. Chem. Soc.*, 1994, **116**, 5969.

145 J. F. Hartwig, M. Kawatsura, S. I. Hauck, K. H. Saughnessy, and L. M. Alcazar-Roman, *J. Org. Chem.*, 1999, **64**, 5575.

146 A. S. Guram and S. L. Buchwald, *J. Am. Chem. Soc.*, 1994, **116**, 7901.

147 K. T. Kamtekar, C. S. Wang, S. L. Bettington, A. S. Batsanov, I. F. Perepichka, M. R. Bryce, J. H. Ahn, M. Rabinal, and M. C. Petty, *J. Mater. Chem.*, 2006, **16**, 3823.

148 Y. Liang, Q. Zhou, Y. Cheng, L. D. Wang, D. Ma, X. Jing, and F. Wang, *Chem. Mater.*, 2003, **15**, 1935.

149 W.-Y. Wong, Z. He, S.-K. So, K.-L. Tong, and Z. Lin, *Organometallics*, 2005, **24**, 4079.

150 A. B. Tamayo, B. D. Alleyne, P. I. Djurovich, S. Lamansky, I. Tsyba, N. N. Ho, R. Bau, and M. E. Thompson, *J. Am. Chem. Soc.*, 2003, **125**, 7377.

151 J. K. Stille, *Angew. Chem. Int. Ed.*, 1986, **25**, 508.

152 P.-M. Windscheif and F. Vögtle, *Synthesis*, 1994, 87.

153 A. E. Thompson, G. Hughes, A. Batsanov, M. R. Bryce, P. R. Parry, and B. Tarbit, *J. Org. Chem.*, 2005, **70**, 388.

154 M. A. Bennett and D. L. Milner, *Chem. Commun.*, 1967, **12**, 581.

155 Y.-Z. Lee, X. Chen, S.-A. Chen, P.-K. Wei, and W.-S. Fann, *J. Am. Chem. Soc.*, 2001, **123**, 2296.

156 N. W. Jacobsen and A. E. Philippides, *Aust. J. Chem.*, 1986, **39**, 1911.

157 C. Farren, C. A. Christensen, S. FitzGerald, M. R. Bryce, and A. Beeby, *J. Org. Chem.*, 2002, **67**, 9130.

158 I. R. Laskar, S.-F. Hsu, and T.-M. Chen, *Polyhedron*, 2005, **24**, 189.

159 J. L. Romera, J. M. Cid, and A. A. Trabanco, *Tet. Lett.*, 2004, **45**, 8797.

160 C. Wang, M. Kilitziraki, J. A. H. MacBride, M. R. Bryce, L. E. Horsburgh, A. K. Sheridan, A. P. Monkman, and I. D. W. Samuel, *Adv. Mater.*, 2000, **12**, 217.

161 R. Gedye, F. Smith, K. Westaway, H. Ali, L. Balderisa, L. Laberge, and J. Roasell, *Tet. Lett.*, 1986, **27**, 279.

162 R. J. Giguere, T. L. Bray, S. N. Duncan, and G. Majetich, *Tet. Lett.*, 1986, **28**, 4945.

163 R. S. Varma, *Green Chemistry*, 1999, **1**, 43.

164 L. Perreux and A. Loupy, *Tetrahedron*, 2001, **57**, 9199.

165 'Microwave Assisted Organic Synthesis', ed. J. P. Tierney and P. Lidström, Blackwell, 2005.

166 G. W. Kabalka, L. Wang, R. M. Pagni, C. M. Hair, and V. Namboodiri, *Synthesis*, 2003, 217.

167 N. E. Leadbeater and M. Marco, *Angew. Chem. Int. Ed.*, 2003, **39**, 3596.

168 H. Konno and Y. Sasaki, *Chem. Lett.*, 2003, **32**, 252.

169 K. Saito, N. Matsusue, H. Kanno, Y. Hamada, H. Takahashi, and T. Matsumura, *Jpn. J. Appl. Phys.*, 2004, **43**, 2733.

170 M. J. Frisch, G. W. Trucks, H. B. Schlegel, G. E. Scuseria, M. A. Robb, J. R. Cheeseman, J. A. Montgomery, T. Vreven, K. N. Kudin, J. C. Burant, J. M. Millam, S. S. Iyengar, J. Tomasi, V. Barone, B. Mennucci, M. Cossi, G. Scalmani, N. Rega, G. A. Petersson, H. Nakatsuji, M. Hada, M. Ehara, K. Toyota, R. Fukuda, J. Hasegawa, M. Ishida, T. Nakajima, Y. Honda, O. Kitao, H. Nakai, M. Klene, X. Li, J. E. Knox, H. P. Hratchian, J. B. Cross, V. Bakken, C. Adamo, J. Jaramillo, R. Gomperts, R. E. Stratmann, O. Yazyev, A. J. Austin, R. Cammi, C. Pomelli, J. W. Ochterski, P. Y. Ayala, K. Morokuma, G. A. Voth, P. Salvador, J. J. Dannenberg, V. G. Zakrzewski, S. Dapprich, A. D. Daniels, M. C. Strain, O. Farkas, D. K. Malick, A. D. Rabuck, K. Raghavachari, J. B. Foresman, J. V. Ortiz, Q. Cui, A. G. Baboul, S. Clifford, J. Cioslowski, B. B. Stefanov, G. Liu, A. Liashenko, P. Piskorz, I. Komaromi, R. L. Martin, D. J. Fox, T. Keith, M. A. Al-Laham, C. Y. Peng, A. Nanayakkara, M. Challacombe, P. M. W. Gill, B. Johnson, W. Chen, M. W. Wong, C. Gonzalez, and J. A. Pople, in 'Gaussian 03, Revision N.04', 2004.

171 A. D. Becke, *Phys. Rev. B*, 1988, **38**, 3098.

172 A. D. Becke, *J. Chem. Phys.*, 1993, **98**, 5648.

173 C. Lee, W. Yang, and R. G. Parr, *Phys. Rev. B*, 1988, **37**, 785.

174 S. Portmann and H. P. Lüthi, *Chimia*, 2000, **54**, 766.

175 K. Ng, X. Gong, S. H. Chan, L. S. M. Lam, and W. K. Chan, *Chem. Eur. J.*, 2001, **7**, 4358.

176 S. Hou and W. K. Chan, *Macromlecules*, 2002, **35**, 850.

177 X. Zahn, Y. Liu, X. Wu, S. Wang, and D. Zhu, *Macromolecules*, 2002, **35**, 2529.

178 R. Milcent and G. Barbier, *J. Hetrocycl. Chem.*, 1983, **20**, 77.

179 L. Nie, Z. Li, J. Han, X. Zhang, R. Yang, W.-X. Liu, F.-Y. Wu, J.-W. Xie, Y.-F. Zhao, and Y.-B. Jiang, *J. Org. Chem.*, 2002, **69**, 6449.

180 S. P. Dudek, M. Pouderoijen, R. Abbel, A. P. H. J. Schenning, and E. W. Meijer, *J. Am. Chem. Soc.*, 2005, **127**, 11763.

181 A. L. Kanibolotsky, R. Berridge, P. J. Skabara, I. F. Perepichka, D. D. C. Bradley, and M. Koeberg, *J. Am. Chem. Soc.*, 2004, **126**, 13695.

182 G. Hughes, C. S. Wang, A. Batsanov, M. Fern, S. Frank, M. R. Bryce, I. F. Perepichka, A. P. Monkman, and B. L. Lyons, *Org. Biomol. Chem.*, 2003, **1**, 3069.

183 M. Golfier and M.-G. Guillerez, *Tetrahedron Lett.*, 1973, **17**, 267.

184 W. Li, D. P. Nelson, M. S. Jensen, R. S. Hoerrner, D. Cai, R. D. Larsen, and P. J. Reider, *J. Org. Chem.*, 2002, **67**, 5394.

185 M. Larhed, M. Hoshino, S. Hadida, D. P. Curran, and A. Hallberg, *J. Org. Chem.*, 1997, **62**, 5583.

186 H. Hashizume, H. Ito, N. Kanaya, H. Nagashima, and H. Usui, *Heterocycles*, 1994, **38**, 1551.

187 M. F. Reich, P. F. Fabio, V. J. Lee, N. A. Kuck, and R. T. Testa, *J. Med. Chem.*, 1989, **32**, 2474.
188 T. Itoh and T. Mase, *Tetrahedron Lett.*, 2005, **46**, 3573.
189 V. Bonnet, F. Mongin, F. Trécourt, G. Quéguiner, and P. Knochel, *Tetrahedron*, 2002, **58**, 4429.